Field investigations and reactive transport modelling of biodegrading coal tar compounds at a complex former manufactured gas plant

Suzanne C. Faber

Reading committee:
Prof. dr. ir. T.J. Heimovaara
Prof. dr. R. Helmig
Dr. H. Passier
Prof. dr. M. Petitta
Prof. dr. ir. H.H.M. Rijnaarts

Examination committee:
Prof. dr. ir. T.J. Heimovaara
Prof. dr. R. Helmig
Dr. H. Passier
Prof. dr. M. Petitta
Dr. N.B. Sutton

ISBN:	978-90-6266-660-7
Title:	Field investigations and reactive transport modelling of biodegrading coal tar compounds at a complex former manufactured gas plant
NUR code:	934
NUR description:	Hydrologie
Number of pages:	290
Cover lay-out:	Margot Stoete, Utrecht University
Printed by:	Ipskamp Printing

Field investigations and reactive transport modelling of biodegrading coal tar compounds at a complex former manufactured gas plant

Veldonderzoeken en reactief transportmodellering van biologisch afbreekbare aromatische koolwaterstoffen op een complex voormalig gasfabrieksterrein

(met een samenvatting in het Nederlands)

Proefschrift

ter verkrijging van de graad van doctor aan de
Universiteit Utrecht
op gezag van de
rector magnificus, prof. dr. H.R.B.M. Kummeling,
ingevolge het besluit van het college voor promoties
in het openbaar te verdedigen op
vrijdag 6 oktober 2023 des middags te 12.15 uur

door

Suzanne Catherina Faber

geboren op 17 januari 1987
te Amsterdam

Promotor:
Prof. dr. R.J. Schotting

Copromotor:
Dr. A. Zech

This dissertation has been developed within the *Bestparc Utrecht (Biological Engineered Stimulation in a Public Accessible Recreation Area in the Center of Utrecht)* research project. Bestparc is a scientific collaboration between Utrecht University, Wageningen University and Research and Deltares, and has been made possible with financial support from the Ministry of Infrastructure and Water Management and the Municipality of Utrecht.

Acknowledgements

This promotion trajectory has been quite a journey and I would like to express my gratitude to all those people that supported me along the way.

I would like to thank my promotor Ruud Schotting for thinking of me, five years after graduating from my masters, when looking for a candidate for this research. I am also grateful for your unwavering trust in me to bring the PhD to a good end and for being so personal that I always felt free to be myself. I would like to thank Amir Raoof and Alraune Zech for their support with reviewing chapters and modelling results. Henning Prommer, although without any formal supervising role, I am immensely grateful for your support in setting up the reactive transport model.

I wish to thank the entire Griftpark team, for the many interesting, sometimes turbulent, discussions. From Utrecht municipality, Deltares, Wageningen University, Aveco de Bondt, Mourik and Antea group: Peter, Bart, Gert, Harry, Jan, Johan, Sophie, Annemieke, Tim, Dilan, Andrea, Antoine, Arie, John, Kees. I hope our paths will cross again in the future. A particular shout out to Jan Gerritse and Johan van Leeuwen, thank you for the fruitful conversations and for being such kind colleagues. Also Arie van Lit, I enjoyed my visits to the treatment plant and the 'gevulde koeken' with you and John. Thank you particularly for your generosity with data, if there was such a thing as 'death by Excel'... I also want to thank Dilan Aydin, it was great to build more than a professional relationship with you.

There were many people, within Utrecht University as well as outside, that helped me with my work by taking the time to answer questions. A few that I want to thank in particular are: Tony Appelo for his help with PHREEQC; Maarten Zeylmans van Emmichoven and Marc Bierkens helping me to understand more of the geology of the Utrecht region; Thilo Berendts for helping me grasp (a bit of) geochemistry; Sebastian Müller for his knowledge on indicator kriging; and Wolfgang Nowak for the exchanges on isotopes and uncertainties.

I would like to thank my paranymphs Alejandra Reyes-Amézaga and Vahid Nikpeyman. Ale, it was really great to have you around in that last year. Our walks through the botanic gardens and our open conversations did me good. Vahid, 'gedeelde leed is halve leed' and it was warming we could look out for each other a bit those last months. I also thank all the group members, office mates and visitors of the environmental hydrogeology group. It was great to know each other, despite corona keeping us at home for quite some time. Jan van Lopik, I enjoyed our irregular chats on the phone. Annuska Exel, you have a way to brighten moods. Also thanks to Marco Veloo for your practical support and kindness. I am also grateful to all the students that I have had the

pleasure to teach, whether mathematics or numerical modelling, and all the BSc and MSc students whose theses I supervised, it has been a fun part of my activities at Utrecht University. Particular thanks to Michaela Bhend, Tom Bastiaan and Arnaud Lacoste, whose work contributed to this dissertation. Last but not least in the colleague category: a shout out to all the three-o'clock-handstand-geochemists. Thanks to you I felt more integrated in the faculty. Furthermore, the practice became a motivation to get on the train to Utrecht in the morning, and surely the fresh supply of oxygen to my brain sped up the writing.

I am grateful to both my mother and my father for teaching me to enjoy and support me to develop my creativity, which is such an important part of my life, whether dance, music, literature or nature. Dancing keeps me sane through periods of madness and sadness. From this follows my gratitude to all the various dancing teachers I have had the pleasure to learn with, as well as for my piano teacher Petros, you are truly wonderful. Mom, I thank you for your unconditional love and support. Thank you, Peter, for always making me feel welcome. To my sister Camille, I am glad about what we have always been as well as what we have grown into. Thank you and Barnaby for making me the best niece ever, Ada, oh my, melt. The extended family, Simone, Josephine, Cecile, Johan, you will always be an important part of my life. Dear oma and opa, what a blessing to come from such a warm family. Although opa did not live to know, graduating at the same faculty where he was a professor has been special.

A deep thanks also to my housemates, who have made me feel at home and supported on darker days. To Amir, you and your family, and everything we shared, mean a lot to me. Finally, here's to all my friends. On this page I can't do justice to you all, but Nina and Laisvie, you know what you mean to me. Dear Sara, Kiki, Laurie, René, Mirko, Philip, Mariëtte, Klaas, Florine, Wiebe, Rutger, Dorus, Alina, etc., you colour my life (pink and the whole rainbow)!

Contents

Chapter 1

General Introduction

1.1 Manufactured gas plants

Since the industrial revolution, a wide variety of aromatic hydrocarbons has been introduced into the environment through human activities [137, 192]. Some of these substances have carcinogenic properties and pose risks human health and the environment [147]. The manufacturing of gas is an industrial activity often associated with significant hydrocarbon contaminant spills [214, 130, 288, 131].

1.1.1 Gas manufacturing

During the early 1800s, large commercial manufactured gas plants (MGP) were built in nearly every European and American city for the production of gas for municipal lighting [307, 133]. A conservative estimate suggests 8.700 FMGPs and coke-oven plants existed worldwide, excluding China, Russia and India [307]. Other estimates suggest between 21,200 to 32,600 FMGPs in the US alone [131].

At MGPs, gas production involved gasifying and carbonising coal, followed by tar extraction to purify the gas [280]. These tars consist of mixtures of primarily mono- and poly-cyclic aromatic hydrocarbons, phenols, aliphatic compounds and hetero-cyclic compounds [21, 40, 110, 210]. The tars were often disposed of, intentionally or unintentionally, at the production and purification locations or elsewhere on the industrial site [71, 214]. Coal tar contamination is believed to be present at the majority of FMGPs [89, 130, 132].

1.1.2 Remediation of former manufactured gas plant sites

Coal tars are a class of dense non-aqueous phase liquids (DNAPL). DNAPLs are heavier than water and have high viscosity so that they, once the entry-

pressure of the soil pores is exceeded, migrate down into the subsurface as a separate phase [205]. The depths to which DNAPLs can penetrate can make it impractical to excavate the source zone and treat contaminants ex-situ [33]. Although it may be possible to remove some of the pure-phase DNAPL directly by pumping, this approach does not provide an effective solution for the remediation of FMGP sites [205, 301]. Firstly, soil contamination at FMGP sites is often characterised by extreme heterogeneity due to the random deposition of coal tars and relocation of contaminated soil during construction works [307]. This heterogeneity makes it challenging to locate source zones for pumping [301]. Additionally, a considerable amount of residual DNAPL mass remains in the subsurface due to capillary forces after the bulk mass of DNAPL has drained [318, 33, 205].

In-situ treatment of source zones through methods such as thermal or chemical treatment or biodegradation, may be more efficient than pumping [33, 111, 198, 210]. However, during the 1980s and 1990s, when remediation efforts were undertaken at many contaminated sites, the high costs associated with these methods rendered them economically unfeasible in numerous cases [71, 111, 284, 307]. In many cases, the most economic method became to physically contain contaminant source zones by using groundwater cut-off walls [198]. Cut-off walls prevent clean groundwater from passing through the contaminated source zone, avoiding further contamination of groundwater down-gradient of the site. While physical containment barriers, typically constructed from materials like cement-bentonite or sheet piling, are not completely impermeable, they effectively protect the surrounding aquifer, if necessary through additional measures such as pumping [267, 198].

The Netherlands, a small but densely populated country, has extensively employed the containment method at many contaminated sites. The total number of contained locations is estimated to be 2,388, of which some include permanent groundwater pumping and treatment to establish an inward flux, along with intensive monitoring of the measures' effectiveness [11, 219].

Although the containment method effectively protects the groundwater, it fails to reduce the total contaminant volume, thus requiring perpetual operation and monitoring. The yearly costs for a single site may reach up to millions of euros, without any prospect of an end date.

In recent decades, innovative in-situ technologies have emerged, particularly using natural and stimulated biodegradation. Advances have also been made in non-destructive and rapid monitoring and analysis of water quality, as well as in numerical modeling software [84]. These new technologies have prompted the Dutch Ministry of Infrastructure and Water Management to revisit existing contain-and-manage sites with the aim to come to a terminal management plans [38].

1.1.3 The Griftpark

In 1840, a manufactured gas plant (MGP) was established on the outskirts of Utrecht. By the time of its closure in 1960, the industrial site contained multiple gas factories and was surrounded by the expanding city. In the 1980s, the extensive coal tar contamination existing at the site became public and lead to an uproar among the neighbouring residents [44]. Due to its urban location and the depth range of the coal tar contamination (down to more than 30 m below ground level), excavation or in-situ treatment were deemed unfeasible. Given the shallow groundwater table (around 2 m below ground level in Utrecht) the dissolved plume of aromatic hydrocarbons posed a threat to neighbouring residents. To prevent further development of the contaminant plume, a cement-bentonite wall was built around the site in 1990.

Field investigations prior to installation of the vertical barrier revealed the aquitard to be discontinuous [122]. As a results, the aquitard may not protect contamination of leaking into the deeper groundwater, an important source of drinking water in the Netherlands. Therefore, groundwater wells in the contained zone are continuously operated to maintain a lower water table. Figure 1.1 shows a cross-section and top view of the measures. The extracted water is biologically treated at a purification plant [221].

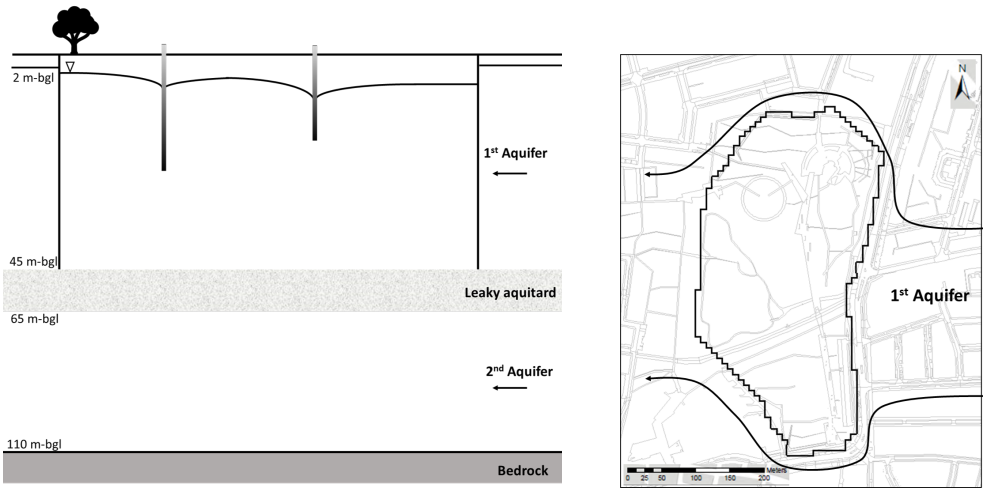

(a) (b)

Figure 1.1: (a) Cross-sectional representation of the containment measures initiated in 1990 at the Griftpark, consisting of a cement-bentonite wall (black vertical lines) surrounding the coal tar source zone and pumping wells to create an under-pressure. (b) The park from a bird's-eye view, showing the outline of the vertical barrier and subsequent diversion of groundwater flow around the park.

The already existing contaminant plume was addressed through a pump

and treat method. Based on calculations conducted at the time, this remediation measure was expected to need to last for at least 100 years to reduce contaminant concentrations downstream of the Griftpark to intervention levels. However, these levels were nearly achieved within 20 years. Recent advancements in knowledge have lead researchers to attribute this rapid reduction in contaminants to natural biodegradation processes.

Natural attenuation, including dispersion, sorption and biodegradation, can reduce the concentration and size of organic contaminant plumes over time. Over the last three decades, many studies have shown that biodegradation is a relevant natural attenuation process [180, 203, 228, 274]. Meanwhile, monitored natural attenuation (MNA) has become an accepted management option for low-risk contaminated sites [307, 193, 228, 313]. These findings prompted the municipality of Utrecht to reconsider the management strategy for the Griftpark, aiming to phase out the costly active management procedures and instead relying on MNA as a management approach.

1.2 Basics of groundwater flow and organic contaminant transport

1.2.1 Groundwater flow and anisotropy

Groundwater flow is generally described by Darcy's law [67], yielding

$$\vec{q} = \frac{\vec{Q}}{A} = -\overline{\overline{K}}\nabla h \tag{1.1}$$

where $\vec{q}$ and $\vec{Q}$ are, respectively, the specific discharge and volumetric flow rate through the aquifer in the direction of flow, and A is the cross-sectional area perpendicular to the direction of flow. The hydraulic gradient is denoted by ∇h and the hydraulic conductivity tensor of the aquifer material in the main direction of flow by $\overline{\overline{K}}$. The hydraulic conductivity depends on the aquifer's intrinsic permeability $\overline{\overline{\kappa}}$, and the density ρ and viscosity μ of the fluid, according to

$$\overline{\overline{K}} = \frac{\overline{\overline{\kappa}}\rho g}{\mu}, \tag{1.2}$$

where g is the gravitational acceleration. In nature, aquifers are generally heterogeneous and anisotropic and therefore the hydraulic conductivity varies in space [105].

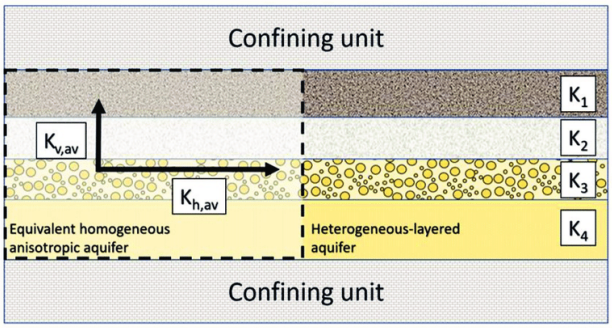

Figure 1.2: Heterogeneous-layered aquifer with various hydraulic properties for the different layers (1-4) and its equivalent homogeneous anisotropic approximation [299]

1.2.2 Groundwater flow at the Griftpark

The geologic formation below the Griftpark consists of mostly marine and fluvial deposits originating from Holocene and Pleistocene eras [32]. In the Utrecht region, the direct subsurface consists of two aquifers separated by an aquitard. The aquifers, that contain most of the groundwater reserves, consist of unconsolidated sand and gravel, whereas the aquitard consists of finer material, such as clay and silt, and has a low hydraulic conductivity. Figure 1.3 shows a schematic of a 34 km cross-section of the subsurface lithology of the Utrecht region. The figure shows that Utrecht is situated at a geological fault line, which has caused the clay from aquitard to be interspersed with sand from the second aquifer, causing a reduction in the aquitard's insulating properties.

Groundwater flow is usually a slow process. Around Utrecht, groundwater flows with a velocity of approximately 12 meters per year in an east-west direction. The first aquifer is unconfined, indicating it is in contact with the atmosphere and the water table may rise and fall with changes in atmospheric pressure, as well as with precipitation and evapotranspiration. Due to the discontinuity of the aquitard, communication between the first and second aquifer may take place and therefore the second aquifer is labeled semi-confined. The hydraulic pressure in the first aquifer is higher than in the second, so that groundwater may leak from the first down into the second aquifer. To avoid contaminated leaking out from the park into the second aquifer, groundwater is continuously pumped up from the park at a rate of at least 7.5 m^3/h.

Groundwater flowing in the first aquifer gets diverted by the vertical barrier at the Griftpark. This diversion causes an increase of water pressure on the up-gradient side and a decrease at the down-gradient side of the park. As the vertical barrier is not entirely impermeable, both the pressure on the up-

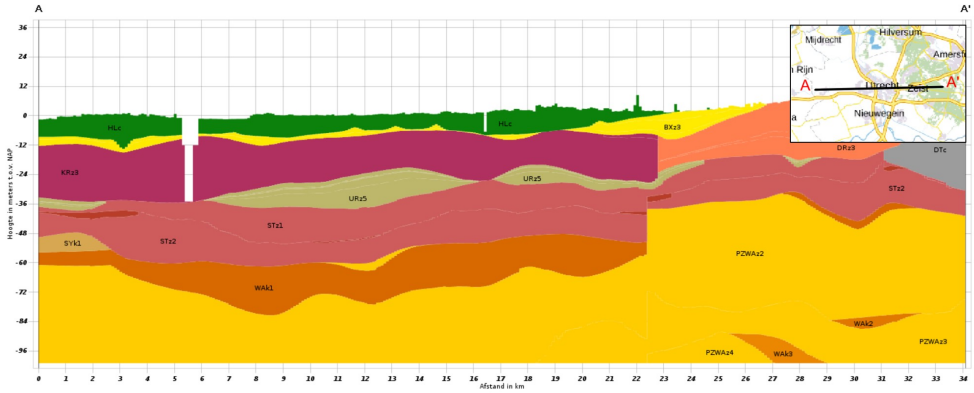

Figure 1.3: Lithology to a depth of 100 m of a 34 km cross-section through Utrecht. The confining aquitard, the Waalre (formerly Kedichem) formation, is indicated in a dark orange, the second aquifer in a light orange. The inset shows the cross-section from a top view

gradient side of the wall and the lowered water table within the park (due to groundwater extraction), causes the percolation of some groundwater through the wall into the park.

1.2.3 Fate of organic contaminants in the subsurface

Organic contaminants often enter the subsurface in the form of non-aqueous phase liquids (NAPL) [205]. NAPLs, such as oil, gasoline or tar, do not naturally mix with water and exist in water as separate phase. NAPLs are divided into two categories: light non-aqueous phase liquids (LNAPLs), that are lighter than water and dense non-aqueous phase liquids (DNAPLs), that are heavier than water. When an LNAPL is released on the ground surface, it tends to spread horizontally along the capillary fringe, which is the zone of pores above the water table where groundwater is sucked up through capillary forces [97].

In the context of this thesis, the focus is on coal tars, a class of DNAPLs. In the following subsections, we will discuss DNAPL movement and dissolution in more detail.

DNAPL movement

When a DNAPL is spilled and reaches the groundwater table, it can continue to seep downward into the saturated zone under gravity and capillary forces as a distinct liquid phase [75, 226]. During downward percolation, the DNAPL forms highly non-uniform interconnected ganglia, the distributions of which

are mostly determined by subsurface heterogeneity [144, 205, 75, 223]. Furthermore, as DNAPL passes through the subsurface, it leaves behind residual zones of low saturation in the form of fingers, blobs and droplets, entrapped in the porous medium by capillary forces, while high saturation pools can form on top of permeability barriers and macro-scale entrapment zones [52, 305, 170]. Consequently, the final DNAPL distribution is highly heterogeneous and unpredictable [75].

Figure 1.4 shows the results of a two-dimensional laboratory-scale tank experiment, as carried out by Luciano et al. [185]. It shows the influence both of medium heterogeneity as well as the existence of a hydraulic gradients on DNAPL infiltration through a water saturated medium.

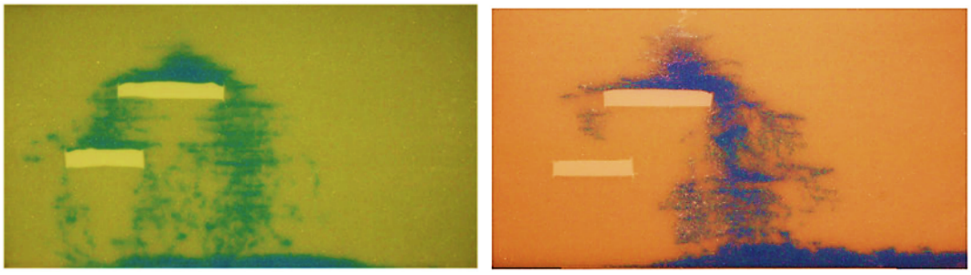

(a) (b)

Figure 1.4: (a) DNAPL leaking through a saturated stratified medium in the absence of water flow. (b) DNAPL leaking through the same medium with left to right water flow. Figures adapted from [185].

DNAPL dissolution

Upon entering the groundwater, DNAPL compounds can dissolve and form a plume that may contaminate large volumes of groundwater and pose significant environmental risks [205]. As many of the DNAPL compounds have low solubility and slow dissolution rates, they present persisting sources of groundwater contamination that may last centuries [33, 82].

The rate at which compounds dissolve from the pure phase DNAPL is primarily influenced by the contact area between the pure phase and water. As a result, the distribution of the pure phase zone plays a crucial role in contaminant dissolution [43, 108, 264, 325]. Residual zones, characterised by large surface areas, have high dissolution potential, whereas pool zones have less interfacial area available for mass transfer.

During dissolution, an equilibrium establishes between the concentration of each compound in the pure-phase mixture and the concentration of that compound dissolved in the aqueous phase [205, 231]. This means that the

dissolution rate of individual compounds is affected by the presence of other compounds and therefore that individual dissolution rates should be corrected [173, 82, 157]. Furthermore, the varying solubilities and mole fractions of compounds in coal tar result in different depletion rates from the pure-phase mixture, a phenomenon referred to as source zone ageing, causing also the dissolved contaminant fractions to change over time [158].

Transport of dissolved contaminants

After dissolution, contaminants are transported with the groundwater through advection. While transported by the groundwater, contaminants are subjected to natural attenuation, which includes all naturally occurring processes that reduce contaminant concentrations, such as dispersion and diffusion, sorption and biochemical transformation processes [251].

Dispersion causes the plume to spread in all directions and lower in concentration. Dispersion is caused by both microscopic and macroscopic effects of non-ideality of flow. Microscopic dispersion is caused by the diversion of contaminants by soil grains. Molecular diffusion is often included in microscopic dispersion. Macroscopic dispersion describes the spread of solutes caused by large-scale heterogeneities in a porous medium. In groundwater science, microscopic and macroscopic dispersion are mostly treated as one.

Many of the coal tar hydrocarbons transported through the subsurface by groundwater are hydrophobic and sorb to natural organic matter in the soil matrix. Sorption includes all physical and chemical processes that cause contaminants to get either adsorbed to or absorbed in the porous material. Sorption causes a delay in the migration of the plume front. The three dimensional reactive transport equation describing the rate of change of contaminant concentration $C(x, y, z, t)$ at any location, reads

$$nR\frac{\partial C}{\partial t} = \nabla \cdot \left(n\vec{D}\nabla C - C\vec{q} \right) + r_{reac}, \tag{1.3}$$

where n is the porosity of the porous medium. The advective transport of solutes in the direction of flow is determined by the groundwater velocity $\vec{q}$, whereas dispersion in all three-dimensional directions is determined by the hydrodynamic dispersion tensor $\vec{D}$. R is the retardation factor caused by equilibrium sorption of solutes to the soil organic matter. All other biochemical processes that may transform the contaminants are described by the r_{reac} term.

Biodegradation of organic contaminants

In the case of sites contaminated with aromatic hydrocarbons like coal tar, naturally occurring microorganisms in the subsurface have been observed to

possess the potential for breaking down aromatic hydrocarbons at significant rates [193, 228, 314, 313]. The biodegradation reaction is essentially a redox reaction where micro-organisms obtain energy for growth by transferring electrons from electron donors to electron acceptors. During biodegradation the substrate, i.e. the hydrocarbons, serves as the source of electrons. Aerobic biodegradation of aromatic hydrocarbons, where oxygen acts as the electron acceptor, has been well studied since the 1960s [116, 115, 263]. Under aerobic conditions, aromatic hydrocarbons are degraded through the mono-oxygenase and di-oxygenase enzymes [150]. The enzymes introduce oxygen atoms as hydroxyl groups to the aromatic ring, facilitating its cleavage into fragments that are more easily metabolised [127]. Through multiple oxidation and ring cleavage reactions, compounds are transformed into various intermediary metabolites before being completely oxidised to CO_2 and H_2O or transformed into simpler compounds that can be used for bacterial cell-growth, see Figure 1.5 [150].

In the mid-1980s it was discovered that microbial degradation of organic compounds can also occur under anaerobic electron acceptors using a range of electron acceptors including as nitrate [19, 143, 171, 324], sulphate [26, 70, 85, 104] and iron [183, 182], and even CO2, which results in the production of methane, through a relatively slow process [120, 316]. Several pathways for the anaerobic degradation of aromatic hydrocarbons have been identified, including fumarate addition and carboxylation, which insert a more oxidised group into the molecule [100]. For example, in the case of benzene degradation, benzoyl-CoA is created before the compound is further metabolised in a similar manner as during aerobic respiration, see Figure 1.5 [60]. The reduction capacity of anaerobic electron acceptors is lower than that of aerobic acceptors as anaerobic respiration yields less energy [274].

In the conventional interpretation, if the organic pollutants act as electron donors, distinct zones of specific redox potential (redox zones) evolve down-gradient of contaminant source zones, depending on the concentration and reactivity of the electron acceptors present in the aquifer [17, 188]. However, overlapping redox zones have been observed at many contaminated sites, as redox reactions may not always occur sequentially along a hypothetical thermodynamic order, but also simultaneously [148, 146]. For instance, the simultaneous occurrence of sulphate and iron reduction along with methane production has been observed in plumes [153, 34, 186, 253].

For risk assessment at contaminated field sites, it is useful to make predictions on plume progression using numerical models. To achieve this, it is necessary to establish kinetic expressions for contaminant removal through biodegradation. The biodegradation of hydrocarbons, expressed in Equation 1.3 with the term r_{reac}, can be described with kinetic rate expressions

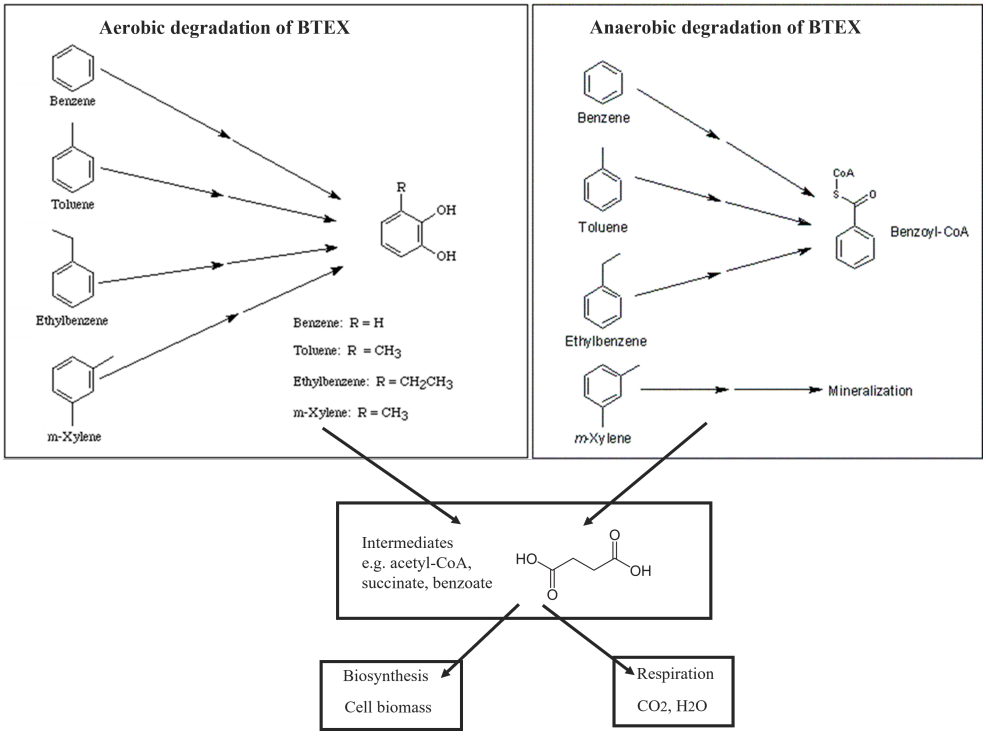

Figure 1.5: Simplified illustration of aerobic and anaerobic pathways of BTEX degradation. Figure adapted from [68] and [271].

of varying levels of complexity. For example, the transformation rate of the substrate may be described by a first order degradation model, where the rate linearly depends on the concentration of the substrate, or by a Monod kinetic model, in which degradation rates slow down at low substrate concentrations. The kinetic model may include terms for biomass growth and decay, as well as electron acceptor consumption and rate limitations. Furthermore, studies have revealed that degradation rates of individual hydrocarbons are different in mixtures than in single-substrate experiments [86, 159, 254]. Some studies have attempted to quantitatively model different substrate interaction mechanisms, such as competitive, non-competitive or uncompetitive, using kinetic expressions with data from batch experiments [48, 96, 181, 286]. It depends on the purpose of the model and the amount of data available which level of precision and complexity of the kinetic degradation reaction is useful in a specific case.

Biodegradation may be stimulated by supplying electron acceptors (such as oxygen or nitrate), nutrients (such as nitrogen and phosphorus), trace

elements (such as vitamins), co-solvents (such as ethanol), or microorganisms to the groundwater [228, 2, 193, 307].

1.2.4 Contamination and biodegradation at the Griftpark

Due to the significant subsurface heterogeneity at the Griftpark, it is extremely challenging to predict the total amount and distribution of pure-phase DNAPL contamination and to assess dissolution fluxes and source zone depletion. While measuring mass flux in the plume exiting from the source is often used to analyse the rate of dissolution from source zones [20, 82, 190, 157], this approach is not feasible at the Griftpark due to the vertical barriers surrounding the contaminated zone, that prevent the progression of a contaminant plume.

During site investigations conducted in the 1980s prior to the installation of the contain-and-manage technique, contamination was discovered all over the site, to depths of at least 30 m below ground level [252]. However, when it was decided to contain the contaminant source zone, investigation of the contaminants was stopped, so no complete map was ever made [6].

The investigations also revealed that the dissolved contamination existing at the park consisted primarily of poly-cyclic aromatic hydrocarbons and the mono-aromatic compounds benzene, toluene, ethylbenzene and the o/p/m-xylene isomers (BTEX), usual suspects in coal tars [252]. Some non-organic compounds were also found, such as cyanide, originating from the coal-gas factory, along with certain heavy metals as well as sulphate, potentially originating from the gas purifiers [252].

Although literature suggests a good potential of coal tar aromatic degradation at field sites, this potential should be investigated at the Griftpark specifically, especially considering the limited availability of fresh groundwater carrying electron acceptors due to the presence of vertical barriers, which could act as a limiting factor.

Biodegradation of organic contaminants at field sites is typically assessed along three main research lines [36] based on proving (1) changes in the contamination, such as the disappearance of substrate, (2) the presence of microbial DNA associated with the potential respiration processes and (3) the potential of the groundwater to support biodegradation, mostly by the presence of available electron acceptors. Conclusive evidence of biodegradation can be obtained only if several research lines were able to indicate its occurrence [36, 46, 246]. Therefore, all these research approaches will be employed at the Griftpark to assess biodegradation.

1.3 3D reactive transport modelling

1.3.1 Reactive transport modelling codes

To determine the viability of biodegradation (natural or stimulated) for source remediation and plume management at specific contaminated sites, reactive transport models provide valuable insights. Reactive transport models may integrate all available hydrological, hydrogeological and hydrogeochemical information to develop a quantitative framework to evaluate the long-term groundwater risks posed by a contamination. The first multi-component reactive transport models that treat any combination of transport and biogeochemical processes were developed by the mid-1980s [178, 269, 320]. With these models, phenomena as observed in the field could be more easily interpreted.

Currently, there are numerous modelling codes available that can include three-dimensional flow and reactive transport. Examples are HP1/HPx, PHT3D, OpenGeoSys, ParCrunchFlow, HYTEC, eSTOMP, HYDROGEOCHEM and PFLOTRAN [268]. The codes may vary in some features. For example, not all can handle two-phase flow and only some have graphical user interfaces. With a thorough understanding of the environmental problem and the aim of the numerical simulation, a choice can be made regarding which physically occurring processes need or need not be included in the model and what software is appropriate.

1.3.2 Concise literature discussion

Numerous modelling studies have been conducted to assess the occurrence of natural biodegradation in contaminated aquifers [41, 146]. In this section, we present a selection of reactive transport model studies that addressed biodegradation at sites contaminated with organic DNAPLs.

Essaid et al. [90] developed a two-dimensional, multi-species reactive transport model to study the transport and degradation of a pollution plume originating from a crude oil spill site at Bemidji, Minnesota, US. The model incorporated sequential aerobic and anaerobic degradation processes, as well as bacterial growth. Despite considerable uncertainty in the model parameter estimates that were mainly taken from literature, the model could generally reproduce measured levels groundwater plume and bacterial concentrations. Sensitivity analysis revealed that although simulation results were minimally sensitive to changes in aerobic degradation parameters, they were highly sensitive to the anaerobic degradation parameters. Other influential factors were found to be dispersivity, nutrient availability and sorption.

Brun et al. [42] investigated a pollution plume, primarily composed of aromatic compounds, at the Vejen landfill, Denmark. They compared field

measurements with two-dimensional simulations of the attenuation processes, including sequential aerobic and anaerobic degradation processes. Representing biodegradation kinetics with a partial equilibrium approach lead to satisfying reproductions of observed redox zones. The results also showed that using bulk values for first-order degradation rates (i.e. neglecting the presence of redox zones) could lead to incorrect assessments of the plume's attenuation. Furthermore, pH inhibition was found to be an important aspect of degradation kinetics. The authors emphasised that the initial solid Fe(III) concentration is significant for estimating the correct attenuation of the hydrocarbon plume.

Prommer et al. [234] developed a reactive transport model to study a tar-oil contaminated site in Düsseldorf-Flingern, Germany. The field data had high spatial resolution and could be used for the calibration of biodegradation rates. The model was used to simulate both biochemical and isotope gradients. The simulations successfully reproduced the observed isotope depth profiles for various aromatic hydrocarbons and revealed the effects of core versus fringe degradation. This concept describes the phenomenon, previously observed in other studies, when degradation occurs across the whole plume near the source zone, , while being limited to the plume fringes in the down-gradient direction due to the depletion of electron acceptors.

D'Affonseca et al. [65, 66] constructed a three-dimensional model for the interpretation of data from a well-characterised coal tar contaminated former wood-treatment plant in Buchholz, Germany. Their simulations incorporated dissolution from the source zone, reactive transport of dissolved compounds and the aquifer's geochemical response. The results highlighted the diverse fates of individual compounds due to variations in their physiochemical characteristics, such as reduction capacity, solubility, dissolution rate, isotope enrichment factors and weight percentages in the mixture. The study also demonstrated the importance of the spatial distribution of the source zone in determining the contaminant mass fluxes, as well as the influence of transient release from the source zone on biogeochemical conditions and isotope signatures over the lifetime of the contamination. Additionally, the modelling results illustrated the difficulty in assessing contaminant fate if the collected data covers only a small time window relative to the transport time scale.

From these studies, several insights were obtained:

- Accurate knowledge of anaerobic degradation parameters is crucial for estimating dissolved contaminant concentrations effectively.

- The distribution and characteristics of source zones are the main factor determining contaminant release fluxes.

- The quantity of minerals in the subsurface that serve as electron ac-

ceptor sources can significantly impact the long term development of contaminant plumes.

- Varying physiochemical characteristics of compounds in a mixture dictate their individual behaviour and fate.
- The potential need for pH buffering in the reactive module should be assessed to capture accurate degradation kinetics.
- High-resolution field data, both spatially and temporally, is essential for the precise calibration of biodegradation rates and capturing transient contaminant releases.

1.3.3 Challenges in reactive transport modelling

Many hydrogeological characterisation techniques rely on a limited number of measurements taken at specific locations, such as collecting groundwater samples from sampling ports or analysing drilling profiles to assess subsurface stratigraphy. Given the inherent heterogeneity of the subsurface, this means that predictions made by deterministic hydrogeological models will always carry a degree of uncertainty [304]. The uncertainties can arise from incomplete site characterisation, but also from parameter ambiguity due to spatial and/or temporal scaling issues and incomplete process understanding [236].

In academia, rigorous models are often used to evaluate risks associated with parameter uncertainty and heterogeneity. In stochastic hydrogeology, model progressions are made while employing the parameter's statistical properties. The uncertainty of a parameter can be represented by a probability density function (pdf), which depicts the range of possible parameter values and their likelihood of occurrence. We refer to Refsgaard et al. [241] for a comprehensive overview of commonly applied methods that can be used for simulation of statistical uncertainty assessment.

The most widely used method in hydrogeological applications is Monte Carlo (MC) analysis [35, 103, 243]. Although MC is a very rigorous and useful tool, there are also some issues concerning its use. Firstly, conducting a full MC analysis demands a high amount of computing power considering the large amount of uncertain parameters that should be taken into account in many reactive subsurface modelling applications (e.g. permeability, porosity, DNAPL source zones and biochemical reactions,) [241]. For many real-world risk assessments and management applications, mapping the entire heterogeneity may not be feasible [59, 98, 225]. Secondly, probabilistic model outcomes represented with statistics are not always well-accepted by practitioners and managers in applied research [257, 76].

Alternatives to sophisticated stochastic methods are the consensus or multi-model approach [88]. Within the consensus approach, a single model is constructed that integrates all available data and knowledge of the site, aiming to comprehensively capture the system's behaviour and address conceptual uncertainties [37]. With the multi-model approach, several variations of the base model are used that represent diverging conceptual understandings of the modelled system [218]. Without rigorous stochastic methods, uncertainty in these models can be investigated using parameter sensitivity analysis (PSA) [327]. During a PSA, the impact of parameter variations on model responses are investigated. Another tool that may be applied for strategic management is the uncertainty matrix (UM), that systematically represents uncertainties occurring at different stages of decision support activities [290, 304].

1.3.4 Contaminant transport modelling at the Griftpark

Figure 1.6 presents a comprehensive overview of the various processes at the Griftpark that potentially contribute to the spread, concentration and longevity of contamination. Not all these factors can be incorporated in the model and in this section we shortly address the most essential considerations for the reactive transport model of the site.

To construct a physical flow model of the Griftpark, knowledge needs to be acquired on crucial subsurface parameters, such as hydraulic conductivities, aquitard heterogeneity and the resistivity of the cement-bentonite barrier. Additionally, precipitation and evapotranspiration fluxes, and groundwater flow need to be understood. The aquitard's heterogeneity is particularly significant, as it acts as the pathway for contamination to reach the second aquifer. investigating subsurface heterogeneity poses challenges due to its inherent variability and limited applicability of research techniques due to the site setting. For example, advanced three-dimensional imaging techniques such as seismic and electric resistivity tomography surveys were considered, but deemed too costly considering their impracticality and low chance of success caused by, for example, the large pond lined with cement-bentonite present in the park, and the rubble and pipelines presumed present in the shallow subsurface.

The amount, location, and distribution of pure phase coal tar play a crucial role as they determine the dissolution mass fluxes. However, predicting the spatial distribution of source zones is challenging due to the numerous industrial activities at the former manufactured gas plant, uncertainties in spill locations and the irregular spread of DNAPL through caused by subsurface heterogeneity. Therefore predictions should be based on field measurements.

With high uncertainty in subsurface and contaminant source zone parameters, information about the spread and level of dissolved contamination

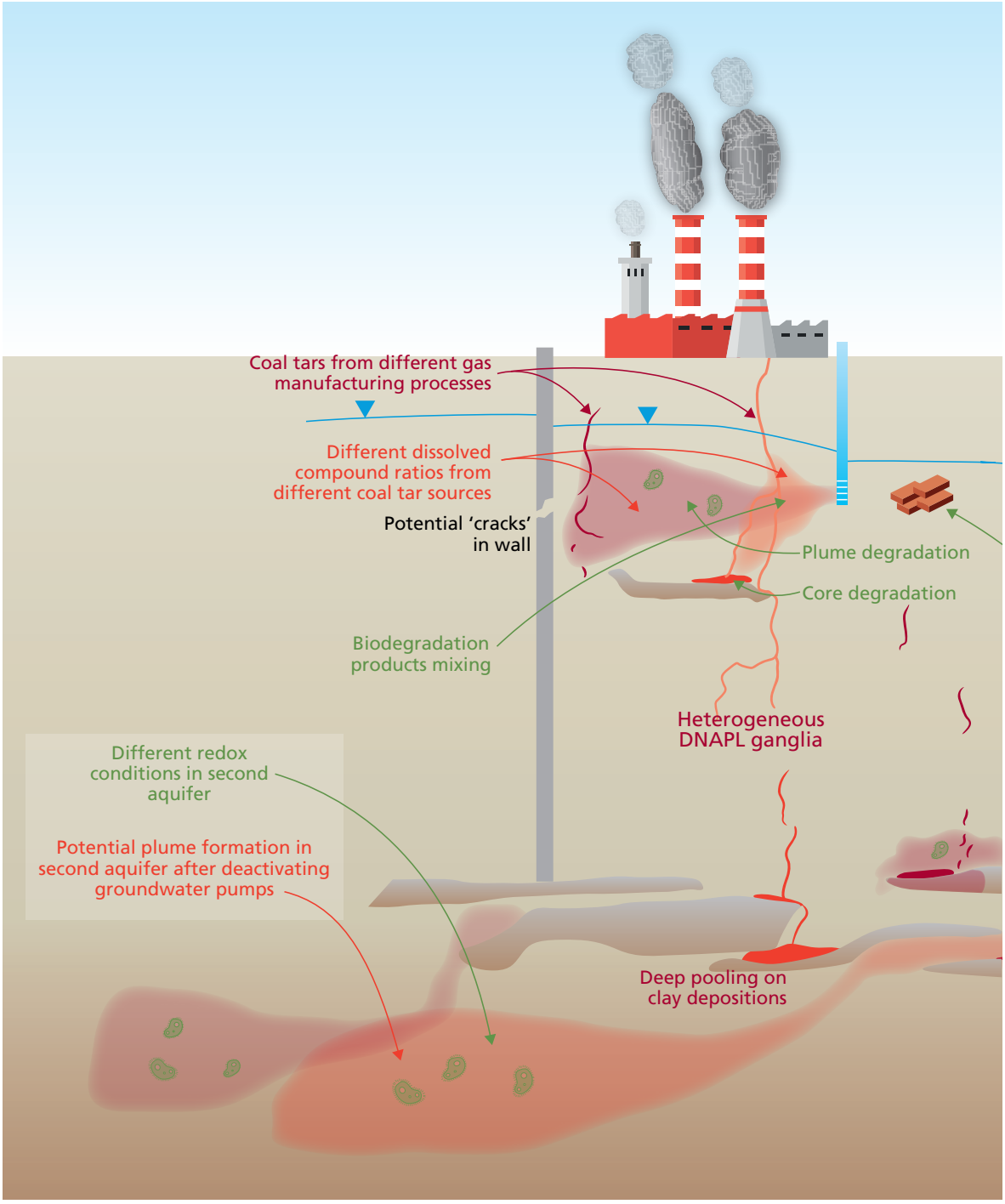

Figure 1.6: Comprehensive overview of various processes that may contribute to the spread, concentration and longevity of contamination at the Griftpark.

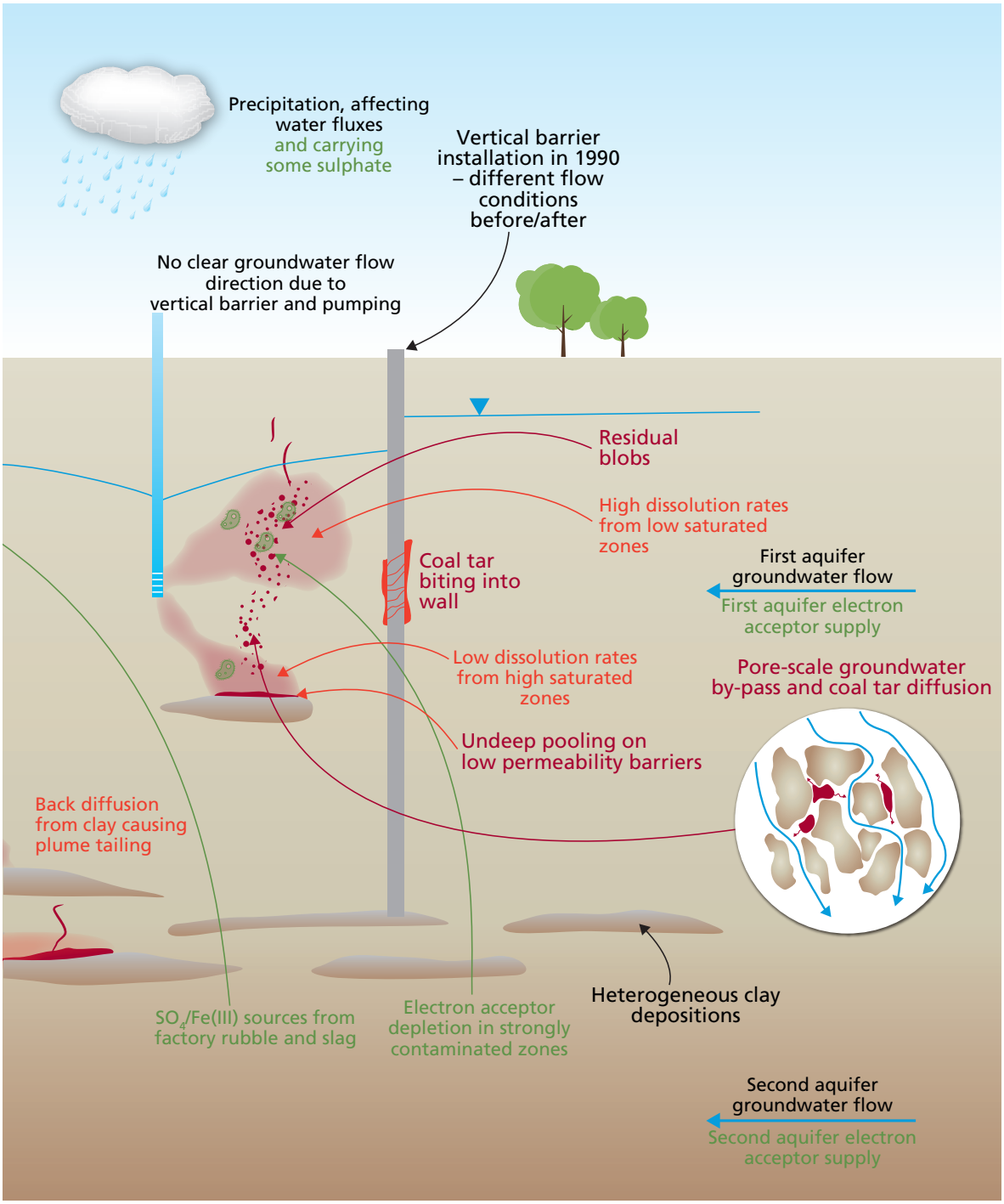
Precipitation, affecting water fluxes and carrying some sulphate
Vertical barrier installation in 1990 – different flow conditions before/after
No clear groundwater flow direction due to vertical barrier and pumping
Residual blobs
High dissolution rates from low saturated zones
Coal tar biting into wall
First aquifer groundwater flow
First aquifer electron acceptor supply
Low dissolution rates from high saturated zones
Pore-scale groundwater by-pass and coal tar diffusion
Undeep pooling on low permeability barriers
Back diffusion from clay causing plume tailing
Heterogeneous clay depositions
SO_4/Fe(III) sources from factory rubble and slag
Electron acceptor depletion in strongly contaminated zones
Second aquifer groundwater flow
Second aquifer electron acceptor supply

presents a valuable extra tool to validate model outcomes. Additionally, groundwater samples should be collected to analyse contaminant composition and measure other parameters essential for evaluating biodegradation potential (e.g. levels of electron acceptors). The fact that the hydraulic barrier and groundwater pumping from multiple wells prevents the development of a contaminant plume in a clearly defined direction of flow, complicates decision-making regarding sampling locations and depths.

The absence of a distinct contaminant plume further complicates the analysis of biodegradation, as it is difficult to obtain firm mass balance estimates. Consequently, it will be challenging to obtain biodegradation rates from the site and relying on literature values may be necessary. However, reaction rates obtained under laboratory conditions are not directly applicable on a field scale and rates can vary between sites and change over time [69, 78]. As such, incorporating parameters such as biodegradation rates and electron acceptor consumption, presents significant challenges in the modeling process.

1.4 Research questions and thesis outline

The primary aim of this research was to enhance the understanding of the hydrogeological and biochemical processes occurring at the Griftpark site. The insights gained from this research can support the municipality of Utrecht in planning future site investigations and designing effective management strategies relying on monitored natural attenuation. The following research questions were addressed in this thesis:

- How does groundwater flow beneath the Griftpark?
- What are the principal biodegradation processes that occur at the Griftpark?
- What is the oxidation capacity of the Griftpark subsurface and how does this influence the potential effectiveness of monitored natural attenuation as a management option?
- What are the critical parameters when using a three-dimensional reactive transport model for risk assessment at the Griftpark?

This thesis presents methodologies used and insights obtained during the investigation of the Griftpark. The performed investigations are subdivided in five Chapters:

Chapter 2: In this Chapter, methodologies and analyses of field investigations performed to improve the understanding of aquitard heterogeneity

and aquifer connectivity are presented. The Chapter includes investigations of contaminant source locations.

Chapter 3: This Chapter focuses on characterising the natural biodegradation processes occurring at the Griftpark. It discusses the applicability of standard research approaches typically applied to analyse field data obtained along contaminant plumes for the interpretation of data from a contained site.

Chapter 4: Here, a slight detour is taken from the field-scale investigations described in the other Chapters. The Chapter focuses on laboratory bench-scale tests conducted to examine the degradation of BTEX in varying mixtures with indene, indane and naphthalene under aerobic conditions. The objective is to improve knowledge of the inhibiting effects these compounds have on each other's biodegradation rates.

Chapter 5: This Chapter presents the development of a three-dimensional groundwater flow model for the Griftpark. It includes the description of an interpolation strategy to obtain heterogeneous conductivity fields for the aquitard, as well as a thorough analysis of grid convergence. The flow model is the foundation for the reactive transport model presented in Chapter 6.

Chapter 6: In this Chapter, the qualitative understanding of biodegradation of tar aromatic hydrocarbons and subsequent geochemical response at the Griftpark is enhanced through the implementation a reactive transport model. The model enables the investigation of the effects of parameter variations on breakthrough concentrations in the second aquifer. Recommendations for further site investigations necessary to perform a comprehensive risk analysis are also provided.

Chapter 2

Griftpark site setting: geology and contamination source zones

Abstract

The Griftpark field site, a former manufactured gas plant, is highly contaminated with coal. The 8 ha contaminant source zone is contained by a slurry wall and further managed with groundwater extraction. Accurate assessment of environmental risks associated with the coal tar contamination at the site, requires a comprehensive understanding of three-dimensional subsurface properties, as well as the identification of contaminant source zones, including their locations and sizes.

In pursuit of these objectives, a large set of field investigation methods are employed with the primary objectives to (a) enhance the understanding of the physical subsurface conditions at the site and (b) identify locations of pure-phase contaminant source zones. Investigation methods utilised include cone penetration tests, membrane interface probings, sonic drillings, groundwater sampling and pumping tests. The results demonstrate that the first and second aquifers are connected in the general area of the Griftpark. Furthermore, the analysis reveals that underlying the Griftpark site, the aquitard consists of a series of overlapping clay lenses with varying thicknesses, that leave for a hydraulic connection between the first and second aquifers within the contained area. The investigation findings also confirm the widespread presence of pure-phase coal tar contamination at various depths throughout the site, with the deepest coal tar deposits found perched on top of the aquitard at depths approaching 50 meters below ground level.

In order to obtain more knowledge of the total number as well as the

sizes of contaminant spills at the site, more field investigations are required. Overall, it is concluded that although the clay lenses comprising the aquitard considerably impede the downward migration of pure-phase coal tar, it is crucial to acknowledge that without groundwater extraction, there remains a potential risk of dissolved contamination leakage into the second aquifers.

The results of this Chapter are integrated in a manuscript under preparation in *Advanced water resources*. Title: A comprehensive description of the characterisation and reactive transport modelling of a complex contaminated field site.

2.1 Introduction

The Griftpark, situated in the city of Utrecht, the Netherlands, is located at the site of a Former Manufactured Gas Plant (FMGP). Between 1860 and 1960, the industrial activities caused intense coal tar contamination of the site's subsurface. Coal tar, the toxic waste product of gas purification, is a dense non-aqueous phase liquid (DNAPL), which is heavier than water and can sink below the water table under gravity and capillary forces [1]. Soil contamination on FMGP sites is characterised by extreme heterogeneity due to the random deposition of coal tars and relocation of contaminated soil during construction works as well as the DNAPL's non-linear downward due to subsurface heterogeneity [307, 223, 205]. Consequently, it is challenging to fully map coal tar distributions at FMGP sites.

The immediate subsurface of Utrecht is known to consist of two sandy aquifers, separated by a clay aquitard situated at a depth ranging between approximately 30 to 40 until around 60 to 70 metres below sea level (New Amsterdam Water Level, NAP, which lies 2 to 3 metres below ground level at the Griftpark). In the 1990s, the contaminated zone was encapsulated by a vertical barrier to prevent further propagation of the dissolved contamination plume in the first aquifer. Field investigations prior to installation of the vertical barrier revealed that the aquitard is discontinuous. As the hydraulic pressure in the groundwater is higher in the first than in the second aquifer, there is a risk of contaminated groundwater leaking downward. A leaky aquitard also brings a risk of downward migration of pure phase coal tar. To mitigate these risks, groundwater extraction pumps have been continuously operating within the zone contained by the vertical barrier since 1990. The extracted groundwater is transported to a treatment plant [221]. Although this method effectively protects groundwater outside of the barriers, it fails to reduce the total contaminant volume, thus requiring perpetual management. With improved understanding of natural attenuation processes obtained over the three last decades, there is an interest to redesign the contamination control measures at the Griftpark to reduce energy use and operating costs. When considering changes to the park's management strategy, the primary concern is the contamination of the second aquifer, which is strictly protected as a vital source of drinking water in the Netherlands. To assess the risk of contaminated groundwater and pure phase DNAPL leakage from the first to the second aquifer, it is crucial to understand the three-dimensional hydraulic connectivity of the two aquifers and the locations and sizes of contaminant source zones.

Various methods are available for studying physical subsurface properties at field sites. These methods include drilling techniques providing vertical

profiles of soil properties, or lab analysis of soil samples to find grain size distributions for hydraulic conductivity calculations. Drilling and sampling are local techniques that yield information on soil parameters at the exact location where the drilling or sampling was performed. To obtain enough information to predict three dimensional groundwater flow and contaminant spread in a heterogeneous aquifer, the required number of data points should be high enough in order to allow for extrapolation of the parameters to untested locations. Depending on the scale of the heterogeneity, this number of data points may increase significantly, which may become too costly and labour intensive for most purposes [9].

With hydraulic methods such as slug and pumping tests, hydraulic conductivity values can be experimentally investigated at larger scales. With a slug test the average conductivity in the vicinity of a well is obtained, whereas a classical pumping test yields relatively large-scale estimates of transmissivity from which the conductivity is calculated. During a pumping test, the aquifer is pumped at a controlled rate and the change in water level is measured in one or more surrounding wells. Analysis of these tests is typically based on the transient Theis or steady state Thiem solution for non-leaky confined aquifers (including Jacob's correction to Theis' solution for unconfined aquifers). However, these solutions do not help to understand subsurface heterogeneity as they yield only averaged conductivity values, while the results are strongly dependent on the level of heterogeneity of the subsurface and the volume tested [119]. Additionally, pumping tests are primarily conducted to gather information on horizontal conductivity, as groundwater predominantly flows horizontally between sedimentary layers. Therefore, the practicality of using a pumping test to obtain information on vertical conductivities at the Griftpark site may be limited.

With a tracer test, information on subsurface conductivity and heterogeneity can be obtained. During a tracer tests designed to estimate physical parameters such as flow velocity, hydraulic conductivity and dispersivity, involve the injection of a conservative tracer into an aquifer and measuring its concentration in down-gradient wells. An advantage of the tracer test is that it may reveal preferential flow paths and therefore structural anisotropy. It can therefore be applied to test the vertical connectivity between different aquifers [239]. A disadvantage of the tracer test is that a high resolution monitoring network is needed to 'capture' the tracer, especially in strongly heterogeneous aquifers where the solute will spread in unpredictable directions, which may significantly increase costs [239].

In addition to the application of various drilling and sampling techniques to investigate the subsurface and locate pure phase coal tar source zones, as well as hydraulic tests to assess the connectivity between the two aquifers,

advanced techniques were also considered for three-dimensional imaging of the subsurface. These techniques included the seismic refraction survey [128] and electrical resistivity tomography [256]. However, due to practical constraints and the low probability of success resulting from factors such as the presence of a large pond lined with cement-bentonite in the park and presumed rubble and pipelines in the shallow subsurface, these techniques were deemed impractical and too expensive.

2.2 Methods and data

2.2.1 Description of the field site

Geology

The geologic formation below the Griftpark consists of mostly marine and fluvial deposits originating from Holocene and Pleistocene eras [32]. The first aquifer is composed of four main geological units. The top layer, the Westland formation, extends to a depth of about 5 m-NAP. The second layer, extending to 10 to 15 m-NAP, is the Kreftenheye formation that consists of moderately-course to course sand with some gravel depositions. The third layer, the Urk formation, is composed of middle to course sand with regions of gravel and extends to approximately 30 m-NAP. The fourth layer is the Kreftenheye formation that consists of fine sand with some clay lenses. The second aquifer, the Harderwijk formation, is relatively homogeneous. It is composed of fine to middle fine and some course sand and extends from about 65 to 110 m-NAP. The first and second aquifer are separated by the Waalre formation (formerly known as Kedichem), characterised by clay and silt deposits. As the Griftpark is situated at a geological fault line, as shown in Figure 2.1, clay from the Waalre formation is interspersed with sand from the Harderwijk formation. Consequently, the aquitard is not fully confining.

Contamination source zones

Figure 2.2 shows a map with locations of industrial activities that took place on the site between 1860 and 1960, as well as associated suspect locations of a number of contaminants [252]. The site contained two types of water gas factories, a coal gas factory, two oil gas factories, a benzene factory, sulphate factory, ten gas tanks, three coal storage containers, eight tar pits, ten oil tanks, two benzene and sulphuric acid tanks and four gas purifiers [252]. The terms coal gas, water gas and oil gas describe the different methods through which gas was produced. As the carbon source, applied distillation process, carbonisation temperature, gas purification and storage techniques

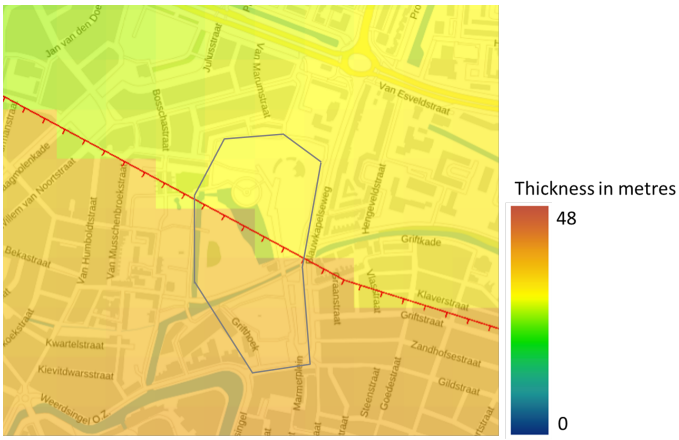

Figure 2.1: Thickness of the Waalre formation at the location of the Griftpark, the fault line is indicated with a red line [79]. The vertical barrier around the Griftpark is indicated by a dark blue line.

used all have a direct influence on the composition of tar, the composition and physiochemical properties of tars at FMGPs vary a lot even at a single industrial site [40, 129, 214, 307]. We refer to the study by Gallacher et al. [110] for a comparison of constituents of coal tar produced during different processes.

When it was found that the site was contaminated in the 1980s, research was conducted at the site to locate contaminant source zones. However, when it was decided to contain the contaminant source zone, investigation of the contaminants was stopped, so no complete map was ever made [6]. It was found that poly-aromatic hydrocarbons (naphthalene and phenanthrene) exist throughout the complete park, at the north side of the park they were found deeper than 15 metres below ground level (m-bgl). Mineral oil was encountered in the north and south of the park, to a maximum depth of 15 m-bgl in the north. Cyanide was encountered in the south of the park to a maximum depth of 5.5 m-bgl. Of benzene contamination no maps were made. A sulphate factory in the south is suspected to have left a sulphate contamination, which should have a positive effect in the Griftpark as sulphate is an important chemical in the biodegradation processes occurring at the site, see Chapter 3. Heavy metals existed as immobile contamination and occurred only in the top soil layer, which was excavated and levelled with clean sand. These historic data give a general idea of contaminant distributions, indicating that mostly at the north side of the park contamination has penetrated to depths greater than 15 m-bgl.

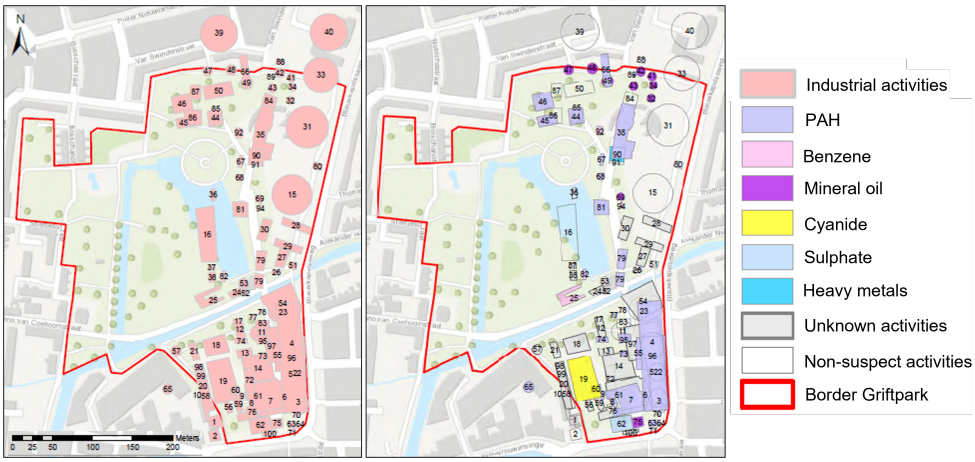

Figure 2.2: Locations of various industrial activities (indicated by numbers) and associated suspect contaminants (indicated by colours) [252]. Note that the red line indicates the border of the park, which does not completely coincide with the trajectory of the vertical barrier.

Management approach

Excavation or in-situ treatment of contamination at the Griftpark was deemed impracticable considering the depth to which pure-phase contaminants were encountered (i.e. below 30 m-bgl) and the urban location of the site. Instead, the contaminant source was contained by a cement-bentonite vertical barrier installed to a depth of approximately 55 m-bgl, into the aquitard separating the first from the second aquifer. During field investigations in preparation of the installation of the vertical barrier, using cone penetration tests (CPTs), it was found that the aquitard is not completely confining. To prevent the leakage of contaminated groundwater from the first to the second aquifer, three pumping wells were installed within the contained area to create an upward flow. Wells B20, B21 and B22 are indicated in Figure 2.3. Yearly, more than 70,000 m^3 of highly contaminated groundwater is pumped up from the park and treated at a station just 2 km from the park. The permeability of the wall, plus any effects of leakage through cracks, was studied by changing pumping rates in the contained area and measuring the effects in wells in- and outside of the containment barrier in the 1990s. It was calculated that a combined pumping rate between 10 to 15 m^3/h is needed to maintain an inward flux into the park [123].

2.2.2 Profiling, drilling and soil sampling

A range of techniques was applied to obtain information on the subsurface's lithological properties. In the 1980s, 46 CPTs were performed mostly along the trajectory of the vertical barrier. Since 2018, during this project, these tests were supplemented by sonic drillings to give detailed soil descriptions to greater depth. Also a number of membrane interface probe (MIP) tests supplemented knowledge of soil type. The main aim of the MIPs was to supply us with vertical profiles of volatile organic carbon concentrations and the technique is explained in the Section 2.2.4. Locations of sonic and MIP tests are shown in Figure 2.3. Depths of all filters are given in Appendix A. Grain size analysis were performed on a number of soil samples.

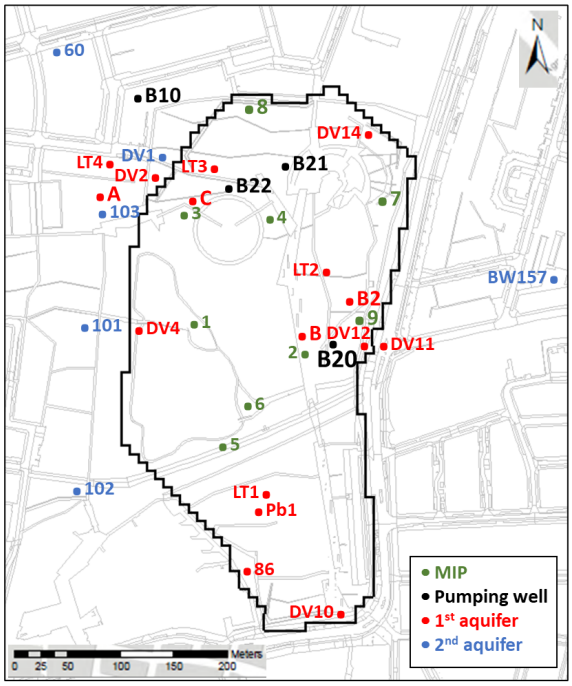

Figure 2.3: Locations of MIPs, sonic drillings and wells at the Griftpark. MIPs are indicated by the numbers 1-9 in green. Pumping wells B20, B21, B22 and B10 are indicated in black. Wells at locations A, B, B2, C, 101, 102 and 103 were installed during this project. BW157, 60, 86, LTs 1, 3 and 4, DVs 1, 2, 4, 10, 11, 12 and 14 are monitoring wells that were installed in 1990. Monitoring wells screened in the first aquifer are indicated in red, those in the second aquifer in blue.

Cone penetration testing

With the cone penetration tests (CPTs), a cone with a diameter of around 4 cm is pushed into soil with a hydraulic jack at constant velocity [247]. During penetration, the probe measures end bearing resistance at the tip (expressed by cone resistance). The side of the tip is equipped with a friction sleeve that measures side friction (expressed by friction ratio). The depth-profile of cone resistance and friction ratio can be interpreted to obtain the soil type using the classification presented by Robertson and Campanella [248, 249].

The 46 CPTs were performed at the Griftpark by *Heidemij* and *Grondmechanica Delft* along the trajectory of the planned vertical barrier. The maximum depth that could be reached was 70 m-bgl, although they mostly achieved lesser depths. Results along linear transects were interpreted to two-dimensional transects to obtain an impression of the structure of the aquitard.

Sonic drilling

With the roto-sonic drill, boreholes are drilled, cored and cased by rotating and vibrating the drill at resonant sonic frequencies that cause liquefaction of the soil, thereby reducing friction [125, 309]. The drill pushes down the core barrel and the well casing. The core barrel, filled with sediments, is retrieved to the surface, where the soil can be visually inspected and sampled. Visual inspection is a fast method to classify soil samples in situ by their looks and feel [297]. Wells are implemented into the borehole before retrieving the well casing. Multi-level Sampling wells (MLS) are wells that contain multiple ports at adjustable depths so that water samples or water level measurements from multiple depths can be obtained. The wells at the Griftpark were sealed with bentonite sleeves that swell when in contact with groundwater in order to avoid vertical flow around the well and a gravel pack was applied to avoid collapse of the borehole.

Seven sonic drillings were performed by *Sialtech* (Houten, the Netherlands) at locations A, B, B2, C, 101, 102 and 103, shown in Figure 2.3. A picture of the drill in operation is shown in Figure 2.4. We selected the locations both for the expected presence of significant levels of contamination, as well as to increase knowledge of subsurface parameters in the middle of the park, away from the vertical barrier, and deep into the second aquifer. B and B2 were placed at locations where little to no clay was expected according to the CPT result analysis from 1988. They were drilled to 61 and 62 m-NAP respectively. C was placed close to pumping well B22, that pumps up highly contaminated groundwater. At C, drilling was halted at a depth of 47 m-NAP, when a pool of pure-phase coal tar was encountered perched on top of clay to avoid creating a downward path for the tar. Boreholes A, 101, 102 and 103

Figure 2.4: Sonic drill in operation in the Griftpark.

are located down-gradient of the Griftpark. A was drilled to a depth of 62 m-NAP. At 101, 102 and 103 wells were drilled deep into the second aquifer to a depth of 110 m-NAP.

Visual determination of the soil cores was performed by *Aveco de Bondt* (Nieuwegein, the Netherlands). After boreholes were drilled, at all locations monitoring wells were installed for groundwater sampling. At all locations standard HDPE monitoring wells with a 3.2 cm diameter and 1 m filter length were installed. At B, B2 and C, also MLS wells (*Solinst Canada Ltd.*, Georgetown, Canada) were installed. The MLS wells consist of HDPE filters with an outer diameter of 10 cm that each contain seven units with an 8 mm inner diameter. They are screened along a length of 25 cm and have a 3-4 mm slot width. All wells were installed in sandy layers to allow easy flow.

Grain size analysis

By analysing grain size distributions, hydraulic conductivity values can be calculated [164, 135]. A range of empirical formulas exist for these calculations. We applies the Breyer formula, which does not consider porosity and is considered most useful for materials with heterogeneous distributions and poorly sorted grains with uniformity coefficient between 1 and 20, and effective grain size (i.e. d_{10}, the grain size than which 10% of the grains are smaller) between

0.06 and 0.6 mm [220, 230]. Accepting the clay samples, this applies at the Griftpark.

The Breyer formula reads

$$K = \frac{g}{v} k_B \cdot \frac{500}{UC} \cdot d_{10}^2, \tag{2.1}$$

where g is the gravitational acceleration, v the kinematic viscosity of water, UC the uniformity coefficient, which is calculated by dividing d_{60} and d_{10} (i.e. the grain sizes of which 60 and 10% of the grains are smaller) and k_B the Breyer constant (0.0006).

To characterise a range of hydraulic conductivity values at the Griftpark, sixteen soil samples were collected for grain size distribution analysis by *Synlab*. Samples of different soil type were collected from varying locations and depths. We compared results with the visual soil classification performed during drilling as well as with regional data. Results have to be used with caution as the small number of samples may not reflect the variability of soil types at the heterogeneous Griftpark site.

2.2.3 Hydraulic field scale testing

To improve our understanding of the three-dimensional hydraulic connection between the first and second aquifer, readily available hydraulic data were studied and supplementary field tests were conducted. As wells in- and outside of the vertical barrier were also considered in the analysis, also information on the leak tightness of the vertical barrier is obtained. As traditional pump-curve analysis is not suitable for heterogeneous aquifers and the wall would further complicate the analysis, the aim of the hydraulic tests is not to find specific hydraulic conductivities, but to increase the understanding of connectivity qualitatively.

Study of hydraulic data 2006 - 2021

During the years of operation of the contain-and-manage site control measures, water level data have steadily been collected by *MOURIK* (Groot Ammers, the Netherlands) and *RoyalHaskoningDHV* (Amersfoort, the Netherlands), that are in charge of the daily operations at the Griftpark. These data provide information on the effects of groundwater pumping and rainfall on water levels at different locations and depths in and outside of the park. For this Chapter, we made a selection of the available data, that can be subdivided in three categories.

The first data set is used to study the effect of seasonal variations in the first and second aquifer. The data consists of hydraulic heads in wells DV1

(screened in the second aquifer) and LT4 (screened in the first aquifer down-gradient of the Griftpark) with four data points per year over the period 2006 until 2021.

The second set is used to measure the effect of turning off groundwater extraction pumps (i.e. B20, B21 and B22) on hydraulic head levels in wells DV1, LT1, LT2, LT3 and LT4. For some of the tests, also groundwater extraction pump B10 is taken into account. This pump is situated north-west of the Griftpark and screened at a depth of 8-18 m-NAP. It was part of the pump-and-treat method used to remediate the contaminant plume down-gradient of the the park. In November 2017, B10 was definitely turned off, as the contaminant plume had disappeared. Wells LT4 and DV1 are situated just outside of the vertical barriers on the north-west side of the park and screened in the first and second aquifer respectively. LT1, LT2 and LT3 are situated within the contained zone, LT3 in the north, relatively close to pumping wells B21 and B22, LT2 in the centre, between wells B21/B22 and B20 and LT1 in the south, further removed from all pumping wells, see Figure 2.3. A selection of these recurring pumping tests will be presented, covering periods with a small precipitation surplus, so that rain and evaporation effects can be left out of the analysis.

The third data set is used to study the effects of pumping and precipitation surplus simultaneously. It consists of monthly hydraulic head levels in DV1 (second aquifer), LT3 (first aquifer inside the Griftpark) and LT4 (first aquifer down-gradient of the Griftpark), and pumping and precipitation surplus data over the period from 2010 until 2022.

All water level measurements were performed with standard divers by *Mourik*.

Pumping test

Within this project, we designed a supplementary pumping test. This test focused primarily on the effects of turning on or off groundwater extraction pumps B20, B21 and B22 on water levels in wells in the vicinity of pumping well B20. The full network of monitoring wells including screen depths is shown in Figure 2.5. Wells B, B2, DV12 and DV11 are located at a lateral distance of 28, 36, 43.5 and 50.5 m from pump B20 respectively. At location B, water levels in the four monitoring wells BU1, BU2, BU3 and BU4, screened between 14-16, 41-43, 51-52 and 60-61 m-NAP respectively, were recorded, as well as the water level in three MLS wells that each contain seven filter ports. At location B2, water levels were recorded at the monitoring well screened between 61.5-62.5 m-NAP, as well as in several ports of the two MLS wells. The two deepest wells (BU4, 60-61 m-NAP, and B2, 61.5-62.5 m-NAP), are interpreted as extending into the upper boundary of the second aquifer, as

no clay was found at these depths. Deeper wells were unavailable at these locations to test for deeper confining layers. Wells DV12 and DV11, screened between 27-21 m-NAP, are located in the first aquifer on either side of the vertical barrier and are used to obtain information on potential leakages in the wall.

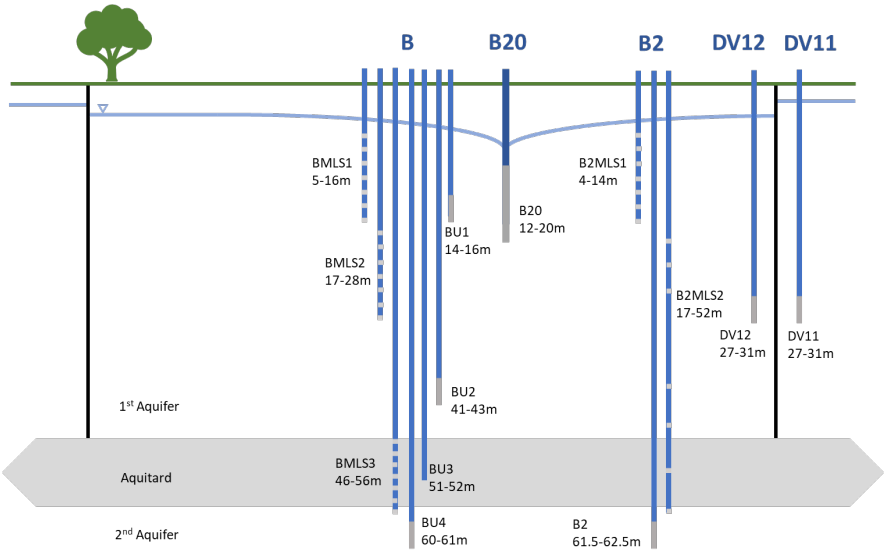

Figure 2.5: Monitoring network for the B20 pumping test, with depths indicated in m-NAP. The aquitard is shown as a grey band that does not represent a solid clay layer but a general zone of lower hydraulic conductivity, the vertical barriers are drawn in black.

Pump B20 was set to either 0 or 10 m^3/h, the pump's maximum rate. As previously calculated, a minimum groundwater extraction rate of 7.5 m^3/h is required at the Griftpark to prevent leakage of groundwater out of the contained zone. During the test, this rate was mostly maintained by pumps B21 and B22, running at 3.5 and 4 m^3/h respectively. The timeline of pumping, diver operation and manual MLS measurements are indicated in Figure 2.6. Preceding this timeline, a round of MLS measurements was conducted on September 20^{th} 2021 (at which time pump B20 was off) which are also included in the data analysis.

Hydraulic head data were collected manually in all wells using a Solinst 102M Mini Water Level Meter after five or fourteen days after pump switches. Manual hydraulic head measurements have an accuracy of approximately ± 1 cm. In wells BU1, BU2 and BU3, hourly hydraulic head measurements were collected with Van Essen Instruments divers. The divers' absolute pressure measurements have a typical accuracy of ± 0.5 cm. Well cap heights were

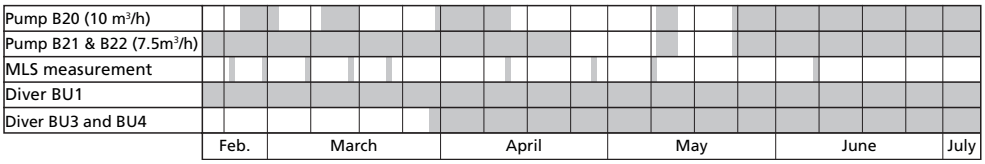

Figure 2.6: Timeline of the B20 pumping test performed in 2022. When groundwater pumps were operating or measurements taken in MLS wells (manually) or in wells BU1, Bu3 and BU4 (with diver) cells are filled in grey.

measured with a land level surveying instrument. All results were converted to metres below sea level (NAP). Atmospheric pressure values were used to correct the diver data and were downloaded from the *Royal Netherlands Meteorological Institute* (*KNMI*) [163].

The effects of pumping were compared with effects of precipitation on water levels in the wells. Precipitation surplus was calculated from hourly precipitation and daily evapotranspiration data from the KNMI taken at the De Bilt station located 3.5 km away from the Griftpark. This means that single rain events cannot be presumed to correspond exactly between De Bilt and the Griftpark, but can be used to indicate precipitation intensity. Daily evaporation data was roughly translated to hourly data by dividing the total daily amount over 12 day-hours. As the evaporation data supplied by the KNMI is a reference value based on the evaporation from a wet grass field, a correction factor of 0.4 is applied for the evaporation based on the foliage and land usage at the Griftpark [123].

To study the effects of fluctuations in atmospheric pressure on groundwater levels, the barometric efficiency (BE) of the system was calculated according to

$$BE = \frac{\rho g \Delta h}{\Delta P}, \tag{2.2}$$

where Δh indicates the change in hydraulic head, ΔP the change in atmospheric pressure, ρ the density of water and g the gravitational acceleration. For the calculation, measurements from BU1 during periods with little rainfall were used. The BE was used to verify whether or not atmospheric pressure changes could overrule changes in hydraulic heads caused by pumping. An aquifer with a BE of 1 means the aquifer has a full response to changes in atmospheric pressure, whereas an aquifer with a BE of 0 would be completely unaffected. Typically, the BE of aquifers ranges from 0.2 to 0.7 [313].

2.2.4 Locating contaminant source zones

Soil core and well inspection

Soil samples brought up with the core barrel technique can at the ground surface immediately be visually inspected for the presence of pure phase coal tar. Pooled layers, as well as fingers, blobs and droplets of pure phase coal tar can easily be identified due its dark colour and tar smell.

At the Griftpark, all soil cores brought up to the surface during sonic drilling at locations A, B, B2, C, 101, 102 and 103 were visually inspected for the presence of pure phase coal tar by *Aveco de Bondt*. Additionally, a camera inspection of the highly contaminated extraction well B22, that is known to regularly produce blobs of pure phase coal tar, was performed by *CTA Watertechnologie* (Hellouw, the Netherlands). B22 is equipped with filters between and 23-33 and 35-43 m-NAP and thus coal tar is expected to have leaked down to at least around 30 m-NAP at this location.

Membrane interface probing

The membrane interface probe (MIP) is a type of direct push probe similar to the CPT [58]. The MIP uses a hydraulic profiling tool (HPT) to measure soil resistance. With a HPT, water is injected from the tip of the cone at a constant rate while the cone is pushed into the subsurface. The ratio between the injection rate and injection pressure yields an estimate of the hydraulic conductivity. The MIP is also equipped with a fluorocarbon polymer membrane, mounted to the tip of the cone, through which, after being heated to approximately 100-120^oC, volatile organic carbons (VOC) partition. They are led up to ground level with a carrier gas, where they pass through a conventional detector system (e.g. GC-MS or PID) so that a quasi-real-time indication of targeted VOC concentrations in soil over depth can be obtained [250]. Thus, a quasi real-time indication of VOC concentrations in soil over depth is obtained. Thus, a quasi real-time indication of VOC concentrations in soil over depth is obtained.

MIP tests were performed at the Griftpark in 2018 to obtain insight in the vertical spread of contaminants at nine suspect locations, shown in Figure 2.3 by the numbers 1-9. The test locations were chosen depending on where contamination was suspected according to historical information regarding industrial activity. The MIP rod achieved a maximum depth of 29 m-NAP. The MIP's GC-MS was set up to analyse the BTEX components as well as naphthalene, 1,2,4-trimethylbenzene, styrene, indene and indane that were found to be present at high concentration during a pre-investigation. The MIP tests were carried out by *EnISSA* (Steenokkerzeel, Belgium).

Groundwater analysis

As pure phase DNAPL occurs in the subsurface not only as high-saturation zones in the form of pools and fingers, but also as low-saturation zones in the form of residual ganglia and blobs, it is possible that pure phase tar exists even where it cannot easily be visually demonstrated. We employed groundwater analysis to further locate source zones. By comparing the contaminant concentrations in groundwater samples to saturation levels, the (near) presence of pure phase contamination can be identified. Compound and concentration analysis of hydrocarbons is often conducted using gas chromatography-mass spectrometry (GC-MS). With this method, gas-chromatography and mass spectrometry are combined to identify different substances in a sample [266]. In the gas chromatograph, volatile hydrocarbons are gasified and separated while passing through a capillary column. In the mass spectrometer, compounds' are ionised and their different mass to charge ratios are used to separate compounds further. The concentration is calculated by comparing the peak area of the signal with the peak area of a known concentration.

Coal tar often consists of a mixture of mono- and poly-aromatic hydrocarbons (MAH and PAH), of which the latter have low water-solubility [109, 110]. In oily mixtures, however, relatively water-soluble components can act as co-solvent for components with higher molecular weight [151, 101]. Thus it is expected that the solubility of the PAHs naphthalene, indane and indene, is increased through the co-solvency effects of the relatively soluble BTEX compounds. This effect causes that coal tar cannot be considered as an ideal solution from which compounds dissolution capacities can be calculated using Raoult's law [191]. Therefore, a groundwater sample from the highly contaminated groundwater well B22 was taken. In this sample, droplets of pure-phase tar could be seen and thus full saturation was presumed. The concentrations of the main contaminants in this sample were used as solubility reference for a typical Griftpark coal tar. Note that coal tars were created at different types of coal gas factories and thus also at the Griftpark coal tars are expected to differ from each other. For simplicity, we assumed the same composition for all coal tar. Compound and concentration analysis was performed by GC-MS at *Synlab*.

Groundwater was collected from the first aquifer inside the contained zone from wells B, B2, B20, B21, C, Pb1, DV4, DV10, DV12, DV14, 86, LT1 and LT3. We analysed concentrations and compared them to the maximum solubility in order to predict the nearby presence of pure-phase tar.

Contaminant concentrations were also analysed in samples from the second aquifer up-gradient (BW157) as well as down-gradient of the Griftpark (A, 60, 101, 102, 103). These wells were sampled to verify if the current measures keep the second aquifer clean. All well locations are shown in

Figure 2.3 and filter depths in Appendix A. Within the current Griftpark project, samples from wells A, B, B2, C, 101, 102, 103, BW157, Pb1 (deep well), DV4 and 60 were analysed for mono-aromatic BTEXIeIaN, 1,2,3 and 1,2,4-trimethylbenzene, propylbenzenes, ethyltoluenes, and styrene and the double-ringed compounds naphthalene and methylnaphthalene concentrations by GC-MS at *Synlab*. More details on the method of analysis is presented in Chapter 3.

Furthermore, throughout the years of operation of the contain-and-manage measures at the Griftpark, groundwater from wells DV10, DV12, DV14, 86, Pb (shallow well), B20, B21, B22, LT1, LT3 were regularly collected by *Mourik*. These samples were subjected to analysis at *Eurofins Analytico* (Barneveld, the Netherlands) to determine the presence of the combined concentration of BTEX compounds and the 16 priority PAHs outlined by the Environmental Protection Agency (EPA), including naphthalene.

2.3 Results and discussion

2.3.1 Profiling, drilling and soil sampling

CPT and MIP tests

The 46 CPT tests from the 1980s, along the trajectory of the vertical barrier, yielded depth-profiles of cone resistance and friction ratio to maximum depths varying between 31 and 67 m-NAP with 50 m-NAP (i.e. 52 m-bgl) on average. An example of seven CPTs, situated along a transect, are shown in Figure 2.7 [6]. The transect itself is also shown in Figure 2.8, that depicts the three dimensional interpretation made in 1989 from eight of such cross-sections [6]. Most prominent is the complete absence of clay around the central zone of the park.

The MIP tests yielded six profiles (MIP1-6) of soil conductivity in the first aquifer. The corrected HPT pressures and estimated K values of two are shown in Figure 2.9. Estimated K values ranged between 0 and 50 m/d, the maximum value the MIP could register (i.e. the field values can be larger). The average value lies of around 18 m/d. Although these values cannot be used as absolute values, they give an indication of the variation range of the hydraulic conductivity within the first aquifer.

Sonic drillings

Seven profiles of soil descriptions were obtained during sonic drilling. The drilling profile of well B is shown in Figure 2.10. The white sections in the profiles indicate where material fell out of the core barrel. For these depths,

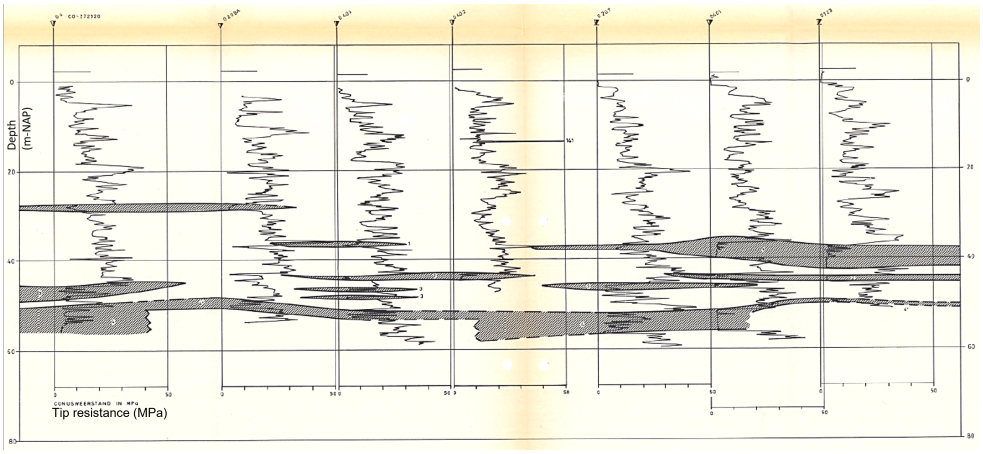

Figure 2.7: Example of a CPT data set along a profile as indicated in in Figure 2.8, with an interpretation of possible clay layering [6]

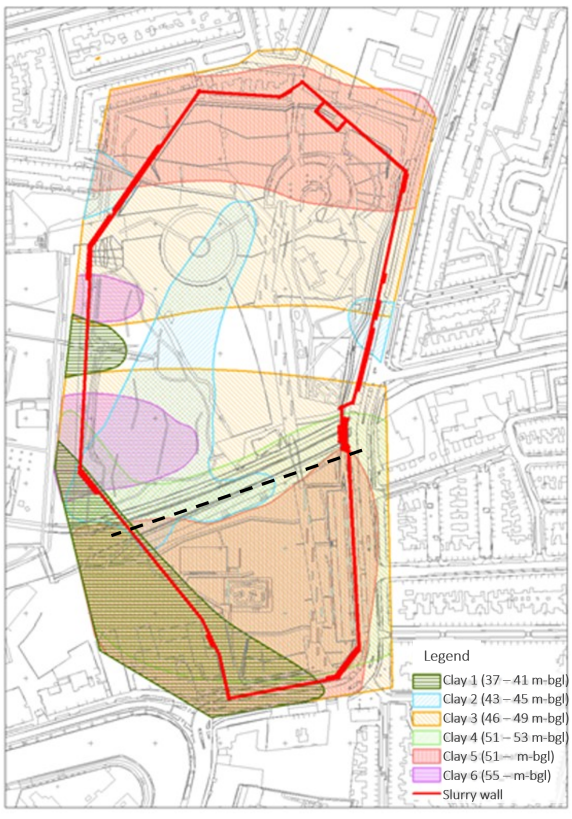

Figure 2.8: Interpretation of clay layering from CPT results [6].

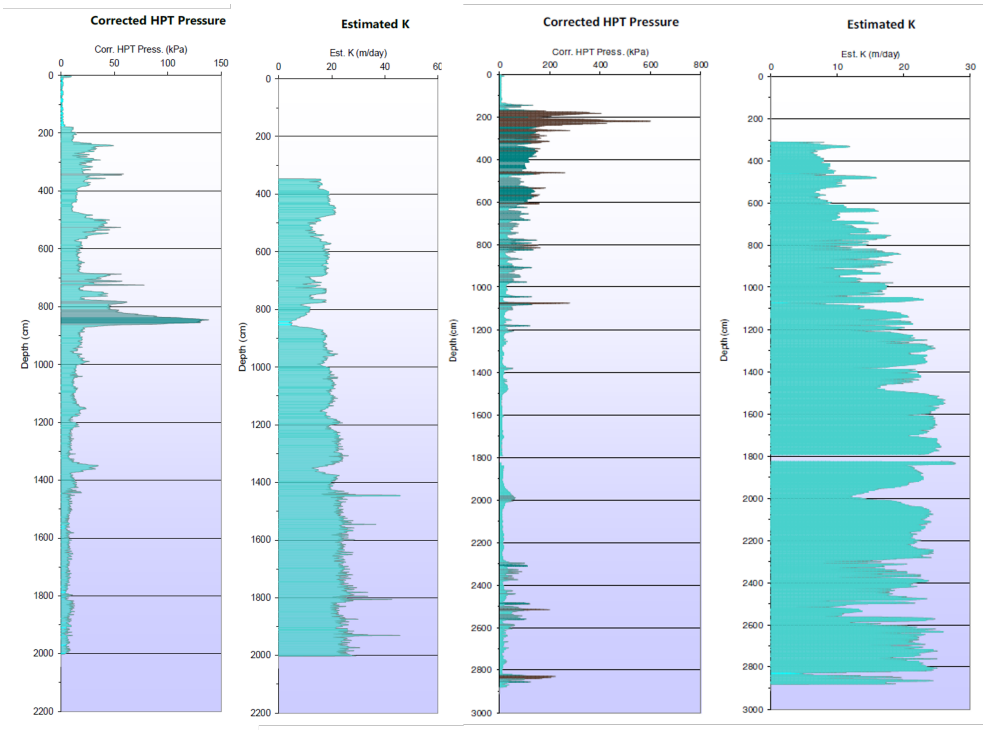

Figure 2.9: Example of one of the MIP profiles showing the HPT pressure and estimated K values.

exact soil type could not be determined, however, the fact that soil fell out is caused by it having a course grain type. Results show that the first aquifer is highly heterogeneous with mostly weak to moderately silty sand and very course sand, interspersed with gravel as well as clayey depositions on sub-half metre scales, as is typical for estuary deposition environments [262]. Clayey depositions were encountered at all drilling locations at depths ranging between 36.5 and 67.5 m-NAP. The thickest continuous clay deposition, encountered at location 102, was 5 m thick. Some clay lenses, however, could not be fully characterised either due to reaching the maximum drilling depth or to prevent the creation of pathways for downward movement of DNAPL by drilling through. The second aquifer was found to be more homogeneous than the first aquifer, with soil types ranging between moderately silty to moderately fine and moderately course sand.

Figure 2.11 presents a visual representation of the CPT, MIP and sonic data. The data was categorised into three distinct sets, corresponding to the northern, southern, and central zones of the park. The Figure reveals that although clay depositions are somewhat scarcer and thinner in the central

Figure 2.10: Sonic drilling profile of location B, with interpretation of visual inspection. Depth indicated in metres below ground level, which is 3.2 m above NAP

zone, clay is present at every drilling location, contradicting the interpretation made in 1989, as depicted in Figure 2.8, where a complete gap in the clay layer was suggested. Although it should be noted that connecting different data points should be done with caution, there are indications that tilted clay lenses may be present. For instance, the clay observed between 52 and 56 m-NAP at A and below 50 m-NAP at C might be part of a single tilted clay lens, rather than two separate ones.

Grain size analysis

Grain size analysis was performed to obtain soil type descriptions and calculate hydraulic conductivities. The results of the soil analysis are summarised in Appendix B. Grain size analyses of soil samples from different locations and depths show soil types ranging from very well sorted to extremely poorly sorted and gap-graded soil (indicating a mix of two soil types), and from clay and silty soil to extremely course sand. Overall, the NEN soil classifications agree rather well with the visual soil descriptions. The hydraulic conductiv-

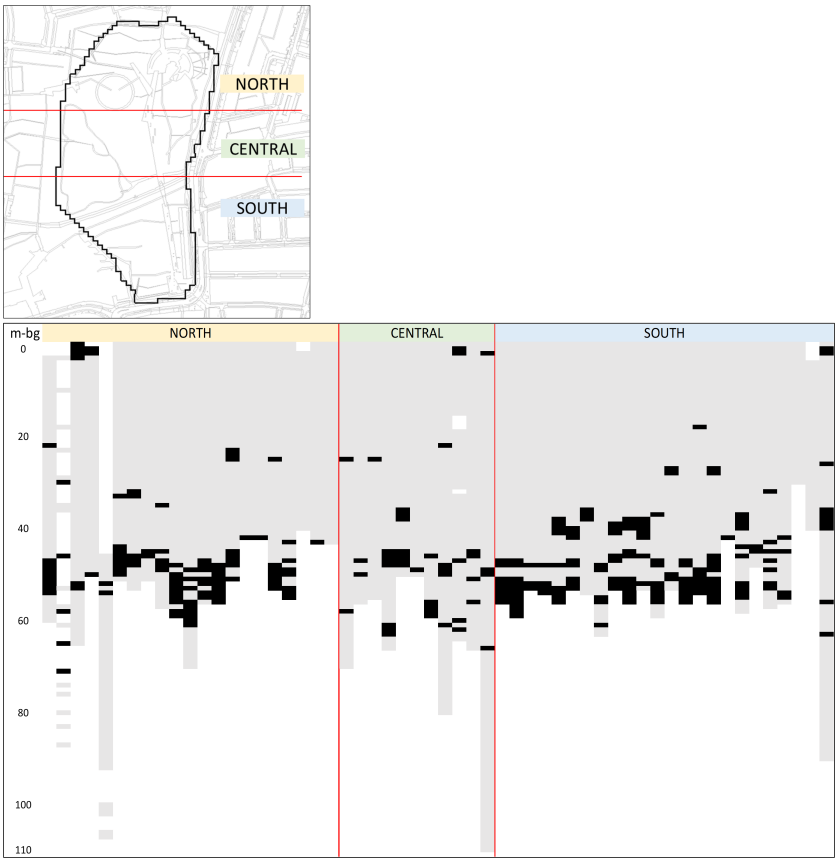

Figure 2.11: Visual representation of the soil analyses, including results from CPT, MIP and soil cores. Top: division of the park in north, central and south zone. Bottom: 2D view of the soil types, black: clay or very fine sand, grey: fine to very course sand and gravel, white: no data.

ity (K) values found generally agree with the conductivity values reported in regional databases. They also show the subsurface's heterogeneity. For example, the B61 sample has a rather low conductivity compared to the other samples containing very course sand. The A30 sample has an extremely low K value (0.002 m/d) despite the moderately fine/moderately course classification as this is a gap graded soil. The high percentage of grains smaller than 0.063 mm has strongly reduces the soil's conductivity.

2.3.2 Hydraulic testing

Seasonal variations in hydraulic heads were studied. Figure 2.12 shows the results in wells DV1 and LT4 in March, June, September and December over

the period of 2006 until 2021. DV1 and LT4 are located close to each other but screened in the second and first aquifer respectively, both slightly downgradient of the Griftpark. Water levels in DV1 and LT4 show the same seasonal response, i.e. lower water levels in summer and higher levels in winter, and both with an average deviation from the mean of 6.0 cm. The hydraulic head in DV1 is, on average, 9 cm lower than in LT4. This result proves that a hydraulic connection exists between the two aquifers. However, the connection may exist over a large regional scale, and does not give distinct information on the hydraulic connectivity right below the Griftpark.

Study of hydraulic data 2006 - 2021

Seasonal variations Between 2017 and 2021, short-term pumping tests were performed multiple times. We made a selection of four of these tests that support the interpretation of the hydraulic test we performed during this project. During the execution of the selected pumping tests, precipitation surplus was low, varying between -2.8 and 4.4 mm over the two-day test period, implying that variations in precipitation can be left out of the analysis. Figure 2.13 shows the combined extraction rates of groundwater pumps B20, B21 and B22 (inside) and B10 (outside) and the hydraulic heads in wells DV1 (second aquifer outside), LT1, LT2, LT3 (first aquifer inside) and LT4 (first aquifer outside). LT2 instead of LT3 is monitored in the 2017 test. Locations and depths of the wells are indicated in Figure 2.3.

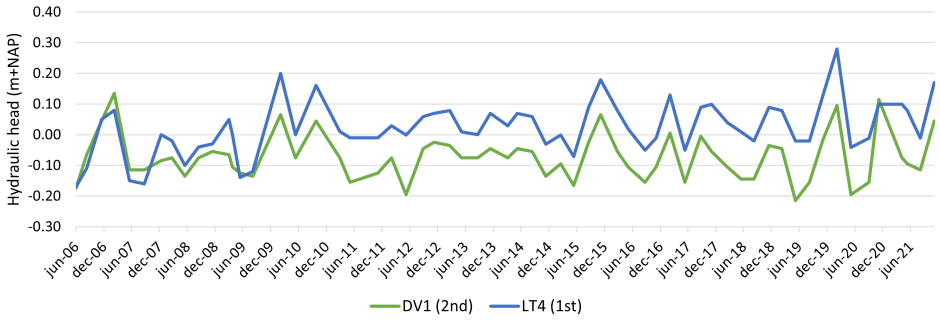

Figure 2.12: Quarterly hydraulic head levels in DV1 (second aquifer outside, in green) and LT4 (first aquifer outside, in blue). Measurements taken in March, June, September and December over the period of 2006 to 2021.

Pump switches Figure 2.13 reveals that water levels in the second aquifer (DV1) do not respond to starting or stopping the pumps at least within the first 48 hours. Water levels in wells screened in the first aquifer inside the contained zone (LT1, LT2 and LT3) all clearly respond to switching the

groundwater pumps on or off. On average, the water level in LT3 (north side contained zone) declines or increases 6 cm more than the water level in LT1 (south side contained zone, further away from pumping wells) after starting or stopping the pumps. This indicates that although pumping lowers the water level throughout the complete park, the current set-up of the pumps, where all three pumping wells are placed in the central/north region of the park, is most effective in the northern region.

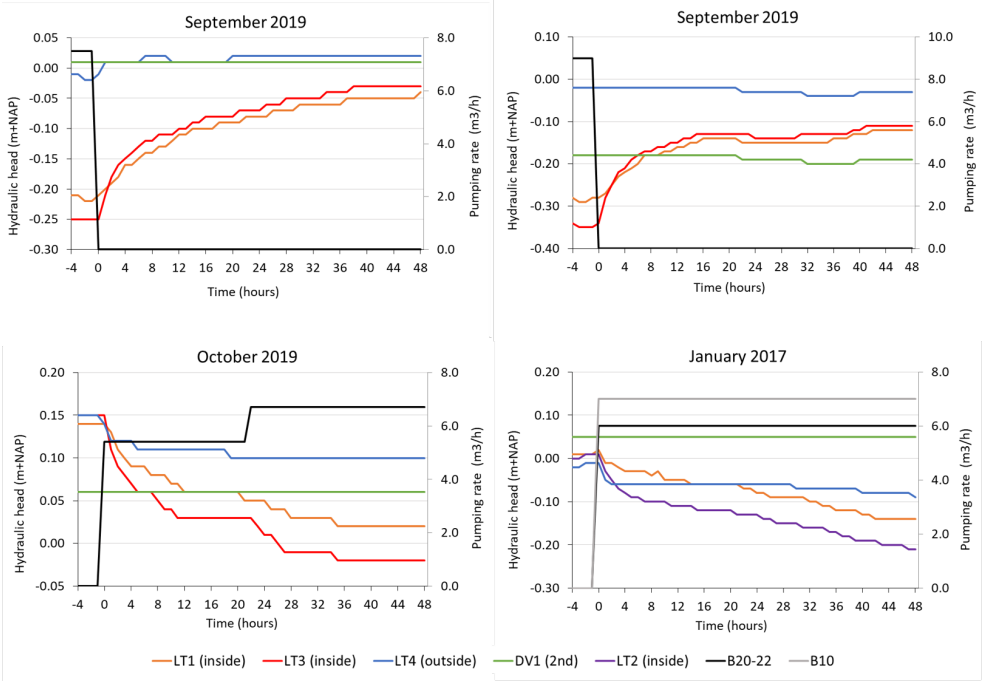

Figure 2.13: Combined pumping rates of B20, B21 and B22 (inside the Griftpark, black), pumping rate of B10 (outside the park down-gradient, grey) and hourly hydraulic head measurements in DV1 (2nd aquifer outside, green), LT1 (1st aquifer inside south, orange), LT2 (1st aquifer inside north, purple), LT3 (1st aquifer inside north, red) and LT4 (1st aquifer outside, blue).

The water level outside the vertical barrier (LT4) declines when the pumps are turned on (tests October 2019 and January 2017), however, this decline is less pronounced than inside the contained zone. Furthermore, the water level declines more when pump B10 (outside) is also included (7 vs 5 cm drop). In the tests during which the pumps are deactivated (performed in September 2019), no noticeable response in LT4 is observed. These findings suggest that the vertical barrier allows for some water flow, but that the strength of the response depends on other environmental factors.

Overall, with the pumps running at rates above 6.5 m^3/h, the hydraulic

head is ensured to be higher outside the park than inside, ensuring an overall inward groundwater flux into the park. This turns around when the pumps are turned off.

Pumping and precipitation We also studies the simultaneous effect of pumping and precipitation on hydraulic heads in- and outside of the park. Figure 2.14 shows monthly hydraulic head levels in DV1 (second aquifer), LT3 (first aquifer inside) and LT4 (first aquifer outside), groundwater extraction rates and precipitation surplus data from 2010 until 2022. The 20% moving averages of the water levels and precipitation surplus are shown to distinguish reactions to precipitation fluctuations and long term trends that may be caused by varying pumping rates. With a moving average, short-term fluctuations are smoothed out to reveal long term trends.

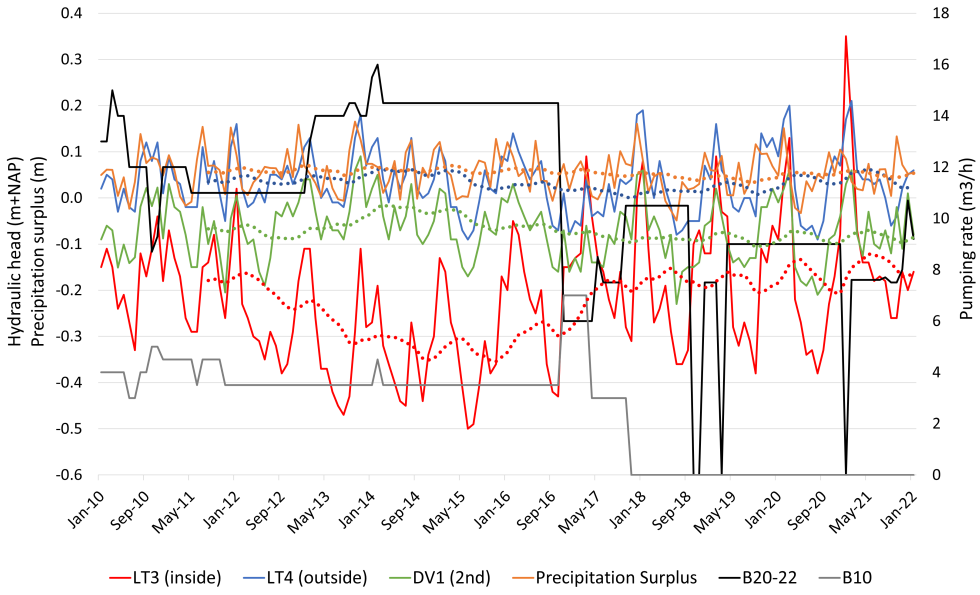

Figure 2.14: Monthly data of combined pumping rates of B20, B21 and B22 (inside of the vertical barriers, in black), pumping rate of B10 (down-gradient of the vertical barriers, in grey), precipitation surplus (in orange), hydraulic heads DV1 (2nd aquifer outside, in green), LT4 (1st aquifer outside, in blue) and LT3 (1st aquifer inside, in red). All measurement sets include their 20% moving averages to show the long term trends.

The average water level in LT3 declines with an increase of the combined pumping rate of B20, B21 and B22 and increases when the rate is lowered. Similar trends are not evident in the wells outside of the contained zone. Consistent with the results shown in Figure 2.12, Figure 2.14 demonstrates

that precipitation has a comparable impact on the water levels in the first aquifer outside the vertical barriers (LT4) and in the second aquifer (DV1) over the testing period. The average deviations from the mean are 5.4 and 5.5 cm, respectively.

Pumping test

In order to enhance our understanding of the hydraulic connectivity between the first and second aquifer near groundwater pumping well B20, a pumping test was conducted. After the CPTs performed in the 1980s, it was conjectured that no clay was present around this location, see Figure 2.8. However, with the inclusion of soil profiles obtained from the current project's sonic drilling, this theory was modified to acknowledge the existence of clay at this location, albeit with potentially thinner depositions, as indicated by the central zone in Figure 2.11. The experimental set-up for the pumping test is illustrated in Figure 2.5. The primary objectives of this test were to improve the qualitative understanding of the connectivity between the first and second aquifer, as well as that of the vertical barrier. In addition to reactions to changing pumping rates, also variations in precipitation were used as a parameter affecting water levels in and outside of the containment and in the first and the second aquifer.

Figure 2.15 shows the hourly water level measurements from divers at location B, at depth units BU1 (first aquifer), BU3 (aquitard) and BU4 (second aquifer). Over the test period, BU1 shows a maximum variation of 72 cm, BU3 of 28 cm and BU4 of 19 cm, indicating the first aquifer has the strongest fluctuations and the second aquifer the weakest.

To determine the aquifer's barometric efficiency (BE), data of water levels in well BU1 and fluctuations in atmospheric pressure over two periods (from the 5^{th} to the 10^{th} of March and from the 15^{th} of April to the 9^{th} of May, periods characterised by little rainfall), were used in Equation 2.2. The calculation yielded a BE of 0.45, indicating that atmospheric pressure fluctuations affect hydraulic heads in the wells. With this BE, it was determined that atmospheric pressure variations occurring throughout the complete pumping test, would result in an average hydraulic head change ranging between a minimum of 0.17 cm and a maximum of 1.6 cm in the monitoring wells. As the recorded hydraulic head variations measured are generally much larger than that (i.e. between maxima of 72 cm at BU1 and 19 cm at BU4), head changes caused by atmospheric pressure fluctuations are deemed negligible.

Figure 2.15 demonstrates that turning on well B20 to 10 m^3/d on the 31^{st} of March results in a significant decline of the hydraulic head in the first aquifer, a relatively smaller decrease at the depth of the aquitard, and a noticeable, but minor decrease in the deepest well. Upon deactivating pump

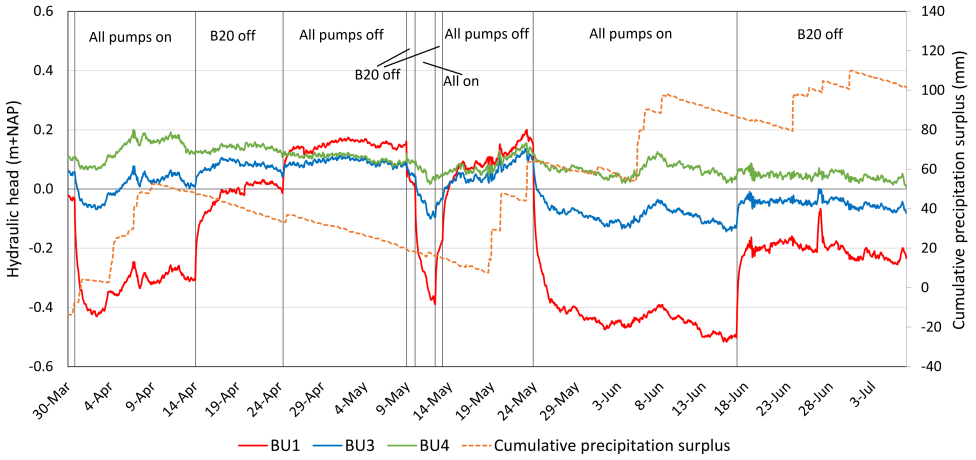

Figure 2.15: Hourly data of water levels at location BU1 (red), BU3 (blue) and BU4 (green) screened at depths of 17-19, 54-55 and 63-64 m-NAP respectively and cumulative precipitation surplus (orange). Moments of pump switching are indicated by vertical black lines.

B20, the water level in the shallowest well rises strongly again, with a lesser increase in the middle well. Although the water level in the deepest well does not rise, the declining trend caused by evapotranspiration is interrupted. Similar effects are observed during subsequent pump switches. Although the effect at 64 m-NAP is relatively weak, the pumps, which are screened in the first aquifer, affect the hydraulic head levels in the second aquifer, indicating a hydraulic connection between the first and second aquifer.

High rates of precipitation surplus occurred between the 30^{th} of March and 10^{th} of April, as well as between May 19^{th} and 24^{th}. Rainfall was also registered around the 8^{th} and 28^{th} of June. In all three wells, a direct response to rain can be distinguished. On the one hand, the minor response to changing pumping rates in well BU4 compared to in the more shallow observation wells, indicates that the connection between the first and second aquifer is not so direct in the vicinity of well B. On the other hand, the response to precipitation suggests that effective communication exists between the two aquifers regionally, as was also shown by response to seasonal variations shown in Figure 2.12.

Figure 2.16 presents the hourly diver data obtained from wells DV11 and DV12, both screened between 29-33 m-NAP and situated just out- and inside of the vertical barrier, respectively. Over the test period, DV12 shows a maximum variation in water level of 72 cm and a clear response to changes in pumping regimes. DV11 shows a maximum head variation of 21 cm and no clear response to pump switches. However, deactivating all pumps, on

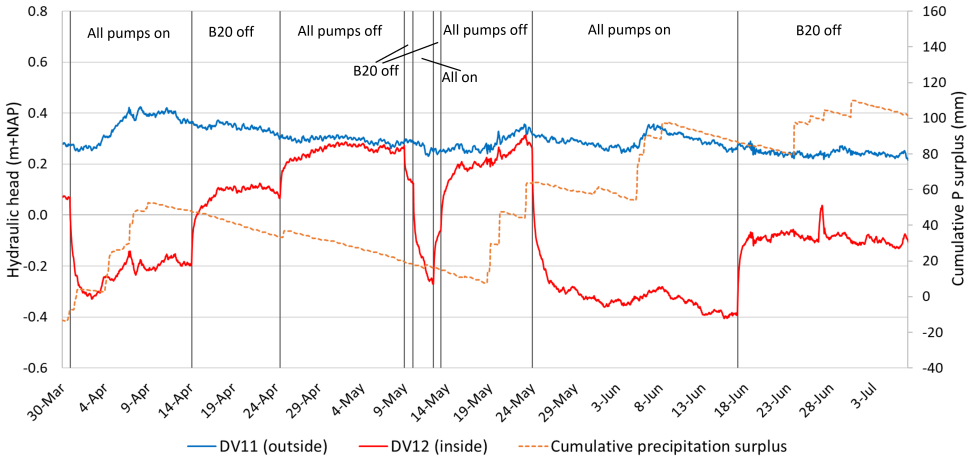

Figure 2.16: Hourly data of water levels in wells DV11 (blue) and DV12 (red), screened between 29-33 m-NAP. They are located just out- and inside of the vertical barrier, respectively. The cumulative precipitation surplus is shown in orange. Moments of pump switching are indicated by vertical black lines.

April 24^{th}, halts the downward trend caused by the declining precipitation surplus. In comparison, Figure 2.13 shows that well LT4 (outside the vertical barrier on the west side) does not respond to changes in pumping rates in, potentially indicating a slightly higher permeability of the barrier at the east side compared to the west side. However, this effect could also be attributed to the fact that the hydraulic gradient over the barrier is larger on the east side. Regardless, our findings indicate that although cement-bentonite is not impermeable, the impact of pumping from within the park on water levels in wells outside is overshadowed by fluctuations caused by precipitation.

Figure 2.16 shows that during intervals with a negative precipitation surplus, the hydraulic head in DV11 experiences a downward trend, while this effect is not visible in DV12. This may be attributed to the system still recovering after pump deactivation.

The water level in DV12 (inside) are consistently lower than in DV11 (outside), regardless of pumping rates or precipitation, although the difference becomes as small as 3 cm. This is an effect of the water storage against the up-gradient side of the wall, where DV11 is situated.

Although precipitation events should not be connected one to one with the changes in hydraulic head measurements as the data were taken from a weather station 3.5 km away from the Griftpark, Figure 2.17 demonstrates that hydraulic head levels vary similarly inside and outside of the hydraulic barrier. In contrast, Figure 2.14 indicates a more pronounced response to rainfall in the well in the contained zone (LT3) compared to the first aquifer

well outside of the contained zone (LT4) on the west side of the park. This can be explained by the fact that falling or rising water levels caused by precipitation in the contained zone cannot be supplemented by, or drained to, the surrounding aquifer, making the contained zone prone to stronger fluctuations. This observation further supports the notion that the vertical barrier may have slightly higher permeability on the east side compared to the west side of the park.

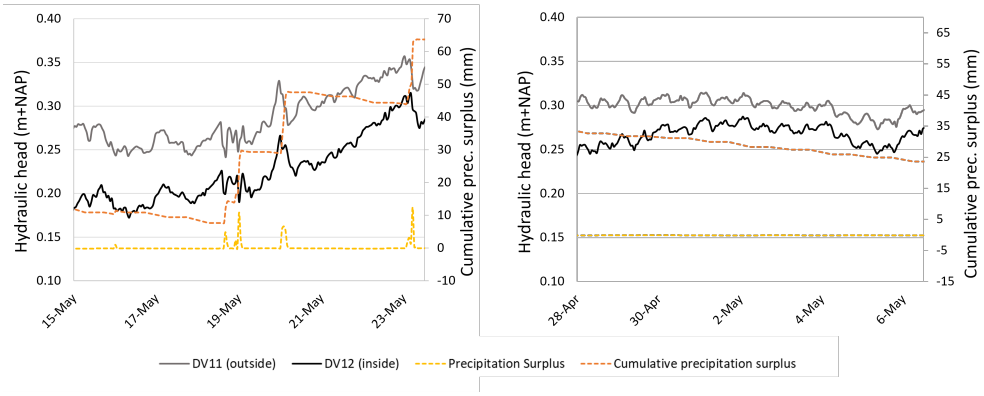

Figure 2.17: Two excerpts of water levels at DV11 and DV12 out of Figure 2.16, shown together with precipitation data.

Figures 2.18a and 2.18b show the results of manual water level measurements in the MLS wells at locations B and B2. At shallow depths, on average, scenarios with pumps on yield the lowest hydraulic heads and scenarios with all pumps deactivated the highest. All measurements were taken during dry periods except the measurement that is indicated by the dark blue squares (measurements from February 22^{nd}), explaining the relatively high hydraulic heads during this period. The results show that deeper into the aquifer the difference in water levels caused by varying pumping rates diminishes. These findings agree with the continuous measurements at location B, shown in Figure 2.15, where a strong reaction to a change in pumping rates could be distinguished in the shallow well, less strong in the second well and only weakly in the deepest.

The results shown in Figure 2.18 allow for more detailed investigation of subsurface properties. At several depths, in both well B and B2, we observed sudden increases in the hydraulic head through depth. These sudden increases indicate impediments to groundwater flow. The most evident cause of flow impediments at the Griftpark are the existing clay depositions, however, also the presence of thick layers of pure phase DNAPL can be a cause. To connect the observed hydraulic increases to clay depositions, depths at which clay was encountered during sonic drilling are indicated by brown horizontal lines

in Figure 2.18. The nature and thickness of these depositions are further explained in Table 2.1.

location	top (m-NAP)	bottom (m-NAP)	thickness (m)	soil type
B	46.5	46.6	0.1	clay, moderately sandy
	51.8	52	0.2	extremely fine sand, clay layers
	54	55	1	very fine sand, clay layers
	59.5	62.5	3	clay, strongly sandy
B2	25	25.5	0.5	moderately fine sand, clay layers
	33	35.5	2.5	moderately fine sand, clay layers
	37	37.5	0.5	moderately fine sand, clay layers
	44.5	47	2.5	clay, strongly sandy
	52	52.5	0.5	clay, weakly silty
	56	56.5	0.5	clay, weakly sandy

Table 2.1: Depths and descriptions of depositions containing clay as found at locations B and B2 during sonic drilling.

At location B, significant hydraulic head increases are observed between 16-18, 41-46, 50-51 and 57-60 m-NAP, with the most pronounced increases between 41-56 and 57-60 m-NAP. By considering the clay deposition descriptions shown in Figure 2.18a, we deduce that the two thicker clay depositions have an effect on vertical hydraulic connectivity and cause the head increases between 50-51 and 57-60 m-NAP. The head increase between 41 and 46 m-NAP could potentially be attributed to the deposition at 43 m-NAP, although its thinness raises uncertainty. The reason behind the slight head increase between 16 and 18 m-NAP remains unclear, however, it is plausible that it may be caused by a measurement error in determining the height of the well cap for B-MLS1 or B-MLS2 since the head increase occurs exactly between the two. Furthermore, based on dissolved contaminant concentrations measured in well B at 18 m-NAP, it is concluded that pure phase coal tar exists around this depth (further explanation given in Section 2.3.3). If pure phase DNAPL exists at this location within the range of 16 to 17.5 m-NAP, it could potentially explain of the flow impediment.

At location B2, head increases were observed between the depths of 16-18, 41-46, 52-53 and 57-60 m-NAP, with the most pronounced increases between 40-47 and 52-57 m-NAP). The 2.5 m thick clay deposition at 44.5 m-NAP has an effect on the vertical hydraulic connectivity, whereas the 2.5 m thick layer

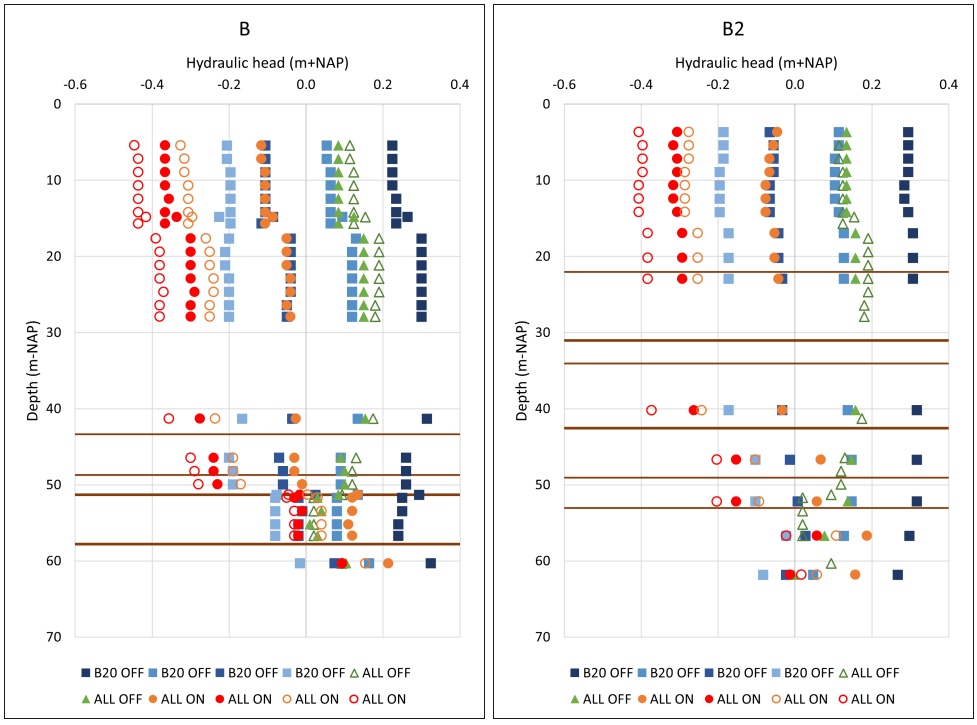

(a) Location B

(b) Location B2

Figure 2.18: The figure shows hydraulic head levels in the MLS wells at locations B and B2. Measurements taken at various times (indicated in Figure 2.6) during a range of pumping regimes and after varying periods for equilibration. Measurements taken with pumps B20, B21 and B22 on are indicated by red and orange circles, while only pump B20 was on by blue squares and when all pumps were off by green triangles. Measurements taken five days after switching pumps are shown by solid shapes, when taken after fourteen days by empty shapes. Depositions of clay or that contain clay as determined during sonic drilling are shown by brown horizontal lines. The thicker lines indicate depositions thicker than 1 m, whereas the thinner lines indicate depositions of max 50 cm. The clay depositions are further clarified in Table 2.1

at 33 m-NAP, consisting of sand with clay layerings, does not. The deposition at 52 m-NAP appears to have an effect, despite its limited thickness. Between 57 and 62 m-NAP, a decrease in hydraulic head was observed instead of an increase as measured in the other wells. This could potentially indicate the presence of tilted clay lenses, which may lead to a decrease in pore pressure in specific locations. Similar to at location B, the slight head increase between 16 and 18 m-NAP could potentially be caused by land level measurement error.

In conclusion, clay depositions of more than 1 m thickness have been shown to have an effect on vertical hydraulic connectivity. Furthermore, there are indications that even clay depositions as thin as 20 cm may cause flow impediments. The variability in the observed effects may be attributed to variability in size and thickness of the depositions, as well as their texture and inclination.

2.3.3 Contaminant source zones

Soil core and well inspection

During sonic drilling, pure phase tar was visually found at several locations: at well B between 34-35.3 m-NAP tar fingers were encountered; at B2 pure phase DNAPL was found between 1 and 2.5 m-NAP and until 4 m-NAP droplets of pure product; at well C pure phase DNAPL interspersed with fingered zones were found between 23-27.5 m-NAP, 28.8-36.5 m-NAP and 44.5-46.5 m-NAP. As some very course soil cores fell out of the core barrel, it was not possible to inspect the soil and contamination throughout the complete depth of all drillings. Furthermore, the camera inspection of well B22 showed a clear presence of pure phase coal tar from 27 to 28.5 m-NAP as well as at 32.0, 36.7 and 40.1 m-NAP.

Membrane interface probings

The MIP drillings reached a maximum depth of 26 m-NAP, encountering coal tar compounds at all test locations. When the MIP rod passes through pure phase tar, it may cause disproportionately high concentration readings [45, 114]. During the MIP tests conducted at the Griftpark, disproportionate concentrations, as high as 100 mg/L of individual compounds, indicating the presence of pure phase coal tar, were recorded at multiple locations and depths. Based on these observations, it was concluded that the following locations contain pure phase tar zones: MIP2, close to well B, between 12-19 m-NAP; MIP3, close to well C, below 23 m-NAP; MIP4 between 7-16 m-NAP; MIP5 around 5 m-NAP; MIP7 at 1, between 7-12 and at 22 m-NAP; and at MIP9, close to well B2 between 2 and 4 m-NAP.

Groundwater analysis

In the groundwater sample from well B22, 36 types of mono-aromatic hydrocarbons, 25 double- and triple-ring poly-cyclic aromatic hydrocarbons (PAH) and four aliphatic hydrocarbons, components of mineral oil, were identified. The found mono-aromatic benzene, toluene, ethylbenzene and o/m/p-xylene isomers (BTEX) as well as the double-ringed naphthalene are usual suspects in coal tars [65, 40, 308], together with trimethylbenzenes, propylbenzenes, ethyltoluenes, styrene, indane, indene and methylnaphthalenes, acenaphthylene, anthracene, fluoranthene, pyrene and phenanthrene, that have also previously been identified at other FMGPs [109, 110]. Based on the total detected GC-MS peak areas and individually identified components, these compounds constitute about 90% of the total dissolved contaminant concentration at B22.

Compound	C B22	C_{max}	S_{max}
Benzene	6.380	2.503	6.380
Toluene	3.131	501	3.131
Ethylbenzene	4.035	1.690	4.035
M/P-Xylene	7.217	1.058	7.217
O-Xylene	3.260	506	3.260
Cumene	128	104	128
M-Ethyltoluene	1.307	232	1.307
P-Ethyltoluene	204	n.a.	204
O-Ethyltoluene	141	91	141
1,2,4-Trimethylbenzene	656	367	656
1,2,3-Trimethylbenzene	212	177	212
Indene	64	1.126	1.126
Indane	2.375	1.602	2.375
Naphthalene	11.174	7.626	11.174

Table 2.2: Maximum concentration of tar aromatic compounds measured in the saturated B22 groundwater sample, as well as the maximum concentration measured in groundwater samples collected from wells B, B2 and C. Maximum solubilities, are for all compounds taken from the concentration in the saturated B22 sample, except for indene, for which a higher concentration was measured in well B2. All concentrations are given in (mg/L).

As the B22 groundwater was completely saturated with coal tar compounds, the concentrations measured in this sample are used as an estimation of the maximum solubilities for the Griftpark coal tar compounds. As the concentration of indene in the B22 sample was very low, i.e. much lower than the average concentration in the other groundwater samples taken from wells B, B2 and C (also much lower than a duplicate sample that yielded a lower total dissolved concentration), it was assumed that this result was erroneous,

and the concentration was replaced with the maximum concentration measured in the B, B2 and C samples (i.e. B2 8 m-NAP), see Table 2.2. The maximum (saturated) total concentration, i.e. the sum of the maximum solubilities displayed in Table 2.2, is 40 mg/L. Of this mass, 27% is naphthalene, 17% m/p-xylene, 15% benzene, 10% ethylbenzene, 8% o-xylene, 8% toluene, 6% indane, and 3% indene.

During soil core analysis at well C, pure phase DNAPL was encountered between 23 and 27.5 m-NAP, 28.8 and 36.5 m-NAP and 44.5 and 46.5 m-NAP. In water samples collected from the MLS well installed in this borehole at these depth ranges, dissolved contamination concentrations between 8.5-13.6 mg/L were measured. This indicates that even at locations where direct proof of pure phase coal tar presence is available, dissolved concentrations stay well below the maximum dissolved concentration of 40 mg/L. This suggests that biodegradation effectively reduces contaminant concentrations close to source zones. Therefore, we used threshold value of 8.5 mg/L to indicate the nearby presence of pure phase coal tar at a sampling location. Groundwater samples taken from well B show peak concentrations of tar aromatics between 9 and 18 m-NAP (between 3.4 and 10.5 mg/L). Groundwater samples taken from well B2 show peak aromatic concentrations in samples taken from 4 m-NAP (9.7 mg/L) as well as 11 m-NAP (10.1 mg/L). In groundwater samples from wells Pb1 (deep well 17 m-NAP) and DV4 (31 m-NAP) no significant hydrocarbon concentrations were found.

Routine monitoring of the Griftpark involves regular analysis of aromatic hydrocarbon concentrations in groundwater collected from a variety of wells. The measurements are conducted by *Eurofins Analytico* and include BTEX and 16 EPA PAHs. Notably, the analysis conducted by *Eurofins Analytico* indicates higher total concentrations than those observed in the samples collected during this project. High concentrations occur mostly in samples from wells in the southern region of the park, which were not included in our sampling.

For example, in the sample collected from Pb1 (shallow well 7 m-NAP), an average concentration (inclusing BTEX+PAH over the period of 2005-2021) of 53 mg/L was recorded. Samples from well 86 (9 m-NAP) yield an average concentration of 65.2 mg/L. Within these analyses, the most contaminated samples contain a significantly higher fraction of BTEX (more than 80%) compared to PAHs, in contrast to the average fraction of BTEX across all samples (around 45%). A potential explanation for the discrepancies may be the presence of different types of factories around this part of the park, during which manufacturing processes waste products were produced that contained relatively more MAHs.

In the samples from LT1, DV10, DV12 and DV14 no significant concen-

trations were measured. At LT3 the average concentration is 3.6 mg/L. In water from groundwater extraction wells B20, B21 and B22 the average concentrations measured were 1.25, 5.04 and 17.2 mg/L respectively.

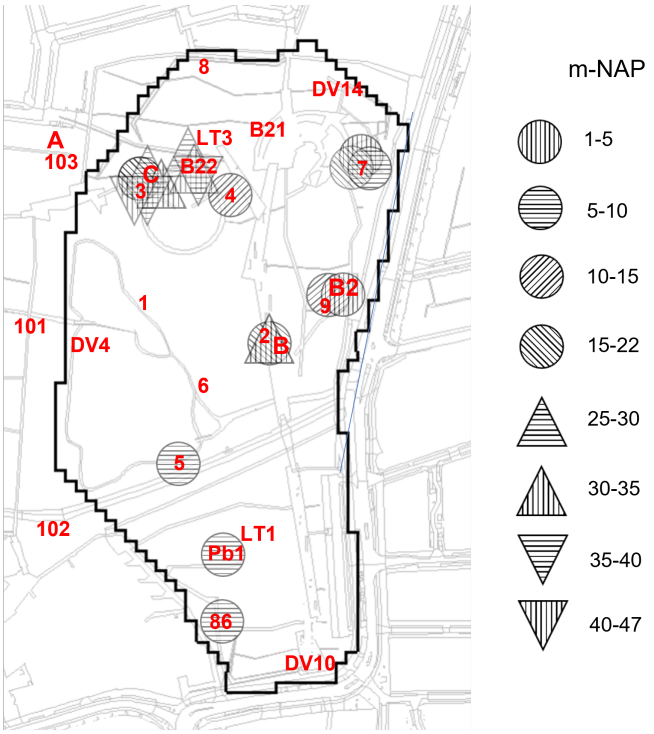

Figure 2.19: Locations and depths of pure-phase coal tar contamination interpreted from field investigations and groundwater sampling in the Griftpark. Presence of pure phase tar is depicted by different shapes and shape fills that indicate different depths as indicated in the legend.

Following the above results, Figure 2.19 depicts all suspected source zone locations, with different shapes and shape fills indicating different depths. The Figure shows the variety in coal tar deposition locations at the site, as is common at FMGP sites [307]. As the source zone locations found during the recent field investigations are taken from one-dimensional vertical profiles or single point measurements, the shape sizes do not represent the actual extent of the pure tar zones. Furthermore, pure phase zones may exist at locations where no measurements were performed. Consequently, the resulting map of contaminant source zones as presented in Figure 2.19 can only be used as an indication of the distribution of pure phase contamination.

We cross-checked locations and depths of source zones with soil type descriptions from drilling profiles. The results confirm that pure phase product is mostly situated on top of lower permeability layers in the subsurface. At lo-

cation C, tar was found pooled on top of the clay at the depth of the aquitard. Considering our previous conclusions that no direct hydraulic pathways exist in the aquitard around the Griftpark, the risk this involves for further downward migration is presumed to be small. As validation, we conducted a compound analysis on water samples collected from the second aquifer (i.e. from wells BW157 (upgradient), A, 60, 101, 102 and 103). None of the samples showed significant concentrations of aromatic hydrocarbons and the found aromatic compounds (below 0.05 mg/L) are not representative of the contamination occurring at the Griftpark. Data on concentrations in the second aquifer can be found in Appendix C.

These findings provide evidence that contaminants originating from the Griftpark have not spread through the second aquifer. This suggests that, firstly, the current pumping scheme is effective in preventing leakage of groundwater into the second aquifer. Secondly, it implies that in the case that coal tar would have reached the second aquifer, the pumps generate sufficient upward seepage to transport dissolved contaminants upward. If coal tar were present in the second aquifer, the biodegradation process would alter the concentrations of electron acceptors. Therefore, to investigate the potential presence of coal tar in the second aquifer, electron acceptor analysis was also performed, confirming an absence of changes in electron acceptor concentrations between up-gradient and down-gradient wells, leading to the conclusion that no pure phase coal tar exists in the second aquifer.

2.3.4 Potential for tracer test

The potential for a tracer test at the Griftpark was studied but rejected. Usually, tracer tests are performed in the horizontal plane along the main direction of groundwater flow. Vertical spread is measured to account for dispersion and diffusion, or, as in the case of a dipole tracer test to study anisotropy ratios on small scales [276]. Although at the Griftpark vertical groundwater flow from the second to the first aquifer is forced by groundwater from the first aquifer, the hereby established flow velocity is very low, even if pumping rates from existing wells are maximised. Furthermore, the existence of low conductivity depositions in the aquitard would cause the tracer to spread considerably. The combination of the low flow velocity and expected spread of the injected tracer are considered to make the chances of a successful vertical tracer test at the Griftpark low as well as not useful.

2.4 Conclusions

In Chapter 2, we presented studies performed to collect information on the geometry and properties of the Griftpark subsurface of the site and to map

locations of contaminant source zones. With a combination of field-based methods, it was found that:

- Both physical drilling and hydraulic field scale tests confirm the Griftpark subsurface consists of two aquifers separated by a leaky aquitard, between about 37 and 70 m-NAP.
- The first aquifer is a heterogeneous sandy aquifer where soil type varies on sub-half metre scales from very fine to very coarse sand, here and there interspersed with gravel or finer depositions, mostly sandy clay. The second aquifer is more homogeneous, moderately silty to moderately course sand.
- The aquitard consists of a collection of clay lenses of varying sizes and thickness. Clay depositions exist everywhere below the Griftpark, but are somewhat scarcer and thinner in the central zone. Results show that the first and second aquifer are hydraulically connected, but the connection is not so strong as to suspect a 'hydraulic corridor', i.e. a large gap in the clay layer.
- Due to the limited hydraulic connection over the aquitard, the chance of a successful vertical tracer test between the two aquifers is low.
- Changes in precipitation rates have a large effect on hydraulic head levels within the park due to the contained zone being cut-off from the surrounding aquifer. Despite the head levels that therefore rise more strongly inside the park, the hydraulic tests have confirmed that with a pumping at rate above 6.5 m^3/d, the hydraulic pressure within the contained zone (first aquifer) is kept below the pressure in the first aquifer outside the contained zone as well as in the second aquifer below the park. Thus, seepage is inward into the park and dissolved contamination is prevented from leaking out.
- Dissolved contamination was encountered in all groundwater samples from the contained zone and it is concluded the complete Griftpark subsurface is contaminated.
- Pure phase coal tar was encountered throughout the complete site, at depths ranging between 4 to 49.5 metres below ground level (i.e. 1-46.5 m-NAP). Only in the north and central regions (i.e. around the locations of wells B, C and B22), tar was found at depths greater than 13 metres below ground level (i.e. 10 m-NAP).
- No proof of contamination was found in the second aquifer. Including the absence of an indication of a 'hydraulic corridor' in the aquitard, it

is concluded that the chance of DNAPL presence in the second aquifer is low.

Overall, we may conclude that the current contain-and-monitor measures applied at the Griftpark are successful in maintaining an under-pressure within the contained zone and keeping the second aquifer free from contamination. In Chapter 3 we will investigate the occurrence of biodegradation at the site, which, like the groundwater pumping, is another potentially important factor limiting contaminant spread. Biodegradation potential and subsurface geometry are both crucial factors when considering phasing out the active management procedures at the Griftpark and investigating the potential of relying on monitored natural attenuation as a new management approach.

Chapter 3

Characterisation of natural biodegradation at the Griftpark

Abstract

Investigations of natural biodegradation at field sites commonly rely on monitoring sediment and groundwater along or across a transect of a contaminant plume. However, at the Griftpark field site, due to the presence of containment barriers and groundwater extraction from multiple locations, a traceable contaminant plume is absent. The standard lines of evidence are employed at the Griftpark site to investigate the occurrence of natural biodegradation and identify potential biodegradation pathways. The applicability of these standard analysis methods under the specific field conditions is evaluated.

The results show that gradients in aromatic hydrocarbon concentrations and changes in compound ratios provide an initial indication for the occurrence of biodegradation of the primary contaminants at the site. Examination of varying electron acceptor concentrations and the presence of reduced electron acceptors in sediment and groundwater allow for the identification of specific reduction reactions taking place. However, the considerable heterogeneity in chemical composition among groundwater samples poses challenges in determining spatial trends. The presence of signature metabolites and microbial DNA further confirm the occurrence of biodegradation and elucidate biodegradation pathways for the primary contaminants at the site. Although carbon and hydrogen isotope ratio shifts can serve as additional confirmation of biodegradation occurrence and type, the absence of a traceable contaminant plume hinders the calculation of biodegradation rates, a typical advantage of isotope fractionation analysis.

This study demonstrates that the occurrence of natural biodegradation can successfully be proven even in the absence of a traceable contaminant plume. However, given the hydrogeological and biochemical subsurface heterogeneity, these investigation methods do not enable the estimation of biodegradation rates and the prediction of future development of oxidation and contamination conditions at the site. In order to gain deeper understanding of the dynamics and long-term implications of biodegradation processes in such complex environments, the utilisation of three-dimensional numerical models may provide essential support.

The results of this Chapter are being prepared for publication in *Science of the Total Environment*. Title: Characterisation of aromatic hydrocarbon biodegradation at a physically contained field site.

3.1 Introduction

During the early 1800s, the first large-scale commercial manufactured gas plants (MGP) were constructed to produce gas for municipal lighting [133]. Subsequently, MGPs were built in nearly every Central European and North-east American city [307]. Estimates of the total number of former MGPs (FMGP) vary widely. A conservative estimate suggests 8,700 FMGPs and coke-oven plants worldwide, excluding China, Russia and India [307], whereas other estimates suggest between 21,200 to 32,600 FMGPs in the US alone [131].

In MGPs, gas was created by gasifying and carbonising coal in retorts or coke ovens [280]. Next, tars were extracted to purify the gas. These tars consist mainly of mono- and poly-cyclic aromatic hydrocarbons, phenols, aliphatic compounds and hetero-cyclic compounds [21, 40, 110, 210]. The tars were often disposed of, intentionally or unintentionally, at the production and purification locations or elsewhere on the industrial site [71, 214]. One example of an FMGP is the Griftpark in the city of Utrecht, the Netherlands, where industrial activities with a risk of tar spillage took place on an eight hectare terrain between 1840 and 1960.

Tars are a class of dense non-aqueous phase liquids (DNAPLs). In the subsurface, they sink through the unsaturated zone into the saturated zone through connected ganglia under gravity and capillary forces [75, 226]. Due to subsurface heterogeneity, the pure phase coal tar forms highly non-uniform distributions in the subsurface [91, 169, 75], consisting of low-saturation zones in the form of residual ganglia and blobs, and high-saturation zones in the form of pools that may collect on top of permeability barriers [264]. Due to the low solubility and dissolution rates of many of the coal tar compounds, such groundwater contamination may persist for centuries [33, 82], posing a threat to human health and the environment [147, 156].

The potentially deep penetration of DNAPLs into the subsurface makes it challenging to excavate source zones to treat the contaminants ex-situ [33]. Therefore, at many locations contaminated with DNAPLs, source-zones have been physically contained with vertical barriers, often combined with groundwater extraction [198]. This 'contain-manage' technique has been applied at over 2,388 contaminated sites in the Netherlands [11]. Although the method effectively protects the groundwater, it fails to reduce the total contaminant volume, thus requiring perpetual management, including monitoring.

Currently, in the Netherlands, the contain-and-manage sites are being revisited, with a focus on exploring the feasibility of monitored natural attenuation (MNA) as a management option. MNA entails relying solely on naturally occurring physical, chemical and biological processes to reduce contaminant mass in the subsurface and groundwater, potentially offering a

cost-effective and environmentally friendly alternative to current management strategies [313, 51].

For sites contaminated with the aromatic hydrocarbons present in coal tar, biodegradation has been found to have a high potential to break down aromatic hydrocarbons and MNA has become an accepted alternative for active remediation at low-risk sites contaminated with organic compounds [193, 228, 314, 313]. Before implementing MNA, it is crucial to evaluate if natural biodegradation occurs at a site, and if so, at rates high enough to maintain a safe environment. Suitable methods to investigate the potential of natural biodegradation at field sites have been well-established in recent decades.

Biodegradation in the field is typically demonstrated through three research lines [36, 27]. Conclusive evidence of biodegradation can be obtained only if several research lines were able to indicate its occurrence [36, 46, 246].

The first line of research involves monitoring changes in the contamination itself. This includes monitoring changes in total contaminant concentrations as well as changes in the ratios of the different contaminant compounds which can indicate different biodegradation rates [274]. It also includes finding evidence in the presence of metabolic intermediates generated during biodegradation of hydrocarbons [87, 46, 229, 24]. The metabolites are often less complex and harmful than the parent compounds and can be further degraded and mineralised to CO_2, CH_4 and H_2O [311, 95]. Some metabolic intermediates are specific to the parent compound and the degradation pathway, and their detection can indicate the occurrence of specific enzymatic reactions [63, 25, 30]. Finally, the first line also includes monitoring shifts in carbon and hydrogen isotope ratios. For many contaminants, biodegradation leads to a shift towards heavier fractions of the isotopes as lighter compounds are more easily catabolised during biodegradation [302]. By studying these shifts, biodegradation rates can be calculated based on biotic processes only, opposed to basing calculations on decreasing substrate concentrations, which also includes effects of sorption and dispersion [203, 36, 281].

The second research line entails the investigation of the chemical potential the sediment and groundwater to support biodegradation. Many studies have provided evidence for biodegradation of aromatic hydrocarbons under various redox conditions, such as oxygen reduction [116, 115, 263], nitrate reduction [19, 143, 171, 324], sulphate reduction [26, 70, 85, 104], iron reduction [183, 182] and methanogenesis [120, 316]. The presence and depletion of electron acceptors in sediment and groundwater, as well as the occurrence of their reduced products, are important indicators of biodegradation at a field site. Also the availability of nutrients for biomass growth is a prerequisite for biodegradation [217].

The final research line is based on the presence of prokaryotic microor-

ganisms with biodegradation capacity that exist in the subsurface [310, 13]. As biodegradation is mediated by these organisms, the presence of specific microbial DNA associated with the potential of specific degradation processes can provide proof of the potential for biodegradation [161].

Changes in contaminant and electron acceptor concentrations, and in isotopic ratios are mostly monitored along or through contaminant plumes [212, 312, 322, 57, 121]. In that way, chemical changes can, with known groundwater flow velocity, be related to time and as such biodegradation rates can be obtained. However, at locations with contained sources, the absence of apparent contaminant plumes requires a different approach for the analysis of field data.

In this chapter, the Griftpark is used as a case study to evaluate the applicability of the aforementioned research lines for characterising biodegradation at sites without a traceable contaminant plume. To our knowledge, no previous studies have assessed biodegradation at contained contaminated sites. The findings presented here may contribute to risk and cost reduction at contained sites contaminated with aromatic hydrocarbons.

3.2 Site description

The Griftpark, located in Utrecht, the Netherlands, is built on a former industrial site, which hosted several MGPs. The geologic formation at the location of the Griftpark consists primarily of marine and fluvial deposits originating from the Holocene and Pleistocene eras [32]. The first aquifer, composed of the Westland, Kreftenheye, Urk and Kreftenheye formations, extends to a depth of about 50 m-bgl. It has a heterogeneous structure with both fine and course depositions [6]. The second aquifer, the Harderwijk formation, extending from about 70 to 110 m-bgl, is relatively homogeneous. The first and second aquifer are separated by the Waalre formation, characterised by clay and silt deposits. During a set of cone penetration tests (CPTs) performed in 1988, it was found that the Waalre depositions are interspersed with sand from the Harderwijk formation, causing this layer to not be fully confining [6]. Figure 3.1 shows an impression of the Griftpark lithological layering.

The FMGPs left behind extensive coal tar contamination. Pure phase coal tar was found at depths varying between 4 to 49.5 m-bgl across the eight hectare terrain during site investigations performed in the 1980s. Aromatic hydrocarbons, in particular monoaromatic compounds benzene, toluene, ethylbenzene and the o/m/p-xylene isomers (BTEX) and the double-ringed aromatic hydrocarbon naphthalene, were found to make up most of the contaminant mass [252]. Some non-organic compounds were found as well, including cyanide from the coal-gas factory and some heavy metals. There is also a

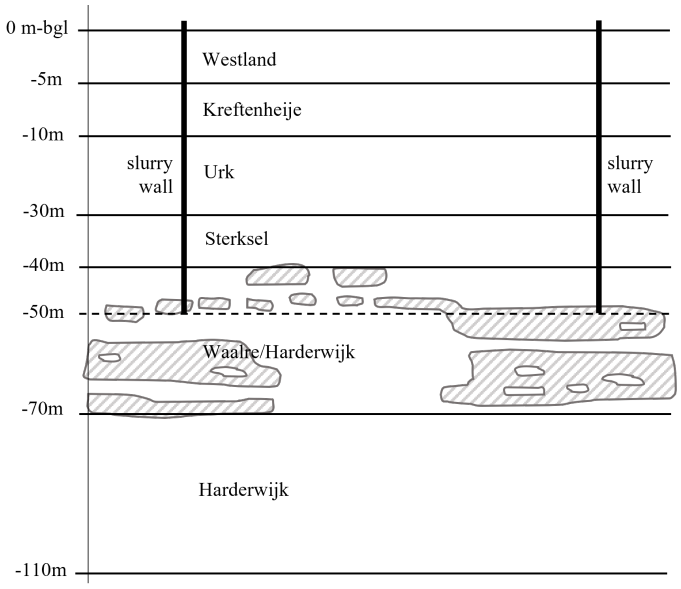

Figure 3.1: Sediment layers below the Griftpark.

source of sulphate pollution at the southern edge of the site, most likely originating from gas purifiers [307].

Due to the depth to which pure-phase tar was encountered when the contamination was discovered, remediation or in-situ treatment was deemed impracticable. Therefore, in 1990, a cement-bentonite vertical barrier was installed around the site to prevent further development of the contaminant plume down-gradient. After installation of the vertical barrier, mapping of the pure phase tar zones was halted and a complete map was never made [6]. The wall spans an eight-hectare area and is installed up to a depth of approximately 55 m-bgl. As the aquitard is not completely confining, a risk exists for contaminated groundwater to leak from the first to the second aquifer. To establish inward seepage, both through the cement-bentonite wall and the aquitard, groundwater is extracted from three wells, B20, B21 and B22, see Figure 3.2, within the contained zone. B20 and B21 are filtered between 12 and 20 m-bgl and B22 between 25.75-36.40 and 38.40-46.50 m-bgl.

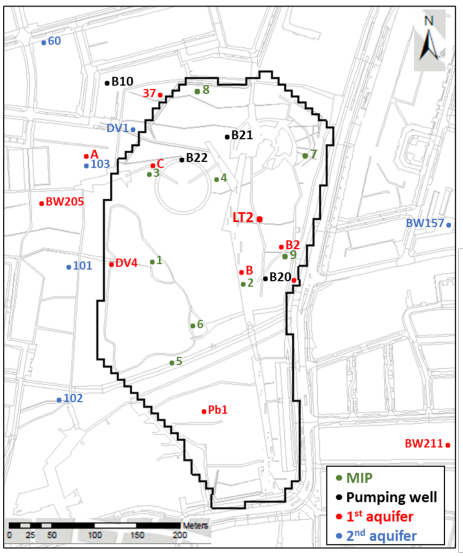

Well	Filter depths (m-bgl)						
B	17.0	44.0	54.0	63.0			
B MLS1	8.5	10.5	12.0	14.0	15.5	17.0	19.0
B MLS2	20.5	22.5	24.0	26.0	28.0	29.5	31.0
B MLS3	49.5	51.5	53.0	55.0	56.5	58.5	60.0
B2	64.5						
B2 MLS1	7.0	8.5	10.5	12.0	14.0	15.5	17.5
B2 MLS2	20.0	23.0	26.0	43.0	50.0	55.0	60.0
C	38.5	40.5	43.0	45.5			
C MLS	15.5	17.0	19.0	20.5	22.5	24.0	26.0
101	54.0	57.0	64.5	67.5	72.0	81.0	87.0
102	46.5	53.0	62.0	68.0	73.0	75.5	82.0
103	47.5	61.0	66.5	72.5	80.0	99.5	

Figure 3.2: Locations and filter depths of wells at the Griftpark. MIPs indicated by the numbers 1-9 in green. Pumping wells B20 and B21, filtered between 12 and 20 m-bgl, and B22, filtered between 25.8-36.4 and 38.4-46.5 m-bgl, indicated in black. Locations B, B2, C, 101, 102 and 103 are equipped with both normal and MLS wells. Monitoring wells filtered in the first aquifer are indicated in red, those in the second aquifer in blue.

3.3 Materials and methods

3.3.1 Field investigations

Cone penetration testing and membrane interface probing

At Griftpark, we conducted nine membrane interface probe (MIP) tests at locations suspected of contamination (numbers 1-9 in Figure 3.2). The selection of these locations was based on previous research and historical data on industrial activity. MIP is a direct push probe that measures soil resistance and records a profile of relative soil conductivity. Equipped with a membrane, MIP can also partition volatile organic carbons (VOC) after heating, providing quasi-real-time indications of VOC concentrations in sediment at different depths [250]. An on-site gas-chromatograph mass-spectrometer (GC-MS) was used to measure the VOCs, and the MIP rod could reach a maximum depth of 29 m-bgl. BTEX components, naphthalene, 1,2,4-trimethylbenzene, styrene, indene and indane were selected for analysis based on their high concentrations during pre-investigation. EnISSA (Steenokkerzeel, Belgium) conducted the MIP tests.

Sonic drilling and monitoring well installation

The roto-sonic drilling method [125] was applied to collect (anaerobic) soil samples, describe soil profiles and install sampling wells. The sonic drillings were carried out by Sialtech (Houten, the Netherlands), at locations A, B, B2, C, 101, 102 and 103 shown in Figure 3.2. Borehole A was positioned down-gradient of the Griftpark at a depth of 65.5 m-bgl. B and B2 were drilled at locations where little to no clay was expected according to the 1988 CPT result analysis [6], and where contaminant concentrations were high according to the MIP analysis. B was drilled to a depth of 64.0 m-bgl, and B2 was drilled to a depth of 65.5 m-bgl. C was installed to a depth of 50.5 m-bgl, near pumping well B22, which pumps up highly contaminated groundwater from a depth of 25.75-36.40 and 38.40-46.50 mg-bgl. Drilling through clay lenses where pure phase DNAPLs lie pooled on top can cause a risk downward DNAPL spread [61]. Therefore, when such a risk was expected at the Griftpark, the drilling was halted.

Following the drilling of boreholes, standard HDPE monitoring wells with a 3.2 cm diameter and 1 m filter length were installed for groundwater sampling at locations A, B, B2, and C. Multi-level sampling wells (MLS) from Solinst Canada Ltd. (Georgetown, Canada) were also installed at B, B2, and C to enable water sampling at higher depth-resolution than is possible with standard monitoring wells. The MLS wells consist of HDPE filters with an outer diameter of 10 cm, each containing seven units with an 8 mm inner diameter. They are filtered along a length of 25 cm and have a 3-4 mm slot width. The filter depths (top of the filter) are indicated in the table included in Figure 3.2. Besides the groundwater wells, also DNAPL collection wells were installed at B2 filtered between 3.5-8.0 m-bgl and at C between 25.5-29.5 m-bgl. These HDPE wells have a 63 mm diameter and 3 mm slot widths.

Soil samples were obtained using the corebarrel technique [309]. DNAPL distribution was visually assessed from the undisturbed soil samples. Where pure phase tar was expected, transparent lexan liners (polycarbonate) were used so that the presence of pure phase tar could be visually inspected. However, it was found that the liners burst upon extended contact with pure tar.

3.3.2 Laboratory analyses

For groundwater sampling, a selection was made of monitoring wells covering a range of conditions and levels of contamination. Groundwater was sampled from the first aquifer inside (B, B2, B22, C, PB1, DV4) and outside (BW205, 37, BW211) of the contained zone. Wells B, B2, 101, 102 and 103 contain MLS filters in the second aquifer. The locations of all wells are shown in Figure 3.2.

Contaminant analysis

Groundwater samples were examined for their BTEX, PAH, mineral oil and cyanide content by standard gas chromatography-mass spectrometry (GC-MS) at Synlab (Munich, Germany). Initially, we analysed a groundwater sample saturated with coal tar from the highly contaminated B22 well. The aromatic hydrocarbon compounds that together constitute 90% of the total dissolved concentration in this sample were used to prepare calibration solutions for the quantification of compounds in other samples from the Griftpark.

To investigate the presence of additional aromatic compounds not included in the standard analysis, groundwater samples were analysed on an Agilent 7890A GC-MS system with an ATTM-624 60 m x 0.25 mm x 1.4 μm Heliflex column (Grace). Groundwater samples were taken in completely filled vials and stabilised with an NaOH pellet. For analysis 8 ml samples were transferred in 22 ml butyl/teflon capped GC-vials (Grace) with 10 μM deuterated benzene as an internal standard. Five-point concentration calibration samples were prepared similarly using >99% pure aromatic hydrocarbons. An MPS 5975C autosampler (Gerstel) was used to agitate the GC-vials for 20 min. at $75°C$. Subsequently 250 μl headspace samples were injected at an inlet temperature of $200°C$ with a split mode of 5:1. After injection the column oven was held for 1 min. at $40°C$, with a subsequent increase of 10 °C/min. until $200°C$, followed by an increase of $20°C$/min. until $300°C$. This temperature was held for 1 min. The chromatograms were analysed in MSD ChemStation software.

Analysis of redox conditions

Cations, anions and elements in groundwater samples were determined to assess redox conditions and to compare conditions in contaminated versus uncontaminated zones. The concentrations were determined using a combination of DIONEX ion-exchange chromatography and inductively coupled plasma-optical emission spectrometry (ICP-OES) analysis. The method has been described by van Leeuwen et al. [294]. Additionally, soil samples were analysed to determine the concentrations of electron acceptors to provide insights into the mass of electron acceptor available for biodegradation in the subsurface. The soil analyses were performed at Synlab.

Metabolite analysis

To provide evidence for active biodegradation and obtain insight in the degradation pathways at the Griftpark, 26 groundwater samples were collected for metabolite investigation from wells in zones with different conditions, namely A, B, B2, C, Pb1, 60 and BW205 from depths ranging from 7 to 72 m-bgl.

The zones included areas in- and outside the contained zone and the first and second aquifer. Also, two tar samples, from wells B (5.7 m-bgl) and C (48 m-bgl), were taken for analysis. A suspect list was created for 170 potential metabolites based on literature data on both aerobic and anaerobic degradation pathways of the present hydrocarbons and is provided in Appendix E. The suspect analysis was carried out at the University of Amsterdam using a qualitative tandem liquid chromatography quadrupole time of flight mass spectrometry method (LC-qTOF-MS) according to a protocol that was developed for samples from FMGPs as reported by van Leeuwen et al. [296]. For 35 of the detected metabolites calibration lines could be made and concentrations could be determined.

Multi-element compound specific isotope analysis

Isotopic fractions of aromatic contaminants in groundwater samples from sampling points with different levels of contamination from MLS wells B, B2 and C as well as a pure phase sample from well C were analysed by multi-element compound specific isotope analysis. Both $\delta^{13}C$ and $\delta^{2}H$ fractions of BTEX, indene, indane and naphthalene (BTEXIeIaN) were measured by gas chromatography-isotope ratio mass spectroscopy (GC-IRMS) at Hydroisotop (Schweitenkirchen, Germany). For a full explanation of the method we refer to van Leeuwen et al. [295].

In the $\delta‰$ notation, $\delta^{13}C$ and $\delta^{2}H$ fractions are calculated using the Pee Dee Belemnite standard isotope ratio R_{PDB}, here written for hydrogen, according to

$$\delta^{2}H(t) = \left(\frac{R(t)}{R_{PDB}} - 1\right) * 1000,$$

where $R(t)$ is the carbon or hydrogen isotope ratio at a certain time t. First order biodegradation rates can be calculated from changing isotope ratios using the Rayleigh equation. The Rayleigh equation reads

$$F(t)^{\alpha-1} = \frac{R(t)}{R(0)}, \tag{3.1}$$

where $\alpha = \frac{\epsilon}{1000} + 1$ is the kinetic fractionation factor as obtained from the per mil enrichment factor ϵ and $F(t)$ is the unreacted fraction (i.e. $C(t)/C(0)$, with $C(t)$ the concentration of the degrading organic compound at a certain time t). The Rayleigh equation can be rewritten as [194]

$$\epsilon * ln(F(t)) = ln\left(\frac{10^{-3} * \delta^{2}H(t) + 1}{10^{-3} * \delta^{2}H(0) + 1}\right) * 1000. \tag{3.2}$$

Next, the percentage of biodegradation $B\%$ for a compound can then be calculated through

$$B\% = (1 - F) * 100\% = 1 - exp\left[\frac{ln\left(\frac{10^{-3} * \delta^2 H(t) + 1}{10^{-3} * \delta^2 H(0) + 1}\right) * 1000}{\epsilon}\right] * 100\%. \quad (3.3)$$

As $F(t) = \frac{C(t)}{C(0)} = e^{-kt}$, the percentage of biodegradation $B\%$ can be used to calculate the first-order degradation rate k

$$k = \frac{-ln\left(1 - \frac{B\%}{100}\right)}{t}. \quad (3.4)$$

Furthermore, relative changes in the carbon and hydrogen isotope ratios can indicate the occurrence of specific enzymatic degradation reactions [302, 99, 167]. The relative changes are indicated by the lambda value $\Lambda^{H/C}$ and are calculated with the slope of linear regression of hydrogen versus carbon isotope signatures according to

$$\Lambda^{H/C} = \frac{\delta^2 H}{\delta^{13} C}. \quad (3.5)$$

DNA analysis

To indicate the presence of bacteria, archaea and determine biodegradation pathways, genes encoding 16S rRNA or genes encoding specific functional enzymes were quantified by the real-time polymerase chain reaction (qPCR) according to van der Waals et al. and van Leeuwen et al. [295, 292]. In particular, DNA of micro-organisms that are able to perform fumarate addition or carboxylation to initiate breakdown of BTEX, naphthalene or alkanes were quantified.

A selection of groundwater samples from wells A, B, B2 and C were analysed, as well as two soil samples containing pure phase tar from locations B (5.7 m-bgl) and C (48 m-bgl). For the groundwater analysis, 1 L samples were collected in clean amber bottles, stored on ice, and transported to the laboratory. Within 24 h the microbial cells were collected on membrane filters (47 mm diameter x 0.22 pore size) by vacuum filtration. The filters were stored at -80^oC until DNA was extracted using the MoBio Power-lyzer kit (MoBio, CA, USA). The filters were crushed with sterile toothpicks and cells were lysed by bead beating. DNA was subsequently extracted according to the supplier's protocol.

qPCR assays were performed on a Bio-RadCFX real-time PCR machine as described by van der Waals et al. [292]. An overview of the assays and primers is given by van Leeuwen [295].

Soil physics

As soil permeability controls whether diffusive or advective transport dominates and may thus impact the conductance of contaminants, electron acceptors and bacteria, it may play a role in biodegradation potential [240]. In order to investigate the influence of soil type across the Griftpark on biodegradation, physical properties of a number of soil samples were analysed. Grain size analysis was performed in a selection of soil samples selected from different depths from locations A, B and C. The analyses were performed by Synlab. Results were translated to hydraulic conductivity values using the Breyer method that is considered applicable for materials with heterogeneous distributions and poorly sorted grains [220].

3.4 Results and discussion

3.4.1 Contamination

From a groundwater sample from well B22 that was saturated with coal tar, 36 types of mono-aromatic hydrocarbons, 25 double- and triple-ring polycyclic aromatic hydrocarbons (PAH) and four aliphatic hydrocarbons, components of mineral oil, were identified. The found mono-aromatic BTEX compounds as well as the double-ringed naphthalene are usual suspects in coal tars [65, 40, 308]. Other compounds encountered include trimethylbenzenes, propylbenzenes, ethyltoluenes, styrene, indene, indane and methylnaphthalenes, acenaphthylene, anthracene, fluoranthene, pyrene and phenanthrene, that have also previously been identified at other FMGPs [109, 110]. Based on the total detected GC-MS peak areas and individually identified components, the BTEXIeIaN compounds (BTEX, indene, indane and naphthalene), constitute about 90% of the total dissolved tar aromatic hydrocarbon concentration and will receive most focus in this work. In the saturated samples from well B22, BTEXIeIaN was measured at a maximum total concentration of 37.6 mg/L, which was taken as maximum saturation concentration of typical Griftpark coal tar.

3.4.2 Biodegradation

Changes in contaminant composition

In this section we explore changes in contaminant compositions that may indicate the occurrence of biodegradation. Figure 3.3 shows the summed concentrations of the main compounds and their individual fractions in groundwater samples from wells B, B2 and C, as well as the saturated sample from well B22. Notably, maximum measured concentrations in the B, B2 and C wells

were found to be less than half of the maximum solubility of 37.6 mg/L measured in the saturated B22 sample, even in the near presence of pure phase coal tar, which was found at location C at depths between 26-50 m-bgl, as well as at B2 around 7 m-bgl. These findings suggest that biodegradation effectively reduces dissolved coal tar aromatics in the subsurface.

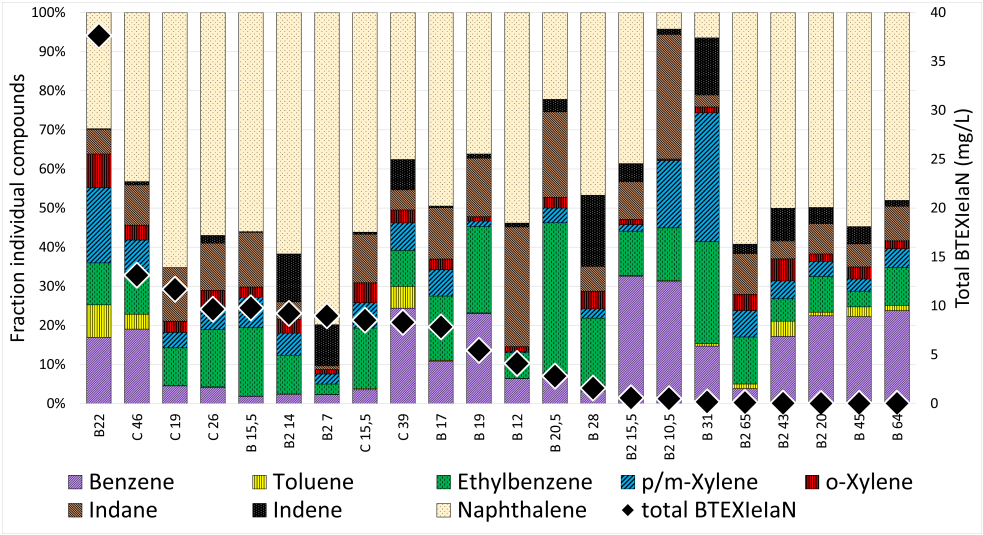

Figure 3.3: BTEXIeIaN fractions (coloured bars, left axis) along decreasing total dissolved BTEXIeIaN concentrations (black diamonds, right axis) in samples from various depths from wells B22, B, B2 and C.

Comparing contaminant ratios between different samples at the FMGP site is a challenging task, as the applied carbon source, carbonisation temperature, gas purification and storage techniques all have a direct influence on the composition of contamination at FMGPs [40, 110, 307]. Additionally, the various solubilities of different compounds within coal tar, causes the pure phase composition to change over time. Lower molecular weight compounds dissolve more easily, so that the molar fraction of heavier, less soluble, compounds increases in molar fraction over time [158, 102, 33]. As the Griftpark industrial site hosted several types of gas factories, it is expected that coal tars at the site vary in composition. Without a plume along which changes in contaminant concentrations can be measured, only general trends in varying ratios of contaminants in samples throughout the combined data set can be used to indicate biodegradation.

In the saturated groundwater sample from B22, naphthalene comprises nearly 30% of the dissolved BTEXIeIaN mass, followed by 17% m/p-xylene, 15% benzene, 10% ethylbenzene, 8% o-xylene, 8% toluene, 6% indane and 4% indene. On average, in the groundwater samples from wells B, B2 and

C however, naphthalene comprises 46% of the dissolved BTEXIeIaN mass, with the rest consisting of 7% m/p-xylene, 14% benzene, 13% ethylbenzene, 3% o-xylene, 1% toluene, 11% indane and 5% indene. As such, the change of contaminant ratios between the B22 sample and the combined set of samples from B, B2 and C, suggests that that poly-aromatic hydrocarbons have relatively low degradation rates compared to the mono-aromatic compounds, especially the xylenes and toluene, which is in line with previous findings in the literature.

Electron acceptors

Analysis of groundwater samples from several locations in the Griftpark shows that O_2 and NO_3^- are not present in the groundwater of the first aquifer. The presence of highly variable concentrations of SO_4^{2-}, ranging from 0 to 237 mg/L with an average of 79 mg/L, and its reduced compound sulphide, S(-II), ranging from 0.04 to 27.7 mg/L with an average of 3.5 mg/L, in the groundwater samples from wells B, B2 and C, indicates the occurrence of sulphate-reducing biodegradation. Figure 3.4 shows plots of tar aromatic and SO_4^{2-} concentration at different depths in MLS wells B, B2 and C. Generally, samples with higher aromatic concentrations exhibit lower SO_4^{2-} concentrations, indicating that sulphate reduction likely occurs in the presence of tar aromatics in the Griftpark.

Figure 3.5 shows SO_4^{2-} concentrations, on a log-scale, plotted against total tar aromatic concentrations in all groundwater samples taken from the Griftpark. A general trend of decreasing SO_4^{2-} concentrations with increasing contamination levels is observed when all the data is considered together, although no clear direct relationship is apparent. Fluctuations in the sulphate levels, even at high tar aromatic concentrations, may be caused by the aforementioned presence of sulphate sources in the subsurface and indicate that reduction potential throughout the park varies. Possible sources of sulphate include gypsum created during gas purification or cement rubble from former factories.

We measured total Fe(III) content in soil samples from locations A, B and C. The results for locations B and C were plotted in Figure 3.4. At the uncontaminated location A, soil samples were collected from 50, 53 and 61.5 m-bgl. The samples contained 2.7, 29.0 and 8.1 g/kgdm of Fe(III), respectively. In soil collected at location B, Fe(III) concentrations ranged from 2.0 to 17.0 g/kgdm (with an average of 6.9 g/kgdm), while at location C they ranged from 0.9 to 5.1 g/kgdm (with an average of 3.9 g/kgdm).

Figure 3.4 does not reveal a direct correlation between levels of aromatic hydrocarbon and sulphate and the iron content per well. The lack of detailed iron speciation makes it difficult to predict the reduction potential from iron

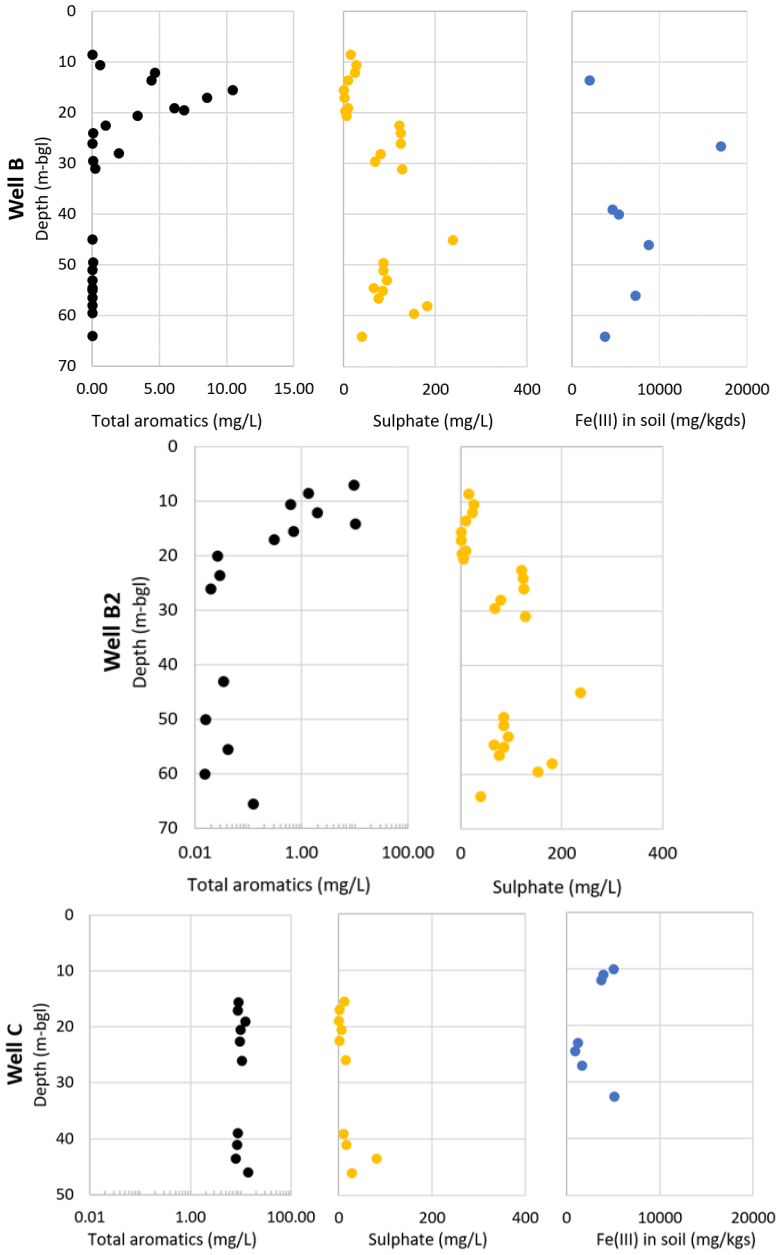

Figure 3.4: Dissolved tar aromatic (black) and SO_4^{2-} (yellow) concentrations from groundwater samples collected from different depths in MLS wells B, B2 and C, as well as total $Fe(III)$ content (blue) in soil samples collected from wells B and C.

in the subsurface. Furthermore, at FMGPs, fluctuations in iron content in the sediment may be caused by slag dumped at the site, resulting in heterogeneous

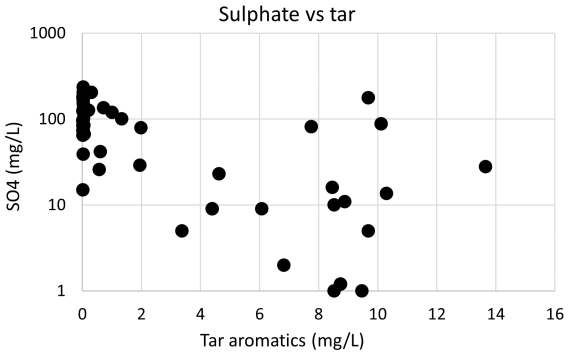

Figure 3.5: Sulphate versus total tar aromatic hydrocarbon concentrations.

iron content and availability [29]. Furthermore, variations in Fe(III) concentrations may also be influenced by peaty depositions occurring at the Griftpark. Despite these limitations, we observed that least contaminated locations had the highest concentrations of Fe(III), which could indicate biodegradation causing an extraction of Fe(III) from the sediment. The detection of reduced iron, Fe(II), in all groundwater samples, at a maximum concentration of 15 mg/L and average of 5.3 mg/L, provides more conclusive evidence of iron reduction.

Likewise, Mn(IV) in sediment was measured between 81-1,000 mg/kgdm at A, 78-290 mg/kgds at B and 8.3-160 mg/kgdm at location C. Reduced manganese, Mn(II), was measured in all groundwater samples, at a maximum concentration of 1.7 mg/L and average of 0.6 mg/L These results indicate the occurrence of manganese reduction. However, considering manganese concentrations in the subsurface are significantly lower than that of iron, suggests manganese reduction is a minor contributor to the overall degradation at the Griftpark.

Figure 3.6 depicts concentrations of S(-II), Fe(II), Mn(II) and CH_4 in all groundwater samples collected from locations B, B2 and C, against total tar aromatic concentrations. Figure 3.6b shows that S(-II) concentrations are generally low and not strongly correlated to aromatic hydrocarbon concentrations. This is likely due to the precipitation of S(-II) with Fe(II) to form iron-sulphide ($Fe^{2+} + HS^- \leftrightarrow FeS + H^+$). Figure 3.6a shows that Fe(II) concentrations were high mostly at low aromatic concentrations, suggesting iron reduction occurs mostly at these concentrations. This observation is consistent with the iron depletion in the sediment at locations with significant contamination exposure. Figure 3.6c shows that Mn(II) concentrations were also high mostly at low aromatic concentrations, but are around ten times lower than those of Fe(II).

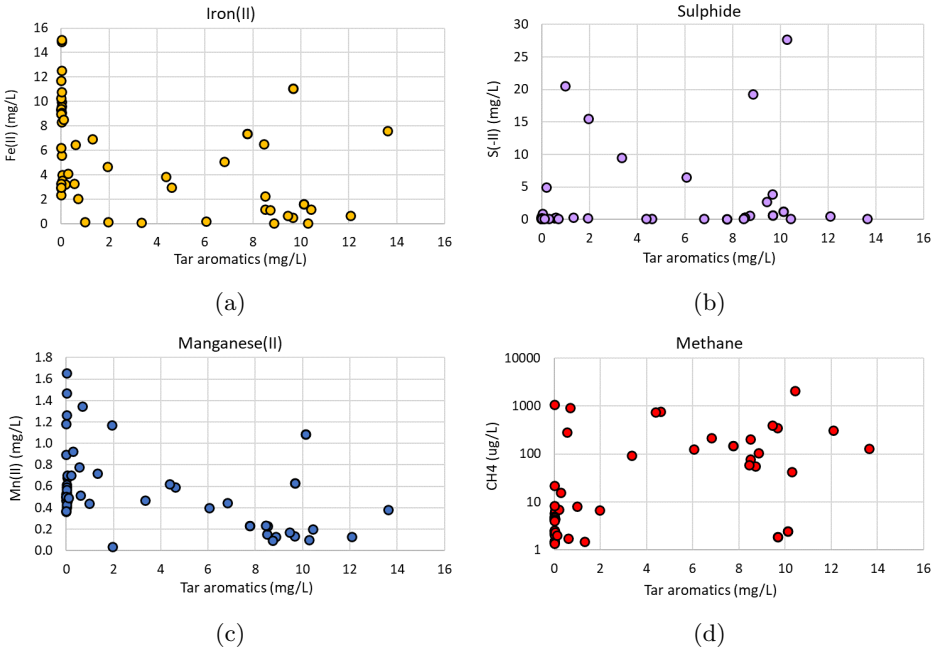

Figure 3.6: Concentrations of $Mn(IV)$, $S(-II)$, $Fe(II)$ and CH_4 versus total tar aromatic concentrations. Because of the large variations in methane concentrations, methane is shown on a log-scale.

Methane was detected in all groundwater samples, with concentrations peaking up to 2000 $\mu g/L$, indicating that methanogenesis occurs widely throughout the site. Figure 3.6d shows that CH_4 concentrations are generally low at low tar aromatic concentrations, but no clear relationship exists between the two. Methanogenesis has previously been demonstrated to be able to support significant biodegradation, including that of poly-aromatic hydrocarbons such as naphthalene, and can occur simultaneously with sulphate and iron reduction [242, 56, 50, 28, 148]. Although the plots in Figure 3.7 illustrate that at the Griftpark, methane production is most pronounced when sulphate or iron reduction is limited, as indicated by low levels of sulphate and Fe(II), respectively, methane is measured at high concentrations at locations where sulphate and iron reduction are likely occurring as well. Considering the stability of methane in groundwater, the heterogeneous flow conditions and multiplicity of contamination source zones, it is challenging to estimate the location of methane production in the park. We refrained from plotting all reduced species against depth, as was done for tar aromatics, sulphate and mineral iron in Figure 3.4, as the results do not provide additional insight into the biochemical processes.

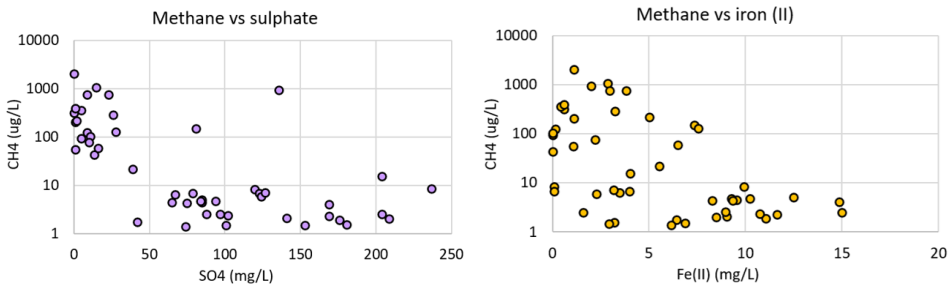

(a) (b)

Figure 3.7: Concentrations of CH_4 versus SO_4^{2-} and $Fe(II)$. Because of the large variations in methane concentrations, methane is shown on a log-scale.

The absence of a dominant groundwater flow direction and the presence of multiple coal tar source locations, poses significant challenges for contaminant plume tracking and mass balance analysis. In most groundwater samples, reduced products resulting from various electron-accepting processes were observed simultaneously. This could be attributed to either concurrent reduction processes in the subsurface, as has been reported at other sites [148, 253], but also to the mixing of chemicals in groundwater that has passed multiple tar source zones. The visualisation in Figure 3.8 illustrates the concept of groundwater mixing resulting from subsurface heterogeneities and multiple zones of pure phase coal tar, explaining the effects on dissolved contaminant composition, electron acceptor reduction and isotope fractionation.

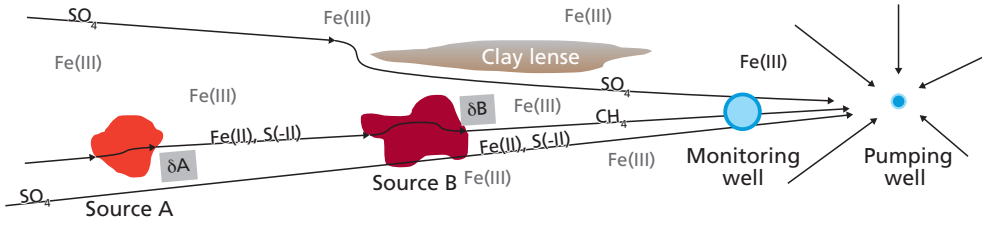

- Dissolution of source A with fraction δA
- Degradation and fractionation of compounds source A
- Reduction of SO_4 and Fe(III)

- Dissolution of source B with fraction δB
- Mixing of compounds source A and B
- Degradation and fractionation of compounds source A and B
- Methanogenesis
- Reduction of SO_4 and Fe(III)

- Continued fractionation and mixing of A and B
- Mixing of EAs and their reduced forms through dispersion and diffusion

Figure 3.8: Conceptualisation of the mixing of groundwater at locations with multiple pure phase tar zones, in heterogeneous aquifers with low flow velocities. Straight arrows represent generalised groundwater flow direction.

We employed a stoichiometric analysis approach to gain insight into the relative contribution of different electron-reducing processes to the total reduction of tar aromatics. Equations 3.6 and 3.7, depicting the stoichiometric relations of sulphate and iron reduction of benzene, toluene and naphthalene, reveal that when iron and sulphate reduction are responsible for oxidising the same number moles of hydrocarbon, Fe(II) would be created at eight times higher molar concentrations than S(-II). On average, the molar concentrations of Fe(II) were found to be 43 times larger than the molar concentrations of S(-II) in the B, B2, and C groundwater samples, which would indicate that iron reduction facilitates the reduction of more than five times as many moles of substrate as sulphate reduction.

In the samples with tar aromatic concentrations below 1 mg/L, the molar concentrations of Fe(II) were found to be 62 times larger than the molar concentrations of S(-II) in the B, B2, and C groundwater samples, indicating that iron reduction facilitates the reduction of almost eight times as many moles of substrate as sulphate reduction. In the samples with tar aromatic concentrations above 1 mg/L this ratio decreased to an average of 18 (above 8 mg/L to 16), indicating that iron reduction facilitates the reduction of approximately twice as many moles of substrate as sulphate reduction. This further proves the importance of iron reduction at locations where iron minerals are not yet depleted from the subsurface. Notably, the stoichiometric calculation did not consider the disappearance of Fe(II) and S(-II) through FeS precipitation. As the stoichiometric yield of S(-II) is smaller than that of Fe(II) for the oxidation of a mole of hydrocarbons, FeS precipitation has a stronger impact on the disappearance of S(-II) than Fe(II). Assuming that Fe(II) and S(-II) precipitate exclusively as FeS, we calculated that if a theoretical 60% of the moles of created S(-II) precipitated in samples with hydrocarbon concentrations above 1 mg/L, the contribution of iron and sulphate reduction would be equal. However, in reality, Fe(II) also precipitates in other minerals, such as magnetite and siderite, leading to a higher ratio of Fe(II) to S(-II) than anticipated from this calculation. Overall, these results suggest that iron is the most important electron acceptor in the Griftpark and that the concentration and depletion of bio-available iron-oxides in the subsurface is the determining factor for biodegradation rates.

$$
\begin{aligned}
C_6H_6 + 3.75SO_4^{2-} + 3H_2O &\rightarrow 6HCO_3^- + 3.75HS^- + 2.25H^+ \\
C_7H_8 + 4.5SO_4^{2-} + 3H_2O &\rightarrow 7HCO_3^- + 4.5HS^- + 2.5H^+ \\
C_{10}H_8 + 6SO_4^{2-} + 6H_2O &\rightarrow 10HCO_3^- + 6HS^- + 4H^+
\end{aligned} \tag{3.6}
$$

$$
\begin{aligned}
C_6H_6 + 30Fe^{3+} + 18H_2O &\rightarrow 6HCO_3^- + 30Fe^{2+} + 36H^+ \\
C_7H_8 + 36Fe^{3+} + 21H_2O &\rightarrow 7HCO_3^- + 36Fe^{2+} + 43H^+ \\
C_{10}H_8 + 48Fe^{3+} + 30H_2O &\rightarrow 10HCO_3^- + 48Fe^{2+} + 58H^+
\end{aligned} \tag{3.7}
$$

Although the results show some general trends in redox conditions at the site, the results also demonstrate a large level of variability and therefore unpredictability of subsurface conditions at the Griftpark. Similar variations at a single site were documented by Kharey et al. at two fuel-contaminated groundwater sites [155]. They found that nitrate, sulphate and iron reduction occurred with varying levels of potential at different locations of the sites, making it challenging to discern clear trends between hydrocarbon concentrations with the electron accepting processes.

Metabolites

In total, 76 different metabolites were found in the 28 groundwater samples taken from the Griftpark (full results shown in Appendix E). Metabolites found include hydroxylated, carboxylated, succinylated and methylated intermediates. Some of the detected metabolites are signal metabolites that indicate the active anaerobic degradation of toluene, ethylbenzene, xylenes, styrene, trimethylbenzene, acenaphthylene, anthracene, fluoranthene, pyrene, phenanthrene. As indicators of the anaerobic degradation of benzene, putative metabolites were detected (benzoate, toluene, phenol and para-hydroxybenzoate). Twelve different metabolites were encountered that can be related to the anaerobic degradation of naphthalene (e.g. naphthyl-2-methyl-succinic and naphtoic acids). For indene and indane degradation, 18 metabolites were detected (e.g. 2-indane-carboxylic acid, 1H-indene-3-carboxylic acid and 1H-indene-2-carboxylic acid). Furthermore, in many of the groundwater samples, metabolites were found that indicate the anaerobic degradation of aliphatic hydrocarbons in mineral oil, as well as nitrogen-, sulphide- and oxygen-containing aromatics, indicating the presence of other hydrocarbons that were not taken up in the 90% mass representation used for GC-MS analysis.

Figure 3.9a displays the total concentration of the 35 metabolites for which concentrations could be determined, versus the total concentration of tar compounds. Although it is evident that low concentrations of aromatic hydrocarbons lead to low metabolite concentrations, no clear correlation between metabolite and contaminant concentrations can be discerned. This suggests that active biodegradation occurs both at low and high contamination levels, a finding that has previously been reported at other sites contaminated

with aromatic hydrocarbons [296] and in laboratory [321, 77]. Even in simpler systems, such as bench-scale batch tests and at field sites with known tar locations and plume distributions, it is challenging to use metabolites as a quantitative measure for the extent or rate of biodegradation as their presence is part of a continuous process of formation and degradation which is influenced by many factors [87, 195, 46].

Figure 3.9b shows the diversity of detected metabolites versus the total concentration of tar compounds. It indicates that with increasing tar concentrations, the variety of metabolites increases until a maximum in diversity is reached.

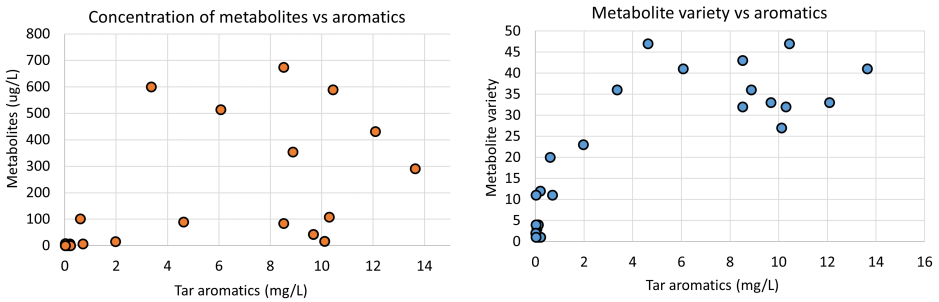

(a) (b)

Figure 3.9: Concentration and variety of metabolites versus total concentration of tar aromatics.

Isotopic ratios

We analysed the isotope fractions of $\delta^{13}C$ and $\delta^{2}H$ for coal tar compounds in groundwater samples collected from wells B, B2 and C, as well as a pure-phase tar extract from 48 m-bgl at well C, as shown in Table 3.1. The various gas manufacturing methods deployed across the site may have caused a maximum variability of approximately 3‰ in $\delta^{13}C$ values of different pure phase coal tars [201, 200]. Using this threshold, we conclude that the observed variations in isotope ratios signal biodegradation of all compounds except naphthalene and ethylbenzene, although the metabolite analysis did prove their degradation at the site. The maximum variation in $\delta^{13}C$ between all samples is smallest for naphthalene (0.9‰) and largest for o-xylene (11.7‰). For naphthalene, that occurs at the highest concentrations of the investigated contaminant mixture, it is suspected that dissolution limitation to biodegradation masks isotope fractionation. Such masking effects are known to occur with the more hydrophobic compounds, such as naphthalene, indene and indane [302].

It was found that groundwater samples with highest tar aromatic concentrations did not necessarily show the lightest isotope fractions. This may be interpreted caused by mixing of groundwater carrying contamination with heavier isotopic ratios originating from up-gradient sources, as explained in Figure 3.8.

Well	B						B2			
Depth	12	15.5	17	19	20.5	28	7	10.5	14	15.5
Hydrogen										
δ^2H-B	-106 ± 2	-110 ± 10	-118 ± 3	-117 ± 10	-90 ± 11	dl	-77 ± 4	-75 ± 9	-51 ± 6	-61 ± 2
δ^2H-T	dl	dl	+78 ± 2	dl	dl	dl	dl	dl	+38 ± 5	dl
δ^2H-E	+80 ± 20	-154 ± 16	-169 ± 7	-170 ± 8	-173 ± 7	-162 ± 5	-179 ± 4	-161 ± 2	-164 ± 6	+2 ± 2
δ^2H-m/pX	+62 ± 2	-99 ± 10	-115 ± 2	-49 ± 9	-65 ± 9	-58 ± 6	-165 ± 2	-136 ± 11	dl	-121 ± 2
δ^2H-oX	+70 ± 14	-43 ± 16	-64 ± 6	+9 ± 4	-22 ± 7	-97 ± 6	-138 ± 6	dl	-126 ± 8	-11 ± 4
δ^2H-Ia	-142 ± 11	-145 ± 11	-159 ± 11	-140 ± 13	-136 ± 2	dl	-132 ± 6	-150 ± 8	-106 ± 2	-81 ± 2
δ^2H-N	-43 ± 14	-54 ± 4	-39 ± 8	-42 ± 2	-34 ± 2	-28 ±2	-55 ± 2	-60 ± 6	-27 ± 7	-60 ± 5
Carbon										
δ^{13}C-B	-26,1 ± 0,5	-25,8 ± 0,5	-24,1 ± 0,5	-24,1 ± 0,5	-25,3 ± 0,5	-20,9 ± 0,5	-26,5 ± 0,5	-26,2 ± 0,5	-25,2 ± 0,5	-25,7 ± 0,5
δ^{13}C-T	-22,8 ± 0,5	-17,8 ± 0,5	-22,1 ± 0,5	-20,2 ± 0,6	-18,7 ± 0,5	-23,8 ± 0,5	-21,0 ± 0,5	-20,6 ± 0,5	-23,8 ± 0,5	-18,1 ± 0,5
δ^{13}C-E	-21,5 ± 0,5	-23,2 ± 0,5	-23,4 ± 0,5	-24,2 ± 0,8	-23,7 ± 0,5	-24,2 ± 0,5	-24,1 ± 0,5	-22,8 ± 0,5	-24,1 ± 0,5	-22,5 ± 0,5
δ^{13}C-m/pX	-17,5 ± 0,5	-24,5 ± 0,5	-25,1 ± 0,5	-22,0 ± 0,5	-23,1 ± 0,5	-21,0 ± 0,5	-26,2 ± 0,6	-23,7 ± 0,5	-26,0 ± 0,5	-25,0 ± 0,5
δ^{13}C-oX	-14,0 ± 0,5	-21,1 ± 0,5	-22,1 ± 0,5	-18,0 ± 0,5	-19,4 ± 0,5	-23,8 ± 0,5	-25,7 ± 0,5	-18,1 ± 0,5	-25,1 ± 0,5	-21,1 ± 0,5
δ^{13}C-Ia	-24,7 ± 0,5	-24,7 ± 0,6	-24,9 ± 0,5	-24,0 ± 0,5	-24,6 ± 0,5	-26,9 ± 0,5	-27,6 ± 0,5	-26,9 ± 0,5	-25,6 ± 0,5	-23,0 ± 0,5
δ^{13}C-N	-26,3 ± 0,5	-26,8 ± 0,5	-26,7 ± 0,5	-26,7 ± 0,5	-26,7 ± 0,5	-26,3 ± 0,5	-27,0 ± 0,5	-26,8 ± 0,5	-27,2 ± 0,5	-26,9 ± 0,5
δ^{13}C-Ie	-23,2 ± 0,5	dl	dl	dl	-23,0 ± 0,5	-23,7 ± 0,5	-25,7 ± 0,5	-25,4 ± 0,6	-25,8 ± 0,5	-24,4 ± 1,1

Well	C					Pure tar C
Depth	15.5	19	26	38,5-39	45,5-46	48
Hydrogen						
δ^2H-B	-99 ± 2	-67 ± 6	-93 ± 4	-72 ± 5	-91 ± 2	dl
δ^2H-T	+170 ± 6	dl	+139 ± 10	-46 ± 2	+13 ± 4	dl
δ^2H-E	-165 ± 6	-167 ± 7	-155 ± 2	-155 ± 2	-163 ± 5	-147 ± 6
δ^2H-m/pX	-131 ± 2	-122 ± 10	-134 ± 2	-127 ± 3	-138 ± 3	-112 ± 8
δ^2H-oX	-108 ± 3	-101 ± 7	-96 ± 3	-100 ± 2	-113 ± 2	-129 ± 6
δ^2H-Ia	-153 ± 4	-155 ± 6	-147 ± 9	-109 ± 11	-159 ± 6	-89 ± 8
δ^2H-N	-52 ± 3	-49 ± 3	-55 ± 2	-47 ± 8	-56 ± 6	-62 ± 4
Carbon						
δ^{13}C-B	-26,7 ± 0,5	-25,8 ± 0,5	-26,0 ± 0,5	-26,0 ± 0,5	-25,5 ± 0,5	-26,1 ± 0,5
δ^{13}C-T	-18,8 ± 0,6	-16,9 ± 0,5	-21,6 ± 0,6	-25,3 ± 0,5	-24,9 ± 0,5	-25,8 ± 0,5
δ^{13}C-E	-25,2 ± 0,5	-24,2 ± 0,5	-24,3 ± 0,5	-24,4 ± 0,5	-24,3 ± 0,5	-25,0 ± 0,5
δ^{13}C-m/pX	-26,2 ± 0,5	-24,7 ± 0,5	-25,7 ± 0,5	-25,5 ± 0,5	-25,4 ± 0,5	-24,6 ± 0,5
δ^{13}C-oX	-25,6 ± 0,5	-24,6 ± 0,5	-24,6 ± 0,5	-24,7 ± 0,5	-25,2 ± 0,5	-24,6 ± 0,5
δ^{13}C-Ia	-23,8 ± 0,5	-24,8 ± 0,5	-25,2 ± 0,5	-25,2 ± 0,5	-25,1 ± 0,5	-25,2 ± 0,6
δ^{13}C-N	-27,0 ± 0,5	-26,6 ± 0,5	-26,7 ± 0,5	-26,8 ± 0,5	-26,8 ± 0,5	-26,6 ± 0,5
δ^{13}C-Ie	-21,1 ± 0,5	dl	-24,0 ± 1,0	-25,9 ± 0,5	-26,3 ± 0,5	-25,6 ± 0,9

dl below detection limit
lightest
heaviest
aromatics > 9 mg/L

Table 3.1: Isotope fractions of $\delta^{13}C$ and δ^2H for a selection of samples from well B, B2 and C, as well as a pure tar sample. Per well, the lightest and heaviest fraction measured for each compound is indicated by dark and light grey cells respectively. The locations near which the presence of pure tar is expected are indicated with dotted cells.

Figure 3.10 shows plots of the $\delta^{13}C$ versus δ^2H signatures of the BTEXIaN compounds at locations B, B2 and C (indene is excluded as no δ^2H data was obtained for it). By fitting linear regressions between the hydrogen and carbon isotope signatures, we obtained $\Lambda^{H/C}$ values, shown in the figure, alongside their R^2 values. We find good fits (R^2 >0.9) for benzene (B2), toluene (C), m/p- xylene (B) and o-xylene (B and B2). Using the $\Lambda^{H/C}$ values,

we could identify corresponding enzymatic reactions as reviewed by Vogt et al. [302, 303]. The fits for benzene points at putative carboxylation, the fits for toluene, m/p-xylene and o-xylene correspond with anaerobic fumarate addition. We obtained less satisfactory ($0.9 > R^2 > 0.8$) fits for ethylbenzene, indane and naphthalene and the thus obtained $\Lambda^{H/C}$ values could not be linked to any known enzymatic reactions. Although the application of the Rayleigh model can lead to successful evaluation of biodegradation in field studies, if dissolution from NAPL is involved, the Rayleigh model may not apply [270]. Mass-transfer limitations impede describing the isotopic fractionation with a constant enrichment factor, causing a masking of kinetic isotope effects [7, 283]. The slower the groundwater flow and the smaller the dissolution rate, the less reliable the quantitative interpretation of isotope signatures will be. Thus, the effects will be strongest for the less soluble PAHs. Poor correlation for $\Lambda^{H/C}$ values for naphthalene have been observed in previous field studies [295, 282, 302, 168].

To study the significance of the measured isotopic ratio variations, unreacted fractions were calculated per sampling well, see Equation 3.1. For the analysis, the lightest sample from each MLS well was interpreted as the original fraction $\delta^2 H(0)$ at that location. The percentage of biodegradation $B\%$ in the other samples was then calculated for each compound using Equation 3.3, with maximum and minimum per mil enrichment factors ϵ taken from literature, see Table 3.2 [302]. The lack of a clearly defined connection between two sampling locations at the Griftpark site, because samples are not collected along flow paths and source zones are unknown, prevents the calculation of biodegradation rates using Equation 3.4, which is typically a key advantage of isotope fractionation analysis [142, 245, 244, 121]. Instead, the results are used solely as a general indicator of biodegradation at the site and the degradation percentages of the samples at each MLS were averaged.

	ϵ(max)	ϵ(min)
δ^2H-Benzene	-29	-79
δ^2H-Toluene	-17	-126
δ^2H-Ethylbenzene	-78	-189
δ^2H-m,p-Xylene	-19	-50
δ^2H-o-Xylene	-19	-50
δ^2H-Naphthalene	-47	-100
δ^{13}C-Benzene	-0.6	-3.6
δ^{13}C-Toluene	-0.7	-6.7
δ^{13}C-Ethylbenzene	-1.3	-4.1
δ^{13}C-m,p-Xylene	-0.7	-2.7
δ^{13}C-o-Xylene	-0.7	-2.7
δ^{13}C-Naphthalene	-0.4	-5

Table 3.2: Min and max values for ϵ used in the calculations [302].

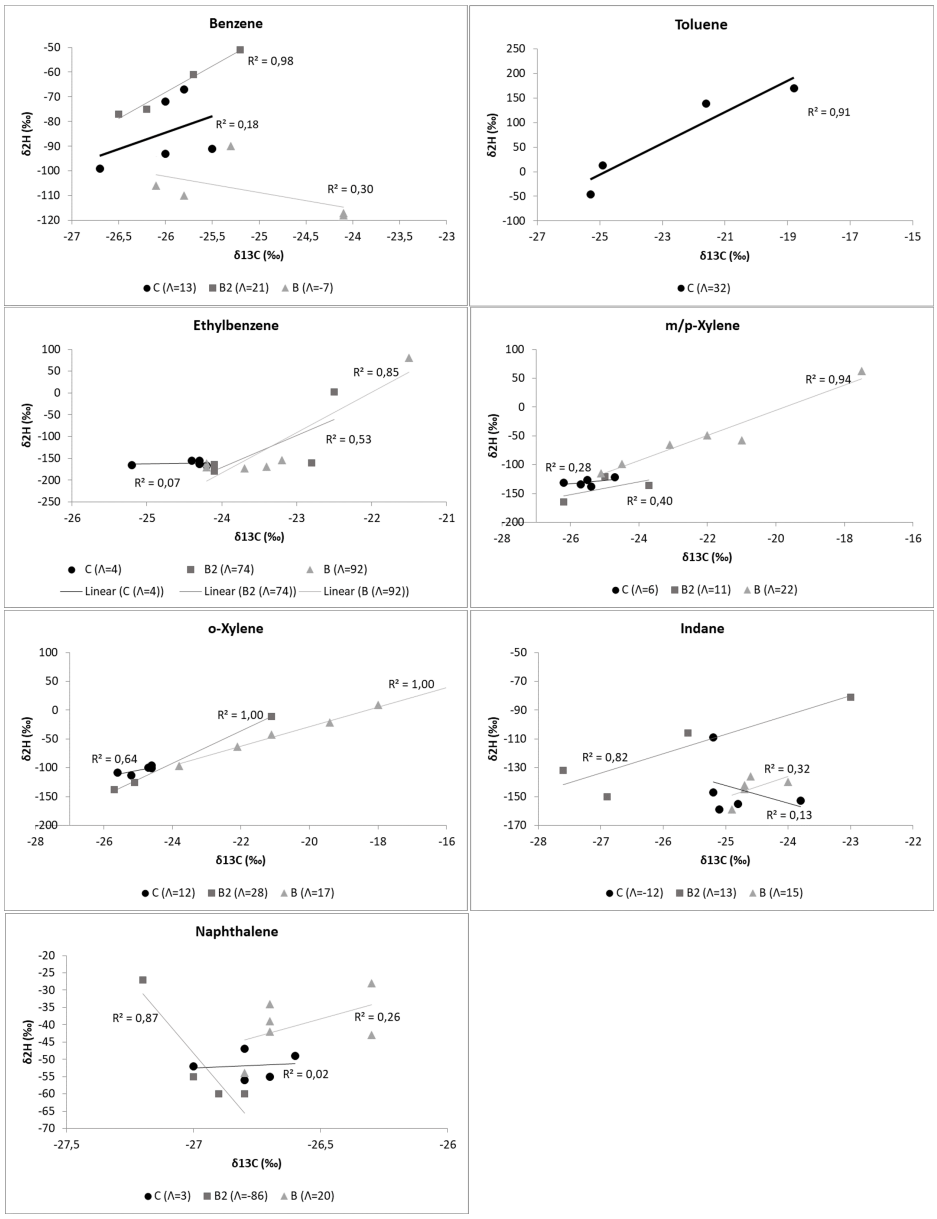

Figure 3.10: Linear regression fits of $\delta^2 H$ versus $\delta^{13} C$ for the BTEXIaN compounds at wells B, B2 and C.

The results for the BTEX and naphthalene compounds shown in Table 3.3, indicate that especially toluene and xylene isomers degrade well and that benzene, ethylbenzene and naphthalene are the least degraded compounds. Also from literature, toluene and xylenes are known to degrade fastest under

iron- and sulphate reducing conditions [274]. No biodegradation percentages were calculated for indene and indane, as no ϵ values are reported in the literature for these compounds. However, the $\delta^{13}C$ isotope fractions of indane and indene show variations of 4.6‰ and 5.2‰, above the maximum variation of 3‰ that could be caused by the deployment of different gas manufacturing methods, indicating indane and indene degradation in the subsurface.

Compound	Well	Biodegradation %			
		low ϵ		high ϵ	
		δ^{13}C	δ^{2}H	δ^{13}C	δ^{2}H
Benzene	B	82	33	39	15
	B2	68	38	20	17
	C	76	45	22	21
Toluene	B	94		39	
	B2	99		44	
	C	86	99	46	65
Ethylbenzene	B	55	30	25	20
	B2	68	46	30	28
	C	51	11	20	5
p/m-Xylene	B	90	90	63	68
	B2	69	88	35	57
	C	69	42	28	19
o-Xylene	B	98	96	76	77
	B2	86	76	66	59
	C	68	48	27	23
Naphthalene	B	43	31	5	16
	B2	53	31	6	17
	C	50	11	5	5

Table 3.3: Average biodegradation percentages of the BTEXN compounds per sampling well, calculated using the lightest sample in each well as $\delta^{13}C(0)$ or $\delta^{2}H(0)$) in Equation 3.3 and using min and max ϵ values found in literature.

Microbial presence

The DNA analyses revealed the presence of the benzyl succinate synthesis enzyme (*bssA*) of sulphate and iron reducing bacteria at a maximum of 472,000 gene copies/mL, confirming the subsurface capacity of biodegradation of toluene and xylenes through succinylation reactions [136]. The 16S rRNA gene copies of *Peptococcaceae* bacteria were detected in over 50% of the groundwater samples, albeit at low concentrations (maximum 477 genes/mL within the contained zone), suggesting a degradation potential of benzene and naphthalene [3, 293, 167]. Benzene carboxylase (*abcA*), that catalyses the degradation of benzene [3], was detected in only two out of 23 samples from the contained zone (at maximum 30 gene copies/mL). Since also *Pep-*

tococcaceae was present at low concentrations, it indicates that the potential for anaerobic benzene degradation at the Griftpark is relatively limited. The presence of genes encoding naphthalene carboxylase (*ncA*), naphtyl-2-methyl succinate synthase (*nmsA*) and naphthoyl-CoA-reductase (*ncrA*) genes (combined at maximum 22,100 gene copies/mL) indicate a strong potential for anaerobic naphthalene degradation [215, 202, 255, 208]. Presence of the 1-methylalkyl succinate synthesis (*assA*) gene in almost all samples indicates the potential of anaerobic degradation of the aliphatic hydrocarbons present in mineral oil [47].

Archaea 16S RNA genes were observed in concentrations 10 to more than 1,000 times lower than those of the iron and sulphate reducing bacteria. While genes encoding benzyl succinate synthase (*bssA*) of nitrate reducing bacteria were found at low concentrations in only some wells within the contained zone (maximum 397 gene copies/mL), they were found at higher concentrations in samples from the second aquifer in well A just outside the contained zone (max 12,300 gene copies/mL). This suggests the low potential for nitrate reduction at the Griftpark site, which aligns with the absence of nitrate in the groundwater of the first aquifer but indicates some potential in the second aquifer, where nitrate is present. Additionally, there appears to be a slight correlation between archaea and methane concentrations (not shown), as expected due to the involvement of archaea in methanogenic processes.

Figure 3.11 depicts the total 16S rRNA and target gene counts versus total tar aromatic concentrations. The results indicate that at low aromatic concentrations, the total gene count is relatively high compared to that at higher aromatic concentrations, while the target gene count is low at lower aromatic concentrations but increases at higher concentrations. This observation suggests a shift in the bacterial community towards a more favorable state for degrading the aromatic hydrocarbons present at the site.

In order to assess the trend in the targeted microbial community, the ratios of the targeted genes are plotted against increasing total tar aromatic hydrocarbon concentrations in Figure 3.12. The figure demonstrates that the ratio of gene copies of *bssA* of sulphate and iron reducers tends to increase as the aromatic concentration rises, providing further proof for the potential of iron and sulphate-reducing biodegradation at the Griftpark.

The abundance of naphthalene as a dissolved contaminant in the Griftpark makes the genes associated with naphthalene degradation a valuable indicator for assessing microbial conditions. In Figure 3.13 we show the total count of targeted genes involved in naphthalene degradation against increasing total aromatic concentrations. The results suggest that highest microbial potential exists in the moderate range of tar aromatic hydrocarbon concentrations. It is well-established that biodegradation can occur even in source zones, indicating

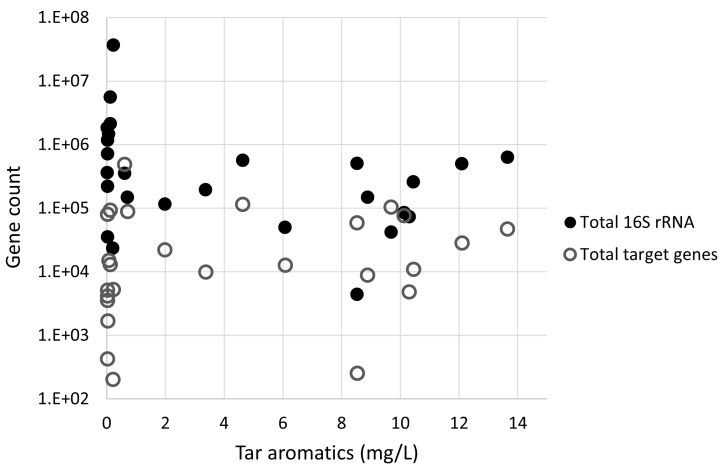

Figure 3.11: Total 16S rRNA and total target gene counts versus total tar aromatic concentrations.

that it remains feasible within the high range of total aromatic concentrations measured at the Griftpark (10-14 mg/L) [296, 204]. Therefore, we attribute the decline in microbial potential at these higher concentrations to the depletion of electron acceptors rather than toxicity resulting from high aromatic concentrations.

No correlation was observed between the concentration or diversity of total bacteria and metabolites in the groundwater samples. This finding contrasts with a previous laboratory study by Zhong et al. (2011) where mixed bacterial cultures were found to produce a broader range of metabolites [329].

Influence of soil type

A minor investigation was conducted to verify whether soil conductivity has a potential influence on biodegradation at the Griftpark. Results (not shown) indicated that contaminants, bacteria, metabolites and reduced electron acceptors occur at similar concentrations in all soil types and therefore that biodegradation has equal potential across the site.

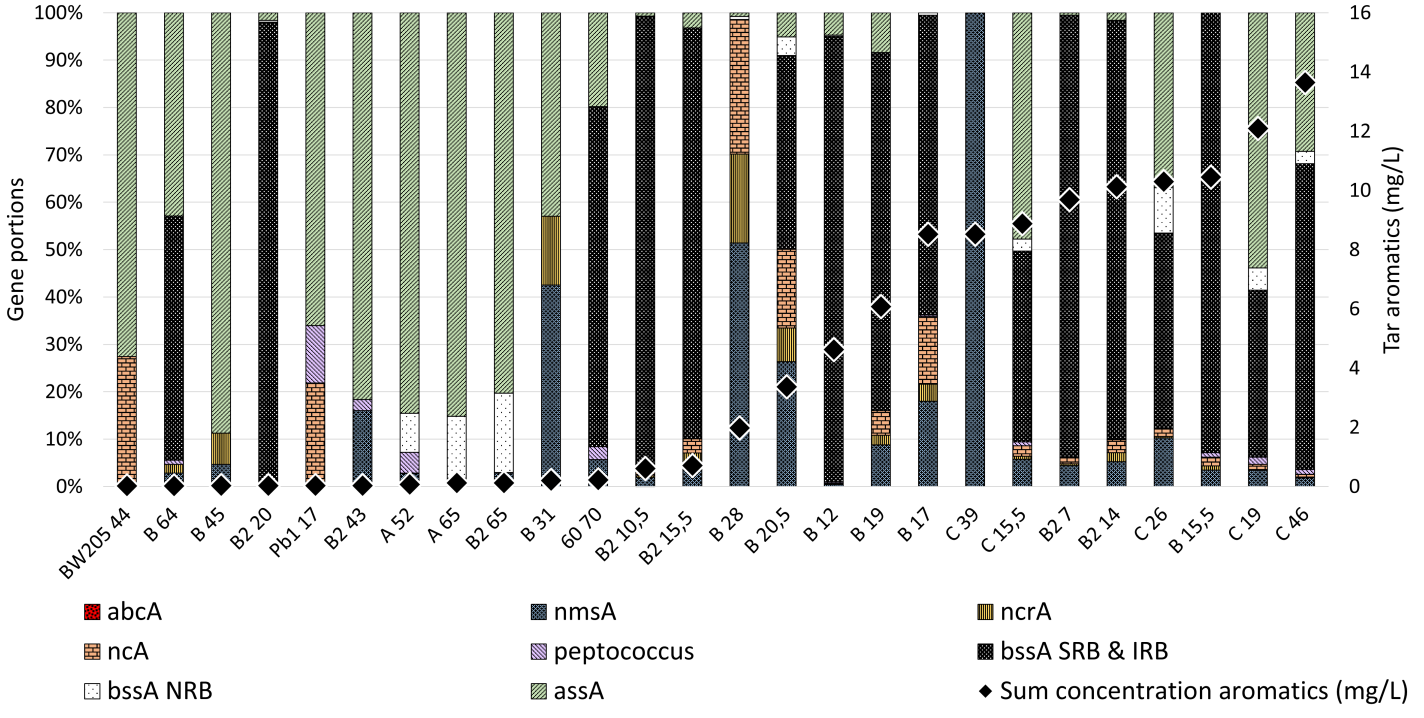

Figure 3.12: Gene portions (coloured bars, left axis) along increasing total dissolved BTEXIeIaN concentrations (black diamonds, right axis).

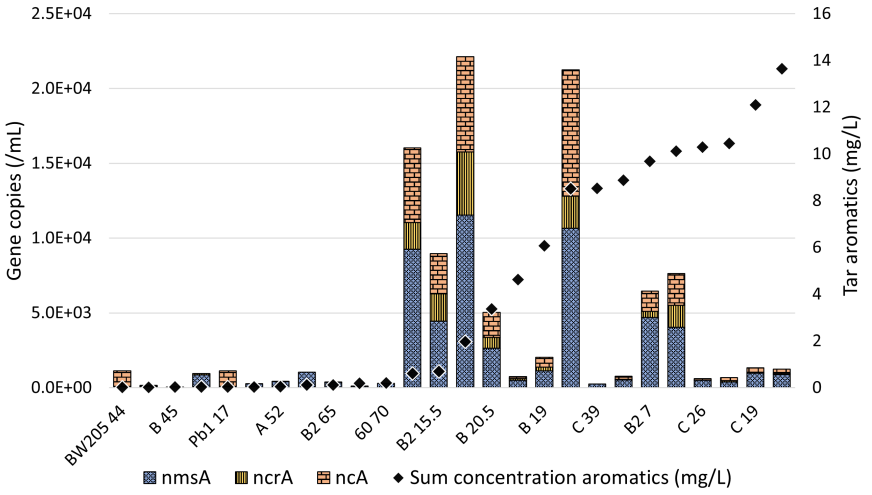

Figure 3.13: Enzymes that take part in the degradation of naphthalene, the most occurring contaminant at the Griftpark (coloured bars, left axis), along increasing total dissolved BTEXIeIaN concentrations (black diamonds, right axis).

3.5 Conclusions

To investigate the occurrence of biodegradation at the Griftpark, three standard lines of evidence were followed: (1) changes in the contamination (i.e. contaminant concentrations, metabolites and isotope ratios); (2) the physiochemical conditions of the groundwater (i.e. the available electron acceptors); and (3) the presence of microbial DNA associated with the potential respiration processes.

The investigation of natural biodegradation at field sites commonly relies on monitoring soil and groundwater along or across a contaminant plume. However, at the Griftpark, a traceable contaminant plume is absent. This is due to several factors, including the containment of the site by a vertical barrier, the use of groundwater pumping from various locations and depths (with fluctuating rates over time), the strong heterogeneity of the subsurface, and incomplete knowledge of all source zone locations. As a result, it becomes impractical to relate sampling locations to each other in time or space. These factors lead to a number of site-specific considerations regarding the standard assessment of in situ biodegradation.

We found that:

- The monoaromatic compounds benzene, toluene, ethylbenzene, o/m/p-xylene, 1,2,4-trimethylbenzene, propylbenzenes, ethyltoluenes, indene, indane and styrene and the double-ringed compounds naphthalene and

methyl-naphthalenes constitute the major mass of dissolved contaminants

- We found that hydrocarbon concentrations well below their solubility levels close to contaminant source zones indicated the occurrence of biodegradation
  - Due to the absence of a traceable contaminant plume and the presence of multiple and unknown source zones, contaminant concentrations cannot be used to make mass balance analyses to obtain biodegradation rates
- Shifting ratios between individual compounds in the contaminant mixture indicated relatively fast degradation of mainly toluene and xylenes
  - Because coal tars occurring throughout the site are expected to vary in composition, only general trends in changing ratios of contaminants throughout the combined data set can be used to indicate biodegradation
- Sulphate and ferric iron are the major electron acceptors used for the degradation of coal tar aromatics at the Griftpark. Manganese reduction and methanogenesis also occur
  - The mixing of groundwater and absence of a traceable plume causes that no easily distinguishable redox zones form. Therefore, it is difficult to predict what processes occur where
  - Without the presence of a traceable contaminant plume, no mass balance calculations of electron acceptors can be made to obtain biodegradation rates
- Signature metabolic intermediates encountered indicated the active degradation of toluene, ethylbenzene, xylene, styrene, trimethylbenzene, acenaphthylene, anthracene, fluoranthene, pyrene and phenanthrene under sulphate- and iron-reducing as well as methanogenic conditions. Metabolites that indicate the putative degradation of benzene, naphthalene, indene and indane were also found
  - As for metabolites it is their presence per se that is used as indicator of biodegradation and not their concentrations, the site's heterogeneous conditions have no great effect on their interpretation for biodegradation assessment
- Carbon and hydrogen isotope fractions indicated significant biodegradation of benzene, toluene and xylenes. Linear regression fits reveal

anaerobic biodegradation pathways of putative carboxylation for benzene, and fumarate addition for toluene and xylenes, which matches the metabolite and DNA findings

  - The mixing of groundwater may cause freshly dissolved compounds with relatively light isotopic ratios to mix with compounds from previously dissolved compounds that have relatively heavier ratios. Considering the lack of knowledge on number and location of source zones, this means that changes in isotope ratios cannot straightforwardly be used to calculate biodegradation rates at this site
  - Although the CSIA did not exhibit a substantial level of naphthalene degradation, alternative lines of evidence indicated a strong potential for the degradation of this compound. Therefore, we conclude that there is a notable masking effect on isotope fractionation in naphthalene due to its hydrophobic nature

- DNA analyses confirmed the presence of iron and sulphate reducing bacteria. A strong potential for anaerobic naphthalene degradation was demonstrated by the high count of genes involved in naphthalene degradation

  - Just like metabolites, micro-organisms are usually not considered along contaminant plumes. Nevertheless, our study indicated a correlation between the concentration of coal tar aromatics and the presence of bacteria responsible for their degradation

Overall, this study demonstrates that the occurrence of natural biodegradation can well be proven in the absence of a traceable contaminant plume. However, due to heterogeneity in hydrogeological and biochemical subsurface conditions, it is unfeasible to predict how, when and where which biodegradation processes are most important or at what rates biodegradation occurs. To prove whether natural attenuation can provide a sustainable management option for the Griftpark, this study needs to be supplemented with a hydrogeological model to simulate dissolution and reactive transport of mobile tar components in the Griftpark subsurface, and examine required degradation rates that could be compared with literature values.

Chapter 4

Effect of indene, indane and naphthalene on aerobic BTEX degradation and indigenous microbial community development

Abstract

The BTEX compounds (benzene, toluene, ethylbenzene, xylene), as well as contaminants like indene, indane and naphthalene (Ie, Ia, N) are common pollutants found at former manufactured gas plants. In this study, the inhibitory or stimulative substrate interactions between BTEX, and Ie, Ia, N during their aerobic biodegradation are evaluated.

In order to achieve this, batch bottles, containing originally anaerobic subsurface sediments, groundwater and indigenous microorganisms from the coal tar contaminated Griftpark site, are spiked with various substrate combinations (BTEX, BTEXIe, BTEXIa, BTEXN, BTEXIeIa, BTEXIeN, BTEXIaN, BTEXIeIaN). The bottles are left under aerobic conditions and substrate concentrations monitored over time. Within the BTEXIeIaN mixture, all compounds are completely degraded by the microbial consortia within 39 days of incubation. The experimental data are fitted to a first order kinetic degradation model for interpretation of inhibition/stimulation between the compounds.

Results show that indene, indane, and naphthalene inhibit the degradation of toluene, ethylbenzene, o-xylene and especially benzene. M/p-xylene is the

only compound whose biodegradation is stimulated by the presence of indene and indane (individually or mixed) but inhibited by the presence of naphthalene. 16S rRNA amplicon sequencing reveals differentiation in the microbial communities within the batches with different substrate mixtures especially within the microbial groups *Micrococcaceae* and *Commamonaceae*. Indene has more effect on the BTEX microbial community than indane or naphthalene and it increases especially the relative abundance of *Micrococcaceae* family.

In conclusion, co-presence of various pollutants leads to differentiation in degradation processes as well as in microbial community development. These findings shed light on the factors contributing to the recalcitrance of certain aromatic hydrocarbons within coal tar mixtures, providing valuable insights for enhancing bioremediation efforts at contaminated sites.

A version of this Chapter has been accepted for publication as:
Aydin, D.C., Faber, S.C., Attiani, V., Eskes, J, Aldas-Vargas, A., Grotenhuis, T., Rijnaarts, H., Indene, indane and naphthalene in a mixture with BTEX affect aerobic compound biodegradation kinetics and indigenous microbial community development, Chemosphere, 2023, article number 139761

4.1 Introduction

Soil and groundwater contamination with petroleum hydrocarbons is a widespread environmental problem [12]. Aromatic hydrocarbons such as BTEX (benzene, toluene, ethylbenzene, xylene) are commonly used as industrial solvents and materials in fine chemical and petrochemical industries [92]. They are also the waste product of the purification of the coal gas at gaswork sites [214]. Such petroleum products are often released into the environment during industrial activities related to refining, transportation, use and disposal. Due to their high solubility in water, they are easily transported over large distances by the groundwater [73]. This poses a serious threat to the environment and human health, since BTEX compounds are defined as environmental priority pollutants by environmental agencies and classified as toxic and carcinogens [147, 156].

An appealing solution to remove BTEX from the environment is bioremediation. Bioremediation relies on natural biodegradation, which is a sustainable, eco-friendly and cost-effective process for contaminant breakdown. During biodegradation, microbes convert aromatic hydrocarbons to less toxic or non-toxic compounds [138]. Several factors are known to influence biodegradation, such as pollutant characteristics (type, concentration, availability), environmental conditions (temperature, pH, availability of inorganic nutrients and electron acceptors) and microbial communities (adaptation, active biomass concentration, activity degradation potential) [12]. Another factor that should be considered, is that of substrate interactions. The presence of one compound can act inhibitory or stimulative to the degradation performance of another. Because sites contaminated with coal tar typically involve mixtures of hundreds of pollutants, these interactions should be studied carefully [73, 181, 330]. Research on aerobic BTEX degradation and the interaction between BTEX compounds has been documented in earlier studies [73, 12, 175]. There are few studies investigating the multi-substrate effect of BTEX with other organic pollutants such as naphthalene [126], tetrahydrofuran [330], methyl ter-butyl ether [74] and ethanol [64, 55]. However, there is a knowledge gap regarding the interaction between BTEX and other potential co-occurring contaminants such as indene and indane.

Beside the multi-substrate effect, it is important to study the microbial community responsible for the biodegradation process and how microbial community is affected by the presence of complex contaminant mixtures. Although the number of papers on the molecular analysis of microbiomes is increasing, the interaction between microbial community and changes of environmental factors are still far from clear. Jiao et al. (2016) investigated the succession patterns of the microbial community in response to various

pollutants, while Huang et al. (2021) showed that BTEX played a key role in shifting the microbial community in groundwater [149, 139]. Because co-occurrence of various pollutants is the norm in polluted areas like former gaswork sites, understanding potential interactions is helpful for the design and optimisation of engineered bioremediation.

In this study, of the full hydrocarbon mixture existing at the Griftpark, a former gaswork site in Utrecht (the Netherlands), BTEX, indene, indane and naphthalene were selected as the contaminant mixture for laboratory study. The selection was made based on the high concentrations of these compounds that were measured in the groundwater. Information about indene and indane degradation in literature is scarce and substrate interactions between BTEX together with indene, indane and naphthalene is not available. The present study focuses on the effect of indene, indane and naphthalene on the aerobic biodegradation of BTEX compounds under laboratory conditions by indigenous microorganisms from the Griftpark. The soil and groundwater samples used in this study originate from the deep, anaerobic subsurface, so that the study will reveal information on the potential of aerobic degradation in originally anaerobic environments. Ultimately, outcomes of this study help to obtain insights into the biodegradation process of various mixtures of contaminants and additionally contribute to implementing efficient bioremediation strategies towards protecting drinking water sources.

4.2 Materials and methods

4.2.1 Sediment and groundwater sampling

Sediments and groundwater used in this study were collected from Griftpark, Utrecht (the Netherlands), a former gaswork site. From 1859 to 1960 several manufactured gas factories and several other industries existed at this location. Notable contaminants in the subsurface and groundwater of the site were detected as BTEX, indene, indane and naphthalene [134]. Clean sediment was collected from Griftpark from drillings (November 2018) at 38-38.5 m below ground level (m-bgl). Relatively clean groundwater with low sulphate concentration (>0.6 mg/L coal tar aromatics and 26 mg/L sulphate) was pumped from the same location, from 8-10 m-bgl (October 2020). All samples were immediately stored in glass containers at 4^oC, in dark until use.

4.2.2 Chemicals

The chemicals used in this study were reagent or analytical grade. Benzene (>99.7%) was purchased from VWR Chemicals (USA); toluene (>99.9%) from

Merck KGaA (Germany); ethylbenzene, m-xylene, o-xylene (>99%) and indane (>95%) from Alfa Aesar (Germany); p-xylene (99%) from Acros Organics (Czechia) and indene and naphthalene (>99.9%) were obtained from Sigma-Aldrich (Germany).

4.2.3 Experimental set-up

Experiments were conducted in batch reactors of 250 mL autoclaved, clear glass bottles. Each reactor contained 20 g of sediment as the source of inoculum and 150 mL of groundwater as media (pH 7). Air was present in the headspace (˜100 mL) in order to supply enough oxygen for the complete removal of contaminants. Bottles were capped with Butyl/PTFE-coated septa and aluminum crimp caps. Reactors were incubated in a rotary shaker at 120 rpm and 20^oC, in the dark between 13 to 39 days, depending on the experimental set-up.

All bottles were spiked with the contaminant mixture of interest. A pure mix solution was prepared and purely mixed in water instead of being dissolved in a carrier solvent. For this, 100 mg of each compound was pipetted in a 1.5 mL clear glass vial and vortexed for one minute. Once naphthalene crystals were completely dissolved, 10 μL pure mix was injected into the reactors with a 10 μL glass syringe. The aim was to have between 1-5 mg/L of each compound in the reactors. The bottles were incubated overnight to equilibrate the hydrocarbons between gas and liquid phases and then was sampled to determine the initial concentration.

Compounds	BTEX	BTEXIe	BTEXIa	BTEXN	BTEXIeIa	BTEXIeN	BTEXIaN	BTEXIeIaN
Benzene	+	+	+	+	+	+	+	+
Toluene	+	+	+	+	+	+	+	+
Ethylbenzene	+	+	+	+	+	+	+	+
o-Xylene	+	+	+	+	+	+	+	+
m/p-Xylene	+	+	+	+	+	+	+	+
Indene	-	+	-	-	+	+	-	+
Indane	-	-	+	-	+	-	+	+
Naphthalene	-	-	-	+	-	+	+	+

Table 4.1: Eight substrate combinations (set-up) used in the batch experiments. (+); compound present in the bottle, (-); compound missing in the bottle.

To test the effect of indene, indane and naphthalene on BTEX biodegradation, eight different substrate combinations were prepared: BTEX, BTEXIe, BTEXIa, BTEXN, BTEXIeIa, BTEXIeN, BTEXIaN and BTEXIeIaN, see

Table 4.1. Each set-up contained five bottles: three active and two abiotic controls. Control bottles were sterilised by autoclaving for 20 min at 121^oC. Sodium azide (NaN_3) and mercury chloride ($HgCl_2$) were added as biocides to prevent any potential microbial activity during the experiment. Abiotic controls were prepared for each set-up to discern volatilisation and adsorption from biodegradation process. Experiments were performed in triplicate and experimental error was calculated as the standard deviation of triplicate samples.

4.2.4 Analytical measurements

Each contaminant was measured and quantified using HPLC-FLD/DAD equipped with an Acclaim^{TM} Phenyl-1 HPLC column 150 x 4.6 mm, 3μm (*Thermo Scientific Dionex*, USA). The operating parameters and flow rates have been described previously [16]. Compounds were analysed by sampling the liquid phase from bottles using a 1 mL syringe equipped with a 0.4 mm needle. One mL liquid sample containing sediment and groundwater was centrifuged at 15000 rpm for 10 min and 750 μL supernatant was transferred to HPLC vials. Finally, 250 μL methanol was added to the vial in order to limit evaporation losses during HPLC autosampler procedures. Chromeleon software (*Thermo Fischer Scientific*, USA) was used for analysis of the data. Sampling proceeded until one contaminant was left or until contaminant concentrations in the bottles dropped below their detection limits in the HPLC method (2-70 μg/L). After each measurement, the average amount of contaminant present in the samples from the active bottles were normalised to the average amount of contaminants present in the sample of the controls, according to

$$\text{normalised concentration} = \frac{mean^{active}}{mean^{controls}}. \tag{4.1}$$

Gas chromatography (*GC-2010, Shimadzu*) was used for headspace gas measurements for monitoring O_2, CO_2, N_2 and CH_4 with the method of de Wilt et al. (2018) [72].

4.2.5 Kinetic parameters

In order to examine the substrate interactions for all compounds in the various BTEXIeIaN mixtures, kinetic modeling was performed using the experimental data. The most commonly applied model for single substrate systems is Monod-type kinetics. In this study, fitting data with Monod kinetics was attempted, however, due to low sampling frequency and quick degradation, fits would either not converge or not be distinguishable from first-order fits. Therefore, the results of the batch data were fitted with the first-order kinetic

model

$$S_i = S_i(0)e^{-k_i t}, \tag{4.2}$$

where $S_i(t)$ is the concentration of the i^{th} aromatic hydrocarbon and k_i its first order degradation rate constant. The solution was fitted with a non-linear least squares curve fit in Python, with the rate constant k_i and initial concentration $S_i(0)$ as fitting parameters using Equation 4.2. The initial concentration $S_i(0)$ was included as fitting parameter because measured initial concentrations were not reliable as the hydrocarbons dissolve into each other and naphthalene would precipitate. Furthermore, as most compounds were degraded early in the sampling process, data was not fitted in log-space, in order not to over-emphasize the measurements below detection limit.

The control batches showed some decrease in concentrations, indicating the occurrence of sorption and/or volatilisation. Therefore, the concentration data were normalised with the control batch data (Equation 4.2). The geometric mean of the triplicate batches were used for fitting. The lag phase was taken out for the individual compounds of each batch series. Fitted degradation rates of all BTEXIeIaN compounds in the various mixtures were used to assess the effect of indene, indane and naphthalene (individually or mixed) on the other compounds, as well as on each other. To assess the quality of the model fits, the coefficient of determination (R^2) was used. To study inhibitive/stimulative effects of indene, indane and/or naphthalene on the compound of interest more easily, ratios of rate constants were calculated according to

$$\alpha_{BTEX,(Ie/Ia/N)} = \frac{k_{BTEX,(Ie/Ia/N)}}{k_{BTEX}}, \tag{4.3}$$

where $\alpha_{\mathrm{BTEX,\ Ie/Ia/N}}$ is the ratio of the rate constants of each of the BTEX compounds in the presence of indene, indane and/or naphthalene, $\mathrm{k_{BTEX,(Ie/Ia/N)}}$, and the rate of each of the BTEX compounds in the pure BTEX mixture, $\mathrm{k_{BTEX}}$. The ratios for indene, indane and naphthalene follow the same logic. Values of α <1 indicate inhibition and α >1 stimulation of biodegradation through the presence of the added extra compound(s) to the BTEX mixture.

4.2.6 DNA extraction and sequencing

In order to understand the impact of different substrate mixtures on microorganisms, one batch from each set-up was sampled for microbial community analysis. The aim was to investigate the difference in microbial communities between the set-ups and the changes in the microbial community when exposed to different substrate mixtures.

For DNA analysis, nine different samples were collected. For the representation of the native microbial consortium, the sample T0 was collected before spiking the batch bottle with any contaminant. To compare the native microbial community to the final community of each set-up, eight different samples were taken at the end of the experiment (day 13-39 depending to the set-up).

An amount of 5 mL sediment-groundwater mix was collected from all set-ups and T0. Batch bottles were shaken vigorously before sampling in order to have a homogeneous sample of sediment-groundwater mix. Then, to allow cell precipitation, samples were centrifuged for 10 min at 15000 rpm. After centrifuging, the supernatant was discarded, and the pellet was stored at -80^oC until further use for DNA extraction. Microbial DNA was extracted from each sediment sample using the DNeasy PowerSoil Kit (*Qiagen*, Hilden, Germany). After processing the samples in a bead beater to lyse the cells, DNA was extracted according to the manufacturer's instructions. The isolated DNA was used as template for amplifying the V3 and V4 region of 16S rRNA via Illumina sequencing using the primer sets described by Takahashi et al. (2014) [277].

4.2.7 Processing and analysis from sequencing data

Sequence analysis of the raw data was performed in NG-Tax version 2.1.74 using default settings as described in Poncheewin et al. (2020) [232]. Taxonomy was assigned using the SILVA reference database version 138.1. Paired-end libraries were demultiplexed using read pairs with perfectly matching barcodes. Amplicon sequence variants (ASVs) were picked as follows: for each sample, sequences were ordered by abundance and a sequence was considered valid when its cumulative abundance was $\geq$0.1%. ASVs are defined as individual sequence variants rather than a cluster of sequence variants with a shared similarity above a pre-specified threshold, such as operational taxonomic units (OTUs). All analyses were performed in R version 4.2.0 (*https://R-project.org/*).

Raw sequences with barcode and primer removed and supporting metadata were deposited in the European Nucleotide Archive (*http://www.ebi.ac.uk/ena*) under the accession number *PRJEB58637*.

4.3 Results and discussion

4.3.1 Degradation of BTEXIeIaN under aerobic conditions

First the potential of the full BTEXIeIaN was studied. Figure 4.1 shows the concentrations of all compounds in the full BTEXIeIaN mixture over a 31 day period. All compounds except for benzene, o-xylene and indene were

degraded within 13 days. After 31 days, complete removal was also observed for benzene, two out of the three active bottles for indane and one out of three for o-xylene. O-xylene is the most recalcitrant compound in this mixture.

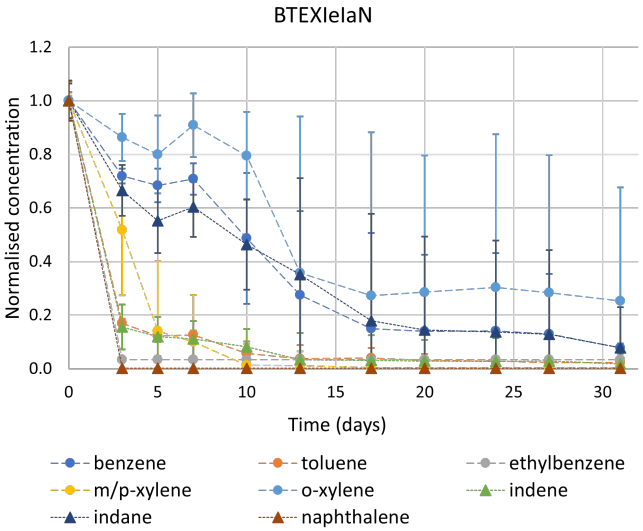

Figure 4.1: Normalised concentrations in the full BTEXIeIaN mixture under aerobic conditions, normalised to the mean of abiotic controls. Error bars show the standard deviations of the three experimental triplicates.

The use of a mixed consortium originated from a polluted site can facilitate the biodegradation of compounds such as BTEXIeIaN. Various studies [12, 49, 222] investigated single strains on BTEX degradation showing that single strains are not capable of removing all compounds simultaneously and efficiently. For BTEX degradation, microbial consortia were found to be more powerful than pure cultures [211]. In this study, a variety of microorganisms were present, apparently with different biodegradation capacities enabling a complete degradation of the complex compound mixture, indicating that in this subsurface sediment system none of the compounds are intrinsically recalcitrant towards aerobic biodegradation. These results showed the intrinsic aerobic degradation potential of microorganisms originating from deep anaerobic subsurface and opens the possibility of using oxygen to stimulate biodegradation of aromatic hydrocarbons, instead of using purely anaerobic strategies.

4.3.2 Substrate degradation patterns during BTEXIeIaN biodegradation

In order to shed light on the effect of substrates on each other, concentrations of each compound are compared in the varying batches. Figure 4.2 depicts the degradation curves of each compound in the varying mixtures. The geometric averages of the compound concentrations of the triplicate batches are plotted with their standard deviations. Substrate degradation patterns of individual compounds in the BTEXIeIaN mixture vary depending on the substrate combinations used in each set-up. Especially in the graph depicting benzene concentrations, the inhibitive effect to benzene degradation of adding indene, indane and naphthalene individually and stronger inhibitive effect when they were added in a mix, can be clearly distinguished. Of the BTEX compounds, m/p-xylene is the only compound for which degradation is not the fastest in the pure BTEX mixture, indicating stimulation to biodegradation of the co-pollutants. From the figure it can also be seen that the standard deviation is highest in the full BTEXIeIaN mixture, indicating that in these batches small variations, in compound concentrations and/or microbial community, strongly affect degradation patterns.

The addition of indene, indane and naphthalene also had an effect on lag times. Generally, naphthalene caused the most increase in lag time.

Table 4.2 shows the order at which compounds were fully removed from the system, i.e. when its concentration declined below the detection limit. Overall, fastest degradation was observed for naphthalene and ethylbenzene. For all cases where naphthalene was present in the mixture (i.e. BTEXN, BTEXIeN, BTEXIaN, BTEXIeIaN), it was the first compound to be fully degraded either with ethylbenzene (BTEXIaN and BTEXIeIaN) or ethylbenzene being the second compound degraded. After ethylbenzene, the order in degradation varied but was often observed as toluene, m/p-xylene, benzene, indene, indane and finally o-xylene.

The degradation order of m/p-xylene was found to be inconsistent in presence of different co-substrates. M/p-xylene was degraded first in the set-up of BTEXIa and BTEXIeIa, and as the second compound in BTEXIeIaN mixture. In BTEXIeN, m/p-xylene was removed one before last. This was the only set-up where indene was degraded sooner than m/p-xylene, which was observed in all triplicate bottles.

Literature studies are in line with our findings that ethylbenzene is the most easily degraded compound in BTEX mixtures. This was observed by Deeb & Alvarez-Cohen (1999) with different BTEX combinations as well as in the presence of BTEX of other co-pollutants as n-propylbenzene or 1,2,4-trimethylbenzene [73]. Isomers of xylene were reported to be degraded last

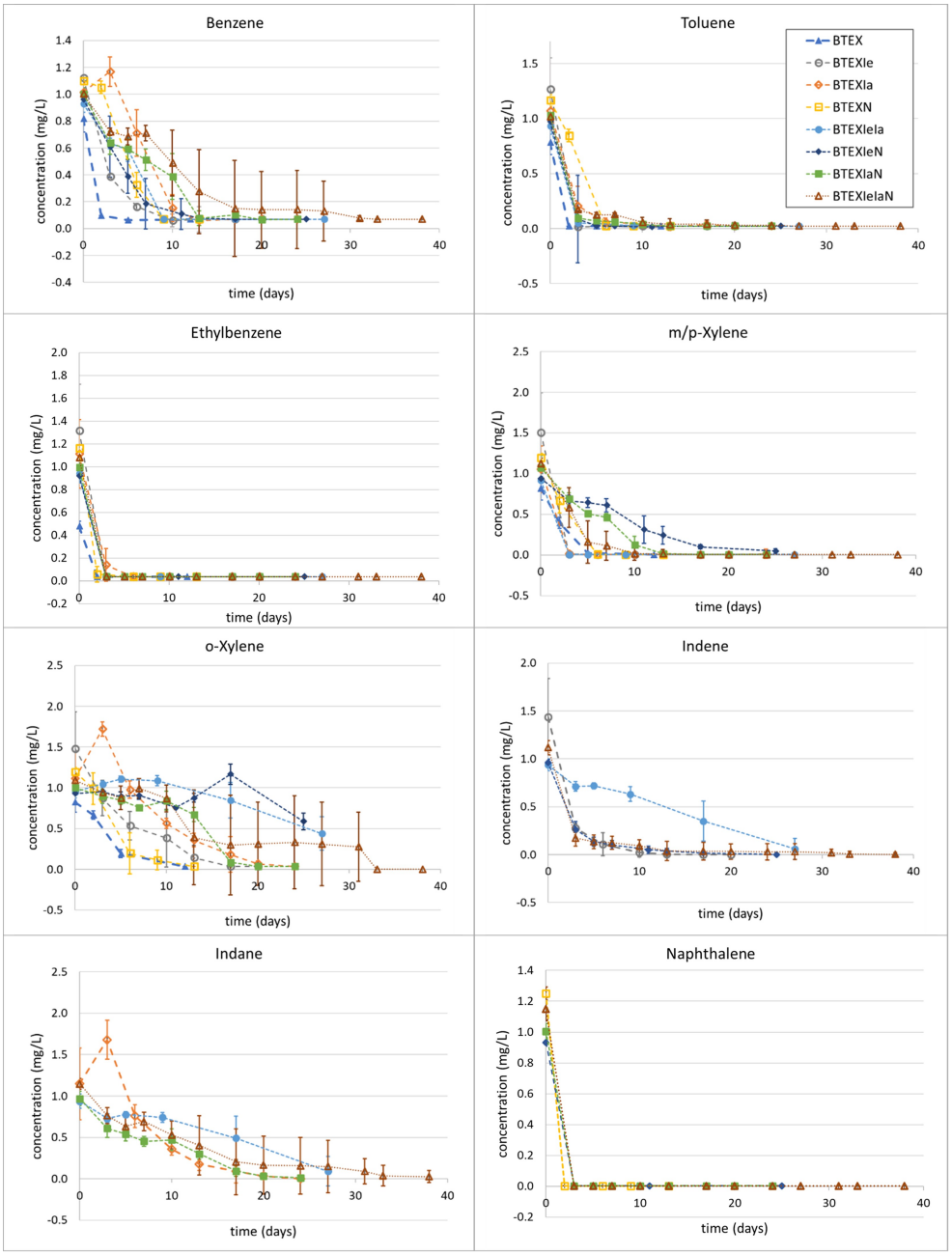

Figure 4.2: Geometric averages of concentrations normalised to control batches of all BTEXIeIaN compounds in the various mixtures. Error bars show the standard deviations of the three experimental triplicates. T=0 is 24hrs after mixing of the compounds.

	BTEX	BTEXIe	BTEXIa	BTEXN	BTEXIeIa	BTEXIeN	BTEXIaN	BTEXIeIaN
Naphthalene				1		1	1	1
Ethylbenzene	1	1	2	2	1	2	1	1
Toluene	2	2	3	4	2	3	2	3
m/p-Xylene	3	3	1	3	1	6	3	2
Benzene	4	4	4	5	3	4	5	4
Indene		5			4	5		5
Indane			5		5		5	6
o-Xylene	5	6	6	6	6	7	4	7

Table 4.2: Degradation order of each compound for each set-up. The compounds were given in the order of degradability starting with easily degradable compound to the most difficult one. The colour is adjusted per column, light blue (1) represents the fastest to reach complete degradation and dark blue (5-7) represents the slowest to reach complete degradation.

among BTEX compounds with o-xylene being more recalcitrant than the others [12, 181, 55].

4.3.3 Effect of indene, indane and naphthalene on biodegradation kinetics of BTEXIeIaN compounds

To study the possible substrate interactions between each compound of the BTEXIeIaN mixture in more detail, the experimental data was fitted to a model. In this model, the first order degradation rate constant (1/day) of each compound in each set-up was calculated, see Equations 4.2. The results were qualitatively interpreted as low sampling frequency reduced the validity of rigorous quantitative analysis. Example plots of the fitting are shown in Appendix F.1 and fitted first order degradation rates in Appendix G.1. Equation 4.3 was used to make a relative comparison of the different degradation rate constants. Lag times were taken out for the model fitting. The resulting ratios between rate constants are shown in Table 4.3.

	BTEXIe	BTEXIa	BTEXN	BTEXIeIa	BTEXIeN	BTEXIaN	BTEXIeIaN
Benzene	0,32	0,23	0,19	0,15	0,19	0,12	0,12
Toluene	0,84	0,31	0,17	0,51	0,48	0,41	0,28
Ethylbenzene	0,93	0,54	1,18	0,81	0,77	0,82	0,85
o-Xylene	0,71	0,74	0,95	0,41	0,04	0,31	0,40
m/p-Xylene	3,74	3,25	0,86	3,89	0,22	0,38	0,68
Indene				0,11	0,77		0,99
Indane				0,21		0,51	0,34
Naphthalene					0,62	0,64	0,66

Table 4.3: Substrate interactions calculated based on the ratio of rate constants in different mixtures. More strongly inhibited biodegradation (α <1) is coloured darker blue and more strongly stimulated (α >1) is coloured darker yellow. Gridded cells indicate no value.

From Table 4.3 it can be seen that benzene is significantly inhibited by the addition of indene, indane and naphthalene, either individually or combined and most strongly of the BTEX compounds. This finding raises environmental concerns, as benzene has high mobility and persistence in the environment due to its low sorption and slow degradation rate compared to the other aromatic hydrocarbons [140]. Besides, benzene is the most carcinogenic among the BTEX compounds [187]. However, while benzene is the most strongly inhibited compound it is not the one degraded last, see Table 4.2.

The results also show that ethylbenzene degradation is least affected by the additions of the IeIaN compounds. Degradation of o-xylene, the most recalcitrant of the BTEX compounds, is little affected by the individual addition of indene, indane or naphthalene, but gets more strongly inhibited when they are added in combinations.

Table 4.3 shows that among the BTEX compounds, m/p-xylene is the only compound stimulated by the presence of indene or/and indane (in the absence of naphthalene). Additionally, naphthalene had a slight stimulative effect on

ethylbenzene degradation. Gülensoy & Alvarez (1999) studied biodegradation capabilities of indigenous microorganisms exposed to different combinations of aromatic hydrocarbons of BTEXN [126]. They reported enhanced degradation of naphthalene by ethylbenzene. Combined with the results of this study, this indicates co-metabolism of naphthalene and ethylbenzene. For all the other compounds, only inhibition was observed in presence of indene, indane and/or naphthalene.

As mentioned, the addition of indene, indane and naphthalene had an effect on lag times. However, when for a compound the addition of indene, indane or naphthalene caused an increased lag time, this was not reflected by lower degradation rates.

The results of these experiments do not only give information on the effect of indene, indane and naphtalene on BTEX, but also on the effects of indene, indane and naphthalene on each other in the presence of BTEX. The results in Table 4.3 indicate strongly competitive inhibition between indene and indane. Adding naphthalene mitigates the effect of indane to indene. Indene and indane reduce the degradation rate of naphthalene to the same extent, whether added individually or together. Indene and indane have previously been found to be co-metabolized by enzymes produced during naphthalene degradation [117], which can explain this mitigating effect.

Our results suggest that substrate interactions between BTEX compounds and indene, indane and/or naphthalene differ in the various mixtures (i.e. strongly or barely inhibited or even stimulated degradation), despite the similarities in the chemical properties and structures of the BTEX compounds. One of the possible reasons for such inhibition/stimulation effects during BTEXIeIaN degradation can be as the presences of broad-spectrum enzymes with different affinities for each compound, repression and induction of genes involved in the degradation of one compound but not another [4]. Even though the focus of this study is far from an enzymatic approach, there was an effort made to study the microbial communities present in the different mixtures to provide an additional perspective to the BTEXIeIaN biodegradation patterns. Insights about the changes in the complex microbial community over time with different substrate combinations might be a first step to elucidate the complex interactions related to inhibition phenomena.

4.3.4 Microbial community is influenced by different substrate mixtures

To get an overview of the differences in microbial community between the set-ups, beta-diversity analyses were performed. The results are displayed in Figure 4.3. The Principal Coordinate Analysis (PCoA), shown in Figure 4.3, allows the visualisation of microbial communities between the different set-

ups by Weighted Unifrac index. In Figure 4.3, Axis 2 explains the variability of microbial communities by 11.1%, while Axis 1 does it by 75%. It should be mentioned that the following results are descriptive and the differences in the microbial community between samples could not be statistically proven due to a lack of replicates for DNA analyses in the different set-ups.

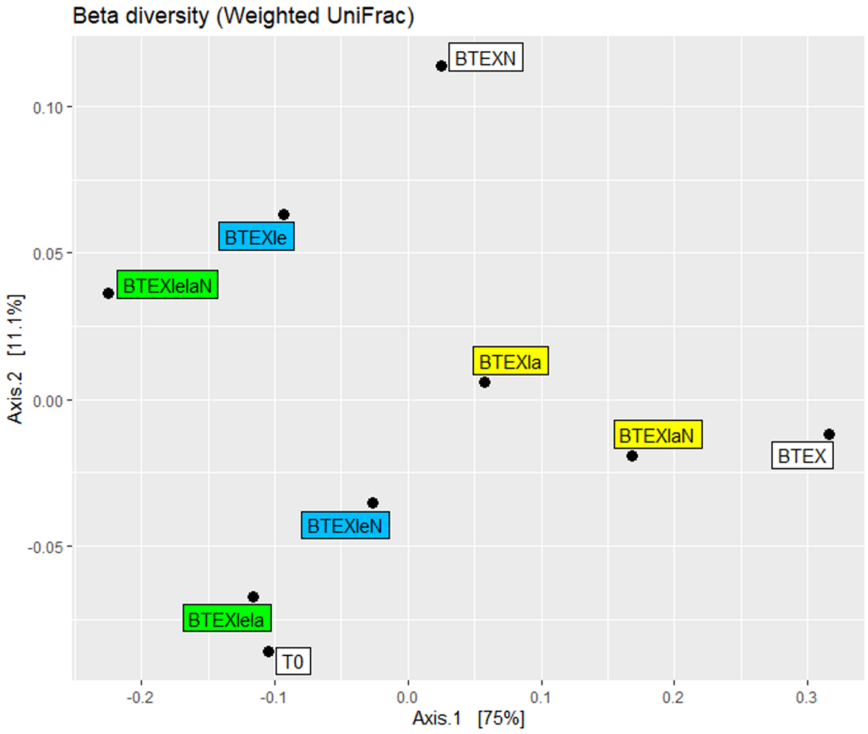

Figure 4.3: Beta-diversity analysis using the Weighted Unifrac distances to investigate the microbial community differences between the set-ups. T0 displays the microbial community in a sediment sample before the addition of contaminants. Samples containing indene are represented in blue, samples containing indane in yellow and samples with indene and indane in green.

Differences in the substrate mixtures lead to differences in the microbial community. In this study, highest differences in microbial composition were found between BTEXIeIaN and BTEX. In Figure 4.3, the BTEX set-up and BTEXIeIaN are positioned in the two different sides of Axis 1. All other set-ups lie in between. This can be expected, as when more compounds are added to the mixture, more changes may occur in the community with an increase or decrease in microbial diversity. This can also depend on the contaminant type (i.e. chemical structure) and the microbial degradation potential rather than the variety of contaminants (i.e. five contaminants vs eight). Although there

is no clear grouping in Figure 4.3 based on the presence of the different substrate mixtures, there is a distinct distribution when either indene (blue) or indane (yellow) are present. While mixtures that contain indene are positioned closely to BTEXIeIaN, gathered on the left side of the graph, samples containing indane are positioned more toward the BTEX mixture, mostly on the right side of the graph. Focusing on the impact of indene, indane and naphthalene on BTEX, comparing differences in microbial composition, BTEXIe is the mixture differentiating from BTEX the most compared to BTEXIa and BTEXN. Thus, it is concluded that indene exerts selective pressure on the BTEX microbial community rather than indane or naphthalene.

The microbial communities in the batches with BTEXIeIaN and BTEXIeIa were rather similar, meaning that naphthalene may not play a significant role in shaping the final microbial community. This is likely due to naphthalene being the first compound to be degraded, see Table 4.2. Therefore, due to its short-time presence, it may not have a major effect in the final microbial consortium. The sediment sample T0 was sampled as the representative starting point of the experiment. The position of T0 is very close to BTEXIeIa, meaning that the final microbial communities between T0 and BTEXIeIa are resembling. Since the initial sample (T0) comes from a former gaswork site, mostly contaminated with an BTEXIeIaN mixture, it is expected that T0 is closer to the BTEXIeIaN position rather than BTEX. However, original sediment samples were collected from 38 m-blg where anaerobic conditions are prevalent, so that the microbial community is expected to have changed significantly. The fact that the indigenous microbial community originating from an anoxic environment has aerobic degradation potential can be explained by the co-existence of aerobic and anaerobic microbes where aerobes consume the oxygen and maintain anaerobic conditions for the anaerobes [113]. Another explanation can be the presence of facultative anaerobes. Members of *Pseudomonas* [94] and *Acidovorax* [4] were reported to be capable to degrade benzene under aerobic, microaerobic and nitrate reducing conditions.

Similar to this study, investigation of different substrates and their effect on the microbial communities and diversity was studied by Banerjee et al. (2022) and Jiao et al. (2016). Banerjee et al. (2022) showed that different bacterial communities played a role in the degradation of the different xylene isomers [18]. Jiao et al. (2016) studied the differences in microbial composition among different pollutants, i.e. phenanthrene (PHE), n-octadecane (C18), PHE and C18, and concluded that different pollutants and their combinations influenced the bacterial community by variations of the composition and relative abundance of the phylogenetic groups [149]. Since changes in microbial community can be associated with functional capabilities [272], this

study shows the importance of microbial community characterisation in response to the pollutant.

4.3.5 Microbial composition in different substrate mixtures

Members of *Proteobacteria* phylum might be related to BTEX degradation, as shown in the compositional plot, see Figure 4.4, this phylum showed high relative abundance in all the set-ups. Contamination with hydrocarbons has been associated with an increase of members belonging to *Proteobacteria* [10]. Chen et al. (2022) reported some indigenous microorganisms coming from polluted groundwater or soil, such as *Actinobacteria*, *Proteobacteria* and some members of *Actinomycetota* such as *Rhodococcus and Arthrobacter* strains to have high BTEX degradation activity in their study [54]. Outcomes of this study showed that the highest relative abundance of *Proteobacteria* was observed in the BTEX mixture and the lowest in BTEXIeIaN. This finding is in line with the differences discussed in Section 4.3.4, where the microbial communities from BTEXIeIaN differed the most from the communities in presence of BTEX without other compounds.

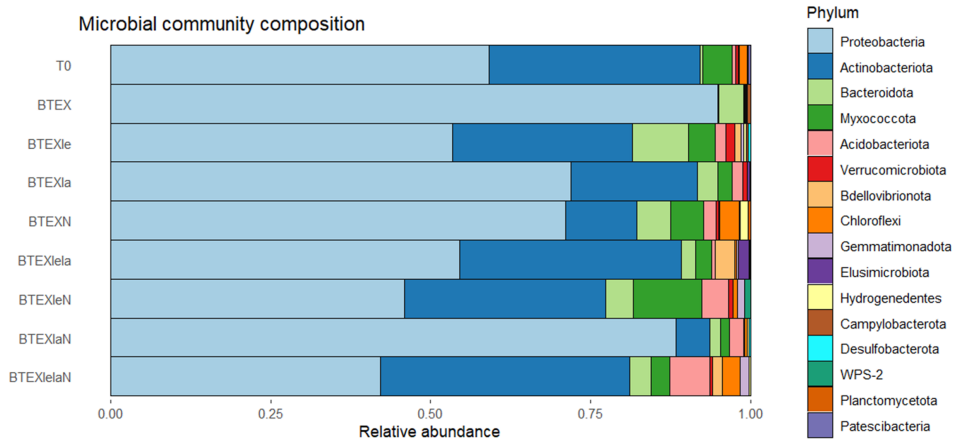

Figure 4.4: Relative abundance of the most abundant phyla for different substrate mixtures.

Presence of indene, indane and naphthalene promotes the abundance of *Actinobacteriota* phylum. As shown in Figure 4.4, higher relative abundance of *Actinobacteriota* is observed in the mixtures containing either indene, indane or naphthalene but not in the BTEX mixture. Especially set-ups including indene have higher relative abundance of *Actinobacteriota.* This was also the case for T0, which is the anaerobic sample taken at the beginning of the experiment prior to spiking with any contaminant. It can be hinted that

Protobacteria might play a role in BTEX degradation while *Actinobacteriota* could be more related with degradation of co-substrates such as indene, indane and/or naphthalene. Further studies are needed to obtain insights about the degradation capacity of the afore mentioned microbial groups.

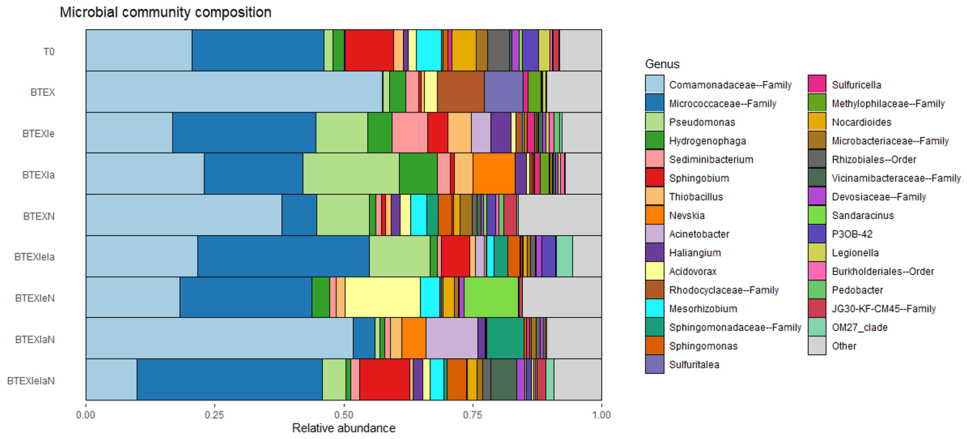

Figure 4.5: Relative abundance of the most abundant genus for different substrate mixtures.

Different substrate mixtures showed different microbial compositions, with varying relative abundances. Figure 4.5 shows a more detailed display of microbial communities analysed at genus level with compositional plots of the top 30 abundant genus present in each set-up. As can be seen, common hydrocarbon degraders reported in literature, such as *Acinetobacter* and *Pseudomonas* [149, 174, 300], *Burkholderiales* [174], *Commamonadacea* [278], *Micrococcus* [300], *Rhodocyclaceae* and S*phingomonas* [174, 300] were also found in the samples. Since the sediment used as inoculum in this study comes from a hydrocarbon-contaminated site and an anaerobic subsurface sample, it is interesting that common aerobic BTEX degraders were detected. However, this is the first study where microbial investigations were performed with indene, indane and naphthalene together with BTEX. Here it is shown that common hydrocarbon degraders can also be detected in the presence of indene, indane and/or naphthalene. Whether these microbial groups play a role in anaerobic biodegradation needs further investigation.

In order to understand which genus showed high abundance and leads to a differentiation among the set-ups, microbial communities at genus level are presented as a heat map in Figure 4.6. The figure shows that the main difference between set-ups concerned mainly two families: *Micrococcaceae* and *Comamonadaceae*. Our results show that the presence of indene increased the relative abundance of *Micrococcaceae* family, indicating that members of

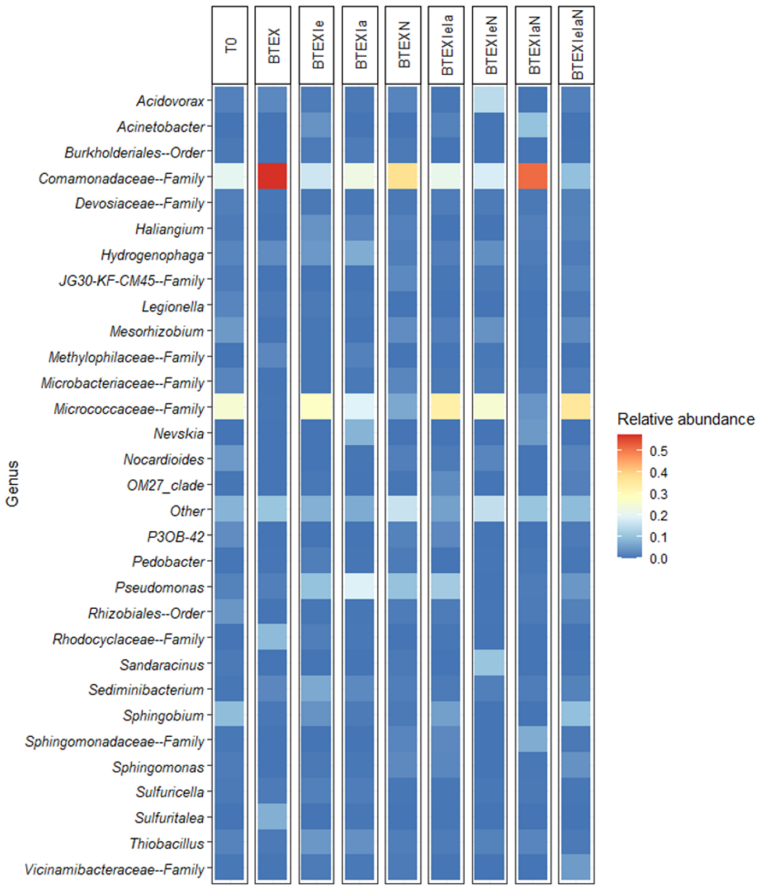

Figure 4.6: Microbial composition of each set-up at genus level, represented as a heat-map. Uncultured and unclassified species were given with the name of the last identified rank.

the *Micrococcaceae* family may play an important role in indene degradation. Also, *Comamonadaceae* showed high relative abundance in the BTEX set-up, suggesting that it might respond to BTEX biodegradation. As previously discussed for the beta-diversity analysis, see Figure 4.3, the biggest differences in microbial communities were found to be between the set-ups BTEX and BTEXIeIaN. In Figure 4.6, a high abundance of *Comamonadaceae* for BTEX was observed with no *Micrococcaceae*, while for BTEXIeIaN, the opposite effect was observed showing higher relative abundance of *Micrococcaceae* than *Comamonadaceae*. Figure 4.6 shows that set-ups showing higher *Micrococcaceae* relative abundance are the mixtures containing indene. In order to combine the results of Figure 4.3 and 4.6, the left side of the beta-diversity

graph, harboring indene-containing mixtures, could be related to the abundance of members *Micrococcaceae* family while the right side to an abundance of *Comamonadaceae*. From these findings, it can be concluded that the differences in the bacterial community structure observed in this study are influenced by different substrate mixtures and that indene had the strongest influence on the BTEX microbial community.

4.4 Conclusion

This study showed that microbial consortia originating from anaerobic subsurface could fully degrade BTEXIeIaN compounds under aerobic conditions. Studying the effects of substrates on each other, revealed that indene, indane, and naphthalene inhibited the degradation of benzene, toluene, ethylbenzene and o-xylene, benzene most strongly. Of the BTEXIeIaN compounds, ethylbenzene, toluene and naphthalene are the fastest degrading. In absence of naphthalene, m/p-xylene was the only compound whose biodegradation was stimulated by indene and indane (individually or mixed).

Understanding the multi-substrate effect in complex mixtures will help to understand why particular compounds may persist at contaminated sites while other compounds are degraded. Mechanisms leading to inhibition in such mixtures are complex, however, it can be hypothesised that the reason of persistent contaminants may not be due to a microbial degradation capacity limitation, but to the effect of mixture inhibition.

Microbial analysis revealed differentiation in the microbial communities within different substrate mixtures, with indene having more effect on the BTEX microbial community than indane or naphthalene. Knowing which microbes can survive in presence of contaminants and be active in biodegradation of those compounds, is relevant for the application of bioremediation technologies. In this study, we found that members of the *Micrococcaceae* family can deal with the presence of indene and indane. However, we cannot conclude yet that these types of microbes are involved in indene biodegradation. Studying this, i.e. by microbial enrichment and molecular physiology studies, would further elucidate the potential for the use of these microbial communities for in-situ bioaugmentation. More detailed studies on microbial dynamics during biodegradation of BTEXIeIaN is needed to understand biodegradation behaviour of such complex mixtures and contribute to improved bioremediation strategies.

Our findings lead to the verdict that indigenous microorganisms from the anaerobic subsurface are versatile and capable to quickly adapt to aerobic conditions to degrade BTEXIeIaN. This is promising for the deployment of aerobic stimulation of degradation for cost effective in-situ remediation strate-

gies at a site that has been contaminated with a hydrocarbon mixture for over 100 years. Similar results were previously reported, where microorganisms enriched from a benzene-contaminated anaerobic groundwater were capable of degrading benzene aerobically [4, 94].

Chapter 5

Geohydrological model of the Griftpark

Abstract

A physical subsurface model of the Griftpark site is developed based on the findings from site investigations. The model incorporates two aquifers separated by a leaky aquitard, a vertical cement-bentonite wall that contains the contamination source zone and three groundwater extraction wells. Refinement of the model grid's layers, rows, and columns is performed until convergence is achieved in water budgets and tracer concentrations.

With various methods, including resistivity profiling and visual inspection of drilling cores, small-scale heterogeneities present in the subsurface of the Griftpark are identified. These heterogeneities are particularly pronounced within the semi-confining aquitard. By utilising 3D Empirical Bayesian Kriging, depth-profile data is interpolated to obtain a three-dimensional representation of the aquitard structure. Simulations conducted using the conceptual subsurface model of the Griftpark demonstrate that considering the aquitard as either a homogeneous or a heterogeneous layered system yields similar plume concentrations, although the plume core progresses further in the case of the heterogeneous simulation. These results suggest that integrating aquitard heterogeneity in the subsurface model is important primarily when studying long-term development of second aquifer plumes.

The developed physical model serves as a basis for the construction of a reactive transport model for the Griftpark site. This reactive transport model will facilitate the examination of the effects of biodegradation on contaminant concentrations.

The results of this Chapter are integrated in a manuscript under preparation in *Advanced water resources*. Title: A comprehensive description of the

characterisation and reactive transport modelling of a complex contaminated field site.

5.1 Introduction

Subsurface and groundwater contamination are a worldwide problem, as many countries rely on groundwater for drinking water, agriculture and industry. The number of potentially contaminated sites worldwide exceeds three million and continues to grow, largely due to the ongoing discharge of waste products into the subsurface or water bodies by numerous industries [261]. In order to secure future groundwater resources, remediation of many of these sites is important. Over the past 40 decades, many remediation techniques have been developed, with an increasing focus on in-situ methods [176]. In-situ methods involve remediating groundwater underground, instead of extracting contaminated water and treating it elsewhere [8]. In the last decades, scientific research has shown that micro-organisms that naturally occur in the subsurface have a high potential to break down aromatic hydrocarbons. At low-risk sites contaminated with organic compounds monitored natural attenuation (MNA) has become an accepted alternative for active remediation [193, 228, 313, 314]. MNA relies on naturally occurring processes, including sorption, dilution and biodegradation, which effectively reduce contaminant concentrations.

The Griftpark, a former manufactured gas plant (FMGP) situated in the middle of the city of Utrecht, the Netherlands, is a contaminated site that has been managed using an active contain-and-management approach for several decades but is currently being reconsidered for management with MNA.

During the FMGPs operation, between 1840 and 1960, a substantial amount of coal tar, consisting of mono-and poly-cyclic aromatic hydrocarbons, leaked into the subsurface during the whole time of operation. Although the severity of the contamination became clear in the 1980s, remediation or in-situ treatment was deemed impracticable due to the depth to which pure-phase contamination was encountered, combined with the urban location of the site. Instead, in 1990, the contaminant source was contained by a cement-bentonite vertical barrier around the site to prevent further contamination of the groundwater downstream. The vertical barrier extends into the aquitard that separates the first aquifer from the second. As the aquitard is not completely confining, a risk exists for contaminated groundwater to leak from the first to the second aquifer. To prevent this, three pumping wells were installed within the contained area to create an upward flow. Yearly, more than 70.000 m^3 of highly contaminated groundwater is pumped up from the contained area and treated at a station just outside the city.

Following the implementation of the contain-and-manage measures, the contaminant plume down-gradient of the contained zone disappeared quicker than predicted [298]. It was concluded that the fast removal of contaminants could be attributed to natural biodegradation processes that were not taken

into account in the calculations. These findings prompted the municipality of Utrecht to reevaluate the management strategy of the Griftpark and explore the potential of relying on biodegradation to make the site's management more sustainable and cost-effective.

In order to facilitate the planning of remediation activities at contaminated sites, three-dimensional numerical groundwater transport models can be utilised to predict flow paths and time scales. There are a number of challenges in the use of numerical transport models, with uncertainty being a crucial concern. Adopting Walker et al.'s definition that uncertainty is "any deviation from the unachievable ideal of completely deterministic knowledge of the relevant system" [304], hydrogeology is an intrinsically uncertain subject. It is characterised by highly heterogeneous subsurface parameters that cannot be fully measured and known at all points in time and space. Model uncertainty can arise from incomplete site characterisation, incomplete process understanding and parameter ambiguity due to spatial and/or temporal scaling issues [236].

To account for uncertainty, subsurface models can be developed while incorporating statistical properties of subsurface parameters. The most commonly used stochastic method in hydrogeological applications is Monte Carlo (MC) analysis [35, 103, 243]. Although MC is a very rigorous and useful tool, a full MC analysis demands a high amount of computing power [241]. Furthermore, probabilistic model outcomes represented with statistics are not always well-accepted by practitioners in applied research [98]. Alternatives to sophisticated stochastic methods are the consensus or multi-model approach [88]. Within the consensus approach, a single model is constructed that integrates all available data and knowledge of the site, aiming to comprehensively capture the system's behaviour and address conceptual uncertainties [37]. With the multi-model approach, several variations of the base model are used that represent diverging conceptual understandings of the modelled system [218]. Without rigorous stochastic methods, uncertainty in these models can be investigated using parameter sensitivity analysis (PSA) [327]. During a PSA, the impact of parameter variations on model responses are investigated.

To assess the viability of MNA as a potential management approach for the Griftpark, contamination risks are evaluated along a source-pathway-receptor conceptualisation [93]. This concept focuses on predicting the impact of contaminant sources on receptors by analysing the vulnerability of the pathway connecting them [273]. The source-pathway-receptor conceptualisation is widely used in hydrogeological risk assessment studies [265, 80, 31, 107].

At the Griftpark site, the source refers to the pure-phase coal tar mass that is present within the vertical containment walls. Several methods have been applied to investigate the locations of coal tar source zones at the Griftpark,

including soil core investigation, membrane inter-phase probing and groundwater analysis, of which the details are reported in Chapter 2.

The receptor is represented by the second aquifer which is subject to strict Dutch regulations to avoiding contamination, as groundwater from the second aquifer is widely used as a source for drinking water supply. This means any proposed management approach must ensure that contaminant concentrations in the second aquifer stay below intervention levels at all times. In the groundwater model, contaminant concentrations in wells in the second aquifer just down-gradient of the Griftpark, situated at the location of three existing multi-level sampling wells, are calculated.

The critical pathway is determined by the discontinuous aquitard that separates the first from the second aquifer. Contaminant transport across the aquitard may lead to contamination of the second aquifer and therefore plays a key factor in the risk assessment. At the Griftpark site, a range of methods has been applied to obtain a three dimensional understanding of the architecture of the aquitard. As described in Chapter 2, methods included sediment core drilling and sampling and hydraulic field scale testing.

The hydraulic field scale tests conducted at the site yielded valuable insight into hydraulic connectivity between the first and second aquifers. However, conventional pump-curve analysis is not suitable for heterogeneous aquifers and cannot provide specific hydraulic conductivity values in three dimensions. Although drilling and sampling techniques provided specific data on subsurface parameters, the information they yield is limited to the exact locations where drilling or sampling took place. To overcome this limitation, geostatistical interpolation techniques are employed, which use data from observed locations to estimate values for variables at locations where no measurements were made. Kriging is a commonly used geostatistical method of interpolation. In this Chapter, we present the results of a three-dimensional kriging interpolation, the 3D Empirical Bayesian Kriging, performed using Griftpark data to obtain a three-dimensional prediction of clay layering in the aquitard.

This Chapter focuses on the development of a hydrogeological model for the Griftpark site that can serve as a basis for a subsequent reactive transport model that can be used to test the viability of MNA for site management. Development of the reactive transport model will be discussed in Chapter 6.

In this Chapter, we evaluate the discretisation of the physical groundwater model by examining water budgets and theoretical solute concentrations in the second aquifer. Two scenarios are considered for modeling the aquitard. The first scenario assumes a homogeneous confining layer representation for the aquitard, while the second scenario incorporates the heterogeneous predictions obtained through kriging. By comparing the outcomes of these scenarios, we

can assess the impact of different aquitard representations on the overall model performance.

5.2 Site description

5.2.1 Lithology

Due to intensive marine and fluvial sediment depositions, Dutch soil profiles often show a complex architecture of layers with different lithological characteristics [291]. Even with dense drilling it is impossible to map the complex textural differences that occur in these deposits and determine three-dimensional conductivity fields with high accuracy [306, 32].

The Griftpark is situated on a sedimentary basin consisting of mostly Holocene and Pleistocene marine and fluvial deposits [32]. The first aquifer, extending from about 2 m above sea level (Normal Amsterdam Water Level, NAP) to 45 m-NAP, consists of four sandy formations, as illustrated in Figure 5.1. The Westland, Sterksel, Kreftenheye and Urk formations are highly heterogeneous, with soil types varying from very fine to very coarse sand and regions of gravel, often alternating on scaled smaller than half a metre. Separating the first and second aquifers is an aquitard known as the Waalre formation (formerly Kedichem). In the Griftpark area, a geological fault line is present, causing the clay to be interspersed with sand intrusions from the underlying sandy Harderwijk formation, making the aquitard semi-confining.

The second aquifer, extending from approximately 65 to 110 m-NAP, known as the Harderwijk formation, is relatively homogeneous and consists of fine to course sands. In Figure 5.1, average horizontal conductivities of the different geologic layers are shown [79]. The figure includes a conceptual representation of clay depositions.

In the 1980s, 46 cone penetration tests (CPT) were conducted along the trajectory of the planned vertical barrier to investigate the subsurface [6]. Between 2018 and 2022, additional investigations were carried out, including six membrane interface probings (MIP) and seven sonic drillings. A detailed description of the investigations and result analysis can be found in Chapter 2, while we here provide a short summary.

The maximum drilling depth achieved using the MIPs was 30 m-NAP, while some of the CPTs reached a maximum depth of 60 m-NAP and certain sonic drillings a maximum 110 m-NAP. All drillings revealed the heterogeneous nature of the first aquifer and aquitard. While the MIPs yielded profiles of relative hydraulic conductivity, CPT resistivity profiles could be translated to soil types using the soil classification chart of Robertson and Campanella [248, 249] and subsequently to hydraulic conductivity estimates

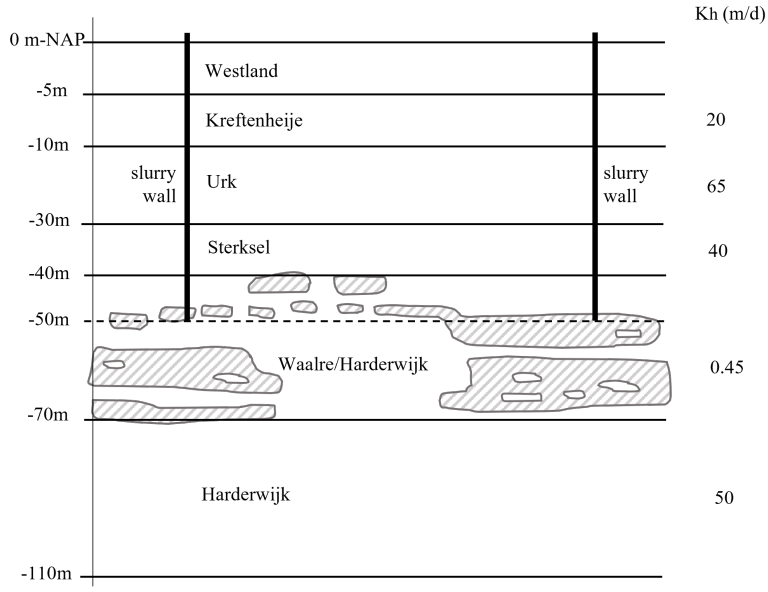

Figure 5.1: Subsurface of the Griftpark, indicating the different geologic depositions and regional average horizontal hydraulic conductivities [79]. The vertical barrier is shown with black vertical lines and clay depositions by grey striped shapes. Due to the heterogeneities in the aquitard around the Griftpark, the hydraulic conductivity of this layer will locally be larger than the average 0.45 m/d indicated in this figure.

based on general soil data as specified in Table 5.1. Visual inspection of soil cores collected during sonic drilling also provided soil type descriptions that could be translated to hydraulic conductivity values. The different test locations are shown in Figure 5.3.

Soil description	K_h (m/d)
peat	0.3
clay	0.005
sandy clay	0.05
extremely fine sand	0.5
very fine sand	1
fine sand	3
medium fine sand	15
medium course sand	40
course sand	50
very course sand	60
extremely course sand	80
fine gravel	100
gravel	200

Table 5.1: Soil descriptions and corresponding horizontal conductivity values used for drilling interpretations.

5.2.2 Groundwater

Regional groundwater flow velocities are about 12 m/yr in both the first and second aquifer, in a south-east/north-west and east/west direction, respectively. The hydraulic head is about 0.5 m higher in the first than in the second aquifer. Figure 5.2 shows the groundwater level contours [79]. The groundwater table at the Griftpark coincides more or less with sea level (0 m-NAP), which is about 2 to 3 m below ground level. Rainfall and evaporation data was obtained from the de Bilt weather station by the National Meteorological Institute [163]. De Bilt situated 3.5 km from the Griftpark and this data is thus generally applicable at the Griftpark site. The averaged values of precipitation and evaporation over the ten-year period from 2011 and 2021 are 656 mm/yr and 1126 mm/yr respectively. For the Griftpark, a correction factor of 0.4 is applied for the evaporation based on the foliage and land usage [123], yielding an average precipitation surplus of 206 mm/yr. There is no sewage run-off at the Griftpark so that all water falling on the park infiltrates the subsurface, with the exception of what falls on the pond and canal, which are lined with cement-bentonite and run off to surfaces waters outside the Griftpark boundaries.

The vertical barrier around the site is made out of cement-bentonite and extents to a maximum depth of 60 m-NAP. The permeability of the vertical barrier, plus any effects of leakage through possible cracks, was studied by changing pumping rates in the contained area and measuring the effects on water levels in wells in- and outside of the containment barrier [123]. The test yielded a resistivity (hydraulic conductivity/thickness) for the vertical barrier of 170 days with an estimated range of 120 to 200 days. Further tests,

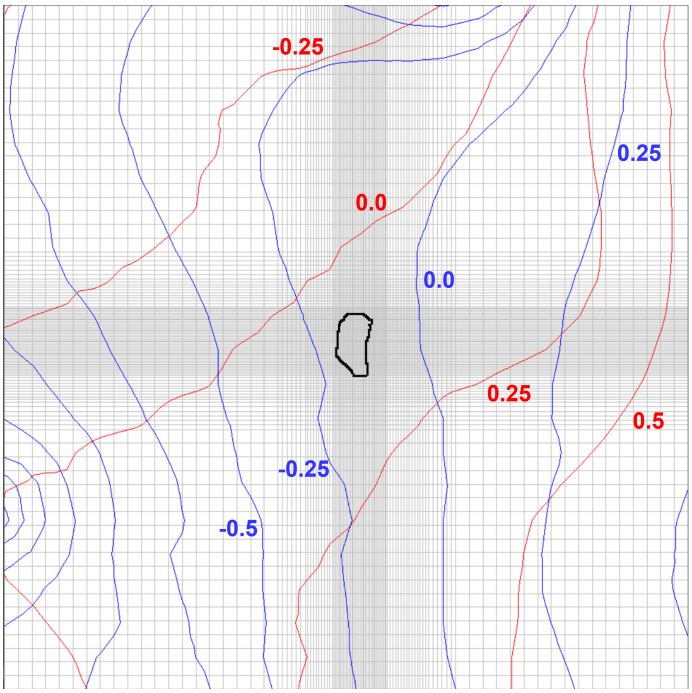

Figure 5.2: Groundwater level contours in a 5x5 km domain with the Griftpark in the centre [79]. Isolines of the first aquifer are indicated in red and the second aquifer in blue. Hydraulic head values of isolines are shown in metres above sea level (m+NAP). On average, the hydraulic head is about 50 cm higher in the first than in the second aquifer. In the initial 5x5 km groundwater model, these isolines were used as constant head boundaries to calculate the hydraulic heads throughout the domain.

described in Chapter 2 have indicated that the vertical barrier performs well, i.e. its transmissivity is determined by the porous nature of cement-bentonite and not by, e.g., cracks. The trajectory of the vertical barrier is shown in Figure 5.3.

During previously performed site investigations it was determined that when maintaining a total pumping rate of 9 m^3/h through the three groundwater extraction wells B20, B21 and B22, shown in Figure 5.3, the total water volume extracted from the system originates for 22% from precipitation, 18% from outside the vertical barrier and 60% through the aquitard [123]. These data will be used to evaluate model discretisations.

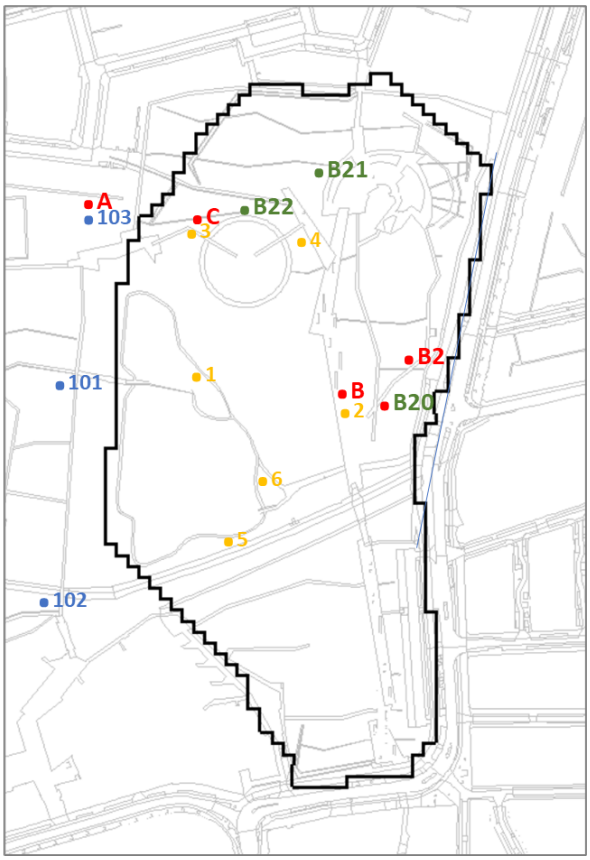

Figure 5.3: Aerial view of the Griftpark, showing the trajectory of the vertical barrier in black. The 6 MIP locations indicated by the numbers 1-6 in yellow; groundwater pumping wells B20, B21 and B22 in green; and MLS wells A, B, B2, C, 101, 102 and 103. The MLS wells indicated in blue extend throughout the complete depth of the second aquifer (i.e. till 110 m-NAP).

5.3 Numerical model

5.3.1 Base model

The three dimensional groundwater flow model of the Griftpark is set up in MODFLOW-2000 using the PMWIN interface [197]. MODFLOW, based on the finite difference method, is a widely used model for simulating groundwater flow in aquifer systems. For the calculation of groundwater levels throughout the aquifer system, the model domain is discretised into rectangular cells. At set time intervals, groundwater flow equations are solved in each cell using the specified aquifer properties and hydraulic boundary conditions.

We used the MT3DMS module to solve solute transport. MT3DMS cal-

culates advective-dispersive transport of particles based on groundwater flow velocities calculated in MODFLOW [328]. MT3DMS uses the finite difference method, just like MODFLOW.

In the base model, the subsurface is structured into three units: (i) first aquifer, (ii) aquitard and (iii) second aquifer. The first aquifer extends from 2 metres above to 45 m-NAP and is implemented as an unconfined layer. It has an average horizontal hydraulic conductivity of K_h=45 m/d. In the first aquifer, the three groundwater pumping wells, B20, B21 and B22 are located.

The second unit is the leaky clay aquitard that extends from 45 to 65 m-NAP. In Chapter 2, we presented our investigations, which demonstrate that the aquitard consists of discrete and often thin clay lenses, causing a hydraulic connectivity between the first and second aquifer. According to site investigations in the 1990s, the average conductivity lies around $K_v = 0.15$ m/d, two orders of magnitude smaller than the values of the 1st aquifer [123]. However, considering the relatively high leakiness of this layer, we also performed simulations using a higher hydraulic conductivity of $K_v = 3$ m/d. The validity of this conductivity is verified using the water budget analysis that was presented in the aforementioned 1990s report [123].

The subsurface third unit, the second aquifer, extends from 65 to 110 m-NAP. At the bottom of this layer we set a no-flow boundary. The unit is more homogeneous than the first aquifer and has an average conductivity of $K_h = 50$ m/d.

In the base model, an anisotropy factor $K_h/K_v = 3$ was applied to the conductivities of all model layers. This value is relatively small for the strongly layered first aquifer. However, we chose a representative vertical conductivity as horizontal flow hardly takes place in this unit due to the vertical barrier, and vertical flow restrictions in the aquitard are modelled through smaller K values. Porosity was chosen using representative porosity values for various unconsolidated sedimentary materials, i.e. 0.35 for the sandy aquifers and 0.4 for the clayey aquitard [207]. All model parameters are listed in Table 5.2.

The vertical flow barrier was implemented using the MODFLOW horizontal flow barrier package with a resistivity of 170 days. It extends over the entire unit depth of the first aquifer until the bottom of the aquitard [123].

Several hydrogeological parameters were chosen uniformly in the entire model. Longitudinal dispersivity is set to 10 m, and both the horizontal and vertical transverse dispersivity to 1 m. These values are large compared to other observed field values [112, 106, 323], reflecting a strongly heterogeneous site. We chose them to account for the fact that flow is mostly vertical in the subsurface volume studied and to overestimate rather than underestimate mixing, as we are interested in the maximum travel distance of the dissolved contamination. The dry bulk density of $\rho_b = 1600$ kg/m^3 is implemented in

Parameter	Value
Large model spatial settings	
Spatial extend $l_x \times l_y \times l_z$	$5000 \times 5000 \times 112$ m^3
Number of rows × columns	119×114
Cell discretisation (including refinement) $\Delta x \times \Delta y$	100×100 - 10×10 m^2
Small model spatial settings	
Spatial extend $l_x \times l_y \times l_z$	$1000 \times 1000 \times 112$ m^3
Number of rows × columns	59×50
Cell discretisation (including refinement) $\Delta x \times \Delta y$	20×20 - 10×10 m^2
Unit specific parameters	
Horizontal hydraulic conductivity K_h, unit 1	45 m/d
Porosity, unit 1	0.35
Regional horizontal hydraulic conductivity K_h, unit 2	0.45 m/d
Local horizontal hydraulic conductivity K_h, unit 2	10 m/d
Porosity, unit 2	0.4
Horizontal hydraulic conductivity K_h, unit 3	50 m/d
Porosity, unit 3	0.35
Global model parameters	
Anisotropy factor K_h/K_v	3
Soil dry bulk density	1600 kg/m^3
Longitudinal dispersivity α_L	10 m
Transversal dispersivities α_T, α_V	1 m
Precipitation surplus	0.0006 m/d
Resistivity hydraulic barrier	170 *days*

Table 5.2: Summary of hydraulic model parameters and spatial model setting for the basic groundwater flow and transport model.

the entire model as it hardly differs between the different units[39]. An average yearly net precipitation surplus of 206 mm/yr (0.0006 m/d) was implemented and no precipitation is modelled above the pond or water canal within the Griftpark.

Initially, a large 5x5 km regional model was set up. Regional conductivity parameters of the three lithological units and regional hydraulic head isolines, shown in Figure 5.2, were used to identify the steady state regional flow pattern. The resulting hydraulic head values were used as constant head boundary to a smaller 1x1 km cut-out model, that only contains the area of the park within the confining walls. The grid cell sizes are refined towards the centre of the domain where the Griftpark is located. Details on grid resolutions are listed in Table 5.2.

5.3.2 Geostatistical interpolation of field data

The accurate representation of the spatial structure of the aquitard layer in the transport model is crucial to assess the flux and concentration of contaminants that may leak from the first into the second aquifer. Local observations

have revealed significant spatial variations in the occurrence and thickness of clay lenses within this geological unit. These variations will likely lead to preferential flow paths that may result in different breakthrough patterns than when assuming a homogeneous representation of the aquitard. To address this, we employed a three-dimensional kriging interpolation method to obtain a hydraulic conductivity distribution for the leaky aquitard.

Kriging is a common geostatistical interpolation method that considers the one and two-point statistics of observed data to provide interpolated values between observations. It produces a continuous and smooth K distribution. The interpolation process relies on the variogram, which quantifies the spatial correlation between sampled points. Unsampled points are assigned weights based on their spatial proximity to the observed points in the surrounding area. In our study, we employed an advanced Kriging method known as 3D Empirical Bayesian Kriging (EBK3D) [166]. Empirical Bayesian Kriging (EBK) is a variation of ordinary kriging that accounts for the errors introduced by relying on a specific semivariogram model. It estimates multiple semivariogram models to create a range of possible true semivariograms. Additionally, EBK it prioritises the interpolation of values based on nearby observations, rather than being influenced by distant values. EBK3D devides the sample point data set into 3D subsets before constructing semivariogram charts. For each location, a prediction is generated using the semivariogram distribution. For our analysis, we utilised the EBK3D tool in the ArcGIS geostatistical wizard (www.pro.arcgis.com).

Parameter	Value
Subset size	100
Overlap factor	3
Transformation	none
Semivariogram type	power
Order of trend removal	none
Elevation inflation factor	7.3
Maximum neighbours	2
Minimum neighbours	1
Sector type	12 sectors
Search radius	58

Table 5.3: Input data for the EBK3D interpolation.

We conducted the EBK3D interpolation on hydraulic conductivity data within the depth range of 30 to 60 m-NAP, covering the lower part of the first aquifer and most of the aquitard. The data points, spaced at one metre depth intervals, are depicted as spheres in Figure 5.4a. Although clay depositions occur even deeper than 70 m-NAP, we lacked the minimum requirement of 10 data points per layer to conduct the interpolation below 60 m-NAP. The

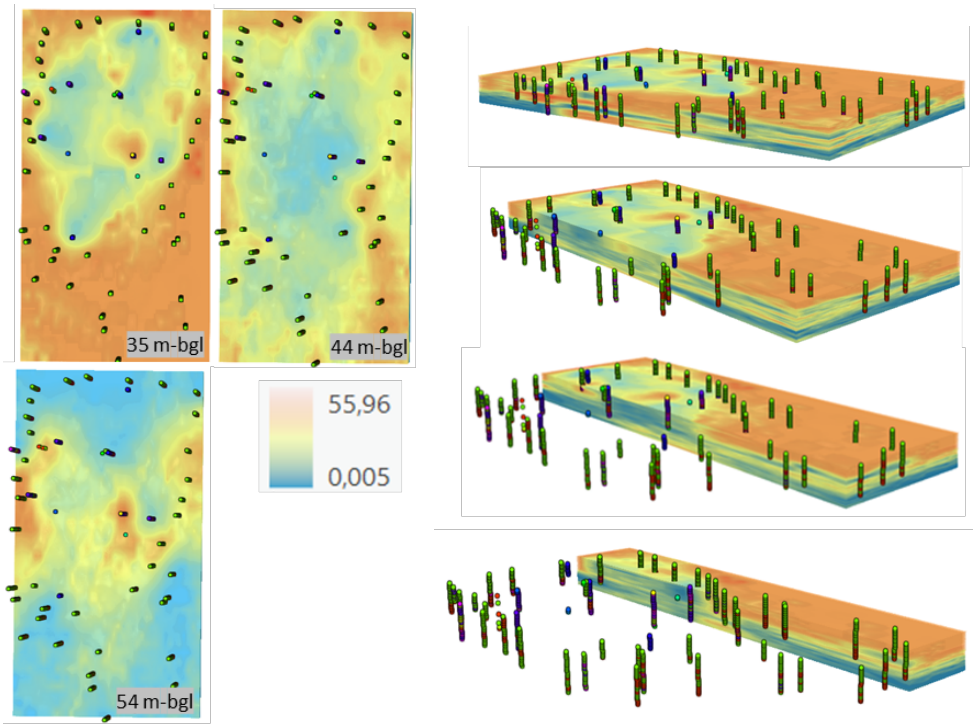

(a) (b)

Figure 5.4: Results of the EBK3D interpolation using vertical per-metre conductivity values between the depths of 30 to 60 m-NAP available at locations depicted as spheres. Figure (a) shows a top view at three depths and Figure (b) shows four cross sectional views in the aquitard. The majority of measurements follow the transect of the wall. The limited number of data points in the centre of the park leads to a reduced reliability of the interpolation results in this zone. A fine alternation of clay and sand layers of the aquitard below the Griftpark can be observed in the results.

majority of measurements follow the transect of the wall and data in the centre of the park is sparse. The quality of interpolated field is dependent on the number of observation points and zones with few data will results in K-field estimates with high uncertainty. Consequently, the reliability of the results in the central zone of the site is relatively low. Secondary input parameters used in EBK3D are listed in Table 5.3.

The EBK3D results, shown in Figure 5.4a, indicate a fine alternation of sand and clay depositions. Results were post-processed for export to the MODFLOW model, for which the vertical domain was subdivided into three and six layers of 10 and 5m, respectively. The division into three layers resulted in average horizontal hydraulic conductivities of 26, 18 and 16 m/d for the depths of 30-40, 40-50 and 50-60 m-NAP, respectively.

5.3.3 Sublayer structuring and grid discretisation

We conducted an evaluation of different conceptualisations of layer discretisations in all subsurface units to determine the optimal representation for our modeling domain. The various scenarios are illustrated in Figure 5.5. Figure 5.5a shows the tested scenarios for different layer discretisations within the first and second aquifer. Figure 5.5b presents the investigated scenarios for layer configurations in the leaky aquitard, including both homogeneous and heterogeneous configurations.

In the initial scenario S1, all three subsurface units were modelled as a single layer with an average hydraulic conductivity (base model). Within this base model, we considered two subscenarios, S1A and S1B, to examine the effect of the aquitards hydraulic conductivity. In scenario S1A, we implemented the reported regional K_h value of 0.45 m/d, while in scenario S1B, we used a higher K_h value of 10 m/d to account for the effect of local distortions in the aquitard. Each subscenario was initially simulated without pumping and then with the three groundwater pumps, B20, B21 and B22, operating at a total extraction rate of Q= 9 m^3/d. These subsequent simulations, referred to as scenarios S1Ap and S1Bp, were conducted to compare the flux ratios through the vertical barrier, aquitard and that from rainwater precipitation.

In scenarios S2-S4, the first aquifer was refined to include four layers. In S2, all layers were assigned the same average hydraulic conductivity K_h of 45 m/d. In scenarios S3 and S4, different hydraulic conductivities were assigned to each sublayer of the first aquifer. These average conductivities of sublayers were based on regional data published by the Dutch National Georegistry, see Figure 5.5a. It should be noted that the model layers do not align precisely with the lithological layering, but were chosen to create a separate layer between 9 and 17 m-NAP, the depth at which pumping wells B20 and B21 are filtered. Within scenarios S2 and S3, subscenarios S2A, S2B, S3A and S3B were introduced to examine the effect of the depth of the contamination source. In scenarios S2A and S3A the contamination source was placed in the first two sublayers, while in S2B and S3B it was placed in all four sublayers of the model. Scenario S4 differed from S3 by incorporating a refined second aquifer consisting of three layers with the same average hydraulic conductivity.

The impact of layer refinement in the aquitard was explored in scenarios S5-S7. While S5 contained three homogeneous layers, S6 and S7 used heterogeneous layers. Notably, with the aquitard subdivided in multiple layers, the vertical flow barrier was positioned until the bottom of the second sublayer, no longer extending through the entire aquitard as in previous scenarios. This was done because in reality, the barrier reaches a maximum depth of 55 m-NAP, not reaching the deepest depth to where clay lenses were encountered. To investigate the significance of barrier depth in scenarios involving a multi-

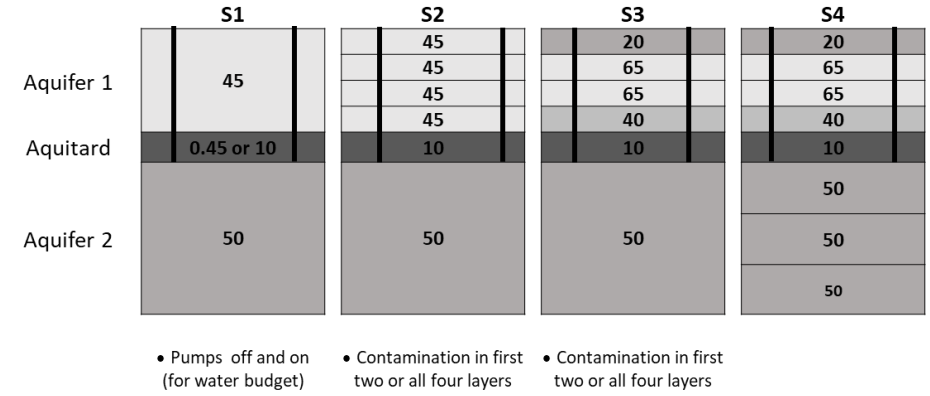

(a)

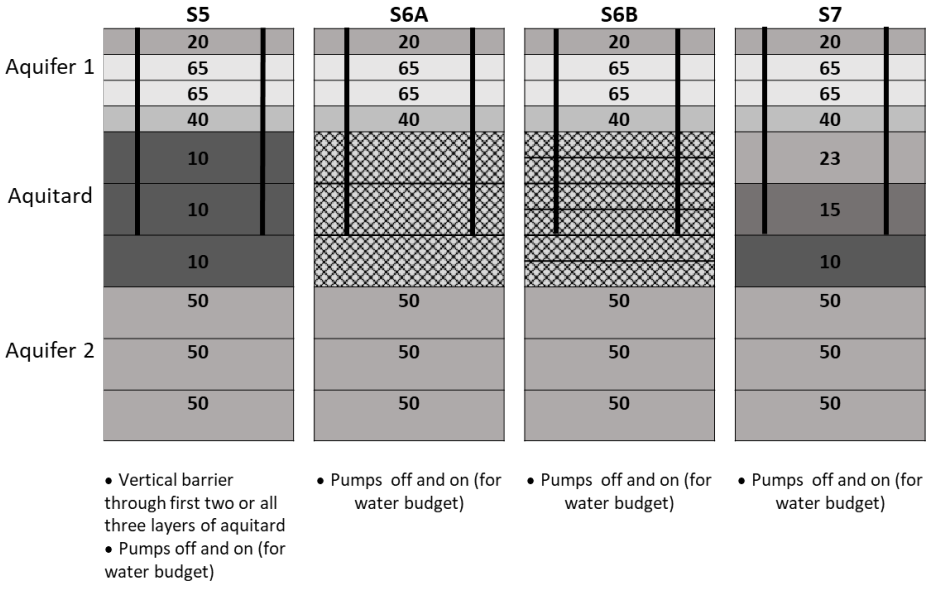

(b)

Figure 5.5: Layer discretisation scenarios in the Griftpark model. Figure (a) depicts the scenarios of first and second aquifer layer discretisations, Figure (b) depicts the scenarios of aquitard layer discretisations. The numbers within the layers indicate the average horizontal hydraulic conductivity K_h (m/d) of each layer. The gridded layers in S6 and S7 in Figure (b) represent heterogeneous K distributions obtained from EBK3D analysis. The images are not scaled to depth.

layered aquitard, S5 was complemented with an additional simulation, S5w, where the barrier extended to the full depth of the aquitard. Scenarios S6A and S6B feature 3 and 6 heterogeneous layers, respectively, with conductivity

distributions obtained from EBK3D. Finally, another scenario was added, S7, which implemented the average hydraulic conductivities of the three sublayers as provided by the EBK3D. All of the subscenarios S5-S7 included subscenarios with groundwater pumps operating, denoted as S5p-S7p.

Grid convergence was also studied in the horizontal plane, i.e. for the number of rows and columns. Using scenario S4 as a reference, the initial grid discretisation, containing 59 rows and 50 columns, was refined two and three times.

We compared the simulation results of each scenario focusing on two target variables: groundwater flow and solute transport. We presumed the grid convergence when the difference between the target outputs of two scenarios was less than 10%.

For the investigation of groundwater flow, we compared water budgets between different scenarios, specifically studying water flow in and out of the contained zone through the aquitard and vertical barrier. To calculate the water budgets, we defined a reference volume, horizontally bounded by the vertical barrier and vertically by the bottom of the aquitard. Using MODFLOW, we calculated both horizontal and vertical fluxes through this reference volume.

In addition to comparing water budgets among different scenarios, we also assessed the relative contributions of rainwater precipitation, leakage through the vertical barrier, and upward seepage through the aquitard to the overall water extraction from the system during groundwater pumping. These results were compared to field estimations of these numbers made in the past, and served as an extra validation of the scenarios.

For the solute transport, we used a conservative tracer, which transport was calculated with MT3DMS. The model incorporated two source zones with fixed mass loading rates, located in the north-west and north-east regions of the park where the deepest contamination was observed. As the contamination levels were not tied to real-world values, they were treated as unitless parameters and compared only relatively between the different scenarios.

The total simulation period for the breakthrough curves spanned 500 years, with a time step size of one year, allowing the plume in the second aquifer to almost completely stabilise. Breakthrough curves were simulated in observation well 101, referred to as Obs1, located in the second aquifer just down-gradient of the park, see Figure 5.3.

Furthermore, to explore the impact of using homogeneous versus heterogeneous aquitard layers, we employed visualisations of vertical flow directions to provide better insight into three-dimensional system dynamics.

5.4 Results and discussion

Results of scenarios S1 to S4 are shown in Table 5.4. The table shows (horizontal) water fluxes (m^3/d) in and out through the vertical barrier and (vertical) through the aquitard, as well as the unitless tracer concentrations in observation well 101. Comparing simulation results of scenarios S1A (K_h=0.45 m/d) and S1B (K_h=10 m/d), both water budgets and tracer concentrations show a significant difference. The results indicate that the more water flows out of the aquitard into the second aquifer, the lower the concentration in the observation well, indicating the plume gets more diluted with the increasing flux.

A comparison of the water budgets between simulations S1Ap and S1Bp revealed that using larger conductivities (10 and 3 m/d instead of 0.45 and 0.15 m/d for K_h and K_v respectively) yields values closer to those previously estimated from field data. These estimates indicated that with a pumping rate of 9 m^3/h, the water volume extracted from the system originates for 22% from precipitation, 18% from outside the vertical barrier and 60% through the aquitard [123]. Thus, the simulation results confirm the high permeability of the aquitard in the Griftpark area compared to the regional-scale average. Therefore, for the following simulations, average K values as used in scenario S1B are employed.

A comparison of simulation results for scenarios S1B, S2A and S3A, indicates that increasing the number of layers in the first aquifer, or using different K values for the layers, makes no significant difference in terms of water budgets or plume concentrations. However, a comparison between scenarios S2A and S2B, and S3A and S3B, shows that the depth at which contamination occurs, in the top two first aquifer layers or all four, changes the plume concentration by 10% and thus, using multiple layers in the first aquifer is considered important, especially as the effect of chemical reactions are still to be examined. As the difference is not larger than 10% and the outflow flux changes less than 5%, four layers are assumed adequate. As using different K values for each layer does not change computing time, this is used for the following simulations, in order to allow for any potential effects this may have in the reactive transport modelling.

Comparing scenarios S3 and S4, reveals that increasing the number of layers in the second aquifer does not have a significant impact water budgets or simulated concentrations in the observation well. However, as the concentration of the plume shows a strongly decreasing depth profile, see Figure 5.6, modelling is continued with three layers. For the breakthrough curves in following simulations, the observation well 1 is applied in the top layer of the second aquifer, as in this layer the highest concentrations occurs.

Name	Source layer	Barrier in	Barrier out	Aquitard in	Aquitard out	C Obs1	Comments
1A	1	18.7	1.5	0	67.9	19.7	No water comes up through the aquitard. What flows out through the aquitard is about 130% times the precipitation surplus
1Ap	-	44%	0%	32%	0%	-	Of the extracted groundwater, 23% comes from rain, 44% through the wall and 32% through the aquitard
1B	1	26	0.2	26.8	103.4	13.3	In this scenario a significant amount of water flows in through the aquitard and about as much as comes in through the barrier. Significantly more water flows out through the aquitard
1Bp	-	15%	0%	68%	-7%	-	Of the extracted groundwater, 23% comes from rain, 15% through the wall and 61% in through the aquitard
2A	1-4	25.6	0.2	30.7	100.5	13.8	In 2A the inward flux through the aquifer is 14% larger than in 1B and the outward flux is reduced by 3%. The concentration in $Obs1$ is 4% higher than in 1B
2B	1-2	”	”	”	”	15.2	In 2B, the contamination concentration in $Obs1$ is 10% higher than in 2A
3A	1-4	25.8	0.1	30.8	100.8	14	There is no significant difference between 2A and 3A
3B	1-2	”	”	”	”	15.3	Between 3A and 3B there is a similar difference as between 2A and 2B
4	1-4	24.4	0.2	35.5	104	14.8	In 4, compared to 3A, the amount of water that comes in through the aquitard is increased by 15% and the amount of water that flows out by 3%. The concentration in $Obs1$ is increased by 6%

Table 5.4: Summary of the results of the system's response to increasing the number of layers in the first and second aquifer as explained in Figure 5.5a. Numbers indicate water fluxes in m^3/d. S1A and S1B were also run with groundwater extraction pumps B20, 21 and 22 running at a total rate of 9 m^3/d (S1Ap and S1Bp). For these simulations flux components are presented in the table as their percentage of the groundwater pumping rate. For scenarios S2B and S3B, the simulations were run with the contamination extending only through the first two instead of all four layers of the first aquifer, but with the same total mass loading rate as the other scenarios.

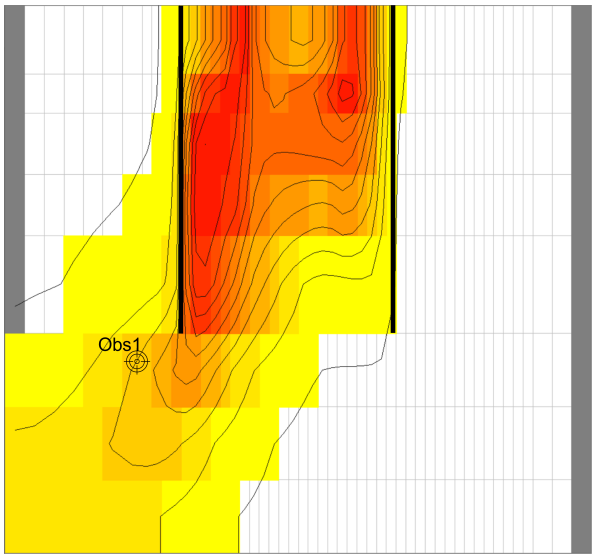

Figure 5.6: A vertical cross-sectional view of the tracer plume after 500 years in scenario S4. Groundwater flow in the second aquifer is east to west. The cross section shows that the plume concentration is highest in the top layer of the three-layered second aquifer. The head boundaries are indicated in grey and the vertical flow barrier in black.

Using scenario S4, which consisted of 59x50 cells of 10x10m, grid convergence was studied. The number of rows and columns was increased by a factor of two and three, creating cells of 5x5m and 3.3x3.3 m, respectively. The findings are summarised in Table 5.5. We found that the refinements had little effect on water budgets. After the first refinement the concentration in the observation well increased by 9%, after which we presume the grid to have converged. Thus, we continue with a domain of size 118x100 cells for the next step of our grid investigation.

The simulation results of scenarios S5 to S7 are shown in Table 5.6. Comparing scenarios S2, see Table 5.5, and S5, indicates that subdividing the aquitard model layer into three homogeneous layers makes only a small difference to water budgets or plume concentration. Comparing S5 and S5w, demonstrates that the difference between scenarios S2 and S5 results from the difference in installation depth of the vertical barrier, rather than by the increase in number of layers.

Comparing scenario S5 to S6, shows that a heterogeneous K field yields a significantly higher flux through the aquitard than a homogeneous K field. Despite the increased flux, the simulated concentration in the observation well is not significantly different between the two scenarios. Figure 5.7 shows that although the plume in the heterogeneous case is more concentrated along the

Name	Barrier in	Barrier out	Aquitard in	Aquitard out	C Obs1	Comments
$D1$	24.4	0.2	35.5	104	14.8	Is scenario 4 of the layer refinement for the first and second aquifer
$D2$	25.4	0.2	36.2	105.7	16.2	9% increase in concentration in $Obs1$ compared to $D1$
$D3$	26	0.4	36.3	106.2	15.9	Significant increase only in what flows out of the flow barrier, which flux is insignificant compared to other fluxes

Table 5.5: Summary of the results of column and row refinement based on Scenario 4 of the layer discretisation. Numbers indicate water fluxes in m^3/d.

centre line, the concentration in the core is lower than in the homogeneous case, exemplifying the non-linearity of such flow problems.

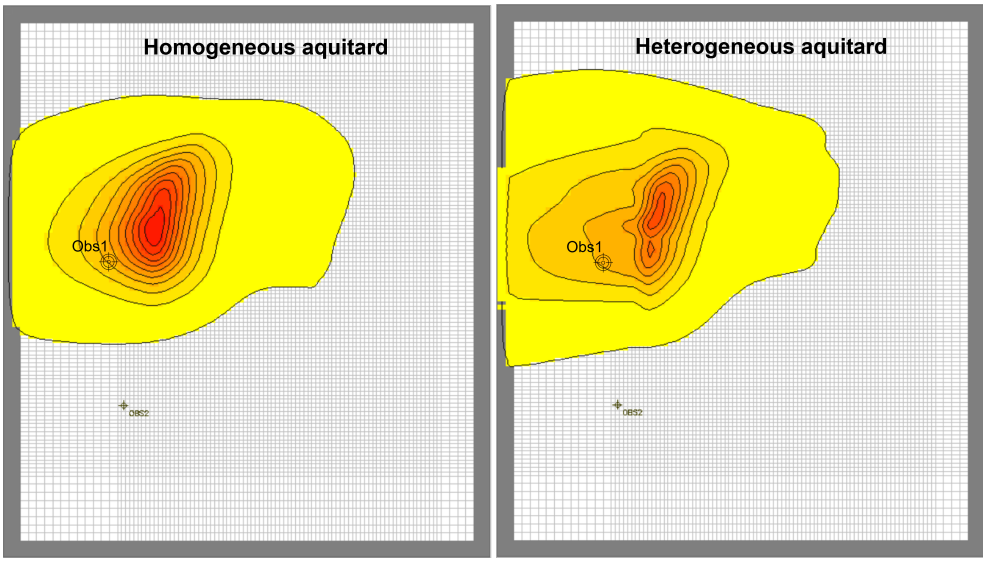

Figure 5.7: Comparison of plume development in the top model layer of the three-layered second aquifer, using either homogeneous (left) or heterogeneous (right) K fields (based on EBK3D interpolation) for the three aquitard model layers. The head boundaries are indicated in grey.

Comparing scenarios 6A and 6B shows that increasing the number of heterogeneous aquitard layers from three to six results in a difference of less than 10% in the water budget and no significant difference in concentration in the observation well. Running scenarios S5, S6A and S6B with pumps on, reveals that the water budgets of the scenarios are similar and approach field findings.

Name	Sublayers	Barrier in	Barrier out	Aquitard in	Aquitard out	$C\ Obs1$	Comments
5	3	23.6	0	36.7	104.6	16.8	Compared to 4, there is less than 5% difference to the water budgets, the concentration in $Obs1$ is 14% higher
$5w$	3	25.3	0.1	37.7	107.1	16.6	No significant difference to the water budget or the concentration in $Obs1$ between 5 and $5w$
$5p$	3	16%	0%	75%	-12%	-	Of the extracted groundwater, 21% from rain, 16% through the barrier and net 63% through the aquitard
$6A$	3	34.4	0	59.9	138.6	17.1	Compared to 5, almost 50% more water flows in horizontally, 63% more water comes in through the aquifer and 32% more out
$6Ap$	3	21%	0%	81%	-22%	-	Of the extracted groundwater, 21% comes from rain, 21% through the barrier and net 59% through the aquitard
$6B$	6	36.2	0	65.4	146.0	17.1	Compared to $6A$, there is almost 100% less outflow horizontally and 27% more outflow through the aquitard, the concentration in $Obs1$ is 25% higher. Compared to $6A$ there is less than 10% difference in the water budget
$6Bp$	6	21%	0%	82%	-24%	-	Of the extracted groundwater, 21% comes from rain, 21% through the barrier and net 58% through the aquitard
7	3	18.6	0.7	60.5	122.7	15.8	20% less water flows in through the barrier than in $6A$, resp. The amount of water that flows out of the aquitard is 11% less than $6A$
$7p$	3	13%	0%	86%	-19%	-	Of the extracted groundwater, 21% comes from rain, 13% through the barrier and net 67% through the aquitard

Table 5.6: Summary of the results of the system's response to increasing the number of layers in the aquitard as explained in Figure 5.5b. Numbers indicate water fluxes in m^3/d except for the simulations that were run with active groundwater extraction. For these simulations, i.e. S5p, S6Ap, S6Bp and S7p, flux components are presented in the table as their percentage of the groundwater pumping rate. Scenario S5 was also run with the vertical barrier extending throughout the complete depth of the aquitard (S5w).

Based on these observations we conclude that incorporating heterogeneous K fields in the subsurface model may be important, particularly when considering future simulations involving biodegradation where groundwater mixing could influence the availability of electron acceptors. The findings suggest that with the K fields provided by the EBK3D, using three sublayers is adequate.

For scenario S7, average hydraulic conductivities as provided by the EBK3D were assigned to each aquitard sublayer. The simulation results show that water budgets in this scenario more closely resemble those of the heterogeneous scenario S6 than that of S5 that utilises a homogeneous K_h value of 10 m/d. This outcome is expected since the value of 10 m/d was merely an estimation. In S7, less water flows out of the aquitard than in S6 when the pumps are off, whereas when pumps are on, the upward flux is stronger in 7, again highlighting the non-linearity of the flow problem.

Figure 5.8a shows the vertical direction of flow in S7, using the homogeneously layered aquitard, while Figure 5.8b shows the vertical direction of flow in 6A, using the corresponding heterogeneous aquitard. In the figures, red indicates upward flux and green downward flux. Note that strength of flow does not have the same limits in the two scenarios, and that for visibility the colour scales in the figures have been normalised for each subfigure separately. The figures show that in both scenarios, flow seeps up on the east side of the park and leaks down on the west side when the pumps are off. In the heterogeneous scenario, the flow is more local and stronger on the east boundary. The figure also shows that even with the pumps on, some groundwater escapes to the second aquifer in both the homogeneous and heterogeneous case.

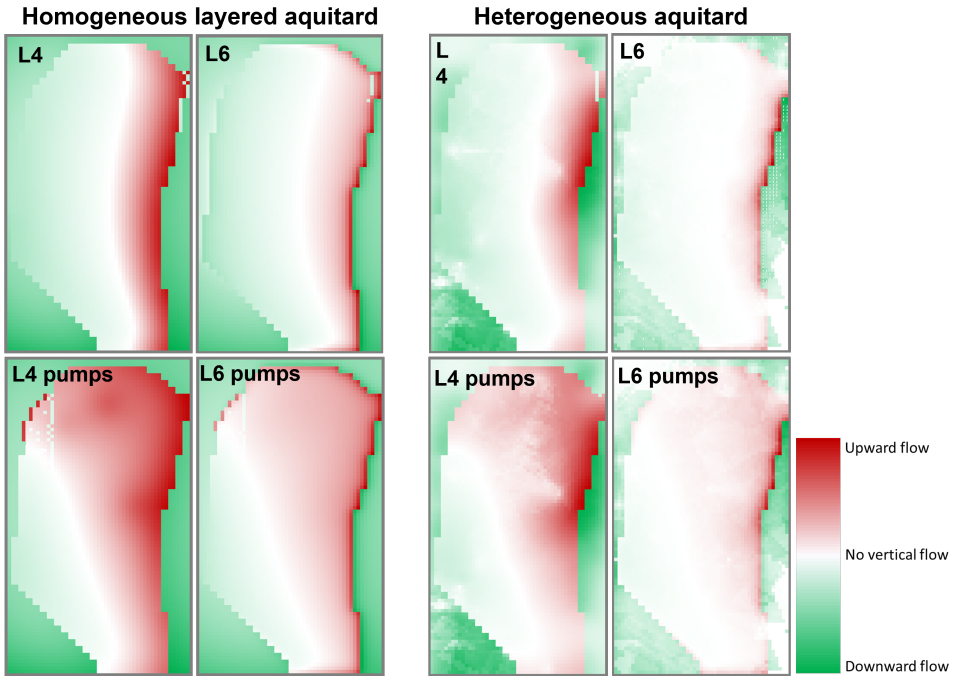

(a) (b)

Figure 5.8: Planar views of vertical flow exchange between the 1st aquifer and aquitard (model layer 4) and inside the aquitard through the plane where the bottom of the vertical barrier is located (model layer 6) when using a homogeneous (a) or a heterogeneous (b) layered aquitard. The colours indicate strength of vertical flow, upward flow in red and downward flow in green, and was normalised for each subfigure.

5.5 Conclusions

The use of physical subsurface investigation techniques such as resistivity profiling and visual soil inspection allowed the identification of small-scale heterogeneities in the Griftpark's subsurface that are particularly strong in the semi-confining aquitard.

Addressing subsurface heterogeneities that are smaller than grid size remains a challenge in field scale modelling. In our most refined simulation, we subdivided the aquitard in 5 m thick layers (i.e. the aquitard subdivided into 6 model layers), whilst clay depositions as thin as 20 cm were encountered in the field. For general flow simulation purposes, these heterogeneities can be accounted for by representational values of the hydraulic conductivity and dispersivity values.

Our simulations showed that treating the aquitard as a homogeneous or a

heterogeneous layered system has an impact on water fluxes into and out of the contained zone, but not significantly on tracer concentrations entering the second aquifer. Nevertheless, when considering biodegradation, the changes in water fluxes may affect contaminant concentrations more strongly. For instance, more tortuous flow paths resulting from heterogeneities can increase retention time, stimulate mixing and thereby modify biodegradation rates. As our simulations using a conservative tracer already revealed, these flow-related challenges exhibit highly non-linear behaviour. Therefore, it is hard to make prediction without numerical models.

In Chapter 6, we discuss the construction of a reactive transport model for the Griftpark. The impact of simulating the aquitard as a three layered homogeneous system, scenario S7, or as a three layered heterogeneous system, scenario S6A, while using reactive transport, will be studied there.

Chapter 6

Reactive transport model including biodegradation of coal tar compounds at the Griftpark

Abstract

This study aims to understand the key mechanisms involved in the biochemical processes occurring at the Griftpark site despite limited knowledge of the coal tar contamination and its biodegradation. To achieve this, a three-dimensional reactive transport model of the Griftpark is developed.

The reactive transport model successfully captures and qualitatively comprehends the crucial subsurface processes and identifies important considerations for continued risk assessment modelling including monitored natural attenuation at the site. Simulations reveal that biodegradation significantly reduces aromatic concentrations, with iron and sulphate as critical electron acceptors.

A sensitivity analysis demonstrates that, based on average degradation rates reported in literature, aromatic concentrations in the second aquifer downstream of the Griftpark remain below intervention levels after a 100-year simulation period, primarily due to biodegradation. However, at the lower end of the range of potential degradation rates reported in literature, contaminant concentrations exceed intervention levels. The analysis highlights that also the volume of subsurface contaminated with coal tar is a crucial factor in determining breakthrough concentrations in the second aquifer.

Furthermore, incorporating heterogeneity in the aquitard leads to increased spread of the contamination plume as well as higher concentrations within the

plume cores. However, the influence of this parameter, compared to the potential range of degradation rates and contaminant source zones, is relatively minor and is considered a valuable addition primarily when specific movement of the contaminant plume in the second aquifer is of importance.

While the numerous assumptions made in the model, e.g., coal tar sources, biodegradation rates, and groundwater composition, limit its direct application for decision-making purposes, the results are promising and provide a good basis for further investigation into the potential application of monitored natural attenuation as a management option for the Griftpark.

The results of this Chapter are integrated in a manuscript under preparation in *Advanced water resources*. Title: A comprehensive description of the characterisation and reactive transport modelling of a complex contaminated field site.

6.1 Introduction

Worldwide, many aquifers have been contaminated with coal tar [307]. Coal tars consist of mixtures of mostly of monoaromatic hydrocarbons (MAH), such as benzene, toluene, ethylbenzene and xylenes (BTEX), and polyaromatic hydrocarbons (PAH), such as naphthalene and fluorene [131, 224]. These dense non-aqueous phase liquids (DNAPL) can sink through the saturated zone as a immiscible phase and form irregular final distributions in the subsurface [75, 226]. Groundwater contamination caused by DNAPL compounds, which have very low solubility and dissolution rates, can persist for centuries and pose a serious threat to human health and the environment due to their carcinogenic effects [33, 82, 147, 156].

Natural attenuation, including dispersion, sorption and biodegradation, can reduce the concentration and size of organic contaminant plumes over time. Over the last three decades, many studies have shown that biodegradation is a relevant natural attenuation process [180, 203, 228, 274]. Monitored natural attenuation (MNA) has become an accepted management option for low-risk contaminated sites, while stimulated biodegradation may be used where the natural potential for biodegradation is limited [307, 193, 228, 313].

To determine the viability of MNA for specific contaminated sites, reactive transport models provide valuable insights. Reactive transport models may integrate all available hydrological, hydrogeological and hydrogeochemical information to develop a quantitative framework to evaluate the long-term groundwater risks posed by a contamination. The first multi-component reactive transport models that treat any combination of transport and biogeochemical processes were developed by the mid-1980s [178, 269, 320, 65].

Constructing a reliable reactive transport model requires a comprehensive understanding of contaminant release rates and the various processes that contribute to natural attenuation. However, the dynamics of microbial degradation reactions are complex and models should account for several, often competing, biogeochemical reactions.

An additional challenge arises when constructing transport models for sites where contaminant source zones have been physically contained. Excavating and treating contaminants ex-situ is often economically unviable due to the deep penetration of DNAPLs into the subsurface [33]. Therefore, at many locations contaminated with DNAPLs, source-zones have been physically contained with vertical barriers, often combined with groundwater extraction [198]. This 'contain-manage' technique has been applied at over 2.388 contaminated sites in the Netherlands [11]. Although the method effectively protects groundwater outside of the barriers, it fails to reduce the total contaminant volume, thus requiring perpetual management. Building on the

knowledge of MNA developed in the past three decades, contain-and-manage sites in the Netherlands are being re-evaluated, aiming to phase out active management procedures and instead relying on MNA as a new management approach.

To make mass balance analyses and determine source release and biodegradation rates, changes in biochemical factors such as contaminant and electron acceptor concentrations are mostly monitored along or through contaminant plumes [212, 312, 322, 57, 121]. However, at contained sites, the absence of a dominant groundwater flow direction and, consequently, a traceable contaminant plume, poses challenges in site assessment, creating an information gap that hinders the development of a reliable reactive transport model. To the best of our knowledge, there have been no previous studies examining biodegradation at contained contaminated sites.

In this Chapter, the Griftpark, Utrecht, the Netherlands, a physically contained coal tar contaminated site, is used as a case study to construct a three dimensional reactive transport model with a focus on MNA. The Griftpark site is characterised by a high level of complexity. The site's subsurface hydrogeological conditions are strongly heterogeneous and a high level of uncertainty exists in knowledge of the locations, sizes and mass transfer rates of DNAPL source zones, biodegradation rates and the mineralogical composition of the subsurface.

With the numerical model, we simulate contaminant release from source zones, subsequent transport through the subsurface and the occurring natural attenuation processes. To calibrate the model we apply a manual, iterative method to match simulation results with field findings. The primary objectives of this study are to use the model to (1) gain insights into the dominant geochemical reactions governing the system, (2) perform a preliminary risk assessment to evaluate the feasibility of MNA and (3) assess the most important subsurface parameters that require further investigation to improve the model.

6.2 Field site description

6.2.1 History and hydrogeology

The Griftpark, located in Utrecht, the Netherlands, was built on a former industrial site that hosted several manufactured gas plants, operated between 1860 and 1960, leaving behind extensive coal tar contamination. Due to the depth to which pure-phase tar was encountered when the contamination was discovered in the 1980s, ation or in-situ treatment was deemed impracticable. Therefore, a cement-bentonite vertical barrier was installed around the site in

1990 to prevent further down-gradient migration of the contaminant plume. The vertical barrier extends to 55 m-bgl, well into the aquitard that separates the first aquifer from the second. As the aquitard is not completely confining, a risk exists for contaminated groundwater to leak from the first to the second aquifer. To establish inward seepage, both through the cement-bentonite wall and the aquitard, groundwater pumps operate within the contained zone.

The geologic formation at the location of the Griftpark consists primarily of marine and fluvial deposits originating from the Holocene and Pleistocene eras [32]. The first aquifer, composed of the Westland, Kreftenheye, Urk and Sterksel formations, extends to a depth of about 50 m-bgl. It has a heterogeneous structure with both fine and course depositions and an average hydraulic conductivity (K) of around 40 m/d [6]. The second aquifer, the Harderwijk formation, extending from about 70 to 110 m-bgl, is relatively homogeneous and has an average K of 50 m/d [6]. The first and second aquifer are separated by the Waalre formation, characterised by clay and silt deposits. The Griftpark is situated on a geological fault line, which has caused clay from the Waalre formation to be interspersed with sand from the Harderwijk formation. As a consequence, the aquitard is not fully confining. Further details on the lithology can be found in Chapter 2.

Outside the barrier, regional groundwater flow velocities are estimated to be about 12 m/yr in both the first and second aquifer in a south-east/north-west and east/west direction, respectively. The hydraulic head in the first aquifer is approximately half a metre higher than in the second [79]. The cement-bentonite vertical barrier around the site, extending to a depth of 55 m-bgl has an estimated resistivity (hydraulic conductivity/thickness) of 170 days [123]. A hydraulic head difference of around 20 cm over the barrier and upward seepage from the second aquifer is maintained through the continuous operation of three groundwater extraction wells (B20, B21 and B22). The vertical barrier and extraction well locations are shown in Figure 6.1.

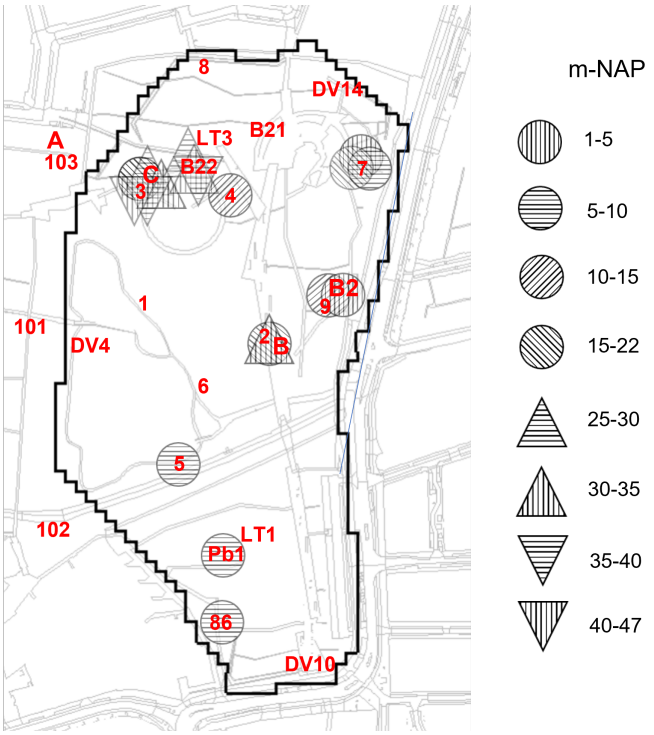

Figure 6.1: Expected pure phase coal tar zones indicated by grey striped symbols. Pumping wells are indicated in blue and the monitoring wells in red.

6.2.2 Contamination

Pure phase coal tar

Coal tars consist of hundreds of different hydrocarbons [110]. The applied carbon source, carbonisation temperature, gas purification and storage techniques all have a direct influence on the composition of sediment contamination at former manufactured gas plants (FMGP) [40, 110, 307]. As at the Griftpark industrial site multiple types of gas factories and purification facilities existed, the composition of different tars at the Griftpark is expected to be diverse. The various solubilities of different compounds within coal tar, causes the pure phase composition to change over time. Lower molecular weight compounds dissolve more easily, so that the molar fraction of heavier, less soluble, compounds increases over time [158, 102, 33].

For this work, we made the simplifying assumption that all coal tar at the Griftpark has the same composition. A pure tar sample was collected from location C, indicated in Figure 4, and weight percentages of mono-aromatic hydrocarbons (MAH) and poly-aromatic hydrocarbons (PAH) of a sample

Compound	WP	MW	S	K_d
benzene	0.1	78.1	0.0228	0.0003
toluene	0.1	92.1	0.0058	0.0012
ethylbenzene	2.3	106.2	0.0015	0.0039
m/p-xylene	2.0	106.2	0.0015	0.0039
o-xylene	0.3	106.2	0.0017	0.0025
indane	5.6	118.2	0	0.0039
indene	0.7	116.2	0	0.0020
naphthalene	42.5	128.2	0.0008	0.0049
1-methyl-naphthalene	14.3	142.2	0.0002	0.0182
2-methyl-naphthalene	24.4	142.2	0.0002	0.0178

Table 6.1: Properties of the MAHs and PAHs that constitute 90 of the weight of a pure tar sample from the Griftpark, i.e. their relative weight percentage (WP %), molecular weight (MW g/mol), solubility at 25 ^oC (S mol/L) and distribution coefficient (Kd m^3/kg)

ten times diluted in acetone were analysed. Table 6.1 shows the compounds that constitute 93% of the total coal tar mass, and their weight fractions in the tar. Naphthalene and methylated naphthalenes are the most abundant compounds in the mixture. Of this representative mixture, less than 5% of the weight consists of the mono-aromatic BTEX compounds.

As naphthalene is the most soluble of the PAHs, the percentage of naphthalene in the coal tar will decrease with aging. In our modelling, we refrain from reconstructing the original coal tar composition and use the measured composition as a starting point for forward modelling.

Similar to the situation found at most FMGP sites, sediment contamination at the Griftpark is characterised by extreme heterogeneity. This heterogeneity is caused by the random deposition of coal tars and relocation of contaminated sediment during construction works [307], as well as the irregular downward migration of DNAPLs through the heterogeneous subsurface [169, 205, 75, 91]. Consequently, fully mapping coal tar distributions is a challenge.

In Chapter 2, the methodology for obtaining information on locations and depths of coal tar source zones was described. The results of the analysis are shown in Figure 6.1. As the data came from vertical profiles (membrane interface profiling and visual sediment core inspection) and point measurements (groundwater sampling), the size and geometry of the encountered pure phase product could not be analysed. As such, the symbol sizes do not represent the actual extent of the pure tar zones.

Dissolved contaminants

Concentrations of coal tar aromatic hydrocarbons were analysed in groundwater samples taken from various locations within the contained zone. In the following, we focus mainly on the results from locations, B, B2, C and B22, see Figure 4. B22 is a groundwater extraction well. At B, B2 and C multi-level sampling wells were used to collect groundwater samples from depths ranging from 7 to 65 m-bgl. The targeted compounds in this analysis are the mono-aromatic hydrocarbons (MAH) benzene, toluene, ethylbenzene and o/m/p-xylene (BTEX), trimethylbenzene, propylbenzenes, ethyltoluenes and the polyaromatic hydrocarbons (PAH) naphthalene, styrene, indane and indene. The procedure of analysis is described in Chapter 3. Figure 6.2 shows the results, including the total dissolved concentrations of the measured compounds and the weight fractions of individual compounds in the mixture.

The sample from B22 was completely saturated with coal tar. The total concentration in this sample was used to indicate maximum solubility of the mix of targeted compounds (40 mg/L). Although during drilling of the borehole of well C, pure phase coal tar was found in core samples at all depths across 26 to 50 m-bgl, even the maximum concentration measured in well C (14 mg/L), at 46 m-bgl, was significantly less than estimated maximum solubility. This indicates that biodegradation effectively reduces dissolved coal tar aromatics in the subsurface.

Figure 6.2 shows that naphthalene alone constitutes around 50% of the total concentration of the targeted mix in most groundwater samples and that benzene generally occurs at highest concentrations of the MAHs.

No detectable level of contaminants was observed in wells 101, 102, and 103, located in the second aquifer immediately downgradient of the Griftpark. This indicates that either or both the groundwater pumps in the park effectively prevent leakage of dissolved contaminants from the first to the second aquifer and biodegradation breaks down dissolved contaminants below the park. Additionally, pumping and/or biodegradation avoids the further spread of contaminants dissolving from pure phase coal tar potentially present in the second aquifer due to downward migration. We will revisit this topic at the end of the next paragraph.

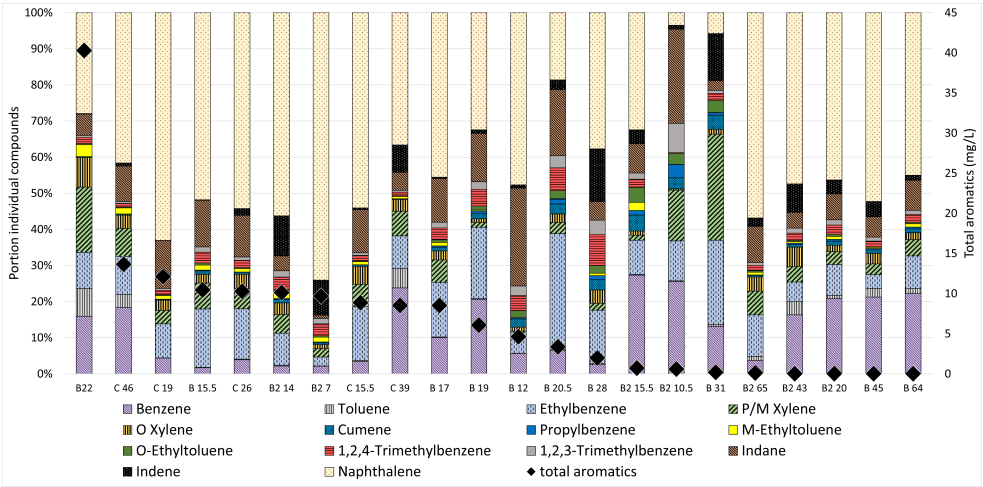

Figure 6.2: BTEXIeIaN fractions (coloured bars, left axis) along decreasing total dissolved BTEXIeIaN concentrations (black diamonds, right axis) in samples from various depths from wells B22, B, B2 and C.

Indications of biodegradation

At contaminated sites, observed hydrogeochemical changes can serve as indicators for the occurrence of biodegradation reactions and reproducing the observed patterns with reactive transport models can be used to quantify at which rate the biodegradation processes occur. Changes in biochemical factors at field sites are mostly monitored and modelled along contaminant plumes [212, 322, 121, 234, 66].

In the conventional interpretation, if the organic pollutants act as electron donors, distinct zones of specific redox potential (redox zones) evolve downgradient of contaminant source zones, depending on the concentration and reactivity of the electron acceptors present in the aquifer [17, 188]. However, overlapping redox zones have been observed at many contaminated sites, as redox reactions may not always occur sequentially along a fthermodynamic order, but also simultaneously [148, 146]. For instance, the simultaneous occurrence of sulphate and iron reduction along with methane production has been observed in plumes [153, 34, 186, 253].

At contained sites, clearly traceable contaminant plumes are absent and it has previously been found that at low groundwater flow velocities, redox zones may become completely indeterminate [17]. At the Griftpark, due to low flow velocities and the absence of a distinct flow direction due to the vertical barrier, groundwater pumping and subsurface heterogeneities, and the overlap in redox conditions enhanced by the presence of multiple pure phase source zones, it is difficult to obtain firm mass balance estimates. As

such, this causes the corresponding determination of biodegradation rates to be uncertain. Figure 6.3 illustrates the concept of groundwater mixing resulting from subsurface heterogeneities and multiple zones of pure phase coal tar, explaining the complex effects on dissolved contaminant composition and electron acceptor consumption.

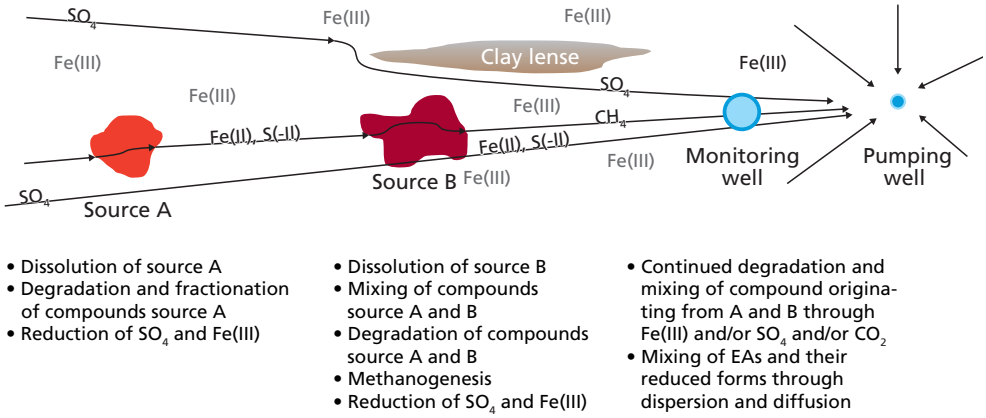

Figure 6.3: Conceptual representation of the mixing of dissolved compounds in the subsurface. Reduced EAs, i.e. S(-II), Fe(II) and CH4, may mix with fresh EAs that are transported with the groundwater, such as sulphate, or present in the sediment, such as iron oxides, due to tortuous flow paths. It also indicates how mixing of the reduced EAs and isotopic finger prints occurs due to the presence of multiple source zones.

With methods explained in Chapter 3, we were able to proof that sulphate and iron oxide minerals are likely the major electron acceptors in the degradation of the aromatic hydrocarbons at the Griftpark, while manganese reduction and methanogenesis may provide minor contributions. Evidence of different redox processes was found to co-occur in groundwater samples at most locations. Oxygen and nitrate do not occur below the first few meters of the first aquifer, while in the second aquifer a low level of nitrate, approximately 0.5 mg/L, exists.

Sulphate was generally measured in high concentrations in the contained zone, at a maximum of 237 mg/L in well B at 44-45 m-bgl where the total targeted aromatic hydrocarbon concentration was 0.025 mg/L. An average of 3.5 mg/L sulphate was measured in samples with aromatic concentrations above 3 mg/L, indicating the occurrence of sulphate reduction. The high concentrations of sulphate at the site in comparison to the 79 mg/L measured in an up-gradient well, indicates a source of sulphate in the subsurface. Potential sources of sulphate include the presence of gypsum created during gas pu-

rification, or cement rubble from old factories. Sulphate concentrations were found to be lower in zones with higher dissolved aromatic concentrations.

Whereas sulphate exists in the groundwater as a dissolved phase, Fe(III) and Mn(IV) occur in minerals in the ground. In groundwater, only their reduced products Fe(II) and Mn(II) can be used as an indicator for biodegradation. Due to precipitation of these products in other minerals, however, they are not suitable as a direct measure of the level of biodegradation.

The highest Fe(II) concentrations are generally measured in samples with low aromatic hydrocarbon concentrations. For example, a maximum of 15 mg/L Fe(II) was measured in MLS well B2 at 23.5 m-bgl with 0.026 mg/L of aromatics, whereas an average of 2.8 mg/L Fe(II) was measured in samples with aromatic concentrations above 3.0 mg/L.

Dissolved Mn(II) was found in all groundwater samples, with a maximum concentration of 1.7 mg/L. The average Mn(II) concentration in samples with aromatic concentrations above 3.0 mg/L was 0.3 mg/L. Considering the significantly lower concentrations of manganese in the subsurface, see Chapter 3, manganese reduction is assumed a minor contributor to the overall degradation at the Griftpark.

Methane concentrations up to 2 mg/L were found. There is no direct trend between the concentrations of aromatic hydrocarbons and methane, however, at hydrocarbon concentrations above 3 mg/L, methane occurs in all samples at an average of 0.3 mg/L. Although methanogenesis is shown to widely occur at the site, it is a slow process, and the speed of biological breakdown of aromatic hydrocarbons at the Griftpark is presumed to be mostly determined by iron and sulphate.

The electron acceptor (EA) assessment in the second aquifer, showed that EA concentrations up- and downgradient of the Griftpark were similar, giving no indication of biodegradation. These findings indicate an absence of pure phase coal tar in the second aquifer.

6.3 Numerical model

6.3.1 Modelling tools and approach

Software selection

As described in Chapter 5, a three dimensional model simulating groundwater flow and contaminant transport at the Griftpark was set up in MODFLOW/MT3DMS. MODFLOW-2000/2005 simulates groundwater flow in aquifer systems using the finite difference method [197]. In this method, the aquifer system is divided into rectangular cells, in which hydraulic heads are calculated by solving groundwater flow equations using specified aquifer properties

and hydraulic boundary conditions at set time intervals. Basic subsurface transport was solved using the MT3DMS module, through which advective and dispersive transport of particles, as well sorption is calculated [328].

For modelling reactive transport, the PHT3D extension was used [235]. PHT3D is a reactive multi-component transport model for saturated porous media that combines the modular MODFLOW/MT3DMS flow and transport simulator with the capabilities of the PHREEQC-2 code. PHREEQC is written in the C programming language and is capable of simultaneously solving geochemical equilibrium and arbitrary, kinetically controlled reactions [227]. Ready geochemical databases are available for PHREEQC that include a broad range of equilibrium and kinetic reactive processes, such as aqueous complexation, mineral precipitation and dissolution and ion exchange. Reactions that are not included in the standard PHREEQC database, such as NAPL component dissolution and degradation, can be defined by the user and included in the database.

MODFLOW and PHREEQC are both widely used in groundwater and geochemistry communities and well tested and documented. In PHT3D, MT3DMS and PHREEQC are coupled via an operator splitting method. For each timestep, firstly the transport of solutes is solved in MT3DMS and secondly chemical transformations are solved in PHREEQC.

For the Griftpark case study, PHT3D was used to simulate (1) dissolution of immobile coal tar aromatic hydrocarbons into the groundwater (through PHREEQC), (2) advective-dispersive transport and sorption of dissolved hydrocarbons in the aquifer (through MT3DMS), (3) the transformation of dissolved hydrocarbons through biodegradation and evolution of the aquifer's biogeochemical conditions (through PHREEQC). In the following Sections we will elaborate on the underlying processes and equations in this order.

Modelling procedures

For the reproduction of field observations by the Griftpark model's simulations, we focus primarily on the vertical profiles of contaminant and EA concentrations obtained from groundwater samples from various depths at three multi-level sampling (MLS) wells, B, B2 and C, depicted in Figure 4. It should be noted that the model's layer structure is coarser compared to the actual sampling depths. Therefore, the numerical model results may not exhibit the same level of depth precision as the field data. In addition to these profiles, we also incorporated concentration data obtained from groundwater samples taken from wells Pb1 and DV4 in the analysis. Furthermore, concentration levels measured during MIP profiling at MIP locations 1, 4, 5, 6, 7, and 8 were included in the analysis. Figure 6.4 illustrates the locations of the wells mentioned above.

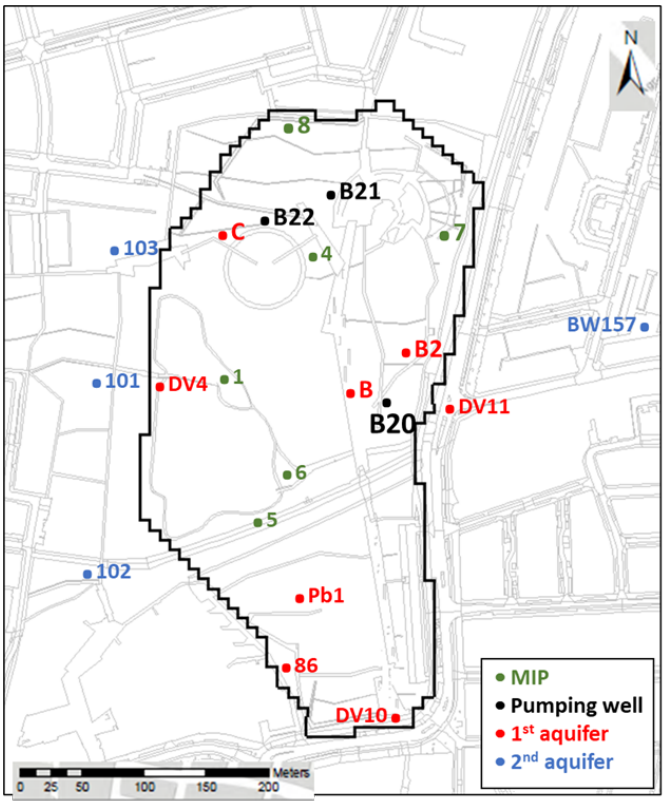

Figure 6.4: Well and test locations at the Griftpark.

We distinguish two main steps in the modelling process. Initially, the conceptual model was used to establish a representative model that reproduces the major patterns of the observed contaminant and EA depth profiles. Considering the significant uncertainty surrounding our understanding of the Griftpark site, including source zone locations, mass transfer, and degradation rates, our objective was not to develop a fully predictive model. Instead, we aimed to employ simulations to provide a general understanding of degradation conditions and subsequent geochemical changes in the field. The acceptability of the model representation was determined based on its ability to facilitate this explanation effectively. Subsequently, the representative model was subjected to a basic sensitivity analysis to enhance our understanding of the system's behaviour. This knowledge will prove valuable for effective decision-making processes.

For the first step, the flow model is run for a 35 year period in a mode reflecting field conditions since the installation of the vertical barrier in 1990, i.e. with groundwater pumps B20, B21 and B22 running at a total average

rate of 10.5 m^3/h. The approach for finding hydraulic conductivities for the various subsurface layer was reported in Chapter 5 . For the reactive transport model an adjustment was made, as explained in the following Section. Because of the wide range of possible interpretations of existing knowledge of the site regarding hydraulic conductivities, flow fields, source zone locations, depths and compositions and biogeochemical conditions, no automated calibration was attempted for any of the simulations. Instead, a manual trial and error approach was used. Furthermore, the number and size of source zone locations, dissolution rates and degradation rates are highly correlated parameters. We therefore decided to apply a dissolution rate that establishes a local equilibrium between the pure and dissolved phase and average field-scale degradation rates found in literature. The size and number of source zone locations were selected as adjustable parameters in the calibration, altering their values with a manual trial and error approach until simulated results approach field values. Additionally, the starting concentration of iron-containing mineral was used as an adjustable parameter.

During the second step, the flow model is run for an additional 100 years with the pumps deactivated. Contamination risks in hydrogeology are commonly evaluated along a source-pathway-receptor conceptualisation [93]. In line with this, our sensitivity analysis focuses on exploring the influence of variations in model parameters on breakthrough concentrations in the second aquifer, specifically in three wells located downstream of the Griftpark (wells 101, 102, and 103, see Figure 6.4. It is important to note that while the sensitivity analysis presented in this Chapter does not provide a comprehensive risk assessment for the Griftpark, as we work with a single conceptual model that entails a considerable level of uncertainty, adopting the source-pathway-receptor conceptual framework contributes to addressing the central research question of the Griftpark project. This question revolves around evaluating the reliability of monitored natural attenuation (MNA) in preventing the occurrence of unacceptable contamination levels in the second aquifer after deactivating groundwater extraction. The parameters investigated during the sensitivity analysis are the use of heterogeneous vs homogeneous hydraulic conductivities in the aquitard, biodegradation rates and dispersivity values.

The procedure to set up a representative model (step one) with which the sensitivity analysis can be performed are explained in the Section 6.3.3 and for the iron-mineral concentration in Section 6.3.3. The results after running the thus obtained representative model for 35 years and their comparison to field data are presented in Section 6.4.2. In Section 6.4.3, the results of the sensitivity analysis are discussed.

6.3.2 MT3DMS model

Construction of the flow model was discussed in Chapter 5. Following additional investigations prior to setting up the PHT3D model, the model was fine-tuned. Updated model parameters and detailed layer information are given in Table 6.2 and Table 6.3. In the x-y plane a coarser version of the model than described in Chapter 5 was used to keep the reactive model computationally viable. The increase in numerical dispersion is deemed negligible compared to the uncertainties inherent to the conceptualisation. We employed an intermediate longitudinal dispersivity value of 4 m [323]. This value is around ten times larger than what is applicable for the relatively homogeneous Borden aquifer but on the small end of that of the highly heterogeneous Colombus Air Force Base aquifer [106, 5]. We set the values of horizontal and vertical transverse dispersivities to $\alpha_T = \alpha_L/10$ and $\alpha_V = \alpha_T/10$, respectively. These values lie in the high range of reliable values obtained at previous studies [323], and are applied considering the high level of heterogeneity in the Griftpark subsurface.

Parameter	Value
Spatial settings	
Model dimensions l_x x l_y x l_z	600 x 680 x 112 m^3
Number of rows x columns x layers	61 x 50 x 16
Cell discretisation refined cells	10 x 10 m^2
Layer specific parameters	
Porosity 1st aquifer	0.35
Porosity aquitard	0.4
Porosity 2nd aquifer	0.35
Anisotropy factor K_h/K_v 1st aquifer	5
Anisotropy factor K_h/K_v aquitard	10
Anisotropy factor K_h/K_v 2nd aquifer	3
General head boundary conductance 1st and 2nd aquifer	500 m^2/d
General head boundary conductance aquitard	1 m^2/d
Global model parameters	
Soil dry bulk density	1600 kg/m^3
Longitudinal dispersivity α_L	4 m
Horizontal transverse dispersivity α_T	0.4 m
Vertical transverse dispersivity α_V	0.04 m
Precipitation surplus	0.0006 m/d
Resistivity hydraulic barrier	170 days

Table 6.2: Flow model parameters.

Two parallel models were set up. Both feature the aquifer system consisting of three lithological layers: the first aquifer, the leaky aquitard and the second aquifer. The first aquifer (2 m+NAP until 30 m-NAP) is in both models represented by four lithological units, each with a different average hydraulic conductivity. The first aquifer is refined to 10 model layers (rang-

Unit	Layer	Top (m-bgl)	Bottom (m-bgl)	Thickness (m)	K_h (m/d)	K_v (m/d)
1st aquifer	1	-2	5	7	20	4
	2	5	12	7	20	4
	3	12	16	4	65	13
	4	16	20	4	65	13
	5	20	24	4	65	13
	6	24	28.5	4.5	65	13
	7	28.5	32	3.5	65	13
	8	32	37	5	40	8
	9	37	41	4	40	8
	10	41	45	4	40	8
aquitard	11	45	52	7	**2.6**	**0.26**
	12	52	58.5	6.5	**1.8**	**0.18**
	13	58.5	65	6.5	**0.92**	**0.092**
2nd aquifer	14	65	80	15	50	17
	15	80	95	15	50	17
	16	95	110	15	50	17

Table 6.3: Model layer depths and hydraulic conductivities. The hydraulic conductivities within the aquitard indicate the average conductivities in the homogeneous model and are shown in bold .

ing from 3.5 to 7 m thickness) to allow for more defined source zone locations and reduce numerical dispersion in the vertical direction.

The aquitard (30-60 m-NAP) is represented by three sublayers (6.5 m thick). The hydraulic conductivity of each sublayer was taken as the average of the heterogeneous values of the corresponding layer that was based on an empirical Bayesian kriging analysis (EBK3D) performed with the available subsurface data, as reported in Chapter 5. To better match field hydraulic head measurements, conductivity values obtained through EBK3D used in Chapter 5, were divided by a factor of 10. These averaged hydraulic conductivities are shown in bold in Table 6.3.

The second aquifer (60 – 110 m-NAP) is represented by a fully homogeneous unit and is subdivided in three model sublayers (15 m thick) to allow for some vertical plume profiling. The model domain spans 1x1 km and features general head boundaries on the east and west ends. When groundwater extraction pumps operate, water may flow inward from both sides of the domain. Equivalent hydraulic conductivity on the head boundaries is set to 500 m^2/d in the first and second aquifer, approaching a fixed head boundary condition. In the aquitard it is set to 1 m^2/d, allowing a stronger response to changes in rates of the groundwater pumps that affect flow between the first and second aquifer.

The cement bentonite vertical barrier surrounding the park is implemented using the MODFLOW horizontal flow barrier package with a resistivity of 170

days. It extends from the first model layer, until the bottom of the second aquitard layer at a depth of 58.5 m-NAP. The model contains three pumping wells, B20, B21 and B22, locations are shown in Figure 6.4. Wells B20 and B21 are screened between 12-20 m-NAP (extending through layers 3 and 4), while B22 is screened between 26-36 m-NAP (extending through layers 6 and 7) and 38-46 m-NAP (extending through layers 9 and 10).

6.3.3 Reactive transport model

Source zone reconstruction

Fractions of aromatic hydrocarbons measured in a recently collected coal tar sample from the Griftpark was chosen as the starting composition in our simulations. To reduce the computational load of the model, only a selection of the full set of compounds encountered in the groundwater is included in the simulations. To ensure a realistic simulation of degradation and travel distances of dissolved hydrocarbons, the selection should cover most of the contaminant mass and the contaminants should cover a range of the geochemical properties such as solubility and sorption. Some important properties of the most abundant compounds are depicted in Table 6.1. Although not used for the current simulations, all compounds shown in Table 6.1 are included in the PHREEQC database for the benefit of potential future simulations.

Benzene and naphthalene were selected as target compounds. They are used to compare the simulation results to field data in order to calibrate the model. Benzene was selected as it has high solubility, low sorption and low biodegradation rates and is therefore an important compound for tracking plume mobility. Despite its low weight percentage compared to ethylbenzene and m/p xylenes in the pure tar, due to its high solubility, it occurs at the highest dissolved concentrations of all MAHs in the groundwater, as shown in Figure 6.2. Naphthalene was selected because it is the most prominent PAHs in the pure tar and was, opposed to the methylated naphthalenes, included in the groundwater analysis used for studying biodegradation, as described in Chapter 3.

To represent the full contaminant load in the model, the other MAHs (toluene, ethylbenzene and m/p/o xylene) were lumped into one specie, represented in the model with the physiochemical properties of ethylbenzene. The remaining PAHs (indane, indene and methylated naphthalenes) were lumped into a single compound with the properties of 1-methylnaphthalene. The cumulative weight percentages of these four species in the pure DNAPL are shown in Table 6.4.

DNAPL is assigned to the source zone cells (specified as immobile species in PHREEQC) using a Dirichlet boundary condition. To prevent DNAPL

depletion throughout the simulation period, a high saturation of DNAPL is assumed, by implementing a total DNAPL concentration of 2 mol/L in the source zone cells. The concentrations of the four representative compounds employed in the source zone cells are shown in Table 6.4.

Compound	WP	C_i
benzene	0.001	0.018
MAH	0.047	0.585
naphthalene	0.425	4.384
PAH	0.527	5.012

Table 6.4: Weight percentage (WP %) and initial mass (C_i (mol/L)) of the selected compounds used in the reactive transport model. Benzene and naphthalene are used as pure compounds, whereas MAH and PAH are used to represent the rest of the mono- and poly-aromatic mass in the tar respectively. In the model, the MAH has the properties of ethylbenzene and PAH those of 1-methyl-naphthalene.

The initial allocation of immobile aromatic hydrocarbon species to model cells was based on the information provided in Figure 6.1. Next, using a manual trial and error approach, source zones cells were added and moved until a satisfactory match between simulated and measured benzene, naphthalene and sulphate concentrations was obtained. For simplicity, the DNAPL distribution was kept the same in layers 2-4, 5-11 and 12-13, where, due to varying model layer thickness, cell volumes vary between 1311 and 2295 m^3. During installation of the contain-and-manage measures, the top soil of the Griftpark was remediated. Therefore, no coal tar sources were allocated to the top model layer.

For the analysis, measured values in groundwater samples collected from a variety of depths in MLS wells B, B2, and C, as well as in samples from Pb1 and DV4, of which the locations are indicated in Figure 4, were used. To aid the positioning of source zones in the model, groundwater flow lines were traced using the MODFLOW extension PMPATH. For illustration, 100-year flow lines retraced from layers 2 (red), 5 (green) and 12 (blue) at MLS wells B, B2 and C are shown in Figure 6.5.

Due to the lack of specific field values, we applied the average of literature-derived degradation rate constants during this modelling process (Table 6.5). To prevent obtaining saturation concentrations in the simulation results, pure phase NAPL was not allocated to cells hosting observation wells.

The source zone architecture chosen for our representative model is depicted in Figure 6.6. The pure phase mass is distributed over 323 model cells with a total volume of 163,600 m^3. With a porosity of 0.35, a tar saturation of 54% in the contaminated cells and a tar density of 1200 kg/m^3, the total initial mass of coal tar in the reference conceptual model is 36,840,000 kg.

This would come down to a saturation of almost 1.5% of the total subsurface volume contained by the vertical barrier and aquitard.

To replicate measured concentrations in the deepest monitoring wells at B and B2 (62 m-NAP) and C (49 m-NAP), pure phase coal tar should be implemented deep into the aquitard of the Griftpark model. Substantial amounts of pure phase tar should be present at significant depths at location C, where during field investigations tar was found perched on top of clay depositions. Water is pumped up from the second aquifer, as the flow lines in Figure 6.5 show, and thus the contamination found in the deepest wells must originate from this direction. However, the presence of clay lenses at these depths in the Griftpark subsurface can significantly alter the flow direction at a local scale, which our homogeneous model cannot reproduce. Therefore, we anticipate significant discrepancies between our modelled and the actual coal tar distributions below 45 m-NAP. Furthermore, just south-east of location B2, pure phase was implemented outside the wall as pure phase contamination was encountered here.

As the aim of this work was not to reconstruct the temporal evolution of the source zone, we accepted the simplification of using the composition of a present-day tar sample as the initial input for our model. However, matching the 35-year simulation results using that composition with again present-day field values of dissolved aromatic hydrocarbon concentrations, will result in discrepancies. Considering the various uncertainties in the conceptual model, including the expected variation in tar compositions throughout the field while only one sample was analysed, this discrepancy is considered of minor concern at this stage in the modelling process. Nonetheless, for future modelling efforts, it may be important to adjust the benzene ratio in the pure phase tar, particularly when estimating biodegradation rates based on modelling results.

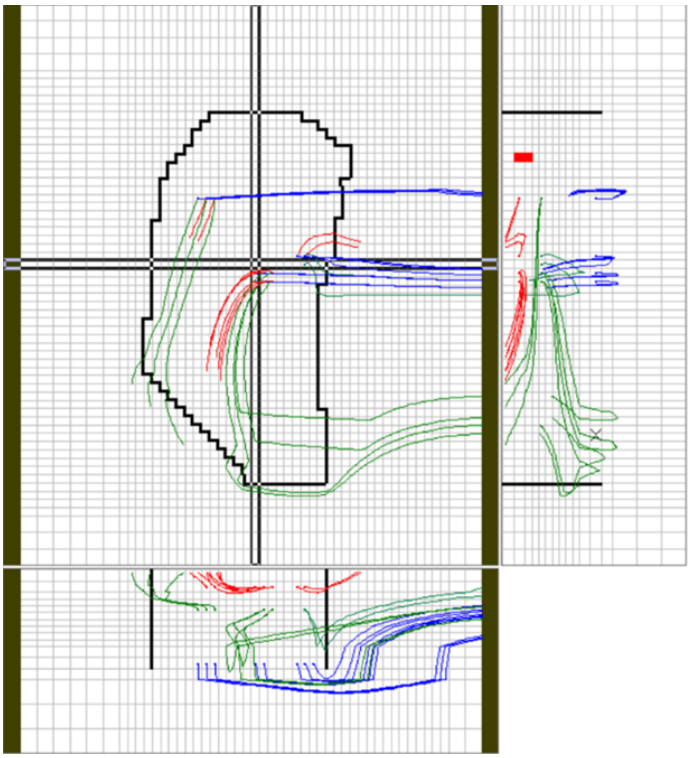

Figure 6.5: Advective flow paths back-tracked for 100 years, that progress to MLS wells B, B2 and C in layers 2 (red), 5 (green) and 12 (blue). The main figure shows a birds eye view, while the side figures offer transects of the black lines highlighted in the main figure. (NB the red cells in the right figure indicate the location of a pumping well).

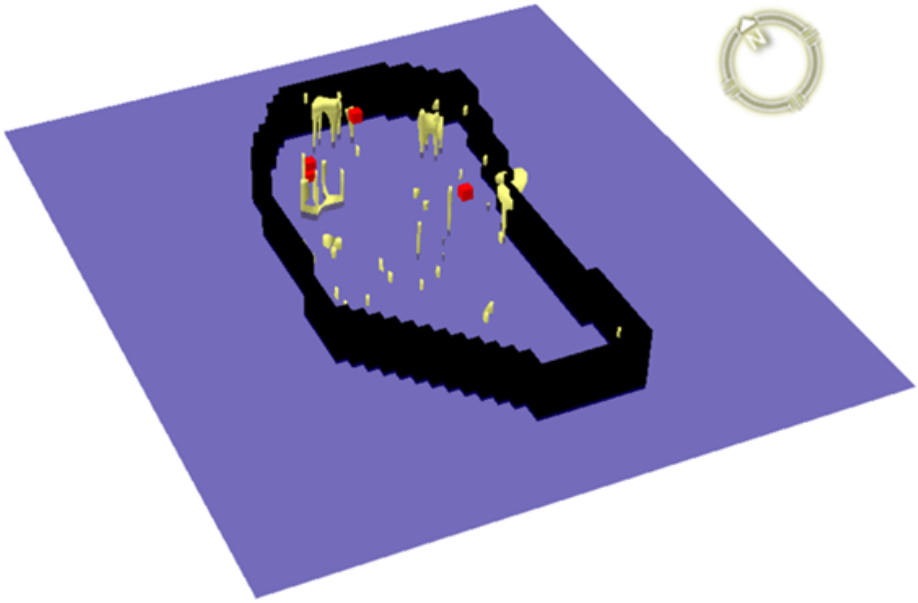

Figure 6.6: Three dimensional visualisation of source zone locations in the Griftpark model. Contamination is indicated in yellow, the flow barrier in black, pumping wells in red and the middle of the aquitard as a partially transparent purple sheet.

Source zone dissolution

In the Griftpark subsurface, pure phase coal occurs in pools, perched on low permeability layers, and blobs, ganglia and droplets in smear zones. While the NAPL distribution plays an important role for mass transfer rates, for example through its effect on local permeability [145], the local equilibrium assumption is typically considered valid for both pool and residual zones [258, 82]. In the Griftpark model, a mass transfer coefficient of 1e-5 /s was found high enough to effectively attain local equilibrium between the NAPL and dissolved phase. The rates at which the coal tar compounds dissolve are calculated through

$$\frac{\partial C^i_{NAPL}}{\partial t} = -\lambda_i (S^i_m - C^i_w) \tag{6.1}$$

where $C^i_{NAPL}(x, y, z, t)$ is the concentration of the i^{th} component in the immobile NAPL phase, λ_i is the mass transfer rate coefficient, $S^i_m(x, y, z, t)$ is the aqueous solubility of compound i in the mixture and $C^i_w(x, y, z, t)$ the aqueous concentration. In mixtures of organic compounds, the aqueous solubility concentration of individual components depends on their portion in the mixture [189]. Assuming ideal behaviour, a modified solubility may be calculated using Raoult's law

$$S^i_m = \chi_i * S^i, \tag{6.2}$$

where $S^i_m(x, y, z, t)$ is the modified maximum solubility of compound i and S^i its aqueous solubility as a pure compound. The time-dependent molar fraction $\chi_i(x, y, z, t)$ of compound i in the coal tar mixture is calculated through

$$\chi_i = \frac{m^i_{NAPL}}{m^B_{NAPL} + m^T_{NAPL} + m^E_{NAPL} + m^X_{NAPL} + m^{Ie}_{NAPL} + m^{Ia}_{NAPL} + m^N_{NAPL}}. \tag{6.3}$$

The dissolution of compounds is calculated in PHREEQC, through the inclusion of Equation 6.1 to 6.3. Solubility values, shown in Table 4, were taken from the study by d'Affonseca et al. [66]. Indane and indene are individually not (well) water soluble, but may co-dissolve with the other compounds. In this study, we calculated the aqueous solubilities of these compounds using their dissolved concentrations in a groundwater sample saturated with Griftpark coal tar and their molar fractions in the tar. The values for all compounds are given in Table 6.1. Although in this work we only use benzene,

naphthalene and the lumped MAH and PAHs, we report all values as they were included in the PHREEQC database.

Reactive transport and geochemical response

Advection, dispersion and sorption Advection and dispersion of dissolved compounds are calculated according to the advection-dispersion equation

$$n\frac{\partial C}{\partial t} = \nabla \cdot \left(n\vec{D}\nabla C - \vec{q}C \right) \tag{6.4}$$

where $C(x, y, z, t)$ describes the solute's concentration at any point in space and time, n is the porosity, $\vec{D}$ the dispersion tensor and $\vec{q}$ the Darcy flux. Advective transport is calculated using the modified method of characteristics (MMOC).

Many of the aromatic hydrocarbons in the coal tar mixture are hydrophobic and sorb to natural organic matter leading to the retardation of the contaminant plume. Assuming linear equilibrium sorption, the relation between the aqueous and sorbed concentrations, C_w^i and C_s^i, is defined by

$$C_s^i = K_d^i \cdot C_w^i. \tag{6.5}$$

For organic compounds, the distribution coefficient K_d between the sorbed and dissolved phase can be estimated from

$$K_d^i = K_{OC}^i * f_{OC} \tag{6.6}$$

where K_{OC}^i is the sediment adsorption coefficient of compound i and f_{OC} the mass fraction of organic carbon in the sediment. For the Griftpark hydrocarbons, the partition coefficient K_{OC}^i is calculated from the octanol-water coefficient K_{WC}^i using an empirical relation obtained from sorption data of mono- and poly-aromatic hydrocarbons in natural sediment samples [154]

$$logK_{OC}^i = 1.00 \cdot logK_{OW}^i - 0.211. \tag{6.7}$$

This relationship has been widely used in previous studies with organic carbons, including coal tar mixtures [102, 66]. To calculate distribution coefficients, octanol-water coefficients, K_{OW}, of the compounds were taken from the American centre of biotechnology
(www.ncbi.nlm.nih.gov) and for f_{OC}, the value of 0.4% for the Utrecht region was obtained from literature [289]. The calculated K_d values are shown in Table 6.1.

Biodegradation kinetics Biodegradation of hydrocarbons and the consumption of electron acceptors (EA) are included and solved through the PHREEQC code. The biodegradation of hydrocarbons and associated chemical reactions, including the consumption of electron acceptors (EA), can be effectively modelled through a range of approaches. These approaches encompass a variety of reactions, such as kinetic and equilibrium reactions, resulting in different levels of model complexity [22]. We have chosen to model hydrocarbon degradation and geochemical response using a two-step approach [233, 199]. In the first step, the substrate is oxidised and electrons are produced, i.e., using benzene as an example reactant,

$$C_6H_6 + 18H_2O \rightarrow 6HCO_3^- + 36H^+ + 30e^- \tag{6.8}$$

The second step simulates the consumption of produced electrons by the reduction of an EA [233], i.e., for sulphate and ferric iron reduction

$$SO_4^{2-} + 9H^+ + 8e^- \rightarrow HS^- + 4H_2O \tag{6.9}$$

$$Fe^{3+} + 1e^- \rightarrow Fe^{2+} \tag{6.10}$$

The reaction steps in Equation 6.8 and 6.10 may be combined, for benzene oxidation under sulphate and iron reduction, respectively, as

$$C_6H_6 + 3.75SO_4^{2-} + 3H_2O \rightarrow 6HCO_3^- + 3.75HS^- + 2.25H^+ \tag{6.11}$$

$$C_6H_6 + 30Fe^{3+} + 18H_2O \rightarrow 6HCO_3^- + 30Fe^2 + +36H^+ \tag{6.12}$$

During methanogenesis, CO_2 is used as the electron acceptor and the overall reaction of benzene degradation under methanogenic condition can be summarised as

$$C_6H_6 + 6.75H_2O \rightarrow 2.25HCO_3^- + 3.75CH_4 + 2.25H^+ \tag{6.13}$$

A partial equilibrium approach can be used to model the kinetics of the two-step process [233, 199]. The oxidation reaction can be approached as the rate-limiting step and is modelled through a kinetic equation. The second step can be modelled using equilibrium reactions. In this study, we use a first-order kinetic reaction for the first step. It incorporates a Monod-type term that accounts for the inhibition effect caused by decreasing EA concentrations [184]

$$\frac{\partial C_{i,EA}}{\partial t} = -k_{i,EA} \cdot \frac{C_{EA}}{K_{EA} + C_{EA}} \cdot C_i, \tag{6.14}$$

where $k_{i,EA}$ is the first order degradation rate constant of the compound i under the reducing conditions of the particular EA, $C_i(x, y, z, t)$ is the concentration of the substrate, and $C_{EA}(x, y, z, t)$ and K_{EA} are the concentration and half-saturation concentration of the EA, respectively.

At the Griftpark, although proof of manganese, iron and sulphate reduction as well as methanogenesis were found, the results indicated that sulphate and iron are the EAs that determine the speed of degradation at the site. As such, we exclude manganese reduction and methanogenesis from the kinetic equations. Although at the Griftpark oxygen exists only in the unsaturated zone, while the model extends over large depth, and nitrate does not occur in the first aquifer on which we focus our current simulations, oxygen and nitrate reduction were included in the kinetic model. This was done to facilitate future simulations, when degradation in the second aquifer and the potential stimulation of biodegradation through oxygen or nitrate dosing may be studied. One way to simply, but still accurately, describe the complete degradation rate of hydrocarbons under several electron accepting processes, is by summing the separate degradation rates under each electron accepting process [184]. Thus, the full degradation reaction for compound i, included in the PHREEQC database, is

$$\frac{\partial C_i}{\partial t} = \left(\frac{\partial C_{i,O_2}}{\partial t} + \left[\frac{\partial C_{i,NO_3^-}}{\partial t} + \left(\frac{\partial C_{i,Fe^{3+}}}{\partial t} + \frac{\partial C_{i,SO_4^{2-}}}{\partial t} \right) \cdot \frac{I_{NO_3^-}}{I_{NO_3^-} + C_{NO_3^-}} \right] \right), \quad (6.15)$$

where the individual degradation terms $\frac{\partial C_{i,EA}}{\partial t}$ are calculated according to Equation 6.14. In this model, the reduction of nitrate is inhibited by the presence of oxygen and the reduction of iron and sulphate is inhibited by both oxygen and nitrate. Iron and sulphate reduction are assumed not to affect each other [66]. The inhibition term depends on an inhibition concentration I_{EA} [184].

The effective kinetic model for biodegradation of aromatic hydrocarbons in this Chapter, with the exclusion of oxygen and nitrate from the groundwater, boils down to

$$\frac{\partial C_i}{\partial t} = \left(\frac{\partial C_{i,Fe^{3+}}}{\partial t} + \frac{\partial C_{i,SO_4^{2-}}}{\partial t} \right) \quad (6.16)$$

Biodegradation rates, used in Equation 6.14, implemented in the model were taken or derived from literature. Following the argument above, we

report on the iron and sulphate reducing rates found for all species, even when in this Chapter only the rates given for benzene, naphthalene, ethylbenzene (used for the lumped MAH) and 1-methyl-naphthalene (used for the lumped PAH) are used. Hydrocarbon degradation rates under iron and sulphate reducing conditions in literature vary greatly [54, 184, 274]. Values for the BTEX compounds were taken from a review study by Suarez and Rifai (1999) [274]. For the other compounds, no readily available data was found in the literature. The sulphate reduction rates for indane and naphthalene were approximated from results published in studies by Mundt, Thierrin and Landmeyer [213, 279, 172]. Given the similarity in molecular structure of indane and indene, their rates were taken the same, although in reality indene might be easier to degrade than indane [213]. The iron reduction rates for indane, indene and naphthalene were calculated by multiplying the sulphate reduction rates by three. The rates for methyl-naphthalene degradation, were taken as half of that of naphthalene. Although D'Affonseca found no proof of methyl-naphthalene degradation at their coal tar contaminated study site [66], methyl-naphthalenes are known to degrade anaerobically [160, 203, 14]. The collected degradation rates $k_{i,EA}$ are summarised in Table 6.5. The average values in Table 6 are used in the representative models, while the effect of different rates will be investigated during the sensitivity analysis. The half-saturation constants K_{EA}, see Equation 6.14, were set to 1e-05 mol/L for all EAs, following Affonseca et al. [66].

	iron rate (/day)			sulphate rate (/day)		
Compound	average	min	max	average	min	max
benzene [274]	0.009	0	0.034	0.008	0	0.049
toluene [274]	0.012	0	0.045	0.062	0	0.21
ethylbenzene [274]	0.003	0	0.017	0.002	0	0.007
m/p-xylene [274]	0.01	0.001	0.037	0.011	0.002	0.022
o-xylene [274]	0.003	0	0.016	0.027	0	0.084
indane	*0.021*	*0.0009*	*0.054*	0.007 [213]	0.0003 [213]	0.018 [213]
indene	*0.021*	*0.0009*	*0.054*	*0.007*	*0.0003*	*0.018*
naphthalene	*0.018*	*0.00015*	*0.021*	*0.006* [279]	0.00005 [172]	*0.007* [279]
methyl-naphthalenes	*0.0036*	*0.00003*	*0.0042*	*0.0012*	*0.00001*	*0.0014*

Table 6.5: Literature values of first order degradation constants under iron- and sulphate reducing conditions. Some values were calculated or deduced from literature, indicated in italic font.

Sedimentary organic matter was found to be low in Griftpark and so the degradation of organic matter other than the tar aromatic hydrocarbons was excluded from the model.

Geochemical response The oxidation of hydrocarbons and reduction of electron acceptors generate alkalinity and cause the consumption or production of protons, initiating secondary reactions like mineral buffering. In PHREEQC, the geochemical response following the kinetic oxidation step, is instigated by adding one mole of carbon in a valence state of zero to the aqueous solution for each mole of carbon that is degraded. Re-equilibration of the subsurface chemistry happens through a range of chemical reactions.

The electron accepting processes occurring in the Griftpark model are iron and sulphate reduction and methanogenesis. Sulphate exists in the groundwater as a dissolved phase. As shown in Equation 6.10, the reduction of sulphate leads to the creation of sulphide. Fe(III) occurs in minerals in the sediment and becomes available for reduction as it dissolves into the groundwater. As dissolved Fe(III) instantaneously transforms to Fe(II) through equilibrium redox reactions, its concentration in the groundwater is no suitable parameter in the kinetic degradation model given in Equation 6.16. Instead, the concentration of iron-containing mineral in the sediment is used to represent the concentration of iron available for redox reactions.

As no detailed sediment analysis was performed at the Griftpark, the source of iron in the ground (and its bioavailable fraction), is unknown. Based on the observed pH values of around 7, it is expected that the groundwater is more likely in equilibrium with goethite (FeOOH) than with iron hydroxide ($Fe(OH)_3$) [233]. Therefore, goethite was used as the source of iron in our model.

As a product of sulphate reduction, sulphide is created, and as a product of Fe(III) reduction, Fe(II) is formed. Fe(II) and S(-II) often precipitate as mackinawite (FeS) in aquifers

$$Fe^{2+} + 2HS^- \leftrightarrow FeS + 2H^+ + 2e^-. \tag{6.17}$$

Due to this precipitation, it is challenging to use Fe(II) and S(-II) concentrations as a measure for the rate of biodegradation. In our model, we include a kinetic precipitation rate of FeS following

$$\frac{\partial FeS}{\partial t} = k_{FeS} \cdot (1 - SR_{FeS}), \tag{6.18}$$

where k_{FeS} is the reaction rate and SR_{FeS} is the saturation ratio of FeS, which is the ratio of the ion activity product and the thermodynamic reaction constant.

In our model, also siderite ($FeCO_3$) and magnetite (Fe_3O_4) are included as sinks of Fe(II). Siderite is included as it is likely to become oversaturated and form at locations where organic carbon is mineralised and ferrous iron is generated during iron reduction

$$Fe^{2+} + CO_3^{2-} \leftrightarrow FeCO_3. \tag{6.19}$$

Magnetite is included as a proxy for mixed-valent Fe-minerals that are likely to form where hydrocarbons degrade under iron-reducing conditions

$$2Fe^{3+} + Fe^{2+} + 4H_2O \leftrightarrow Fe_3O_4 + 8H^+. \tag{6.20}$$

As magnetite consists partially of Fe(III), it can redissolve as a secondary EA source for biodegradation. However, without the presence of nitrate or oxygen in the groundwater this will not occur in the Griftpark subsurface. Magnetite and siderite are modelled through equilibrium reactions. Magnetite, siderite and mackinawite were assumed to be initially absent in the subsurface.

Manganese minerals are excluded from the simulations as they occur at much lower concentrations than iron minerals in the subsurface and manganese reduction was found to play a minor role in the geochemical balance at the Griftpark, see Chapter 3.

Although methanogenesis was not accounted for in the rate equation, the creation of methane is allowed for as a secondary reaction in the model, as it serves as a measure for the shift in redox potential and provides a good basis for model calibration. As the methanogenic process was not incorporated directly into the kinetic degradation reaction, but degradation is expected to slow down when methanogenesis occurs, we included an extra inhibition term to the degradation Equation 6.15, i.e.

$$I_{CH_4} = \frac{C_{CH_4,max} - C_{CH_4}}{C_{CH_4,max}}. \tag{6.21}$$

For $C_{CH_4,max}$ we implemented the maximum concentration of methane measured in the field, i.e. 1.5e-4 mol/L.

Calcite is an important mineral in groundwater chemistry. It buffers the pH through the dissolution and precipitation of carbonate, i.e.

$$CaCO_3 \leftrightarrow CO_3^{2-} + Ca^{2+}, \tag{6.22}$$

$$CO_3^{2-} + H^+ \leftrightarrow HCO_3. \tag{6.23}$$

Carbonate is known to exist in the Westland, Kreftenheye and Urk formations [141], but calcite or carbonate levels were not measured at the study site. An initial concentration of 0.25 mol/L was used in the model. Previous studies have found it is useful to add a pH inhibition term into the rate equation [238]. To slow down degradation when the pH deviates too far from its optimal value, the following term was included in rate Equation 6.15 [317]

$$I_{pH} = \frac{k_{pH}}{\left(k_{pH} + 10^{|\mu_{pH} - pH|}\right) - 1}. \tag{6.24}$$

where μ_{pH} is the optimal pH and k_{pH} is the inhibition factor, for which 7 and 0.5 were used in the Griftpark model, respectively. So that the effective degradation Equation 6.16, is adjusted to

$$\frac{\partial C_i}{\partial t} = \left(\frac{\partial C_{i,Fe^{3+}}}{\partial t} + \frac{\partial C_{i,SO_4^{2-}}}{\partial t} \right) \cdot I_{CH_4} \cdot I_{pH}. \tag{6.25}$$

For this work, we adopted the PHREEQC code used by Prommer et al. [237]. All kinetic and equilibrium reactions are defined in the PHREEQC database, of which the script is included in Appendix H.

Biochemical initial and boundary conditions

Fresh water enters the model with rainwater precipitation and groundwater. In PHT3D, the general head boundaries on the east and west boundaries of the domain were ascribed fixed chemical concentrations. Initial concentrations of ions, pH and pe, were taken from a groundwater sample from the contained zone with a low level of hydrocarbons (DV4) and kept the same for both the first and second aquifer. For rainwater the same chemical composition was used except for the concentration of sulphate, for which the value was taken from the National Institute for Public Health and the Environment (www.rivm.com). HCO_2^{2-} was not measured at the Griftpark and the initial concentration was taken from the study by Affonseca et al. [66].

As discussed in Chapter 3, the high and varying levels of sulphate in the park suggests the presence of sulphate sources. As no compound speciation was performed on sediment samples, a source of sulphate was left out of the model and the maximum value measured (237 mg/L) within the contained zone was used as the initial concentration existing in the groundwater. However, it means that not only biodegradation, but also source dissolution can cause variations in sulphate concentrations in the groundwater at the Griftpark, which may lead to discrepancies between field data and simulation results.

While building the representative model, the initial goethite content in the bulk phase was adjusted. The initial goethite concentration was based, firstly, on matching simulated goethite depletion with iron-content measured in sediment. As no sediment speciation analysis was performed and Fe(III) content was measured in a limited number of soil samples, there is insufficient field data available for a direct comparison with simulation results. However,

in Chapter 3 it was shown that soil analysis indicated that sediment at location C contains less Fe(III) compared to location B, and both less than at an uncontaminated location. Moreover, the level of iron depletion has an influence on the depletion of sulphate and subsequent creation of methane, so that these parameters were also factored in into the adjustment process. We started with a concentration level of 2.5 mol/L and lowered the concentration until, at 0.25 mol/L a satisfactory value was obtained.

At FMGPs iron sources may found in the form of slag, a ferrous waste product of smelting or refining cokes or ores, dumped at the site [29]. As we lack field data to verify this, this was not taken into account in the model. However, as with sulphate, this may lead to discrepancies between results of simulations and field measurements. Furthermore, as a result of the absence of contamination in the top model layer, goethite dissolution does not occur at this depth in the model. Although goethite depletion likely occurred in the top soil over the 100 years of industrial activity prior to remediation, this discrepancy between the model and field data has negligible impact on the calculations, because no contamination passes through this layer due to downward flow.

Both rain- and groundwater solutions were equilibrated (groundwater with the minerals initially present in the subsurface) and charge balanced using chloride in batch mode in PHREEQC. The resulting initial ground- and rainwater compositions are shown in Table 6.6.

Compound	1st aquifer mol/L	Rain mol/L
pH	7.0	7.0
pe	4.4	4.4
CO_3^{2-}	3.83E-03	3.83E-03
Ca	5.22E-03	5.22E-03
Cl	7.68E-03	1.24E-02
Fe^{2+}	1.45E-13	1.45E-13
K	3.69E-04	3.69E-04
Mg	8.68E-04	8.68E-04
NO_3	-	-
Na	3.12E-03	3.12E-03
SO_4	2.37E-03	1.74E-05

Table 6.6: Chemical composition background water

6.4 Results and discussion

6.4.1 Field data matching

Benzene and naphthalene In this Section, the simulation results of the representative model are compared to field data. Using the source zone distribution shown in Figure 6.6, average biodegradation rates given in Table 6.5 and a starting bulk concentration of goethite of 0.25 mol/L, we ran the representative model for a 35 year simulation period. The resulting profiles of benzene and naphthalene concentrations in MLS wells B, B2 and C are shown in Figure 6.7. The figure includes field data, as well as simulation results after running the model without degradation, i.e. with only advective-dispersive transport and sorption, for comparison. The profiles extend to a depth of 75 m-NAP, representing the middle of the top model layer of second aquifer, below which simulated concentrations of (biodegrading) hydrocarbons have dropped to 0.

It should be noted that the field data are obtained from a single measurement taken from samples collected in 2018. Previous analyses have shown that concentrations fluctuate throughout the years, data supplied in Appendix J.1. These fluctuations may be caused by measurement errors, but also by physical effects. For example, the depletion of pure phase product may on the one hand lead to a decrease in dissolved concentration, while on the other hand, reduction of source product in zones with high DNAPL saturation, may lead to an increase in effective permeability, and thereby lead to more contact area and consequently increased dissolved concentrations [216]. This means that when comparing simulation outcomes to measured results, it is important to consider a range of magnitudes rather than aiming for an exact match.

The results depicted in Figure 6.7, show that without degradation, dissolved contamination levels are almost constant throughout the complete depth of the profiles. Comparing simulations with field data shows that we were able to match simulated concentration profiles to measured profiles within an order of magnitude at well B and C, and to a lesser extent at well B2.

The profiles obtained from our simulations demonstrate benzene concentrations that are relatively lower compared to the naphthalene concentrations then when compared in the corresponding field data. Later in this Chapter we will find a potential explanation for this discrepancy.

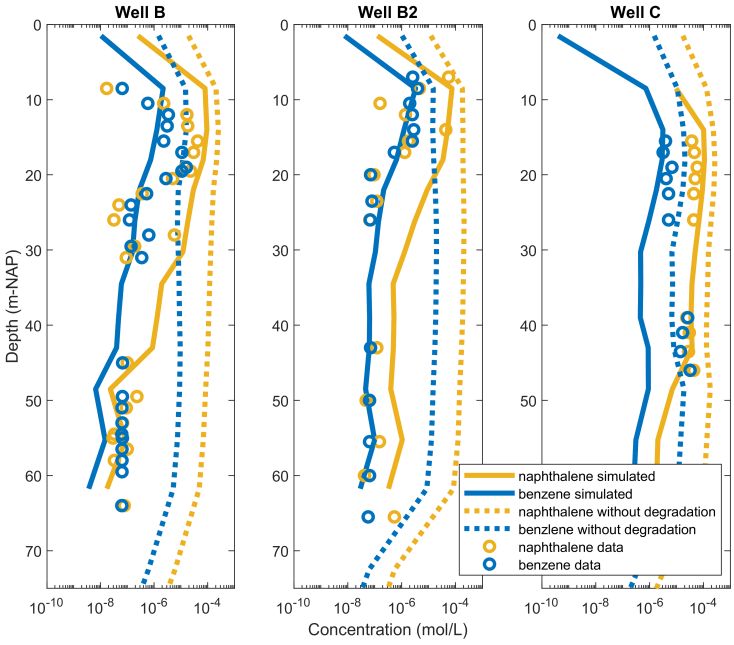

Figure 6.7: Benzene (yellow) and naphthalene (blue) concentration profiles on a log scale at location B, B2 and C, showing simulation results when including degradation (solid lines) and excluding degradation (dotted lines), together with field data (circles). The aquitard extends from approximately 45 to 65 m-NAP.

Results electron acceptors

Electron acceptor and mineral concentrations were calculated throughout the complete model domain using the representative model and compared to available field data. Figure 6.7 presents concentration profiles of simulated and measured values of sulphate, sulphide, ferrous iron, methane and pH, as well as the minerals goethite, magnetite and mackinawite at locations B, B2 and C. To indicate the effects of biodegradation on these species, we also plotted the profiles obtained when running the model without tar aromatics. The most important compounds to study in these simulations are sulphate and goethite, as they most significantly define the amount of degradation that occurs at the site.

The representative model accurately reproduced the sulphate concentrations well at locations B and C, except at depths below 45 m-NAP, where they are overestimated. This discrepancy may stem from using the same sulphate concentration in both the first and second aquifer layers in the model, whereas in reality, sulphate concentrations are lower in the second aquifer.

In well B2, simulations underestimated sulphate concentrations in the top 30 meters of the model, where goethite was depleted, while overestimating the sulphide concentration. This observation suggests that iron may still be available at these depths in reality, which would decrease sulphate reduction and lower simulated sulphide and hydrocarbon concentrations. As discussed in Chapter 3, the presence of heterogeneous iron and sulphate sources in the Griftpark subsurface should be considered.

As can be seen from the field data shown in Figure 6.7, Fe(II) and S(-II) concentrations vary considerably between the three locations B, B2 and C. These variations may be a result of different iron and sulphate reduction rates in different parts of the field, which can be caused by the varying levels of contamination and subsequent level of depletion of iron and sulphate from the ground and groundwater. Whereas in boreholes B and B2, HC contamination levels are similar, fluctuating around an average of 3e-6 mol/L, at B2 S(-II) goes up to 2e-5 mol/L, in B it goes up to 5e-4 mol/L. Meanwhile, Fe(II) levels reach a maximum of around 2.5e-4 mol/L in both wells, at depths where both in B and B2 goethite is depleted. This could indicate a locally lower sulphate degradation rate at B2 or stronger sulphide precipitation [253]. However, it could also be a three dimensional effect, from reduction conditions of upgradient zones.

The results reveal significant differences between simulations and field data with respect to Fe(II). The discrepancies can be attributed to the fact that we modelled magnetite and siderite precipitation as equilibrium processes. Equilibrium precipitation of these minerals almost immediately removes Fe(II) from the system, leading to strong underestimations of Fe(II) in groundwater in our simulations. The results also show that as a consequence of the equilibrium modelling of these precipitates, Fe(II), no siderite is formed at all. Further numerical investigations (not shown) revealed that implementing both magnetite and siderite as kinetic minerals led to the formation of both precipitates. Although the kinetic modelling improved some secondary values (such as pH), it does not improve our conceptual understanding of the site while it does increase the computation time and complexity of manual calibration by adding extra parameters. Therefore, we continued the modelling with only FeS as a kinetic mineral. Following a manual calibration, we implemented a FeS precipitation rate, k_{FeS}, of 1.0e-12 mol/d. At locations where both sulphate and iron reduction occurs, the S(-II) and Fe(II) produced complexes as FeS. Where iron is depleted, S(-II) remains in the groundwater. With the used precipitation rate, the simulation results in somewhat underestimated S(-II) concentrations at locations B and C, but, as discussed above, overestimated it at location B2.

Simulated methane concentrations matched field data within the order

of magnitude and followed a similar trend, indicating the model is able to predict zones with a shift to methanogenesis. Because of the stability of methane in the groundwater and with the three dimensional irregular flow patterns and existence of multiple source zones in the subsurface, it is hard to exclusively tell from which zones methane originates and what the redox conditions are at that location. The simulations showed that sulphate did not deplete completely anywhere in the subsurface and therefore sulphate reduction is likely to occur anywhere as well, so also where methanogenesis occurred.

In the pH profiles shown in Figure 6.7, no field data was included, as measurements of groundwater samples collected from locations B, B2 and C were conducted in a laboratory, which lead to an overestimation of the pH values due to degassing during sampling and storage. On-site pH measurements performed at the Griftpark throughout the years in groundwater, from other sampling wells, indicated that the average pH value within the contained zone is the same as outside of the contained zone, i.e. 7.1, with minimum and maximum values between 6.7 and 7.5. The average background value of 7.1 is shown in the Figure 6.7. The results indicate that our simulations somewhat underestimate the average measured pH values (<10%). The difference between simulated and average field values is not expected to significantly affect the groundwater chemistry and we consider this discrepancy to be of minimal concern.

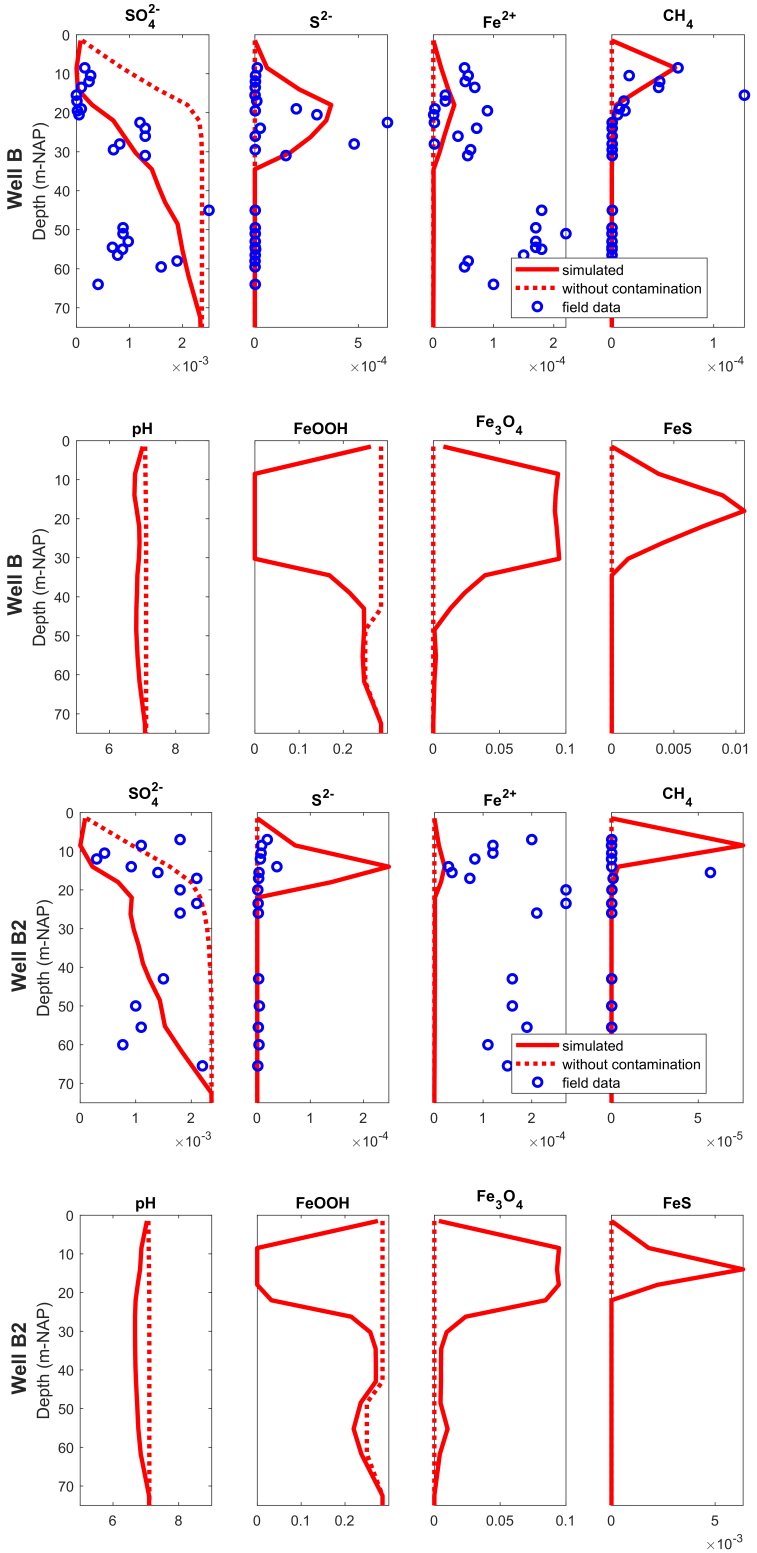
SO4 2-
S2-
Fe2+
CH4
Well B
Depth (m-NAP)
simulated
without contamination
field data
pH
FeOOH
Fe3O4
FeS
Well B2
Depth (m-NAP)
simulated
without contamination
field data
pH
FeOOH
Fe3O4
FeS

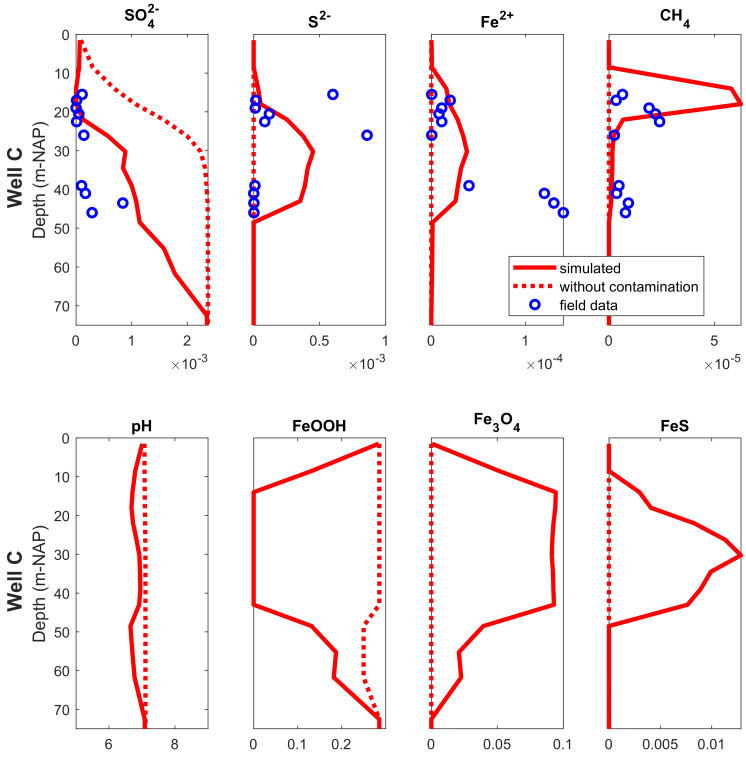

Figure 6.7: Profiles of electron acceptor concentrations and their reduced compounds, as well as mineral concentrations and pH. Concentrations after 35 years of reactive simulation are indicated by red lines, simulated concentrations in the absence of contamination (i.e. showing background values) are indicated with red dotted lines and results of groundwater sample analysis is indicated by blue circles. The aquitard extends from approximately 45 to 65 m-NAP.

6.4.2 Simulated evolution of groundwater contamination and geochemical response

Evolution of source release

The simulation results were used to calculate the average transient change in coal tar composition in the representative model. Figure 6.8 depicts the normalised pure phase mass of the four modelled compounds in the entire model domain. The Figure shows that only benzene, being the most soluble compound, has dissolved from the pure phase to a significant extent (∼50%) within the 35 years simulation period. This observation suggests that the original tar at the Griftpark contained a significantly higher percentage of benzene than what is measured in current field samples and that it is probable that particularly from zones with residual saturation (ganglia and blobs), from which dissolution rates are high, coal tar has been significantly depleted of highly soluble compounds [65, 82].

As mentioned earlier, the implementation of an initial coal tar composition obtained from a present-day sample and the subsequent comparison with dissolved concentration values obtained from field measurements after 35 years of simulation, leads to a discrepancy. This discrepancy may explain the relatively lower benzene concentrations compared to naphthalene concentrations in the simulations when compared in the corresponding field data, as seen in data, as seen in Figure 6.7.

Overall, within the 35 year simulation period almost 2% of the initial mass of tar has been dissolved.

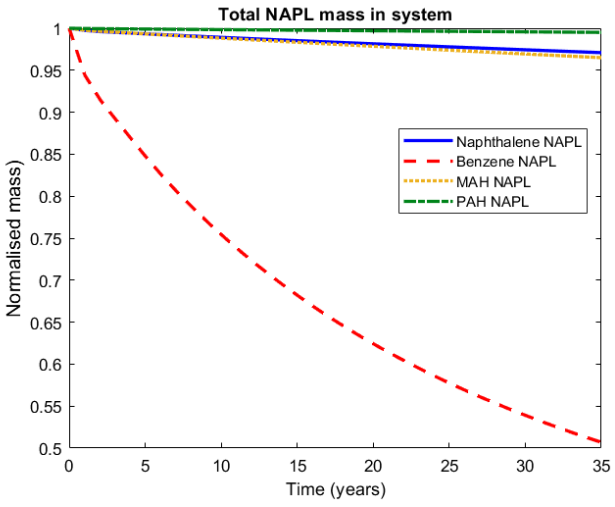

Figure 6.8: Well and test locations at the Griftpark.

Temporal and spatial evolution of redox conditions

The transient change in the system's reduction capacity is closely linked to the initial depletion of iron in sediment and sulphate in groundwater. The availability of iron is limited by the presence of goethite in the model, suggesting that a state of equilibrium will eventually be reached, where biodegradation relies solely on the recharge of sulphate through rainwater and groundwater, as well as methanogenesis. Since oxygen and nitrate are absent in the groundwater, it is not anticipated that Fe(III) will redissolve from magnetite, which contains both Fe(II) and Fe(III) [83]. Furthermore, the restricted groundwater recharge to the contained zone and the relatively low sulphate concentrations in rainwater contribute to a significant reduction in the system's reduction capacity as time progresses. The presence of iron and sulphate sources in the subsurface, resulting from pollution and rubble from the FMGPs (which are not incorporated into the model), may increase the subsurface's reduction capacity in reality.

As mackinawite forms in zones of overlapping iron and sulphate reduction, the depth profiles shown in Figure 6.7 reveal that in the Griftpark model, iron and sulphate reduction occur simultaneously. Fe(III) reduction starts before sulphate reduction as suggested by the fact that zones of magnetite deposition are larger than zones of mackinawite deposition. Wherever Fe(III) is used as an EA, instantaneously magnetite forms in a ratio of about 1:3. In the model, goethite gets depleted before sulphate. Furthermore, the results suggest that methanogenesis occurs when iron has depleted but there are still low levels of sulphate present.

Figure 6.9 depicts the total mass and the transformation rates of goethite and sulphate over the 35 year simulation period. Initially, there is rapid dissolution of goethite, indicating high iron reduction rates, as hydrocarbons start spreading through the groundwater. The dissolution rate decreases as goethite depletion occurs in zones with significant contamination. Concurrently, the sulphate reduction rate initially increases while iron reduction rate decreases, suggesting the dominance of iron reduction at higher goethite concentrations. With decreasing sulphate availability, also the sulphate reduction rate declines. Additional simulations (not shown) revealed that under current pumping conditions, the rate of sulphate reduction decreases until a steady state is reached after approximately 80 years.

Figure 6.10 shows two-dimensional plots illustrating the spatial distribution of goethite and sulphate concentrations at 14 m-NAP after 5, 15 and 35 years. The results show that zones of goethite depletion are sharply delineated. Sulphate levels are affected by both degradation and rainwater precipitation, that creates a lower sulphate concentration percolating through the top layers of the model, as can be seen in the two-dimensional depth profile

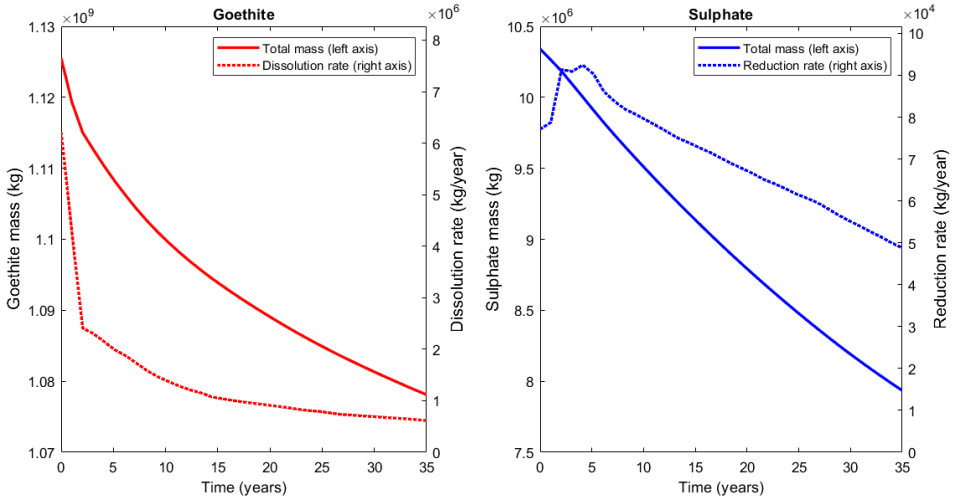

Figure 6.9: Total mass of goethite and sulphate in the whole model domain (left axes), as well as their transformation rates, i.e. the reduction rate of sulphate and the dissolution rate of goethite which is interpreted as the Fe(III) reduction rate (right axes).

shown in Figure 6.11 (note that the depth is not on a distance scale). In this Figure also the effect of boundaries can be seen.

Goethite was fully depleted from cells containing pure phase tar after 2 years. In wells B, B2 and C at 14 m-NAP (in model cells without pure phase tar), goethite was depleted after 17 years. These results indicate the high importance of initial levels of goethite in the subsurface for the correct estimation of hydrocarbon attenuation, as was also reported by Brun et al. in their study at a former landfill [42]. Sulphate levels never reached 0 anywhere in the model. For example, in well C 22 m-NAP, a concentration of 5.6e-5 mol/L was attained after 35 years of simulation.

Using the simplifying assumption that the 35 years of simulation time approaches field conditions since the installation of the vertical barrier, the modelling results suggest that the contain-and-manage strategy employed at the park has not yet reached a steady state condition. However, the near depletion of bioavailable iron oxides, also evidenced by the pH levels that are not increased above background values, implies that it is currently mostly sulphate that controls the biodegradation potential. Our model shows that after 35 years of simulation, some of the initially present sulphate is still available, indicating that the replenishment of sulphate through rainwater and groundwater is not yet the primary limiting factor for biodegradation potential.

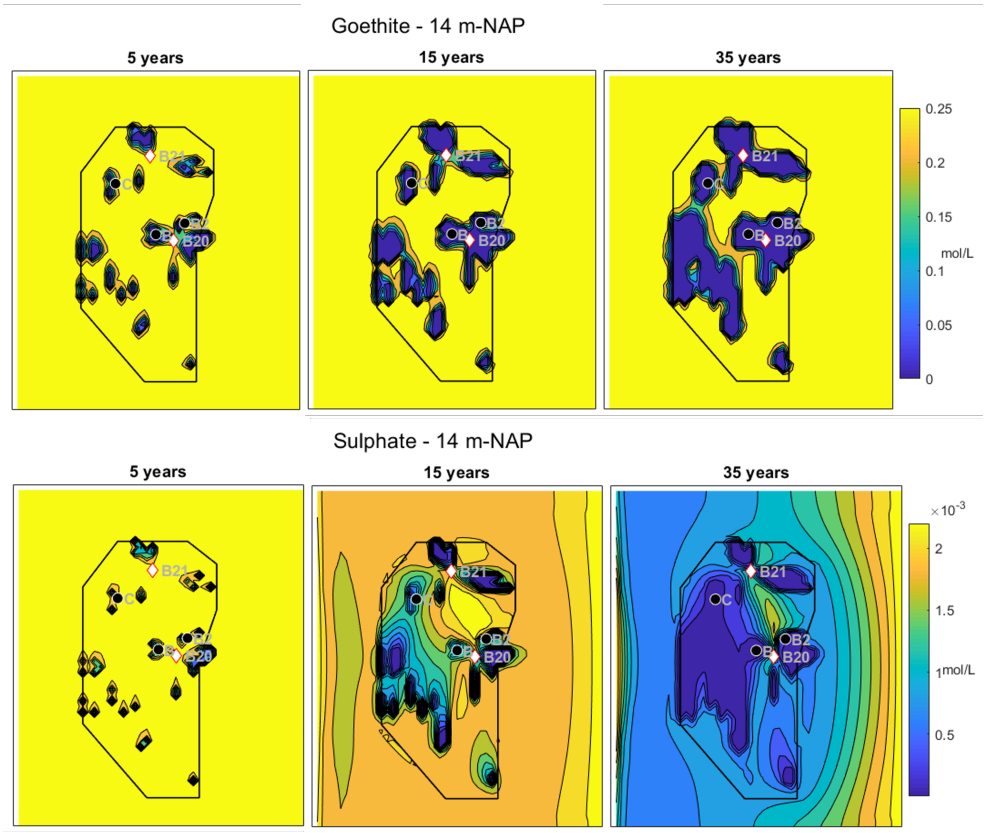

Figure 6.10: Zones of iron and sulphate reduction at 14 m-NAP after various simulation periods. The vertical barriers around the contaminant source are shown in black.

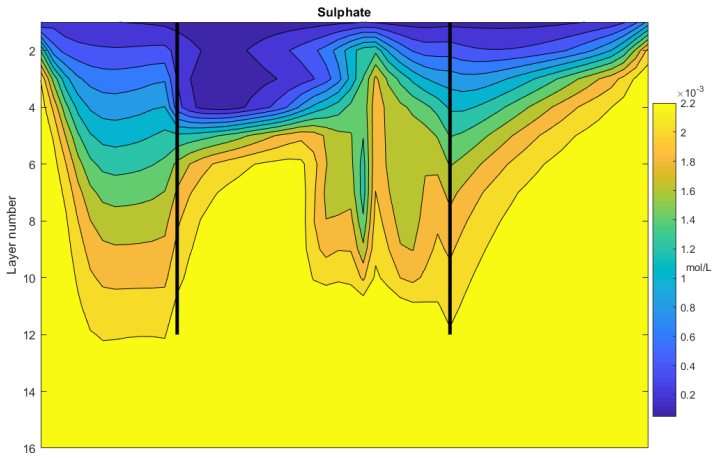

Figure 6.11: Sulphate concentration in a cross section of the park after a 35-year simulation period.

Temporal and spatial evolution of contamination

With the representative model simulations, the changes in total dissolved contaminant concentrations as well as their physical spread was studied. Figure 6.12 plots the total mass of dissolved hydrocarbons in the entire model over the 35 year simulation period. The high rate of benzene depletion, typical for early coal tar aromatic mass discharge, as was shown in Figure 6.8, does not lead to high amounts of dissolved benzene in the system compared to the other MAHs. This can be attributed to the fact that the molar fraction of benzene in the initial composition of pure phase tar in the model is approximately 30% smaller than that of the lumped MAHs and its degradation rate approximately three times larger.

The concentrations of hydrocarbons are expected to gradually rise due to the decreasing reduction potential of the subsurface. Moreover, the rapid depletion of benzene leads to an increase in the molar fractions of other compounds within the coal tar, resulting in an expected increase in mass discharge of these compounds. Figure 6.12 indeed shows increasing concentrations of naphthalene, MAH and PAH. Naphthalene and the lumped PAHs occur in similar mole fractions in the pure phase tar and together constitute 94% of its total molar mass. The higher solubility of MAHs leads to dissolved concentrations that are comparable to the PAH concentrations. In terms of naphthalene and the lumped PAHs, naphthalene has a four times higher solubility and ten times higher degradation rate compared to the lumped PAHs. As shown in Figure 6.12, these differences result in a significantly more pronounced increase in dissolved naphthalene concentrations throughout the entire modelled period.

Figure 6.13 illustrates the total mass transfer rates of pure tar to the dissolved phase and the biodegradation rates of dissolved compounds in the model. Results show that it take about two years for the dissolved contaminants to dissolve and spread into the subsurface environment before a stable phase established. Although dissolution and degradation rates lie close together, the dissolution rate is slightly higher for naphthalene, MAH and PAH, resulting in the still rising dissolved concentrations shown in Figure 6.12.

Benzene shows the strongest reduction in mass transfer rates over time, dropping to less than 20% of the initial peak rate within 35 years (normalised plots not shown) due to the significantly decreasing fraction of benzene in the pure phase tar. The mass transfer rates of naphthalene are significantly higher than that of the other compounds, due to its high molar ratio in tar compared to the MAHs and its notably higher dissolution and degradation rates compared to the PAHs.

Figure 6.14 shows the spread of benzene and naphthalene throughout the model domain at 14 and 43 m-NAP, layers in which respectively pumps B20

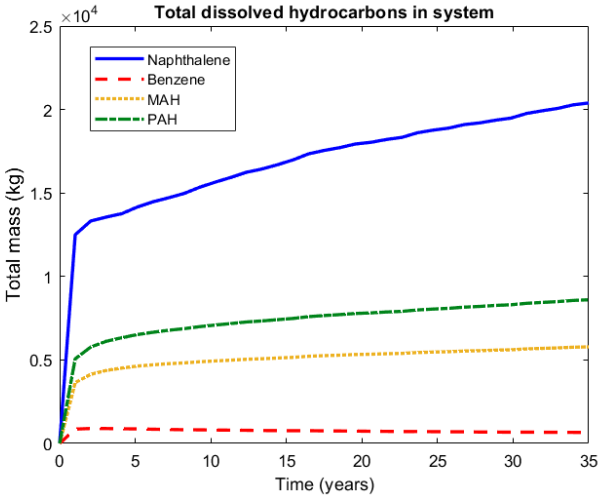

Figure 6.12: Total mass of dissolved hydrocarbons in the model.

and B21, and B22 are screened, after 35 years of simulation time. A cut-off value of 1e-10 mol/L was used for the plot. The results show that concentrations stay below this cut off value in large zones of the park, especially in the deeper layers where less pure phase tar exists. Wells are indicated by white diamonds in the Figure and movement of contamination can be seen to move towards the wells. Comparing Figure 6.14 to Figure 6.15, which shows naphthalene and benzene distributions when degradation is excluded from the calculations, shows that much stronger gradients exist when including degradation. Simulations indicate that the maximum spatial extent of contaminant distribution under current pumping conditions is reached within 10 years. Figures 6.14 and 6.15 show that, despite the inward flow, some contamination passes through the wall on the west side where pure tar was allocated to cells adjacent to it. This indicates the effect of numerical dispersion in the MMOC scheme. Notably, just south east of location B2 pure phase was implemented outside the wall as pure phase tar was found here during field investigations.

To further study the effect of redox conditions on HC concentrations, Figure 6.16 shows the normalised breakthrough curves of the tar aromatic compounds, sulphate and goethite at the locations of wells B20, B21 and B22, as well as, for comparison, at a location with lower contaminant concentrations, location further away from source zones. The naphthalene concentrations in these wells after 35 years of simulation time were 1.5e-4, 6.5e-5, 5.4e-5 and 1.4e-8 mol/L, respectively. Although the goethite concentration is local, i.e. goethite is not transported with the groundwater that carries the hydrocar-

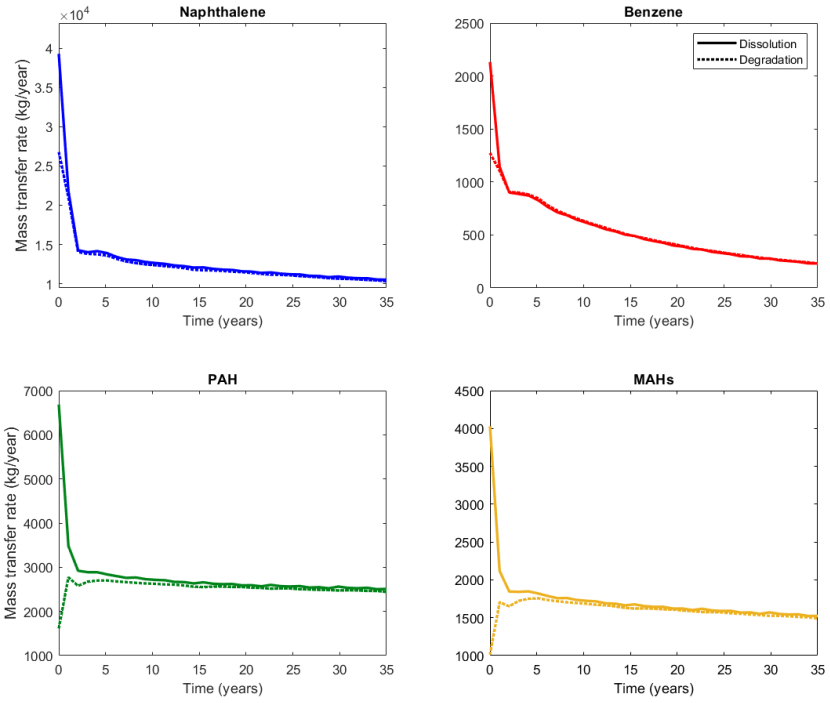

Figure 6.13: Mass transfer (i.e. dissolution and degradation) rates of benzene, naphthalene, lumped MAHs (all MAHs excluding benzene) and PAHs (all PAHs excluding naphthalene) over a 100 year simulation period. Solid lines indicate the mass transfer from the NAPL to the dissolved phase, dotted lines indicate the rate of biodegradation.

bons and sulphate, it is taken as a representative indicator of the iron content in the surrounding of the wells.

Figure 6.16 shows that there is a fast increase in HC concentrations during the first 5 years, as dissolved contaminants spread through the subsurface domain, after which the increase slows down. The gradual depletion of benzene from coal tar source zones causes a significant decrease in benzene concentrations in the contaminated wells over time. The breakthrough curves also show that when goethite depletes, the concentrations of hydrocarbons rise strongly, especially naphthalene. In our model, sulphate reduction does not speed up when the bioavailable iron finishes in the subsurface, which would cause an increased rate of sulphate removal.

The stable level of goethite at the location with a low total level of contamination, indicates that biodegradation at such low concentrations is limited.

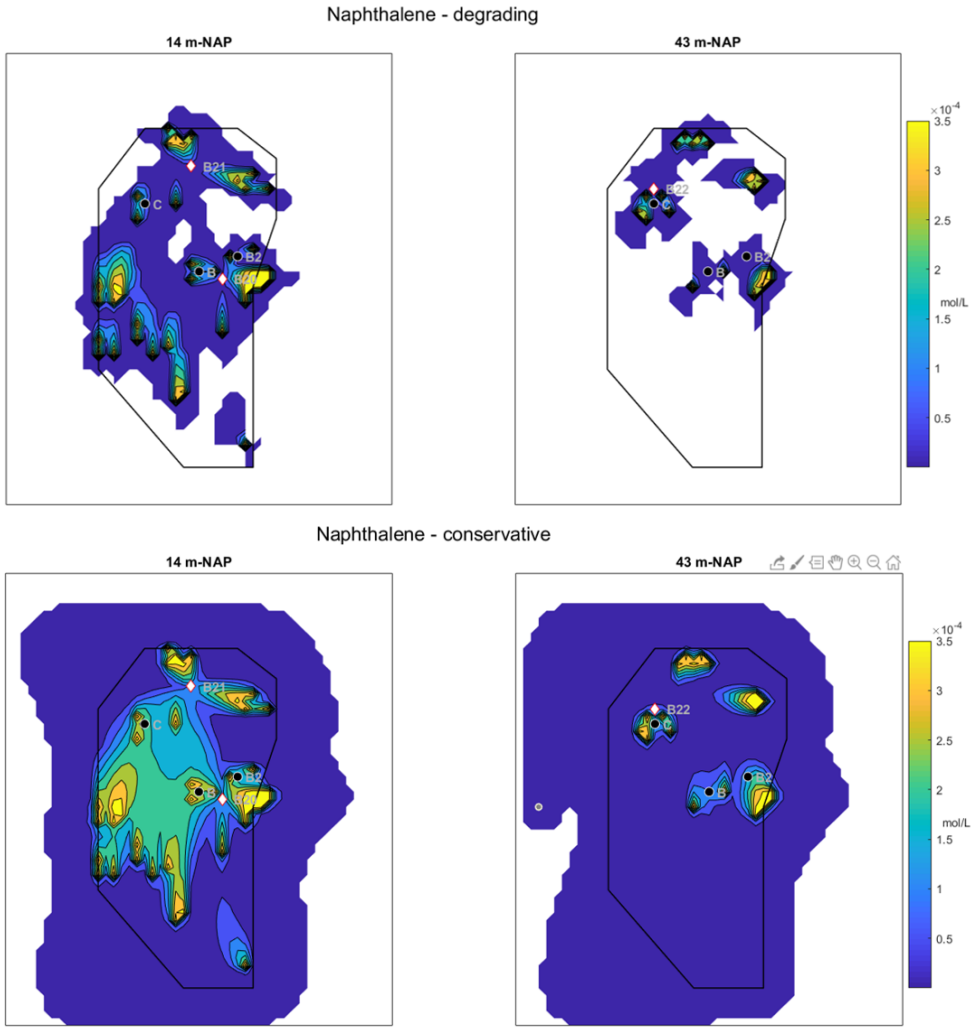

Figure 6.14: 2D distribution of naphthalene at 14 and 43 m-NAP after 35 years of simulation time, both when running the model in- and excluding biodegradation. MLS wells B, B2 and C are indicated by black circles with a white rim. The three pumping wells B20, B21 (screened in model layers 2 and 3 between 5-16 m-NAP) and B22 (screened in model layers 6 and 7 between 24-32 m-NAP and 9 and 10 between 37-45 m-NAP).

Therefore, the reduction in sulphate and HC concentrations in this well are the effect of biodegradation in upgradient zones.

Due to the complex three dimensional setting of the model, the effect of sorption causing a retardation of PAH (i.e. naphthalene and lumped PAHs) plumes from upgradient sources is left out of the scope of this analysis.

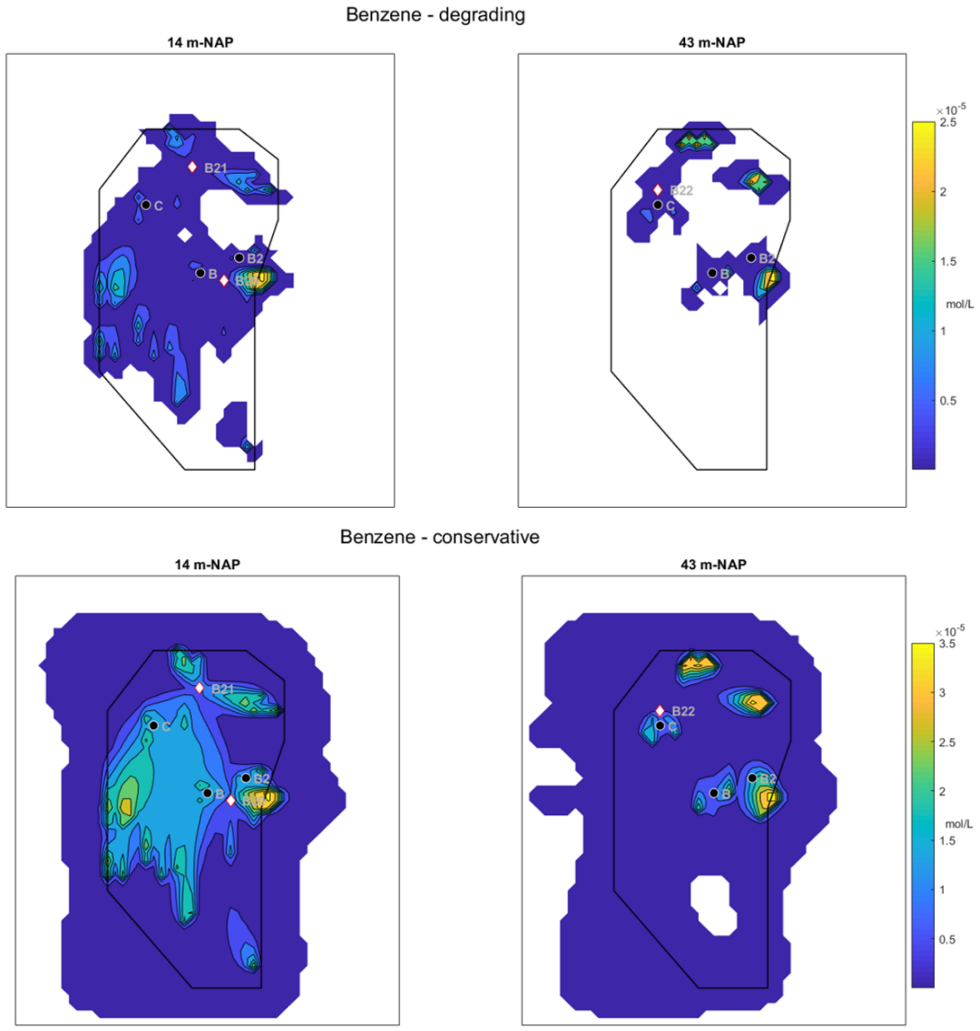

Figure 6.15: 2D distribution of benzene at 14 and 43 m-NAP after 35 years of simulation time, both when running the model in- and excluding biodegradation. MLS wells B, B2 and C are indicated by black circles with a white rim. The three pumping wells B20, B21 (screened in model layers 2 and 3 between 5-16 m-NAP) and B22 (screened in model layers 6 and 7 between 24-32 m-NAP and 9 and 10 between 37-45 m-NAP).

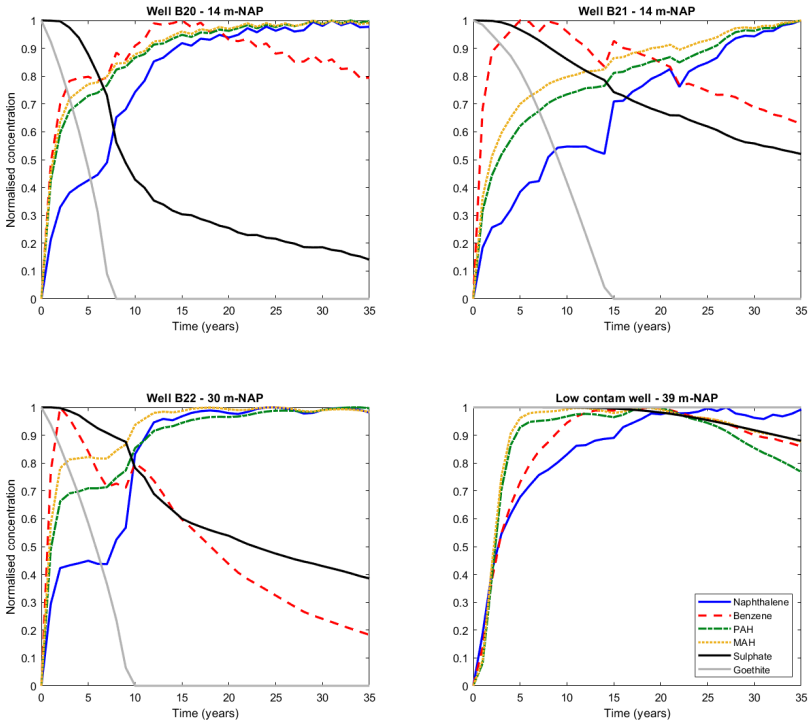

Figure 6.16: Breakthrough curves of the four aromatic species and sulphate at the locations of pumping wells B20, B21 and B22 and another location that has a low total contamination level as well as the concentration of goethite at the well location (used as a representative value of Fe(III) availability around the wells). Values are normalised for each component, for better visualisation of the correlation between contaminant and electron acceptor concentrations.

6.4.3 Sensitivity analysis

For the sensitivity analysis, the model was run for a 35-year simulation period with the groundwater pumps operating at a combined pumping rate of 10.5 m^3/h, as in the representative model. Subsequently, an additional 100 years were simulated with the groundwater pumps deactivated to observe groundwater contamination of the second aquifer. The simulated concentrations in wells 101, 102 and 103 after the total 135-year simulation period were compared to groundwater intervention levels set by the Dutch government. The intervention levels for BTEX and naphthalene can be found in Table 6.7. To determine an intervention level for the lumped MAHs used in the numerical model, the levels for toluene, ethylbenzene and xylenes were summed. Since no references for intervention values for indane, indene or methyl-naphthalenes were found, the analysis excluded an intervention value for the PAHs.

Compound	$C_{intervention}$ mol/L
benzene	3.80E-07
toluene	1.10E-05
ethylbenzene	1.40E-06
m/p/o-xylene	6.60E-07
MAHs (TEX)	1.34E-05
naphthalene	6.60E-07

Table 6.7: Aromatic hydrocarbon intervention levels for Dutch groundwater systems (www.overheid.nl). The value of the lumped MAH was taken as the sum of the values of toluene, ethylbenzene and xylenes.

Figure 6.17 shows the simulated concentrations in wells 101, 102 and 103 over the 135-year period, for both the models that in- and exclude the biodegradation of the aromatic hydrocarbons. In the simulation excluding biodegradation, contaminants are subjected only to advection, dispersion and sorption. The results demonstrate that when employing the biodegradation rates used in the representative model, i.e. obtained from the average literature values, all concentrations remain safe below intervention values, while without degradation, the concentrations of naphthalene and benzene rise significantly above this level. This indicated that biodegradation rates are a crucial parameter for a risk assessment of potential future management strategies at the Griftpark. As the MAHs mostly stay below the intervention value, this value was not included in following plots.

The results also reveal that at very low levels of contamination in the simulation including degradation, the concentration of naphthalene is low, whereas in the non-degrading simulation its concentration is high relative to the other compounds. For comparison, Figure 6.18 presents the contaminant

breakthrough curves in four wells within the contained zone (for which the normalised versions are shown in Figure 6.16). Figure 6.18 shows that also here, in wells with high levels of contamination (i.e. wells B20, B21 and B22), naphthalene is the compound that occurs at highest concentrations, while in the well with low contaminant concentrations, it is relatively lower. As in this simulation biodegradation was included, it proves that the discrepancy between compound ratios in the degrading versus the non-degrading simulations in Figure 6.17 cannot be attributed to degradation only. Instead, it is more likely a combined effect of degradation and transport. Naphthalene has a smaller distribution coefficient, K_d, than that of the PAHs. Therefore the naphthalene plume moves faster through the subsurface than the PAH plume, as the PAHs stronger sorption causes more retardation. Therefore, naphthalene comes into contact with electron acceptors first and partially consumes them before the arrival of other PAHs. Together with its high degradation rate compared to the other species, this may lead to stronger depletion of naphthalene than the lumped PAHs further along the plume, whereas at short distance, the concentration is more defined by its high molar fraction in the pure phase tar.

Figure 6.17 also shows that concentrations are highest in well 101 and lowest in well 102. Figure 6.19a illustrates the three-dimensional development of the naphthalene plume into the second aquifer when using a homogeneous K value throughout the three aquitard layers. For this model run, 100 times reduced biodegradation rates were applied in order to obtain significant breakthrough. The figure demonstrates that the plume concentration is lowest along the southern edge (where well 102 is situated), and highest in the central area (in proximity to well 101). As the aquitard is homogeneous, the heterogeneous distribution of the plume is primarily caused by the distribution of coal tar within the contained zone. Note that the wells are located at their physical position in the field.

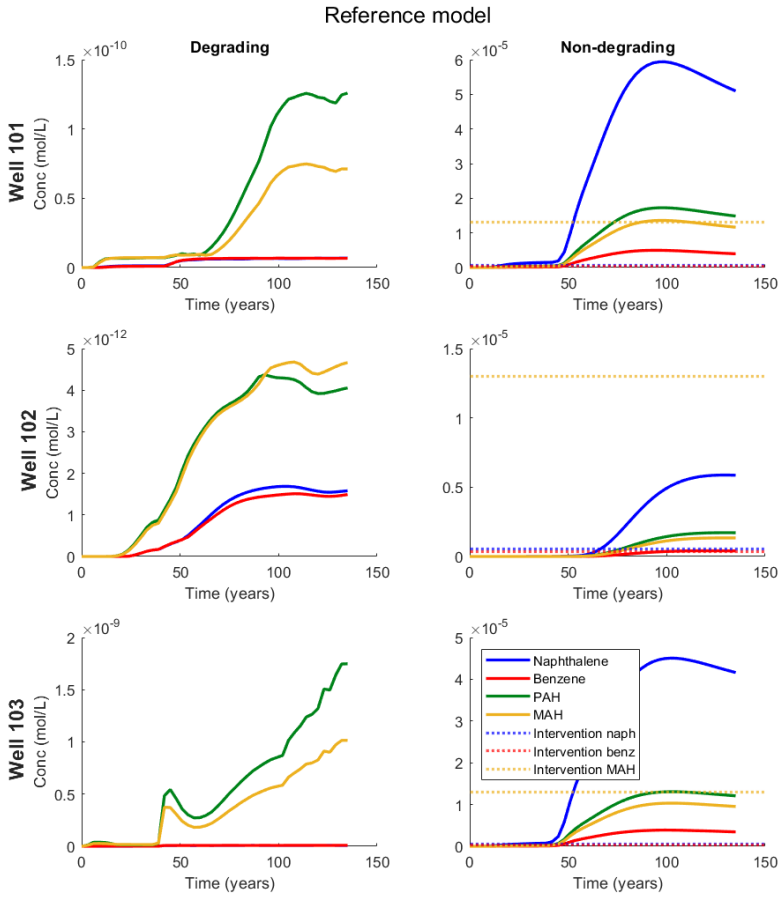

Figure 6.17: Aromatic hydrocarbon breakthrough curves in wells 101, 102 and 103 when running the representative model with and without biodegradation.

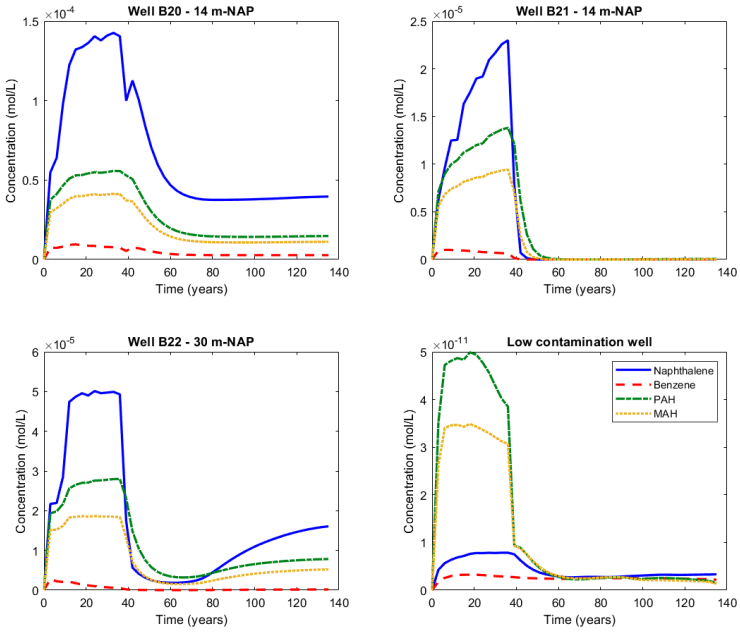

Figure 6.18: Aromatic hydrocarbon breakthrough curves in four wells, B20, B21, B22 and a location with low contamination levels, inside the contained zone.

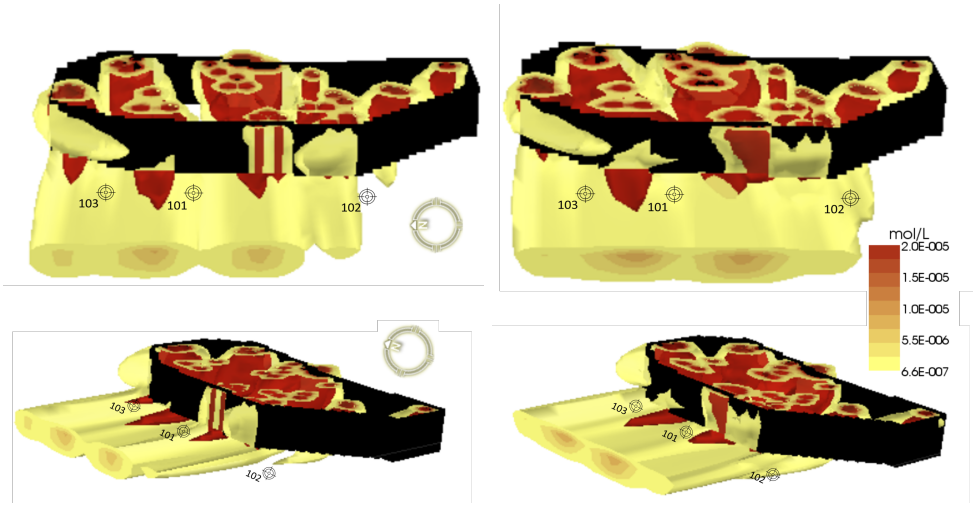

(a) Homogeneous aquitard (b) Heterogeneous aquitard

Figure 6.19: Three dimensional depiction, at two different angles, of the naphthalene plume development (using a 100-fold decrease of the biodegradation rate) in the second aquifer in case of a homogeneous (a) or heterogeneous aquitard (b). The vertical barriers around the contaminant source are indicated in black, the plume on a red to yellow scale. The lower bound cut-off value is the groundwater intervention value, while the higher bound value was chosen for visual clarity.

Biodegradation rates

We investigated the impact of a range of degradation rates on contaminant levels in the second aquifer observation wells. As contaminant concentrations remained well below intervention levels when using average biodegradation rates, we focused only on the impact of lower rates, which can cause risks, and not of higher rates. Table 6.5 presents first order degradation constants under iron- and sulphate reducing conditions reported in literature.

Figure 6.20 shows simulated concentration levels in the three observation wells for various biodegradation rates. The term 'average rate' refers to the average rates derived from literature, as employed in the representative model. Subsequently, these rates were divided by 2, 10 and 100. The smallest value was derived from the lowest field values found for naphthalene and PAHs as given in Table 6.5.

The results indicate that with a 10-fold decrease in degradation rates, simulated concentrations of naphthalene and benzene remain below intervention values in the observation wells. However, when the rates are reduced 100 times, the simulated concentrations significantly exceed intervention values in wells 101 and 103. Compared to the simulation excluding degradation depicted in Figure 6.17, the 100-fold reduced rates yield concentrations of a similar order of magnitude in well 101, but approximately one order of magnitude lower in wells 102 and 103. This difference indicates a spatial non-uniformity in the parameter dependency, caused by the complex three dimensional contaminant flow field resulting from the heterogeneous distribution of source zones, varying electron acceptor availability, layering in the model and hydraulic barrier.

A non-linear dependency on degradation rates is demonstrated by the results depicted in Figure 6.21, that shows the hydrocarbon concentrations in wells 101, 102 and 103 after 135 years of simulation time under varying degradation rates. For visibility, the degradation rates were normalised and plotted on a log-log scale. Normalised rates with a value of 1 correspond to the average literature rates used in the model calibration. Additionally, the non-degrading simulation was included in the plot, represented by a very low normalised degradation rate, i.e. 1e-08.

The analysis reveals that the significant range of sensitivity lies within the order of magnitude range of the 10- to 100-fold reduction of the average rates applied in the representative model. When degradation rates are higher than the 10-fold reduced values, the degradation process occurs so rapidly that arrival of mass becomes the limiting factor for degradation. Under this condition, dissolution and transport play more substantial roles in determining concentration levels. At the other end of the spectrum, when degradation rates are low, i.e. smaller than approximately a 200-fold reduction of the original

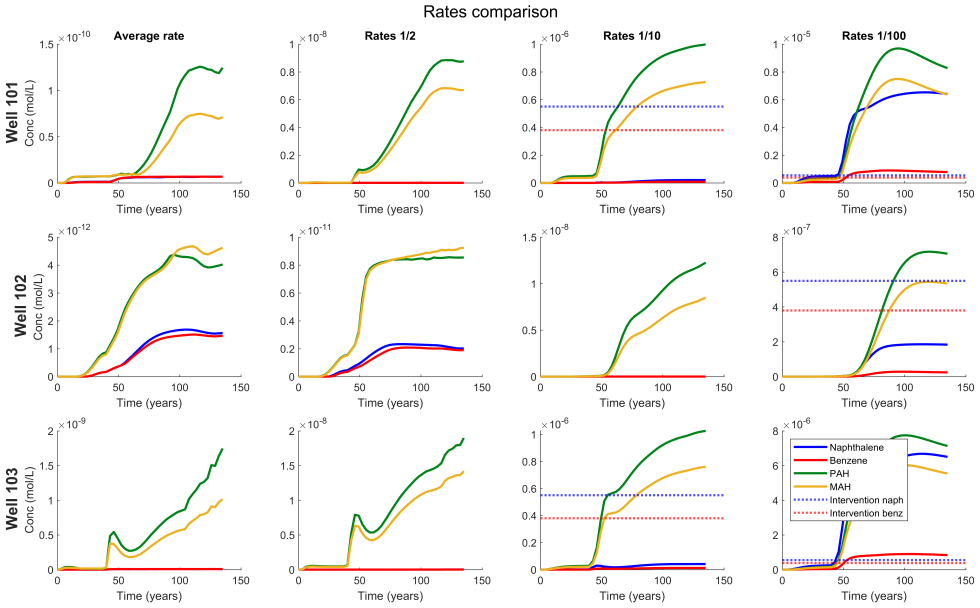

Figure 6.20: Aromatic hydrocarbon breakthrough curves in wells 101, 102 and 103 when applying the average degradation rates (as used in the representative model and given in Table 6.5), as well as half and 10- and 100-fold reductions of those rates.

rates, degradation becomes negligible and different scenarios provide similar solutions.

Steep contaminant concentration gradients occur at the Griftpark. As shown in Figure 6.2, a total BTEXIeIaN concentration of 38 mg/L was measured in a saturated groundwater sample collected from well B22, whereas concentrations of maximum 14 mg/L were recorded in groundwater samples collected from several depths in multi-level sampling well C, at the same depths where tar was encountered during core drilling. Presuming that 38 mg/L is the saturation concentration for the BTEXIeIaN mixture, this means the concentration is halved on very short distance scales.

If the timescale of transport was short, i.e. advection and dispersion would transfer the contaminants faster than biodegradation could break them down, a lower gradient would be expected. Therefore, the results suggest that the considerable concentration gradient is caused by biodegradation. We should note that the complex three dimensional flow field can also create concentration changes by mixing of different streamlines with varying concentrations. However, given the proximity of the sampling well to the source locations, the role of heterogeneous flow field is assumed to be marginal.

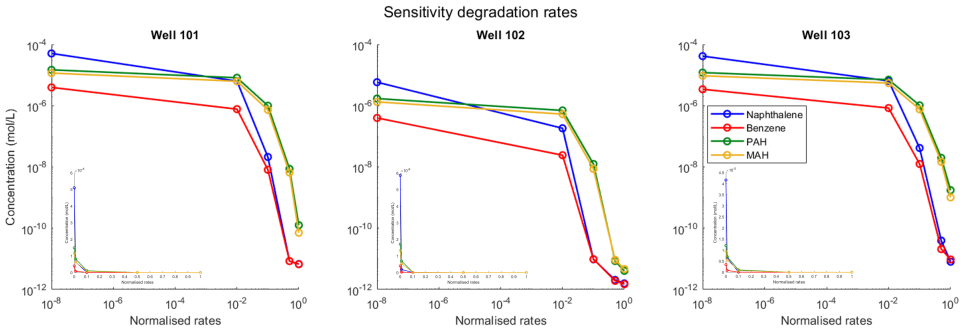

Figure 6.21: Concentrations in wells 101, 102 and 103 after 135 years of simulation time under varying degradation rates. The rates were normalised for all compounds, i.e. the value of 1 indicates the average literature rates as used in the model calibration. The value of 10-8 was used for the simulation excluding degradation. The plots are shown on a log-log scale, the insets show the plots on a normal scale.

Homogeneous versus heterogeneous aquitard

To investigate the effect of aquitard heterogeneity in the model, we compared breakthrough concentrations implementing homogeneous K fields (as used in the representative model) or heterogeneous K fields generated using the EBK3D interpolation method for the three aquitard model layers, as explained in Chapter 5. In order to obtain significant contaminant concentration levels in the second aquifer wells, the biodegradation rates in these simulations were reduced by a factor of 100 compared to the representative model.

Figure 6.22 shows that the heterogeneous aquitard leads to higher contaminant concentrations in the second aquifer. Examining naphthalene concentrations after the 135-year simulation period, there is an approximate increase of 90% in well 101, 65% in well 102 and 70% in well 103. It is expected that heterogeneity in the aquitard causes two contrasting effects. On the one hand, it results in the formation of preferential flow paths along which the plume becomes more concentrated. On the other hand, the heterogeneity contributes to an increase in dispersion, leading to a broader spatial spread of the dissolved contamination. Both these behaviours are illustrated by Figure 6.19b, which depicts the three dimensional development of the naphthalene plume in the second aquifer when the heterogeneous K distribution is applied. Comparing Figures 6.19a and 6.19b, reveals that the heterogeneous case exhibits a larger spatial extent of the dissolved contamination and more dispersed plume cores, indicating increased dispersion. In the homogeneous case, the plume displays three plume cores, that are, as discussed above, primarily influenced by the locations of coal tar in the contained zone. However, in the heterogeneous

case, only two plume cores appear, suggesting more flow through the central part of the aquitard and less flow through the northern part.

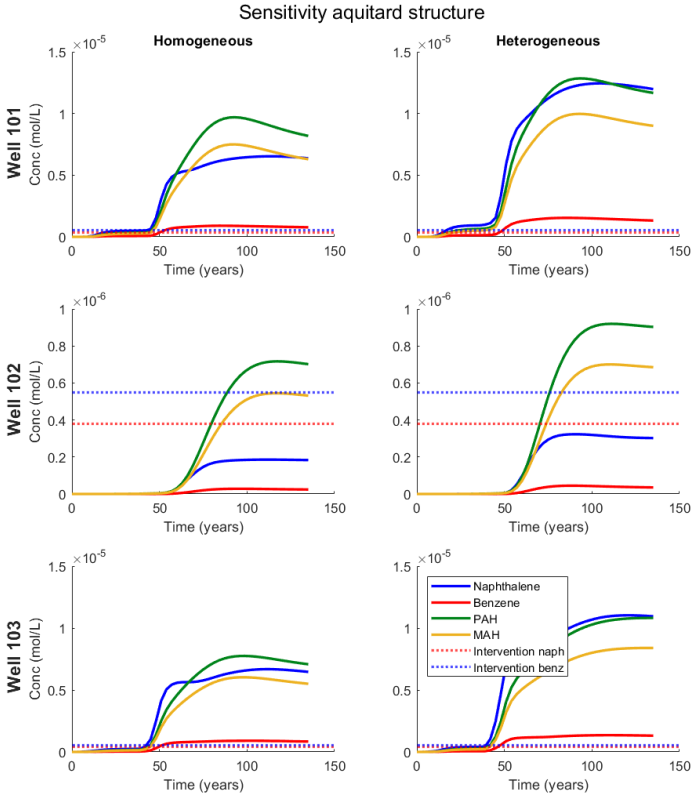

Figure 6.22: Aromatic hydrocarbon breakthrough curves when applying three homogeneous versus three heterogeneous layers to model the aquitard.

Increasing volume of the contaminant source

We possess limited knowledge regarding the total mass of coal tar and its spatial distribution in the Griftpark subsurface. This lack of knowledge makes it challenging to accurately estimate the potential range of coal tar occupied volume in the system. Thus, in order to conduct a sensitivity analysis, we focused solely on the dependency of the system on contaminated volume instead of studying an entire range of potential values. To that purpose, we ran the model (with the adjusted 100-fold lower degradation rates) with double and triple the number of source zone cells as allocated to the representative

model. It should be noted that the additional source zone cells were located within the same regions as the original cells, eliminating the need to consider three-dimensional effects resulting from source zones in completely different locations for this particular analysis.

Figure 6.23 shows the concentration levels in wells 101, 102 and 103 for the three simulations. The results reveal that doubling the number of source zone cells leads to an approximate increase in naphthalene concentrations of 50%, 200% and 40% in wells 101, 102 and 103, respectively, while tripling the number of source zone cells increases the naphthalene concentrations approximately 129%, 320% and 90%. The relationship between the volume of coal tar-contaminated sediment within the contained zone and the concentrations of dissolved contaminants reaching the second aquifer is illustrated in Figure 6.24. The relation between breakthrough concentrations and source zone volume appear linear. The effect of increasing the number of source zone cells is significant, although it varies per compound and observation location. In this case, the effect is strongest in well 102, where the original amount of coal tar keeps dissolved concentrations in the second aquifer below intervention levels, while when using triple the amount of coal tar, the dissolved naphthalene concentration surpasses its intervention level.

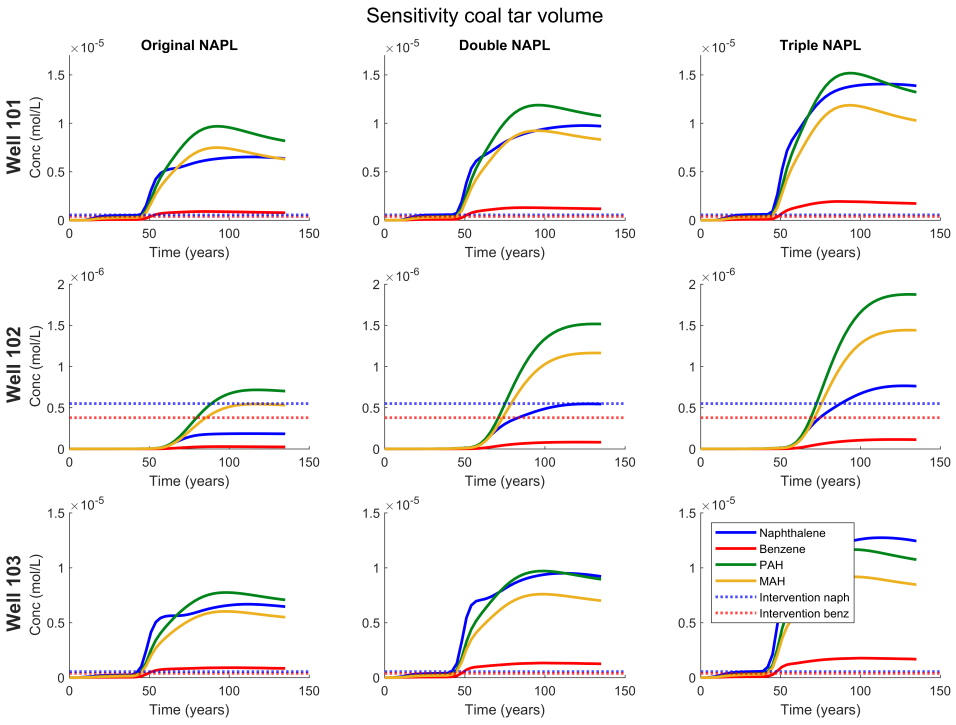

Figure 6.23: Aromatic hydrocarbon breakthrough curves in wells 101, 102 and 103 when implementing the original amount of pure phase coal tar used in the representative model, as well as when doubling or tripling the number of source zone cells.

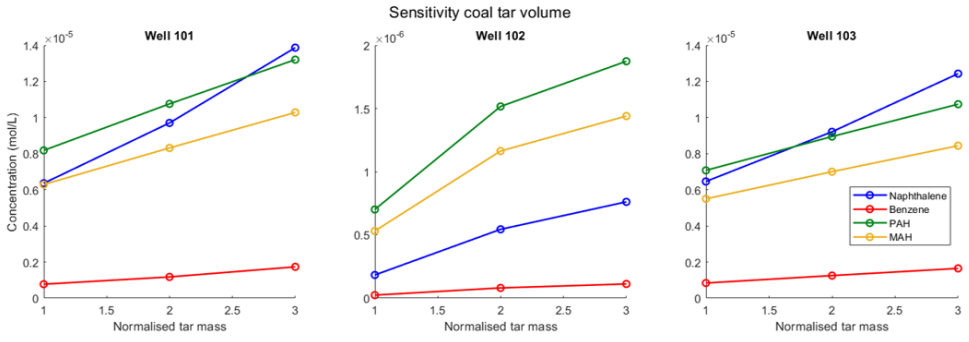

Figure 6.24: Aromatic hydrocarbon concentrations in wells 101, 102 and 103 after 135 years of simulation (100 years after turning off the groundwater extraction pumps) when implementing the original amount of pure phase coal tar used in the representative model, and when doubling or tripling the number of source zone cells.

Dispersion

We investigated the model's sensitivity to a range of dispersivity values. Biodegrading plumes are much more sensitive to changes in transverse than in longitudinal dispersivity, as it is transverse mixing that controls the mixing between clean background water and the plume and thus on how quickly the plume reduces in contaminant load [179]. Therefore, we maintained the original longitudinal dispersivity of 4 m. Based on field-scale transverse dispersivity values from the review study by Zech et al. [323], we used 1 mm as the lowest value for the transverse horizontal dispersivity, in which case modelled dispersion will be dominated by numerical dispersion. For the upper value, we used a rather large value of 0.5 m, 25% larger than the 0.4 m applied in the representative model, to account for the strong heterogeneity of the aquitard through which contaminants pass. For the vertical transverse dispersivity we maintained the ratio α_V=α_T/10.

Simulation results for the four different α_T values (using the adjusted 100-fold lower degradation rates) are shown in Figure 6.25. The results show that with increasing dispersivity, concentrations in wells 101 and 102 increase, while the concentration in well 103 decreases. After 135 years of simulation, the concentration is approximately 165% higher in well 101 when using the maximum dispersivity value compared to when using the minimum value. In well 102 there is an increase of approximately 85%, whereas in well 103 there is a decrease of 25%. These observations are caused by relative locations of the observations points to the moving plume(s), i.e. whether the observation locations lie along the flow path of the plume or with a distance on the lateral sides of the plume. Obviously, varying oxidation potential (caused by the non-uniformity in source zone locations, electron acceptors and flow field) also affects these observations.

Considering the significant heterogeneity of the Griftpark first aquifer and aquitard, it is reasonable to conclude that a higher range of dispersivity values better represents the impact of subsurface heterogeneity. Implementing α_T values of 0.4 or 0.5 m resulted in concentration differences of approximately 2%, 5%, and -1.5% for wells 101, 102, and 103, respectively, indicating a negligible impact within this higher dispersivity range. Therefore, it can be inferred that the precise value of dispersivity is not a critical parameter in the model. For comparison, a simulation was run using the heterogeneous hydraulic conductivity for the aquitard with a horizontal transverse dispersivity of 0.05 m. The results (not shown) indicate that the breakthrough concentrations in wells 101 and 103 are significantly higher (approximately 85%) when implementing α_T=0.05 m with a heterogeneous aquitard than when implementing α_T=0.5 m with a homogeneous aquitard. This indicates that a

high-range but acceptable dispersivity value cannot represent the impact of velocity variations caused by subsurface heterogeneity.

In Figure 6.26, the concentrations at t=135 years are directly compared. It shows that there is a near linear dependency on the dispersivity at least at the lower range of dispersivity values.

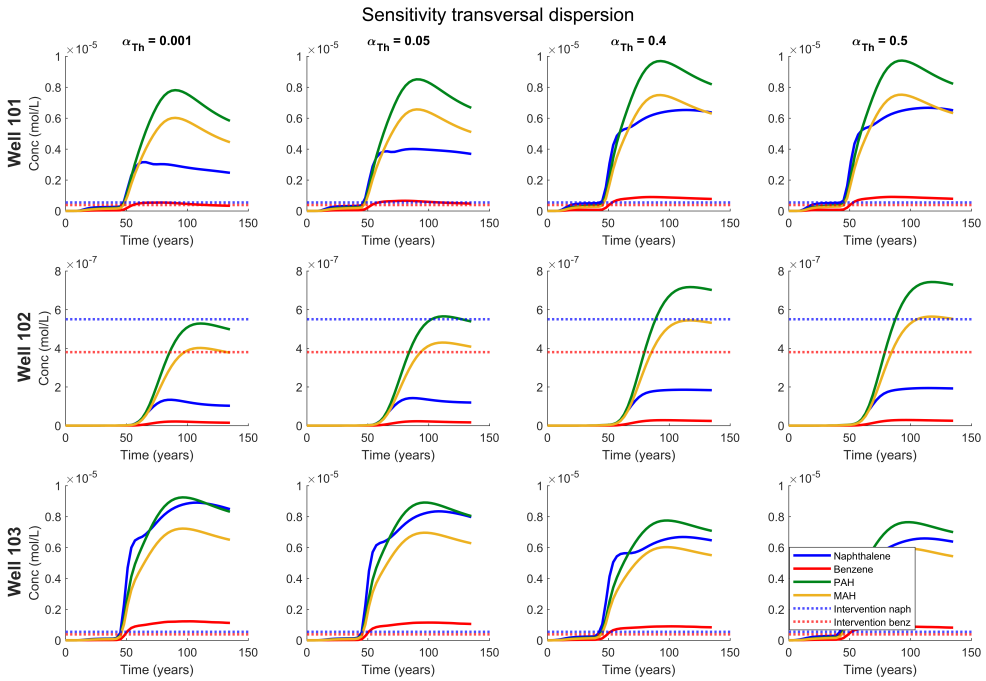

Figure 6.25: Comparison of breakthrough curves in wells 101, 102 and 103 when implementing α_T values of 0.001, 0.05, 0.4 and 0.5 m. The longitudinal dispersivity α_L in these simulations was 4m and $\alpha_V = \alpha_T/10$. The value α_T=0.4 was used in all previous simulations.

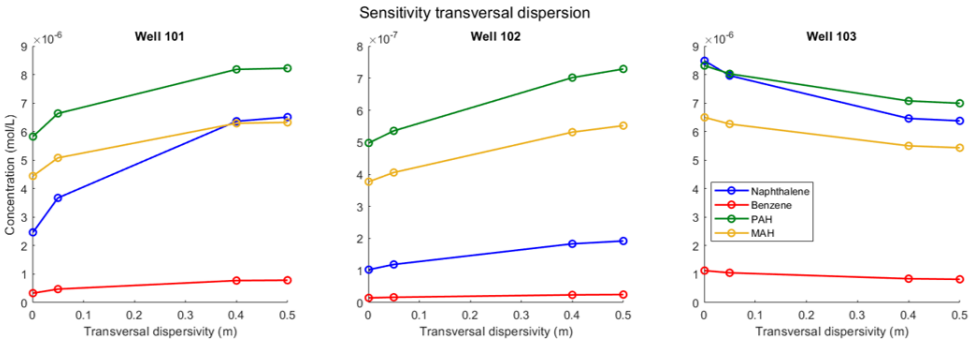

Figure 6.26: Aromatic hydrocarbon concentrations in wells 101, 102 and 103 after 135 years of simulation (100 years after turning off the groundwater extraction pumps) for a range of transverse dispersion values.

6.5 Conclusions and recommendations

In this Chapter, we have described the construction of a three-dimensional reactive transport model of the Griftpark. During the process, we had to work with limited knowledge on the coal tar contamination itself as well as the biodegradation of its dissolved compounds. The full range of organic and inorganic chemical reactions occurring in aquifers is very complex. At a site such as the Griftpark, with a high level of uncertainty in correlated parameters, it is important to stay pragmatic. Therefore, the aim of the model was not to reproduce the full biogeochemical evolution of the contamination, groundwater and sediment, but to make simulations that help us understand the most important mechanisms in the biochemical processes that occur at the site in a qualitative sense.

With the Griftpark model, we were able to acceptably reproduce field measurements and qualitatively describe the biodegradation of the coal tar aromatic hydrocarbons and consequent geochemical reactions at the site. It was found that biodegradation significantly reduces aromatic concentrations at the site and that iron and sulphate are the critical electron acceptors determining degradation. The model was used for a sensitivity analysis that may be used as a starting point for further investigations to investigate the feasibility of turning off groundwater extraction at the Griftpark in the future.

Simulations with deactivated groundwater extraction were run to investigate the potential leakage of contaminants into the second aquifer. The results indicated that, based on average degradation rates reported in literature, aromatic concentrations in the second aquifer observation wells downstream of the Griftpark remained below intervention levels after a 100-year simulation period, primarily due to biodegradation processes. However, at the lowest end

of the range of potential degradation rates reported in literature, contaminant concentrations exceeded intervention levels. Although the many assumptions made in the model, e.g. regarding coal tar sources, biodegradation rates and groundwater composition, prevent its direct application for decision-making purposes, the results are promising and provide a good basis for further investigation into the potential application of monitored natural attenuation as a management option for the Griftpark.

The sensitivity analysis showed that the volume of subsurface contaminated with coal tar and the biodegradation rates of the hydrocarbons are the critical factors in determining the potential breakthrough concentrations in the second aquifer. It was demonstrated that when employing average literature biodegradation rates, all concentrations in the second aquifer remained below intervention values, while without degradation, the concentrations of naphthalene and benzene rose significantly above. The analysis also revealed that significant sensitivity of the model to biodegradation rate lied within the order of magnitude of a 10- to 100-fold reduction of the average literature rates, which is within the range of potential field rates reported in literature, signifying the importance of this parameter for risk analysis.

The results showed a linear dependency of contaminated source volume on the contaminant concentration. In the most contaminated well, concentrations would rise three-fold when the source volume was increased three times. The insufficient knowledge that we possess on total coal tar mass and its spatial distribution in the subsurface, particularly when considering the contribution of low saturated smear zones that have a substantial impact on mass transfer, greatly determines the overall uncertainty of the model.

Modelling results indicated that the presence of intense clay depositions in the aquitard increases both the spread of the contamination plume as well as the concentration in contaminant plume cores and is therefore considered a valuable contribution to the numerical model when specific movement of the contaminant plume in the second aquifer is of importance. It was found that high transversal dispersivity values could not represent the impact of velocity variations caused by the aquitard's heterogeneity when assuming homogeneous hydraulic conductivity fields in the model. The analysis also indicated that within the high dispersivity range there is little sensitivity of the model to variations in this parameter and therefore it is not considered a crucial parameter in the model. We assume that high transversal dispersivity values are appropriate in the highly heterogeneous first aquifer and aquitard.

In order to improve the representative model, we highly recommend additional field investigations. Firstly, obtaining a better picture of the extent of pure phase coal tar contamination is considered a crucial factor in the predictive ability of the model and further investigation of the subsurface.

By applying, for example, the MIP technology at suspect as well as at non-suspect locations, a better estimate of the total contaminated volume and contaminant mass may be obtained.

Secondly, as it is challenging to obtain firm mass balance estimates, and therefore biodegradation rates, in the absence of a traceable contaminant plume, the best way to improve the model's predictive capacity on the long term evolution of hydrocarbons in the field, more detailed investigation of the subsurface' reduction capacity is needed. These investigation should include:

- Iron speciation to analyse the bioavailable iron in the subsurface
  - The performed simulations have shown that iron availability is a crucial factor in determining degradation rates and therefore contaminant concentrations in the Griftpark subsurface
  - The types of iron-oxides in the subsurface influence the availability of iron as electron acceptor and of the rate of sulphate consumption
- Sediment analysis to locate additional sources of sulphate and iron
  - The presence of for example gypsum and slug depositions may present additional sources of sulphate and iron
  - These sources would supply electron acceptors with different dissolution rates and could greatly influence the subsurface long-term reduction capacity
- Determination of biodegradation rates in the first aquifer
  - Our investigations have shown that the wide range of degradation rates available in literature leads to strongly different outcomes for concentrations reaching the second aquifer
  - Regular sampling along radial flowlines towards groundwater extraction wells offers an opportunity to obtain a range of rates, narrowing down the range provided by literature
- Biodegradation potential in the second aquifer
  - In the representative model, the same groundwater composition is assumed for the first and second aquifer, while nitrate reducing conditions prevail over sulphate in the second aquifer
  - Because no coal tar contamination has been observed in the second aquifer, we have no knowledge about the potential of biodegradation of the contaminants under nitrate reducing conditions

Implementing thus obtained additional field data, would lead to increased the reliability of the reactive transport model and provide valuable insights into the potential spread of contamination and potential for biodegradation at the site. For further modelling efforts, a number of additional activities may be considered. However, these are not straightforward and include extra considerations:

- Factor in the ageing of coal tar
  - Our results showed that benzene gets significantly depleted from the source zone over a 35-year simulation period, which means that using the current-day coal tar composition as initial composition for the simulation may not be satisfactory for ensuing model calibration. The representative model may be improved by using a higher initial benzene ratio in the coal tar
  - Consideration: Source zone compositions will vary across the site. Supplemental investigation of the compositions of different coal tars could help to determine whether these variations are significant and whether tar ageing is a crucial factor
- Including compound-specific isotope analysis
  - At many field sites, isotope analysis has proven a valuable tool in estimating biodegradation rates of individual compounds
  - Consideration: With limited knowledge of source zone locations and compositions, the interpretation of isotope analysis may prove very challenging at the Griftpark. Furthermore, isotope fractionation is also redox dependent, which further complicates analysis at the Griftpark where mixed redox conditions occur
- Automated model calibration
  - Exact matching of simulation results and field data is very challenging when using the manual, iterative method we applied whilst building the representative model, especially considering the fact that groundwater composition is strongly influenced by the presence and composition of source zones as well as electron acceptor depletion up-gradient of the monitoring well (as illustrated in Figure 5). Automated calibration (using Monte Carlo analysis) is often a useful tool to study the effect of a wide range of parameter values on model outcomes
  - Consideration: Although relying on a consensus model will result in a significant level of uncertainty that limits the model's predictive

capabilities, conducting an automated calibration for the Griftpark is at this point impractical due to the high number of correlated parameters carrying uncertainty (i.e. source zone locations, sizes, dissolution and degradation rates). Therefore, automated calibration should only be considered after strongly reducing the uncertainties

The full range of organic and inorganic chemical reactions occurring in aquifers is very complex and at a site such as the Griftpark, with a high level of uncertainty in many parameters, it is important to stay pragmatic. Within the Griftpark reactive transport model, we were able to capture and qualitatively understand the most important subsurface processes and use them to find the most important considerations for further developing a model for risk assessment for the potential application of monitored natural attenuation at the site.

Chapter 7

Summary, recommendations and outlook

7.1 Background

Groundwater contamination by coal tar and other aromatic hydrocarbon mixtures poses a worldwide problem. Coal tar, a dense non-aqueous phase liquid, may become a long-lasting source of groundwater contamination when it seeps into the saturated subsurface after being discarded on the ground surface. Once dissolved in the groundwater, aromatic hydrocarbons undergo a range of physical, biological and chemical processes, which are important to quantify when assessing the risks associated with specific contaminant spills. The reliability of quantifying these interdependent processes largely depends on the site conditions and availability of field data. While extensively researched field sites are frequently documented in academic literature and contribute to a better understanding of fundamental processes, real-world scenarios often involve highly complex site settings with limited field data.

The Griftpark is located at the site of a former industrial site that hosted multiple gas factories. The first aquifer below the site is severely contaminated with coal tar, which has been detected at depths ranging between 8 to 50 metres below ground level. To keep the surrounding aquifers safe, the contaminant source zone was contained with a vertical flow barrier. Additionally, to prevent contaminant leakage into the second aquifer through the patchy aquitard, groundwater is continuously extracted from the contained zone. These management measures, the numerous, largely unknown, spill locations, the significant subsurface heterogeneity, as well as the site's urban setting and public usage, limit the prospects for design and execution of comprehensive site investigations.

Traditionally, the enormous complexity and limited availability of liter-

ature, laboratory and field data regarding the characterisation of sites such as the Griftpark have rendered in-depth (model) studies seemingly futile. As a result, there exists a considerable gap in our understanding of numerous real-world sites and their potential for (re)development.

Motivated by this knowledge gap, our study seeks to explore the complex Griftpark field site to evaluate the extent to which field investigations in such complex settings can contribute to system understanding. Despite the inherent challenges posed by the scarcity of data, our objective is to generate valuable insights that contribute to risk assessments and the identification of potential new control and remediation strategies.

This thesis presents the findings from our comprehensive investigation, aimed at improving the understanding of the hydrogeological and biochemical processes that impact the spread and concentration of dissolved aromatic compounds at the Griftpark. The underlying motivation for the research is the aspiration of the municipality of Utrecht to phase out the costly active management procedures and transition to a new approach centered around natural attenuation. The following research questions were addressed:

- What are the hydrogeological conditions beneath the Griftpark?
- What are the principal biodegradation processes that occur?
- What is the subsurface's reduction capacity and how does it influence the potential effectiveness of monitored natural attenuation as a management option?
- What are the critical parameters to be considered when when conducting a risk assessment for potential management options at the Griftpark?

7.2 Methods

To address these research questions, a diverse range of techniques was employed, ranging from laboratory and field investigations to field-scale numerical analysis.

Various drilling techniques were used to obtain information on physical subsurface parameters as well as the presence of coal tar compounds, i.e. cone penetration testing, membrane inter-phase probing and sonic drilling. A range of hydraulic tests was employed to gain more the understanding of connectivity between the first and second aquifer as well as the hydraulic barrier's leak tightness, e.g. pumping test.

Soil, groundwater and tar samples were studied in the laboratory to identify soil types (sieve grain size analysis) and measure contaminant compositions and concentrations (gas chromatography-mass spectrometry). Several

types of analyses were performed to assess naturally occurring biodegradation of dissolved coal tar compounds. These investigations included the determination and quantification of microbial DNA (real-time polymerase chain reaction) and metabolites (qualitative tandem liquid chromatography quadrupole time of flight mass spectrometry), as well as the measurement of multi-element compound- specific isotopes (gas chromatography isotope ratio mass spectroscopy) and electron acceptors present in the groundwater (ion-exchange chromatography and inductively coupled plasma-optical emission spectrometry).

In order to gain deeper insights into the combined impacts of groundwater flow, contaminant transport, biodegradation and subsequent geochemical response, as well as to facilitate a risk assessment of the site, a three-dimensional reactive transport model was made for the Griftpark. The model was constructed in PHT3D, a software that integrates the capabilities of the widely used MODFLOW/MT3DMS flow and transport simulator with the geochemical reaction simulation capabilities of the PHREEQC-2 code.

7.3 Results

Geology

Resistivity profiling and visual soil inspection revealed the presence of small-scale heterogeneities in the Griftpark subsurface, particularly within the aquitard. Further analysis, including hydraulic testing, suggested that although the aquitard allows for water flow between the two aquifers, the flow is impeded by the presence of multiple clay depositions of varying sizes and thicknesses. Contaminant and redox analyses indicated the absence of contamination and biodegradation in the second aquifer, implying that the aquitard in combination with groundwater extraction, effectively prevents both pure phase coal tar and contaminated groundwater from percolating into the second aquifer. This demonstrates the effectiveness of the current contain-and-manage measures.

Numerical modelling showed that including clay depositions in the aquitard, rather than assuming homogeneous model layers, resulted in increased water fluxes into and out of the contained zone. It was also observed that this lead to a stronger spread of the contaminant plume and higher concentrations in contaminant plume cores. However, compared to other parameters, the impact on contaminant concentrations was relatively minor. Therefore, adding explicit heterogeneity is deemed a valuable contribution to the numerical model primarily when specific movement of the contaminant plume in the second aquifer is of importance.

Contaminant source

The numerous potential spill locations at the site and unpredictable nature of distribution patterns of DNAPL in heterogeneous aquifers, posed significant challenges to the determination of contaminant source zones at the Griftpark. During the investigations, pure phase coal tar was consistently encountered at, or inferred to exist in close proximity to, suspect locations. The depth of these encounters varied, with coal tar found as shallow as 4 m below ground level at one location and as deep as 49.5 m below ground level (46.5 m below the water table) at another.

The investigations did not provide sufficient information to obtain a full three-dimensional understanding of source zone distributions. However, the reactive transport model indicated that the volume of contaminated soil significantly influences the dissolved concentrations that reach the second aquifer when groundwater pumps are deactivated, emphasising the importance of thorough site investigations to accurately characterise source zone distributions.

Analysis of a coal tar sample revealed its composition, with 92% of its weight consisting of poly-aromatic hydrocarbons, primarily naphthalene (39% of the total mass) and various methylated naphthalenes (43% of the total mass), as well as indene and indane (1% and 6% of the total mass respectively). The remaining 8% of the sample consisted of mono-aromatic hydrocarbons, with more than half of this fraction consisting of benzene, toluene, ethylbenzene, and xylenes (BTEX) compounds.

Biodegradation

The investigations on natural biodegradation at the Griftpark highlighted the significant role of biodegradation in reducing aromatic concentrations. The study demonstrated that conventional research approaches to assess natural biodegradation, typically applied to study data along contaminant plumes, can effectively prove the occurrence of biodegradation even in the absence of a traceable contaminant plume.

Iron and sulphate were identified as crucial electron acceptors for degradation. The reactive transport model revealed that the transient change in the system's reduction capacity is closely linked to depletion of bio-available iron in sediment and sulphate in groundwater. Whereas sulphate is mostly depleted in groundwater at locations with high aromatic hydrocarbon concentrations, strongly elevated sulphate concentrations at other locations suggest the presence of sulphate sources at the site (e.g. gypsum from factory rubble). Although no sediment analysis was performed to assess the availability of iron in the subsurface, the research findings indicate that iron depletion

has occurred around contaminant source zones. It is expected that over time, biodegradation will become limited by the recharge of sulphate through rainfall and groundwater, as well as by methanogenesis.

Although the data from the Griftpark field site clearly confirmed the occurrence of biodegradation, the absence of a traceable contaminant plume hinders the estimation of mass balances which could be used to calculate degradation rates. Meanwhile, it was demonstrated that degradation rates play a critical role in determining the contaminant concentrations that reach the second aquifer when groundwater extraction is deactivated. Literature values provide a wide range of potential degradation rates due to the variations in physical, chemical and biological conditions at different sites. At the Griftpark, the upper range of literature rates would result in a fully safe situation in the second aquifer after deactivating the groundwater extraction, whereas the lower range would lead to concentrations significantly exceeding intervention values. This emphasises the importance of determining potential ranges of degradation rates specific to the field site in order to conduct more meaningful risk assessments.

Crucial parameters

The Griftpark reactive transport model successfully captured and provided qualitative understanding of significant subsurface processes. The findings provided crucial considerations for the development of a risk assessment model for the potential application of monitored natural attenuation at the site.

Simulations where contamination was allowed to escape the contained zone by turning off groundwater extraction, showed that after 100 years, biodegradation kept aromatic concentrations below intervention levels when using average degradation rates derived from literature. As the many assumptions made in the reference model (regarding coal tar sources, biodegradation rates and the first and second aquifer groundwater composition) currently leave it an unsuitable tool for decision making, the results are promising and give ground for continuing the investigations of monitored natural attenuation as a management option for the Griftpark. The sensitivity analysis revealed that the volume of subsurface contaminated with coal tar and the biodegradation rates of hydrocarbons are the critical factors in determining the potential breakthrough concentrations in the second aquifer.

The comprehensive results of our study demonstrate that despite limited data availability, the combination of field research and numerical modeling can yield valuable insights into the understanding of complex sites. This work signifies the potential value of utilising such tools and methods in investigating sites similar to the Griftpark, whether they possess containment barriers or not.

Aerobic batch experiments

In addition, a series of aerobic batch experiments were conducted to examine the substrate interactions among prevalent contaminants found at the Griftpark site. The experiments demonstrated that Griftpark indigenous microorganisms could fully degrade all tested compounds, i.e. benzene, toluene, ethylbenzene, xylene, indene, indane and naphthalene (BTEXIeIaN), under aerobic conditions. Furthermore, it was found that the presence of indene, indane and naphthalene inhibited the degradation of benzene, toluene, ethylbenzene and o-xylene.

These findings signify that the simultaneous occurrence of multiple pollutants leads to variations in degradation processes and microbial community development. This complexity presents an additional challenge when determining degradation rates at specific field sites, as well as a limitation in the extrapolation of rates obtained from one site to another.

7.4 Recommendations

In order to improve the reference model, we highly recommend additional field investigations to address key knowledge gaps. Firstly, it is crucial to obtain a more comprehensive picture of the extent of pure phase coal tar contamination, as the uncertainty in this parameter significantly affects the model's predictive capacities. Utilising technologies such as the membrane-interface probe at both suspect and non-suspect locations, would provide more insight in the total contaminated volume and contaminant mass.

While obtaining firm mass balance estimates and accurate biodegradation rates presents challenges in the absence of a traceable contaminant plume, regular sampling along radial flowlines towards groundwater extraction wells offers an opportunity to obtain a range of rates, narrowing down the range provided by literature.

In order to improve the understanding of the subsurface's reduction capacity, it is recommended to perform iron speciation analysis on soil samples collected from a range of conditions in the first aquifer as well as from the second aquifer. This analysis would enable the assessment of the amount and type bio-available iron in the subsurface as well as its level of depletion. It is also recommended to identify additional sources of sulphate and iron in sediment (e.g. gypsum and slug depositions) as they can play an important role in the long-term reduction capacity of the Griftpark subsurface.

Furthermore, it is advised to evaluate the biodegradation potential in the second aquifer. Given that nitrate reducing conditions prevail over sulphate in this aquifer and no observed coal tar contamination is present, the potential for biodegradation in the second aquifer remains unknown. This is a signif-

icant knowledge gap as the second aquifer's reduction potential will largely determine the risks associated with the potential seepage of contaminants into this aquifer.

By conducting these investigations, the predictive capacity of the model for long-term hydrocarbon evolution would be substantially improved. This, in turn, would make the model an invaluable tool for conducting risk assessments and evaluating potential future management approaches at the Griftpark.

In addition, considering the inherent heterogeneity and complexity of the subsurface model at this site, it is acknowledged that a certain degree of uncertainty will persist. Therefore, before establishing conclusive future management plans, it is advisable to explore potential contingency measures that could effectively mitigate the entry of unexpectedly high levels of hydrocarbons into the second aquifer. Such contingency scenarios may involve the stimulation of biodegradation, such as through sulphate or oxygen injection. Some of these investigations are already underway at the Griftpark and are discussed in the final part of this summary.

7.5 Outlook

A number of research activities are currently being rolled out that involve the Griftpark. They include a number of specific pilot projects at the Griftpark as well as the international MiBiRem project.

MiBiRem The project 'Microbiomes for bio-based innovation and environmental applications' (MiBiRem) is set up to design an IT modelling tool that integrates microbiological, chemical, hydrological and physical data and processes to support decisions considering if and how to apply bioremediation at contaminated sites. The tool will combine established numerical models solving the physical, chemical, biological and hydrogeological relationships at various scales into a single interface for bioremediation prediction. The Griftpark case study will be used as input for this tool, both by including observation data and through using the reactive transport model, which will for this purpose be translated to the python version of MODFLOW (FlowPy) and PHREEQC (PhreeqPy). The EU-funded project is executed by a large international consortium of which Utrecht University will be involved with the routines on field data handling and the main responsible for the creation of the modelling tool.

Pilots 2023/2024 To investigate the potential of management approaches based on biodegradation at the Griftpark, currently, four pilot projects are being developed.

- Pilot 1: In-situ stimulation of biodegradation by nitrate injection
  - This pilot project involves the installation of an extraction well in the second aquifer for the purpose of extracting nitrate-containing water. The extracted water is then injected into wells located in the first aquifer, where subsequent monitoring will be conducted to assess the biodegradation of coal tar compounds.
  - The primary objective of this pilot is to investigate the potential for biodegradation of the Griftpark coal tar contaminants in the second aquifer, which exhibits nitrate-reducing conditions. The study aims to determine whether natural biodegradation processes alone are capable of sufficiently breaking down dissolved contaminants that may escape the contained zone following the deactivation of current active management measures. Additionally, the pilot will explore the possibility of stimulating biodegradation with nitrate as an additional fallback option
- Pilot 2: In-situ stimulation of biodegradation sulphate injection
  - This pilot entails the installation of wells at a severely contaminated in the Griftpark, characterised by depleted sulphate levels, and the injection of sulphate to stimulate biodegradation
  - The main objective of this pilot is to investigate whether sulphate dosing may stimulate biodegradation of coal tar aromatics to a degree that effectively prevents the migration of contaminants into the second aquifer after deactivating groundwater extraction from the contained zone
  -
- Pilot 3: In-situ aerobic stimulation of biodegradation through micro-bubble injection
  - This pilot study focuses on the installation of wells to facilitate the injection of nano and micro air-bubbles into the groundwater and monitoring the subsequent aerobic biodegradation of coal tar aromatic hydrocarbons.
  - The primary goal of this pilot is to demonstrate the cost-effectiveness of nano- and micro-bubbles compared to macro-bubbles for introducing air into the contaminated subsurface and are therefore expected to be a better option for the stimulated biodegradation of aromatic hydrocarbons

- Pilot 4: Ex-situ treatment of contaminated groundwater in a constructed wetland
  - This pilot entails the installation of a constructed wetland at the groundwater treatment plant, wherein the incoming contaminated groundwater is treated by a combination of helophyte filters, microbubbles and active carbon
  - The main objective of this pilot is to is to demonstrate the capability of wetlands in degrading tar aromatic hydrocarbons, while ensuring no disruption to the surrounding environment. The ultimate goal is to explore the potential of utilising on-site wetlands to prevent the need for pumping contaminated groundwater to the treatment plant located 3 km away from the Griftpark

The first three pilots will be executed by *SARPI/TAUW* and the fourth by *hmvt*. The aim of the pilots is to determine which of these methods are suitable make the management of coal tar aromatic hydrocarbons at the Griftpark and at comparable sites more sustainable and cost-efficient in the future.

Appendices

Appendix A Filter depths

Well	**Filter depths** (m-NAP)						
A	48	62					
B	14	41	51	60			
B MLS1	5.5	7.5	9	11	12.5	14	16
B MLS2	17.5	19.5	21	23	25	26.5	28
B MLS3	46.5	48.5	50	52	53.5	55.5	57
B2	61.5						
B2 MLS1	4	5.5	7.5	9	11	12.5	14.5
B2 MLS2	17	20	23	40	47	52	57
C	35.5	37.5	40	42.5			
C MLS	12.5	14	16	17.5	19.5	21	23
101 MLS1	48.5	50.8	53.8	61	63	64.3	65.8
101 MLS 2	68.8	72.8	77.8	79.8	83.8	85.3	86.5
102	18	23					
102 MLS1	39.5	43.3	49.7	59	63	65	67.5
102 MLS2	69.8	71	72.5	75	79	83	86.5
103	44.5						
103 MLS	58	63.5	67.5	69.5	77	96.5	104
BW157	64						
BW211	24						
BW205	44						
DV1	71						
DV2	31						
DV4	31						
DV10	31						
DV11	31						
DV12	31						
DV14	31						
LT1	$2-7$						
LT2	$2-7$						
LT3	$2-7$						
LT4	$5-8$						
Pb1	7	17					
37	20						
60	67						
86	9						
B10	$8-17$						
B20	$7-17$						
B21	$7-17$						
B22	$23-33$	$35-43$					

Table A.1: Depths of (MLS) filters in wells installed between 2018-2021 (i.e. A, B, B2, C, 101, 102 and 103), wells for groundwater monitoring installed in 1990 (i.e. LTs, DVs etc) and of groundwater pumping wells (i.e. B10 (shut down in 2017) and B20-22).

Appendix B Grain size analysis

Sample	soil description	d_{50} (mm)	soil classification	UC	K (m/d)	$f_{0.063}$ (%)
A 23	very course sand, moderately silty, moderately gravelly	0.39	very course	1.6	81	6
A 25	moderately fine sand, weak silty	0.21	moderately fine, moderately course	2.8	8	7
A 30	moderately course sand, gravelly, clay layers	0.21	moderately fine, moderately course	117	0	33
A 33	very course sand, moderately silty, weak gravelly	0.42	very course	2.4	44	4
A 37	clay, weak sandy	0.01	clay	6.6	-	96
A 47	moderately fine sand, moderately silty	0.23	moderately course	4.4	4	10
B 17	moderately silty, weak gravelly	0.39	very course	1.9	60	2
B 23	very fine sand, moderately silty	0.18	moderately fine	2.8	5	9
B 34	moderately fine sand, weakly silty sand	0.23	moderately course	1.9	22	4
B 53	very fine sand, moderately silty, clay layers	0.11	very fine	191	-	33
B 57	clay, strongly sandy	0.03	clay	5000	-	66
B 61	course sand, weakly silty, moderately gravelly	0.37	very course	4.9	7	9
C 13	course sand, moderately silty, moderately gravelly	0.31	very course	2.4	25	3
C 19	course sand, weakly silty, strongly gravelly, gravel layers	0.39	very course	2.4	37	3
C 26	very course sand, moderately gravelly	0.40	very course	1.7	81	3
C 34	course sand, weakly silty, moderately gravelly, pebbles	0.57	extremely course	3.6	45	5

Table B.1: Sample locations (shown on the map in Figure 2.3 in Chapter 2) and visual soil type descriptions of the samples, as well as d_{50} values, NEN soil classifications, uniformity coefficients (UC), hydraulic conductivities and percentages of soil grains smaller than 0.063 mm resulting from grain size analysis

Appendix C Second aquifer

Well locations	Screen depths	BTEXIeIaN	Nitrate	Sulphate
Up-gradient of the Griftpark				
BW157	65.0	23.9	bdl	60
Below the Griftpark				
B	64.0	0.02	bdl	39
B2	65.5	0.12	bdl	209
Down-gradient of the Griftpark				
A	65.5	0.12	166	
60	72.0	18.8	0.26	26.1
101	60 – 110	2.0	71.0	0.5
102	60 – 110		0.58	25.7
103	60 – 110	0.50	61.6	

Table C.1: Well locations and depths (in m-bg), total concentration (mg/L) of tar aromatics (BTEXIeIaN) and electron acceptor concentrations measured in groundwater samples collected from the 2nd aquifer. Concentrations of nitrate are below detection level (bdl) in some wells.

Appendix D Metabolite suspect list

Parent compound	Suspect metabolites
Fluorene, phenanthrene, benzene, creosote	Phenol
(Tracer)	Fluoresceine
Substrate, potential toluene metabolite	Phenylsuccinic acid - 3 isomers
n-octylbenzene	Phenylbutyrate
Indole; amino acid synthase	Tryptophan - 2 isomers
?	Valeric acid
e.g. Phenol	Adipic acid
Cofactor phenanthrene metabolism	Nicotinic acid
?	2-isopropylmalic acid - 2 isomers
Amino acid synthase	Quinolinic acid - 2 isomers
Amino acid synthase	Acetylphenol
Byproduct toluene+cyanogen chloride reaction	Homophthalonitrile
?	4-Hydroxyphenylpyruvate - 2 isomers
Algemene	Hippurate - 7 isomers
Acenaphtene	Acenaphthyl methylsuccinate - 2 isomers
Acenaphtene, acenaphthylene	Acenaphthene-5-carboxylic acid
Acenaphtene, acenaphthylene	Acenaphthenoic acid - 1 isomers
Acenaphthene	Acenaphthene-1,2-diol
Acenaphthene	Acenaphtnoquinone
Acenaphtylene	Acenaphthylenoic acid - 4 isomers
Addition	Fumaric acid - 2 isomers
Alkanes	2-(1-methyldodecyl)succinate or 2-(2-methyltridecyl)malonate - 2 isomers
Alkanes	2-(1-methyltetradecyl)succinate or 2-(2-methylpentadecyl)malonate - 2 isomers
Alkanes	2-(1-methylhexadecyl)succinate or 2-(2-methylheptadecyl)malonate
Alkanoate	Laurate
Alkanoate	Myristate or myristic acid or tetradecanoic acid
Alkanoate	Butyrate
Alkanoate	2-methyl 2-hydroxy-propanal (isomer of butyrate)
Alkanoate	Hydroxycaproate or hydroxycaproic acid
Alkanoate	Octanoate - 3 isomers
Alkanoate	3-nonenoate
Alkanoate	Nonanoate or nonanoic acid - 2 isomers
Aniline	4-aminobenzoic acid
Ethylbenzene/ acetophenone	Benzoylacetic acid
Ethylbenzene	Phenylethanol

Ethylbenzene/ Phenylethanol	Acetophenone
Ethylbenzene	o-Coumaric acid
Ethylbenzene	p-Coumaric acid
Ethylbenzene	m-Coumaric acid
Fluorene	9-hydroxyfluorene
Fluorene	Fluorene-9-carboxylic acid - 9 isomers
Indene	2-methylindene - 3 isomers
Indene	Dihydro-2-indenoic acid - 7 isomers
Indene	Hexahydro-2-indenoic acid - 2 isomers
Indene	Dicyclononane-2-carboxylate (octahydro-2-indenoic acid)
Indene	1H-indene-2-carboxylic acid
Indene	1H-indene-3-carboxylic acid
Indene	Indyl methyl succinic acid - 2 isomers
Indene	Indenediol - isomer 1
Indene, naphthalene	Carboxylated methyl indene or Dihydro-naphthoic acid - 10 isomers
Indene, naphthalene	Dihydromethyl indenoic acid, Tetrahydro-naphthoic acid or 2,3-dihydro-1H-indene-acetic acid - 14 isomers
Indene, naphthalene	Tetrahydromethyl indenoic acid or Hexahydro-naphthoic acid - 23 isomers
Indene, naphthalene	Octahydro-2-naphthoic acid or Hexahydromethyl indenoic acid
Indene, naphthalene	2-carboxycyclohexylacetic acid
Indene, styrene	Indenediol or styrene carboxylic acid - 7 isomers
Indene, trimethylbenzene	Tetrahydro-2-indenoic acid or Trimethylbenzoic acid - 13 isomers
Indene, trimethylbenzene	Phenylbutyrate
m-xylene/styrene; amino acid synthesis	3-Methyl benzoic acid
m-xylene/styrene; amino acid synthesis	4-Methyl benzoic acid
Naphthalene	1-naphthol
Naphthalene	2,3-dihydroxynaphthalene
Indene, Naphthalene	Decahydro-naphthoic acid or Octahydromethyl indenoic acid
Naphthalene	1-naphthoic acid
Naphthalene	2-naphthoic acid
Naphthalene, phenanthrene	1-Hydroxy-2-naphthoic acid
Naphthalene	1-naphthylacetic acid
Naphthalene	2-naphthaleneacetic acid
Naphthalene	3-naphthalenedicarboxylic acid - 6 isomers
Naphthalene	Dimethyl-naphthoic acid - 15 isomers
Naphthalene	Naphthyl-2-methyl-succinate - 2 isomers
Naphthalene, Benzene, etc. (from salicylic acid)	Gentisic Acid
Gentisic acid	Fumarylpyruvic acid

Xylene	3-o-toluoyl propionic acid
Phenanthrene	Phenanthroic acid - 8 isomers
Phenanthrene, creosote	P-cresol - 4 isomers
Phenanthrene, benzene, phenol, p-cresol, 3-hydroxybenzaldehyde, 2,2,3-trihydroxybiphenyl, anthranilic acid	4-hydroxy benzoic acid
Styrene	Phenylglyoxylic acid - 3 isomers
Products of the skeleton rearangement	Ethylmalonate - 3 isomers
Products of the skeleton rearangement	2-(methylpentyl)malonate
Products of the skeleton rearangement	Butylmalonate - 4 isomers
Solvent	Propanediol
Styrene	2-ethylhexanol
Styrene	Hydroxyphenylacetic acid - 3 isomers
Toluene	Benzylsuccinic acid
Toluene	Cinnamic acid
Toluene, Ethylbenzene, Xylene, Phenol, Benzene	Benzoic acid
Tetramethylbenzene	Trimethylbenzoic acid
Trimethylbenzene, xylenes	Dimethyl-benzoic acid or Benzylacetate - 8 isomers
Xylenes/styrene; toluene	Methylbenzylsuccinic acid - 5 isomers

Table D.1: List of 170 potential metabolites, based on literature data on both aerobic and anaerobic degradation pathways of aromatic hydrocarbons present at the Griftpark.

Appendix E Metabolite analysis

Parent	Metabolite	Conf. level	m/z [M-H]	Formula
Thiophene	(2-/3-)methylthiophene	4	98.01902	C5H6S
Thiophene	(2-/3-)thiophenic acid	3	127.9932	C5H4O2S
Indole	1,3-dihydro-2H-indol-2-one [15, 124]	4	133.1473	C8H7NO
Fluorene	1-formyl- 2-indanone [259]	2b	160.1693	C10H8O2
Indene	1H-indene-2-carboxylic acid [46]	2a	159.0452	C10H8O2
Indene	1H-indene-3-carboxylic acid [46]	1	159.0452	C10H8O2
banzo[a]pyrene, pyrene	1H-phenalen-1-one/Perinaphtenone [319]	4	180.0575	C13H8O
Naphthalene, phenanthrene	1-Hydroxy-2-naphthoic acid [296]	1	187.0401	C11H8O3
Indane, Indene	1-indanone [213]	1	132.0575	C9H8O
Naphthalene	1-Naphthaleneacetic acid [255]	2a	185.0608	C12H10O2
Naphthalene	1-naphthoic acid [326]	2b	171.0452	C11H8O2
Naphthalene	1-naphthol [23]	1	143.0502	C10H8O
Alkanes	2-(1-methyldodecyl)succinate or 2-(2-methyltridecyl)malonate - 2 isomers [30]	4	285.2071	C16H30O4
Alkanes	2-(1-methylhexadecyl)succinate or 2-(2-methylheptadecyl)malonate [30]	4	341.2697	C20H38O4
Alkanes	2-(1-methyltetradecyl)succinate or 2-(2-methylpentadecyl)malonate - 2 isomers [30]	4	313.2384	C18H34O4
Naphthalene	2,3-dihydroxynaphthalene [296]	1	159.0452	C10H8O2
2,4-dimethylphenol	2,4-dimethylenoic acid (2,4-dimethylcyclo- hexanecarboxylic acid)	4	156.115	C9H16O2
Benzofuran	2-[(Benzofuran-2-yl)methyl]succinic acid [255]	4	248.0685	C13H12O5
Indene, naphthalene	2-carboxycyclohexylacetic acid [296, 326]	3	185.0819	C9H14O4
Fluorene	2-formyl-1-indanone [259]	2b	160.1693	C10H8O2
Indane	2-Indanecarboxylic acid	1	162.0068	C10H10O2
Indene	2-methylindene [296]	1	129.071	C10H10
Naphthalene	2-Naphthaleneacetic acid [255]	1	185.0608	C12H10O2
Naphthalene	2-naphthoic acid [326]	1	171.0452	C11H8O2
m-xylene/styrene; amino acid synthesis	3-Methyl benzoic acid [285]	2a	135.0452	C8H8O2
Naphthalene	3-naphthalenedicarboxylic acid - 6 isomers [296]	3	215.035	C12H8O4
Alkanes	3-nonenoate [30]	3	155.1078	C9H16O2
Xylene	3-o-toluoyl propionic acid - 17 isomers [206]	2a	191.0714	C11H12O3

Phenanthrene, benzene, phenol, p-cresol, 3-hydroxybenzaldehyde, 2,2,3-trihydroxybiphenyl, anthranilic acid	4-hydroxy benzoic acid [287, 100, 183]	1	137.0244	C7H6O3
p-Cresol	4-hydroxybenzylsuccinate [209]	4	224.0685	C11H12O5
m-xylene/styrene; amino acid synthesis	4-Methyl benzoic acid [285]	1	135.0452	C8H8O2
Acridine	9(10H)-Acridanone [275]	1	195.0684	C13H9NO
Fluoranthene, Fluorene	9-fluorenone [260, 259]	1	180.0575	C13H8O
Fluoranthene	9-fluorenone-1-carboxylic acid [260]	1	224.0473	C14H8O3
Fluoranthene	9-hydroxy-1-fluorene-carboxylic acid [260]	3	226.063	C14H10O3
Fluorene	9-hydroxyfluorene [296]	1	181.0737	C13H10O
Carbazole	9-methylcarbazole	4	181.0891	C13H11N
Fluorene	9-methylfluorene-9-carboxylic acid	4	224.0837	C15H12O2
Phenanthrene	9-phenanthrol	1	194.0732	C14H10O
Acenaphtene, acenaphthylene	Acenaphthene-5-carboxylic acid [46, 255]	1	197.0608	C13H10O2
Acenaphtene	Acenaphthyl methylsuccinate - 2 isomers [46, 206]	3	283.0976	C17H16O4
Acenaphtylene	Acenaphthylenoic acid - 4 isomers [46, 255]	2b	195.0452	C13H8O2
e.g. Phenol	Adipic Acid [315]	1	145.0506	C6H10O4
Anthracene	Anthracene-2-carboxylic acid	3	222.068	C15H10O2
Benzothiophene	Benzo[b]thiophene-2-carboxylic acid [255]	1	178.0089	C9H6O2S
Creosote	Benzofuran [81]	4	118.0419	C8H6O
Benzofuran	Benzofuran-2-carboxylic acid [255]	3	162.0317	C9H6O3
Toluene, Ethylbenzene, Xylene, Phenol, Benzene	Benzoic acid [46]	1	121.0295	C7H6O2
Creosote	Benzothiophene [81]	4	134.1992	C8H6S
Toluene	Benzylsuccinic acid - 4 isomers [46]	1	207.0663	C11H12O4
Products of the skeleton rearangement	Butylmalonate - 4 isomers [30]	1	157.0506	C7H10O4
Carbazole	Carbazole-3-carboxylic acid	3	211.0633	C13H9NO2
Indene, naphthalene	Carboxylated methyl indene or Dihydro-naphthoic acid - 10 isomers [296, 326]	4	173.0608	C11H10O2
Indane	Cis-1,2-indanediol	3	150.0681	C9H10O2
Indene, Naphthalene	Decahydro-naphthoic acid or Octahydromethyl indenoic acid [296, 326]	4	181.1234	C11H18O2
Indene	Dicyclononane-2-carboxylate (octahydro-2-indenoic acid) [296]	2b	167.1078	C10H16O2

Indene	Dihydro-2-indenoic acid - 7 isomers [46]	3	161.0608	C10H10O2
Indene, naphthalene	Dihydromethyl indenoic acid, Tetrahydro-naphthoic acid or 2,3-dihydro-1H-indene-acetic acid - 14 isomers [296, 326]	4	175.0765	C11H12O2
Tri- methylbenzene, xylenes	Dimethyl-benzoic acid or Benzylacetate - 8 isomers [62]	4	149.0608	C9H10O2
Indane	Dimethylindane	4	146.1095	C11H14
Naphthalene	Dimethyl-naphthoic acid - 15 isomers [118]	3	199.0765	C13H12O2
Alkanes	Dodecanoic acid [30]	2b	199.1704	C12H24O2
Products of the skeleton rearangement	Ethylmalonate - 3 isomers [30]	3	131.035	C5H8O4
Fluoranthene	Fluoranthene-8-carboxylic acid	3	246.0681	C17H10O2
Fluorene	Fluorene-9-carboxylic acid [296]	3	209.0608	C14H10O2
Addition	Fumaric acid - 2 isomers [46]	3	115.0037	C4H4O4
Indene	Hexahydro-2-indenoic acid - 2 isomers [296]	3	165.0921	C10H14O2
Quinoline	hydroxycoumarin - 4 isomers [152]	1	162.0317	C9H6O3
Fluorene, Indane	indanone-carboxylic acid [259]	3	176.0473	C10H8O3
Indene, styrene	Indenediol or styrene carboxylic acid - 7 isomers [296]	4	147.0452	C9H8O2
Indene	Indyl methyl succinic acid - 2 isomers [296]	3	245.0819	C14H14O4
Benzothiophene	methylbenzo(b)thiophene - 4 isomers?	1	148.225	C9H8S
Benzofuran	methylbenzofuran - 4 isomers?	4	132.16	C9H8O
Xylenes/styrene; toluene	Methylbenzylsuccinic acid - 5 isomers [285, 27]	2a	221.0819	C12H14O4
Indane	Methylindane	4	132.0939	C10H12
Alkanes	Myristic acid [30]	1	227.2017	C14H28O2
Naphthalene	Naphthyl-2-methyl-succinate - 2 isomers [14]	2b	257.0819	C15H14O4
Alkanes	Nonanoic acid [30]	1	157.1234	C9H18O2
Indene, naphthalene	Octahydro-2-naphthoic acid or Hexahydromethyl indenoic acid [296, 326]	4	179.1078	C11H16O2
Alkanes	Octanoic acid [30]	1	143.1078	C8H16O2
Ethylbenzene/ acetophenone	P-coumaric acid [46]	1	163.0401	C9H8O3
Acidogenesis	Pentanoic Acid [196]	1	101.0608	C5H10O2
Phenanthrene	Phenanthroic acid - 8 isomers [46, 165]	3	221.0608	C15H10O2
Fluorene, phenanthrene, benzene, creosote	Phenol [46]	1	93.03459	C6H6O
n-octylbenzene, indene, trimethylbenzene	Phenylbutyrate [296, 162]	1	163.0765	C10H12O2
Styrene	Phenylglyoxylic acid - 3 isomers [285]	2b	149.0244	C8H6O3

Substrate, potential toluene metabolite	Phenylsuccinic acid [177]	3	193.0506	C10H10O4
Pyrene	Pyrene carboxylic acid	3	246.0681	C17H10O2
Toluene	t-Cinnamic acid [53]	1	147.0452	C9H8O2
Indene, trimethylbenzene	Tetrahydro-2-indenoic acid or Trimethylbenzoic acid - 13 isomers [296]	4	163.0765	C10H12O2
Indene, naphthalene	Tetrahydromethyl indenoic acid or Hexahydro-naphthoic acid - 23 isomers [296, 326]	4	177.0921	C11H14O2
Creosote	Thiophene [81]	4	84.14	C4H4S

Table E.1: List of 76 different metabolites detected, out of 170 analysed suspect metabolites, in 28 groundwater samples collected from the Griftpark. Indicating the parent compound, metabolite name, confidence levels,mass-to charge ratios and chemical formulas.

Appendix F Plots of degradation rate fitting

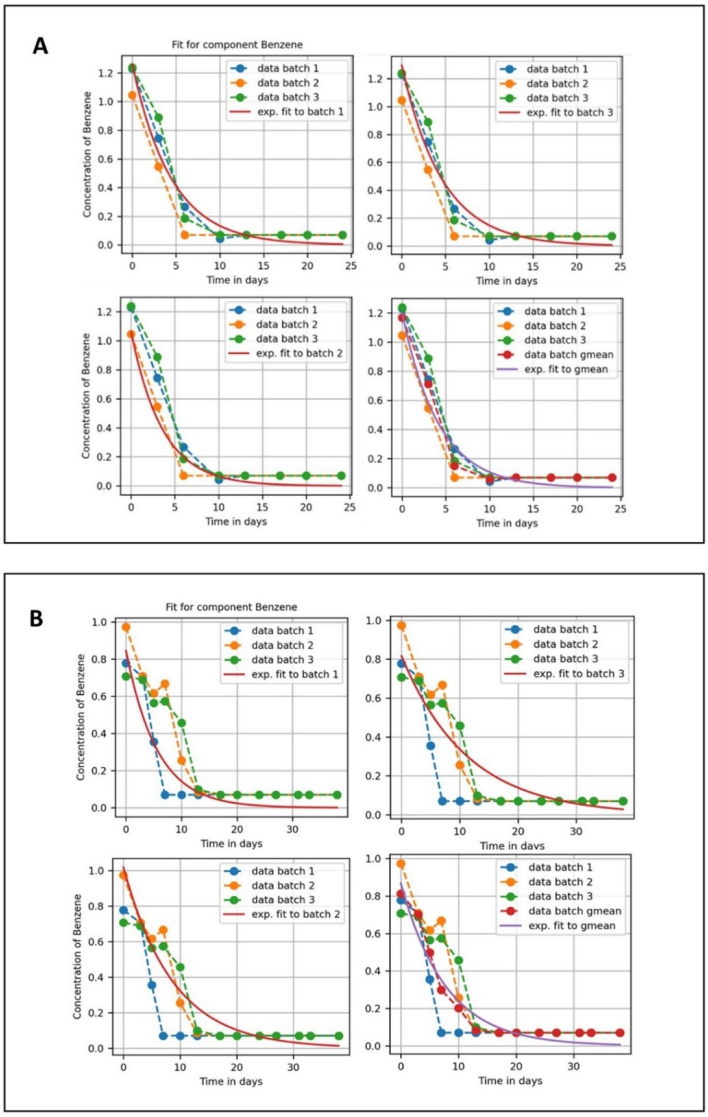

Figure F.1: Plots of the different fits performed for benzene in the BTEXIa (A) and BTEX-IeIaN (B) mixture. For rate calculations the mean of the fits to the three batches was used although they did not differ much from the fit of the geometric mean of the data. Concentrations were normalised with control batches.

Appendix G First order degradation rates

	Literature	BTEX	stdv	BTEXIe	stdv	BTEXIa	stdv	BTEXN	stdv	BTEXIeIa	stdv	BTEXIeN	stdv	BTEXIaN	stdv	BTEXIeIaN	stdv
B	0.34 ± 0.64	1.03	0.05	0.33	0.04	0.24	0.03	0.20	0.01	0.15	0.01	0.20	0.06	0.12	0.02	0.13	0.04
T	0.27 ± 0.42	1.76	0.06	1.47	0.24	0.55	0.23	0.31	0.01	0.90	0.03	0.84	0.40	0.72	0.09	0.48	0.03
E		1.27	0.04	1.18	0.08	0.69	0.26	1.49	0.35	1.03	0.03	0.98	0.06	1.04	0.03	1.07	0.01
oX	0.10 ± 0.14	0.23	0.02	0.16	0.06	0.17	0.02	0.22	0.06	0.10	0.02	0.01	0.01	0.07	0.00	0.09	0.05
mpX	1,21 ± 0,04	0.44	0.08	1.65	0.33	1.44	0.19	0.38	0.04	1.72	0.03	0.10	0.02	0.17	0.00	0.30	0.11
Ie		-		0.51	0.08	-		-		0.06	0.02	0.39	0.08	-		0.50	0.15
Ia		-		-		0.21	0.08	-		0.04	0.01	-		0.11	0.01	0.07	0.05
N		-		-		-		3.22	0.01	-		1.99	0.07	2.06	0.01	2.11	0.02

only one data point above d.l. in:	all batches
	2 batches
	1 batch

Figure G.1: Mean of the degradation rate constants (1/day) of the triplicate batches normalised to control batches. Batches with only one data point above detection limit (d.l.) are colour coded. stdv; standard deviations. Depicted literature rates were taken from Suarez and Rifai, 1999 [274].

Appendix H PHREEQC database

Based on Buchholz database and Affonseca2007 [65]. Text in capitals indicate keywords. Italic text indicates comments

```
SOLUTION_MASTER_SPECIES

element  species   alk gfw_formula gfw
H           H+      -1.0    H      1.008
H(0)        H2      0.0     H
H(1)        H+      -1.0    0.0
E           e-      0.0     0.0    0.0
O           H2O     0.0     O      16.0
O(0)        O2      0.0     O
O(-2)       H2O     0.0     0.0
Ca          Ca+2    0.0     Ca     40.08
Mg          Mg+2    0.0     Mg     24.312
Na          Na+     0.0     Na     22.9898
K           K+      0.0     K      39.102
Fe          Fe+2    0.0     Fe     55.847
Fe(+2)      Fe+2    0.0     Fe
Fe(+3)      Fe+3    -2.0 Fe
Mn          Mn+2    0.0     Mn     54.938
Mn(+2)      Mn+2    0.0     Mn
Mn(+3)      Mn+3    0.0     Mn
Al          Al+3    0.0     Al     26.9815
Si          H4SiO4  0.0     SiO2   28.0843
Cl          Cl-     0.0     Cl     35.453
C           CO3-2   2.0     HCO3   12.0111
C(+4)       CO3-2   2.0     HCO3
C(-4)       CH4     0.0     CH4
Alkalinity  CO3-2   1.0     Ca0.5(CO3)0.5 50.05
S           SO4-2   0.0     SO4     32.064
S(6)        SO4-2   0.0     SO4
S(-2)       HS-     1.0     S
N           NO3-    0.0     N      14.0067
N(+5)       NO3-    0.0     N
N(+3)       NO2-    0.0     N
N(0)        N2      0.0     N
Amm         AmmH+   0.0     AmmH   17.0
Br          Br-     0.0     Br     79.904

NAPL Phase
Naphnapl       Naphnapl       0.0      Naphnapl      128.1732
Meth_naphnapl  Meth_naphnapl  0.0      Meth_naphnapl  142.2
Benznapl       Benznapl       0.0      Benznapl       78.1134
Ethylnapl      Ethylnapl      0.0      Ethylnapl     106.167

Dissolved Phase
Naph         Naph        0.0    Naph      128.1732
Meth_naph    Meth_naph   0.0    Meth_naph    142.2
Benz         Benz        0.0    Benz      78.1134
Ethyl        Ethyl       0.0    Ethyl      106.167


SOLUTION_SPECIES

H2O + 0.01e- = H2O-0.01; log_k -9.0
```

```
H+ = H+
log_k 0.0
-gamma 9.0 0.0

e- = e-
log_k 0.0

H2O = H2O
log_k 0.0

Ca+2 = Ca+2
log_k 0.0
-gamma 5.0 0.1650

Mg+2 = Mg+2
log_k 0.0
-gamma 5.5 0.20

Na+ = Na+
log_k 0.0
-gamma 4.0 0.075

K+ = K+
log_k 0.0
-gamma 3.5 0.015

Fe+2 = Fe+2
log_k 0.0
-gamma 6.0 0.0

Mn+2 = Mn+2
log_k 0.0
-gamma 6.0 0.0

Al+3 = Al+3
log_k 0.0
-gamma 9.0 0.0

H4SiO4 = H4SiO4
log_k 0.0

Cl- = Cl-
log_k 0.0
-gamma 3.5 0.015

CO3-2 = CO3-2
log_k 0.0
-gamma 5.4 0.0

SO4-2 = SO4-2
log_k 0.0
-gamma 5.0 -0.04

NO3- = NO3-
log_k 0.0
-gamma 3.0 0.0

AmmH+ = AmmH+
```

```
log_k 0.0
-gamma 2.5 0.0

Br- = Br-
log_k 0.0
-gamma 3.0 0.0

Naph   = Naph
        log_k           0.0

Meth_naph = Meth_naph
        log_k           0.0

Benz  = Benz
        log_k           0.0

Ethyl  = Ethyl
        log_k           0.0

Naphnapl = Naphnapl
        log_k           0.0

Meth_naphnapl = Meth_naphnapl
        log_k           0.0

Benznapl  = Benznapl
        log_k           0.0


Ethylnapl  = Ethylnapl
        log_k           0.0

H2O = OH- + H+
log_k -14.0
delta_h 13.362 kcal
-analytic -283.971 -0.05069842 13323.0 102.24447 -1119669.0
-gamma 3.5 0.0

2 H2O = O2 + 4 H+ + 4 e-
log_k -86.08
delta_h 134.79 kcal

2 H+ + 2 e- = H2
log_k -3.15
delta_h -1.759

CO3-2 + H+ = HCO3-
log_k 10.329
delta_h -3.561 kcal
-analytic 107.8871 0.03252849 -5151.79 -38.92561 563713.9
-gamma 5.4 0.0

CO3-2 + 2 H+ = CO2 + H2O
log_k 16.681
delta_h -5.738 kcal
-analytic 464.1965 0.09344813 -26986.16 -165.75951 2248628.9

CO3-2 + 10 H+ + 8 e- = CH4 + 3 H2O
log_k 41.071
```

```
delta_h -61.039 kcal

SO4-2 + H+ = HSO4-
log_k 1.988
delta_h 3.85 kcal
-analytic -56.889 0.006473 2307.9 19.8858 0.0

HS- = S-2 + H+
log_k -12.918
delta_h 12.1 kcal
-gamma 5.0 0.0

SO4-2 + 9 H+ + 8 e- = HS- + 4 H2O
log_k 33.65
delta_h -60.140 kcal
-gamma 3.5 0.0

HS- + H+ = H2S
log_k 6.994
delta_h -5.30 kcal

NO3- + 2 H+ + 2 e- = NO2- + H2O
log_k 28.570
delta_h -43.760 kcal
-gamma 3.0 0.0

2 NO3- + 12 H+ + 10 e- = N2 + 6 H2O
log_k 207.08
delta_h -312.130 kcal

AmmH+ = Amm + H+
log_k -9.252
delta_h 12.48 kcal

AmmH+ + SO4-2 = AmmHSO4-
log_k 1.11

Ca+2 + H2O = CaOH+ + H+
log_k -12.78

Ca+2 + CO3-2 = CaCO3
log_k 3.224
delta_h 3.545 kcal
-analytic -1228.732 -0.299440 35512.75 485.818

Ca+2 + CO3-2 + H+ = CaHCO3+
log_k 11.435
delta_h -0.871 kcal
-analytic 1317.0071 0.34546894 -39916.84 -517.70761 563713.9
-gamma 5.4 0.0

Ca+2 + SO4-2 = CaSO4
log_k 2.3
delta_h 1.650 kcal

Mg+2 + H2O = MgOH+ + H+
log_k -11.44
delta_h 15.952 kcal
```

```
Mg+2 + CO3-2 = MgCO3
log_k 2.98
delta_h 2.713 kcal
-analytic 0.9910 0.00667

Mg+2 + H+ + CO3-2 = MgHCO3+
log_k 11.399
delta_h -2.771 kcal
-analytic 48.6721 0.03252849 -2614.335 -18.00263 563713.9

Mg+2 + SO4-2 = MgSO4
log_k 2.37
delta_h 4.550 kcal

Na+ + H2O = NaOH + H+
log_k -14.18

Na+ + CO3-2 = NaCO3-
log_k 1.27
delta_h 8.910 kcal

Na+ + HCO3- = NaHCO3
log_k -0.25

Na+ + SO4-2 = NaSO4-
log_k 0.7
delta_h 1.120 kcal

K+ + H2O = KOH + H+
log_k -14.46

K+ + SO4-2 = KSO4-
log_k 0.85
delta_h 2.250 kcal

Fe+2 + H2O = FeOH+ + H+
log_k -9.5
delta_h 13.20 kcal

Fe+2 + Cl- = FeCl+
log_k 0.14

Fe+2 + CO3-2 = FeCO3
log_k 4.38

Fe+2 + HCO3- = FeHCO3+
log_k 2.0

Fe+2 + SO4-2 = FeSO4
log_k 2.25
delta_h 3.230 kcal

Fe+2 + HSO4- = FeHSO4+
log_k 1.08

Fe+2 + 2HS- = Fe(HS)2
log_k 8.95

Fe+2 + 3HS- = Fe(HS)3-
```

```
log_k 10.987

Fe+2 = Fe+3 + e-
log_k -13.02
delta_h 9.680 kcal
-gamma 9.0 0.0

Fe+3 + H2O = FeOH+2 + H+
log_k -2.19
delta_h 10.4 kcal

Fe+3 + 2 H2O = Fe(OH)2+ + 2 H+
log_k -5.67
delta_h 17.1 kcal

Fe+3 + 3 H2O = Fe(OH)3 + 3 H+
log_k -12.56
delta_h 24.8 kcal

Fe+3 + 4 H2O = Fe(OH)4- + 4 H+
log_k -21.6
delta_h 31.9 kcal

2 Fe+3 + 2 H2O = Fe2(OH)2+4 + 2 H+
log_k -2.95
delta_h 13.5 kcal

3 Fe+3 + 4 H2O = Fe3(OH)4+5 + 4 H+
log_k -6.3
delta_h 14.3 kcal

Fe+3 + Cl- = FeCl+2
log_k 1.48
delta_h 5.6 kcal

Fe+3 + 2 Cl- = FeCl2+
log_k 2.13

Fe+3 + 3 Cl- = FeCl3
log_k 1.13

Fe+3 + SO4-2 = FeSO4+
log_k 4.04
delta_h 3.91 kcal

Fe+3 + HSO4- = FeHSO4+2
log_k 2.48

Fe+3 + 2 SO4-2 = Fe(SO4)2-
log_k 5.38
delta_h 4.60 kcal

Al+3 + H2O = AlOH+2 + H+
log_k -5.0
delta_h 11.49 kcal
-analytic -38.253 0.0 -656.27 14.327

Al+3 + 2 H2O = Al(OH)2+ + 2 H+
log_k -10.1
```

```
delta_h 26.90 kcal
-analytic 88.50 0.0 -9391.6 -27.121

Al+3 + 3 H2O = Al(OH)3 + 3 H+
log_k -16.9
delta_h 39.89 kcal
-analytic 226.374 0.0 -18247.8 -73.597

Al+3 + 4 H2O = Al(OH)4- + 4 H+
log_k -22.7
delta_h 42.30 kcal
-analytic 51.578 0.0 -11168.9 -14.865

Al+3 + SO4-2 = AlSO4+
log_k 3.5
delta_h 2.29 kcal

Al+3 + 2SO4-2 = Al(SO4)2-
log_k 5.0
delta_h 3.11 kcal

Al+3 + HSO4- = AlHSO4+2
log_k 0.46

H4SiO4 = H3SiO4- + H+
log_k -9.83
delta_h 6.12 kcal
-analytic -302.3724 -0.050698 15669.69 108.18466 -1119669.0

H4SiO4 = H2SiO4-2 + 2 H+
log_k -23.0
delta_h 17.6 kcal
-analytic -294.0184 -0.072650 11204.49 108.18466 -1119669.0


PHASES

Calcite
CaCO3 = CO3-2 + Ca+2
log_k -8.48
delta_h -2.297 kcal
-analytic -171.9065 -0.077993 2839.319 71.595

Dolomite
CaMg(CO3)2 = Ca+2 + Mg+2 + 2 CO3-2
log_k -17.09
delta_h  -9.436 kcal

Fe(OH)3(a)
Fe(OH)3 + 3 H+ = Fe+3 + 3 H2O
log_k 4.891

FeS(ppt)
FeS + H+ = Fe+2 + HS-
log_k -3.915

Mackinawite
FeS + H+ = Fe+2 + HS-
log_k -4.648
```

```
Goethite
FeOOH + 3 H+ = Fe+3 + 2 H2O
log_k -1.0

Gypsum
CaSO4:2H2O = Ca+2 + SO4-2 + 2 H2O
log_k -4.58
delta_h -0.109 kcal
-analytic 68.2401 0.0 -3221.51 -25.0627
Hematite
Fe2O3 + 6 H+ = 2 Fe+3 + 3 H2O
log_k -4.008
delta_h -30.845 kcal

Pyrite
FeS2 + 2 H+ + 2 e- = Fe+2 + 2 HS-
log_k -18.479
delta_h 11.300 kcal

Siderite
FeCO3 = Fe+2 + CO3-2
log_k -10.89
delta_h  -2.480 kcal

CO2(g)
CO2 = CO2
log_k -1.468
delta_h -4.776 kcal
-analytic 108.3865 0.01985076 -6919.53 -40.45154 669365.0

O2(g)
O2 = O2
log_k -2.96
delta_h -1.844 kcal

H2(g)
H2 = H2
log_k -3.15
delta_h -1.759 kcal

N2(g)
N2 = N2
log_k -3.26
delta_h -1.358 kcal

H2S(g)
H2S = H2S
log_k -0.997
delta_h -4.570 kcal

CH4(g)
CH4 = CH4
log_k -2.86
delta_h -3.373 kcal

Amm(g)
Amm = Amm
log_k 1.77
```

```
delta_h -8.170 kcal


RATES

      Mineral dissolution/precipitation

-----------------------------------------------
FeS(ppt)
-----------------------------------------------
      -start
30 rate = parm(1)*(1-SR("FeS(ppt)"))
40 moles = rate*TIME
50 Save moles
      -end


            DNAPL dissolution

 -----------------------------------------------
 Naphnapl     Naphthalene
 -----------------------------------------------
    -start
  10  mNaph = tot("Naph")
  11  mNaphnapl  = tot("Naphnapl")
  12  if (mNaphnapl <= 1e-10) then goto 200
  20  mMeth_naphnapl = tot("Meth_naphnapl")
  23  mBenznapl = tot("Benznapl")
  25  mEthylnapl = tot("Ethynapl")
  30  m_napl_tot = mNaphnapl + mMeth_naphnapl + mBenznapl + mEthylnapl
  32  if (m_napl_tot <= 1e-10) then goto 200
  40  solub_Naph = 0.00082440530989838  mol/L
  50  msolub_Naph =  mNaphnapl / m_napl_tot * solub_Naph
  60  rate = parm(1)  * (msolub_Naph - mNaph)
  70  moles = rate * time
  80  if (moles > m) then moles = m
  200 Save moles
 -end

-----------------------------------------------
Meth_naphnapl     1-Methyl-Naphthalene/PAHs
-----------------------------------------------
  -start
   10  mMeth_naphnapl  = tot("Meth_naphnapl")
   11  if (mMeth_naphnapl <= 1e-10) then goto 200
   12  solub_Meth_naph = 0.000207699604225951
   13  mMeth_naph  = tot("Meth_naph")
   20  mNaphnapl  = tot("Naphnapl")
   23  mBenznapl = tot("Benznapl")
   25  mEthylnapl = tot("Ethynapl")
   30  m_napl_tot = mNaphnapl + mMeth_naphnapl + mBenznapl + mEthylnapl
   32  if (m_napl_tot <= 1e-10) then goto 200
   50  msolub_Meth_naph =  mMeth_naphnapl / m_napl_tot * solub_Meth_naph
   60  rate = parm(1)  * (msolub_Meth_naph - mMeth_naph)
   70  moles = rate * time
   80  if (moles > m) then moles = m
   200 Save moles
  -end
```

```
-----------------------------------------------
Benznapl     Benzene
-----------------------------------------------
  -start
   10  mBenznapl = tot("Benznapl")
   11  if (mBenznapl <= 1e-10) then goto 200
   12  solub_Benz = 0.0227873834706977
   13  mBenz = tot("Benz")
   20  mNaphnapl  = tot("Naphnapl")
   23  mMeth_naphnapl = tot("Meth_naphnapl")
   25  mEthylnapl = tot("Ethynapl")
   30  m_napl_tot = mNaphnapl + mMeth_naphnapl + mBenznapl + mEthylnapl
   32  if (m_napl_tot <= 1e-10) then goto 200
   50  msolub_Benz =  mBenznapl / m_napl_tot * solub_Benz
   60  rate = parm(1)  * (msolub_Benz - mBenz)
   70  moles = rate * time
   80  if (moles > m) then moles = m
   200 Save moles
  -end


-----------------------------------------------
Ethylnapl     Ethylbenzene/MAHs
-----------------------------------------------
  -start
   10  mEthylnapl = tot("Ethylnapl")
   11  if (mEthylnapl <= 1e-10) then goto 200
   12  solub_Ethyl = 0.00151836257970933
   13  mEthyl = tot("Ethyl")
   20  mNaphnapl  = tot("Naphnapl")
   21  mMeth_naphnapl = tot("Meth_naphnapl")
   24  mBenznapl = tot("Benznapl")
   30  m_napl_tot = mNaphnapl + mMeth_naphnapl + mBenznapl + mEthylnapl
   32  if (m_napl_tot <= 1e-10) then goto 200
   50  msolub_Ethyl =  mEthylnapl / m_napl_tot * solub_Ethyl
   60  rate = parm(1)  * (msolub_Ethyl - mEthyl)
   70  moles = rate * time
   80  if (moles > m) then moles = m
   200 Save moles
  -end


                 Degradation

-------------------------------------------------------
Naph         Naphthalene
-------------------------------------------------------
-start
Input parameters
  Biodegradation rates
    2  k1_oxid    = parm(1)
    3  k1_denit   = parm(2)
    4  k1_sulf    = parm(3)
    5  k1_iron    = parm(4)
  Half-saturation constants
    6  k12_mNaph   = parm(5)
    7  k12_ox   = parm(6)
    8  k12_no3   = parm(7)
```

```
    9  k12_sulf   = parm(8)
   10  k12_iron   = parm(9)
  Inhibition constants
   11  k_inhib_ox   = parm(10)
   12  k_inhib_no3  = parm(11)
  Definition of the compound moles
   20  mNaph   = TOT("Naph")
   23  IF (mNaph < 1e-11) THEN GOTO 200
  Definition of electron acceptors moles
   30  mOx    = TOT("O(0)")
   31  mNO3   = TOT("N(5)")
   32  mSO4   = TOT("S(6)")
   33  mIron  = EQUI("Goethite")
  pH inhibition
   34  mue_ph = 7   optimal pH
   35  k_inh_ph = 0.5
   36  phdif = sqrt((mue_ph - -LA("H+")) * (mue_ph - -LA("H+")))
   37  ph_inhib = k_inh_ph / (k_inh_ph + 10^phdif - 1)
  Methane inhibition
   38  meth_max = 1.5e-04
   39  meth_inhib = (meth_max - TOT("C(-4)")) / meth_max
Kinetic reactions
  Oxygen reduction
   40  rate_ox    = (k1_oxid) *mNaph*(mOx/(k12_ox + mOx))
  Nitrate reduction
   50  rate_denit = (k1_denit)*mNaph*(mNO3/(k12_no3 + mNO3))*
     (k_inhib_ox/(k_inhib_ox+mOx))
  Sulphate and iron reduction
   60  rate_sulf_iron   = (k1_sulf) * (mSO4/(k12_sulf + mSO4))
   65  rate_sulf_iron   = rate_sulf_iron + (k1_iron) *
     (mIron/(k12_iron + mIron))
   68  rate_sulf_iron   = rate_sulf_iron * mNaph *
     (k_inhib_ox/(k_inhib_ox+mOx)) *(k_inhib_no3/(k_inhib_no3 + mNO3))
   80  rate = (rate_sulf_iron + rate_ox + rate_denit) * ph_inhib *
     meth_inhib
Update and save moles based on the calculated rates
   90  moles = rate * time
   91  if (moles > mNaph) then moles = mNaph
   200 Save moles
  -end


-----------------------------------------------------
Meth_naph      1-Methyl-Naphthalene/PAHs
-----------------------------------------------------
-start
Input parameters
  Biodegradation rates
    2  k1_oxid    = parm(1)
    3  k1_denit   = parm(2)
    4  k1_sulf    = parm(3)
    5  k1_iron    = parm(4)
  Half-saturation constants
    6  k12_mMeth_naph   = parm(5)
    7  k12_ox   = parm(6)
    8  k12_no3   = parm(7)
    9  k12_sulf   = parm(8)
   10  k12_iron   = parm(9)
  Inhibition constants
```

```
   11  k_inhib_ox   = parm(10)
   12  k_inhib_no3  = parm(11)
  Definition of the compound moles
   20  mMeth_naph   = TOT("Meth_naph")
   23  IF (mMeth_naph < 1e-11) THEN GOTO 200
  Definition of electron acceptors moles
   30  mOx    = TOT("O(0)")
   31  mNO3   = TOT("N(5)")
   32  mSO4   = TOT("S(6)")
   33  mIron  = EQUI("Goethite")
  pH inhibition
   34  mue_ph = 7   optimal pH
   35  k_inh_ph = 0.5
   36  phdif = sqrt((mue_ph - -LA("H+")) * (mue_ph - -LA("H+")))
   37  ph_inhib = k_inh_ph / (k_inh_ph + 10^phdif - 1)
  Methane inhibition
   38  meth_max = 1.5e-04
   39  meth_inhib = (meth_max - TOT("C(-4)")) / meth_max
Kinetic reactions
  Oxygen reduction
   40  rate_ox    = (k1_oxid) *mMeth_naph*(mOx/(k12_ox + mOx))
  Nitrate reduction
   50  rate_denit = (k1_denit)*mMeth_naph*(mNO3/(k12_no3 + mNO3))*
     (k_inhib_ox/(k_inhib_ox+mOx))
  Sulphate and iron reduction
   60  rate_sulf_iron   = (k1_sulf) * (mSO4/(k12_sulf + mSO4))
   65  rate_sulf_iron   = rate_sulf_iron + (k1_iron) *
     (mIron/(k12_iron + mIron))
   68  rate_sulf_iron   = rate_sulf_iron * mMeth_naph *
     (k_inhib_ox/(k_inhib_ox+mOx)) *(k_inhib_no3/(k_inhib_no3 + mNO3))
   80  rate = (rate_sulf_iron + rate_ox + rate_denit) * ph_inhib *
     meth_inhib
Update and save moles based on the calculated rates
   90  moles = rate * time
   91  if (moles > mMeth_naph) then moles = mMeth_naph
   200 Save moles
  -end


------------------------------------------------------
Benz     Benzene
------------------------------------------------------
-start
Input parameters
  Biodegradation rates
    2  k1_oxid    = parm(1)
    3  k1_denit   = parm(2)
    4  k1_sulf    = parm(3)
    5  k1_iron    = parm(4)
  Half-saturation constants
    6  k12_mBenz   = parm(5)
    7  k12_ox   = parm(6)
    8  k12_no3   = parm(7)
    9  k12_sulf   = parm(8)
   10  k12_iron   = parm(9)
  Inhibition constants
   11  k_inhib_ox   = parm(10)
   12  k_inhib_no3  = parm(11)
  Definition of the compound moles
```

```
   20  mBenz   = TOT("Benz")
   23  IF (mBenz < 1e-11) THEN GOTO 200
  Definition of electron acceptors moles
   30  mOx    = TOT("O(0)")
   31  mNO3   = TOT("N(5)")
   32  mSO4   = TOT("S(6)")
   33  mIron  = EQUI("Goethite")
  pH inhibition
   34  mue_ph = 7   optimal pH
   35  k_inh_ph = 0.5
   36  phdif = sqrt((mue_ph - -LA("H+")) * (mue_ph - -LA("H+")))
   37  ph_inhib = k_inh_ph / (k_inh_ph + 10^phdif - 1)
  Methane inhibition
   38  meth_max = 1.5e-04
   39  meth_inhib = (meth_max - TOT("C(-4)")) / meth_max
Kinetic reactions
  Oxygen reduction
   40  rate_ox    = (k1_oxid) *mBenz*(mOx/(k12_ox + mOx))
  Nitrate reduction
   50  rate_denit = (k1_denit)*mBenz*(mNO3/(k12_no3 + mNO3))*
     (k_inhib_ox/(k_inhib_ox+mOx))
  Sulphate and iron reduction
   60  rate_sulf_iron   = (k1_sulf) * (mSO4/(k12_sulf + mSO4))
   65  rate_sulf_iron   = rate_sulf_iron + (k1_iron) *
     (mIron/(k12_iron + mIron))
   68  rate_sulf_iron   = rate_sulf_iron * mBenz *
     (k_inhib_ox/(k_inhib_ox+mOx)) *(k_inhib_no3/(k_inhib_no3 + mNO3))
   80  rate = (rate_sulf_iron + rate_ox + rate_denit) * ph_inhib *
     meth_inhib
Update and save moles based on the calculated rates
   90  moles = rate * time
   91  if (moles > mBenz) then moles = mBenz
   200 Save moles
  -end


-----------------------------------------------------
Ethyl      Ethylbenzene/MAHs
-----------------------------------------------------
-start
Input parameters
  Biodegradation rates
    2  k1_oxid    = parm(1)
    3  k1_denit   = parm(2)
    4  k1_sulf    = parm(3)
    5  k1_iron    = parm(4)
  Half-saturation constants
    6  k12_Ethyl   = parm(5)
    7  k12_ox   = parm(6)
    8  k12_no3   = parm(7)
    9  k12_sulf   = parm(8)
   10  k12_iron   = parm(9)
  Inhibition constants
   11  k_inhib_ox   = parm(10)
   12  k_inhib_no3  = parm(11)
  Definition of the compound moles
   20  Ethyl   = TOT("Ethyl")
   23  IF (Ethyl < 1e-11) THEN GOTO 200
  Definition of electron acceptors moles
```

```
   30  mOx    = TOT("O(0)")
   31  mNO3   = TOT("N(5)")
   32  mSO4   = TOT("S(6)")
   33  mIron  = EQUI("Goethite")
  pH inhibition
   34  mue_ph = 7   optimal pH
   35  k_inh_ph = 0.5
   36  phdif = sqrt((mue_ph - -LA("H+")) * (mue_ph - -LA("H+")))
   37  ph_inhib = k_inh_ph / (k_inh_ph + 10^phdif - 1)
  Methane inhibition
   38  meth_max = 1.5e-04
   39  meth_inhib = (meth_max - TOT("C(-4)")) / meth_max
Kinetic reactions
  Oxygen reduction
   40  rate_ox    = (k1_oxid) *Ethyl*(mOx/(k12_ox + mOx))
  Nitrate reduction
   50  rate_denit = (k1_denit)*Ethyl*(mNO3/(k12_no3 + mNO3))*
     (k_inhib_ox/(k_inhib_ox+mOx))
  Sulphate and iron reduction
   60  rate_sulf_iron   = (k1_sulf) * (mSO4/(k12_sulf + mSO4))
   65  rate_sulf_iron   = rate_sulf_iron + (k1_iron) *
     (mIron/(k12_iron + mIron))
   68  rate_sulf_iron   = rate_sulf_iron * Ethyl *
     (k_inhib_ox/(k_inhib_ox+mOx)) *(k_inhib_no3/(k_inhib_no3 + mNO3))
   80  rate = (rate_sulf_iron + rate_ox + rate_denit) * ph_inhib *
     meth_inhib
Update and save moles based on the calculated rates
   90  moles = rate * time
   91  if (moles > Ethyl) then moles = Ethyl
   200 Save moles
  -end

END
```

Appendix I PMWIN database

Definition of Chemistry used by PMWIN for PHT3D (coupled PHREEQC/MT3DMS model)

```
 [Component_mobile_kinetic]
Format:
Line 1: Number of Component_mobile_kinetic
FOR i=0 to (Number Component_mobile_kinetic)-1
  Line 2+i: Name of the Component_mobile_kinetic
  Line 3+i: Number of parameters used in the PHREEQC database
  FOR j=1 to Number of parameters
     Line 4+j: parameter (j)
  NEXT j
  Stoichiometry of the Component_mobile_kinetic (use the exact
  word no_stoichiometry, if stoichiometry is not defined)
NEXT i

4

Naph
11
9.3e-6
7.2e-8
7.2e-8
1e-8
1.0e-5
1.0e-5
1.0e-5
1.0e-5
1.0e-5
1.0e-5
1.0e-5
Naph -1 C10H8 1

Meth_naph
11
4.6e-6
4.6e-8
4.6e-8
0.5e-7
1.0e-5
1.0e-5
1.0e-5
1.0e-5
1.0e-5
1.0e-5
1.0e-5
Meth_naph -1 C11H10 1

Benz
11
3.9e-06
9.3e-8
9.3e-8
1.0e-7
1.0e-5
1.0e-5
1.0e-5
```

```
1.0e-5
1.0e-5
1.0e-5
1.0e-5
Benz -1 C6H6 1

Ethyl
11
6.2e-7
3.1e-6
2.3e-8
3.5e-8
1.0e-5
1.0e-5
1.0e-5
1.0e-5
1.0e-5
1.0e-5
1.0e-5
Ethyl -1 C8H10 1


[Component_mobile_equilibrium]
Format:
Line 1: Number of Component_mobile_equilibrium
FOR i=0 to Number of Component_mobile_equilibrium -1
  Line 2+i: Name of the Component_mobile_equilibrium
NEXT i

19

pH
pe
S(-2)
S(6)
Al
C(4)
C(-4)
Ca
Cl
Fe(2)
Fe(3)
K
Mg
Mn(2)
N(3)
N(5)
N(0)
Na
O(0)


[Component_immobile_kinetic]
Format:
Line 1: Number of Component_immobile_kinetic
FOR i=0 to Number of Component_immobile_kinetic -1
  Line 2+i: Name of the Component_immobile_kinetic
  Line 3+i: Number of parameters used in the PHREEQC database
  FOR j=1 to Number of parameters
```

```
    Line 4+j: parameter (j)
  NEXT j
  Stoichiometry of the Component_immobile_kinetic (use the exact
  word no_stoichiometry, if stoichiometry is not defined)
NEXT i

4

Naphnapl
1
1.0e-5
Naphnapl -1.0 Naph 1.0

Meth_naphnapl
1
1.0e-5
Meth_naphnapl -1.0 Meth_naph 1.0

Benznapl
1
1.0e-5
Benznapl -1.0 Benz 1.0

Ethylnapl
1
1.0e-5
Ethylnapl -1.0 Ethyl 1.0


[Minerals_equilibrium]
Format:
Line 1: Number of Minerals_equilibrium
FOR i=0 to Number of Minerals_equilibrium -1
  Line 2+i: Name of the Mineral_equilibrium
  Line 3+i: Chemical equation
NEXT i

4

Calcite
CaCO3 = CO3-2 + Ca+2

Goethite
FeOOH + 3 H+ = Fe+3 + 2 H2O

Magnetite
Fe3O4 + 8 H+ = 2 Fe+3 + Fe+2 + 4 H2O

Siderite
FeCO3 = Fe+2 + CO3-2


[Gas_equilibrium]
Format:
Line 1: Number of Gases (equilibrium)
FOR i=0 to Number of Gases (equilibrium) -1
  Line 2+i: Name of the Gas
Next i
```

```
7

CO2(g)
O2(g)
H2(g)
N2(g)
H2S(g)
CH4(g)
Amm(g)


[Mineral_kinetic]
Format:
Line 1: Number of Minerals_kinetic
FOR i=0 to (Number Minerals_kinetic)-1
  Line 2+i: Name of the Mineral_kinetic
  Line 3+i: Number of parameters used in the PHREEQC database
  FOR j=1 to Number of parameters
     Line 4+j: parameter (j)
  NEXT j
NEXT i

1

FeS(ppt)
1
1e-14
no_stoichiometry
```

Appendix J Hydrocarbon concentration data

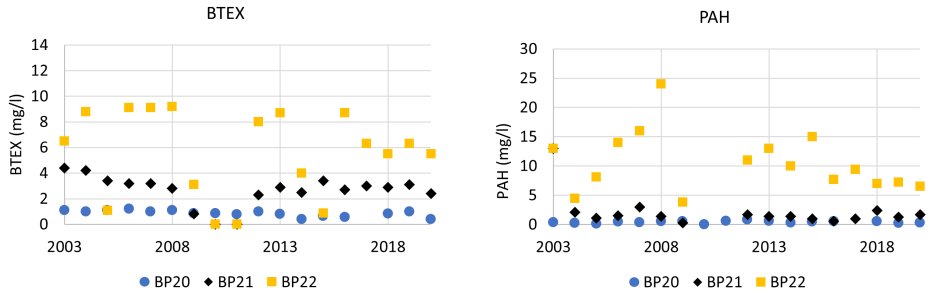

(a) (b)

Figure J.1: BTEX and 16 EPA PAH concentrations in groundwater extraction wells B20, B21 and B22 between 2003 and 2020. The data indicates the variability in concentrations over time.

Bibliography

[1] L. M. Abriola. Modeling multiphase migration of organic chemicals in groundwater systems - A review and assessment. *Environmental Health Perspectives*, 83:117–143, 1989.

[2] L. M. Abriola, J. A. Christ, K. D. Pennell, and C. A. Ramsburg. Source Remediation Challenges. In P. K. Kitanidis and P. McCarty, editors, *Delivery and Mixing in the Subsurface*, chapter 10, pages 239–276. Springer, New York, NY, 2012.

[3] N. Abu Laban, D. Selesi, T. Rattei, P. Tischler, and R. U. Meckenstock. Identification of enzymes involved in anaerobic benzene degradation by a strictly anaerobic iron-reducing enrichment culture. *Environmental Microbiology*, 12(10):2783–2796, 10 2010.

[4] A. Aburto and M. Peimbert. Degradation of a benzene-toluene mixture by hydrocarbon-adapted bacterial communities. *Annals of Microbiology*, 61(3):553–562, 9 2011.

[5] E. E. Adams and L. W. Gelhar. Field Study of Dispersion in a Heterogeneous Aquifer 2. Spatial Moments Analysis. *Water Resources Research*, 28(12):3293–3307, 1992.

[6] Adviesbureau Heidemij. Voorbereiding sanering Griftpark te Utrecht Aanvullend onderzoek omgeving en noordelijk deel van het park. Technical report, Heidemij Adviesbureau, Provincie Utrecht, 1989.

[7] C. Aeppli, M. Berg, O. A. Cirpka, C. Holliger, R. P. Schwarzenbach, and T. B. Hofstetter. Influence of Mass-Transfer Limitations on Carbon Isotope Fractionation during Microbial Dechlorination of Trichloroethene. *Environmental Science and Technology*, 43(23):8813–8820, 2009.

[8] O. Al-Hashimi, K. Hashim, E. Loffill, T. Marolt Čebašek, I. Nakouti, A. A. Faisal, and N. Al-Ansari. A Comprehensive Review for Groundwater Contamination and Remediation: Occurrence, Migration and Ad-

sorption Modelling. *Molecules 2021, Vol. 26, Page 5913*, 26(19):5913, 9 2021.

[9] M. Alexander, S. J. Berg, and W. A. Illman. Field Study of Hydrogeologic Characterization Methods in a Heterogeneous Aquifer. *Ground Water*, 49(3):365–382, 2010.

[10] A. Alfreider and C. Vogt. Bacterial Diversity and Aerobic Biodegradation Potential in a BTEX-Contaminated Aquifer. *Water Air Soil Pollution*, 183:415–426, 2007.

[11] A. P. Alphenaar and A. Van de Velde. Quickscan / karakterisering IBC-locaties. Technical report, TTE, 2015.

[12] P. J. J. Alvarez and T. M. Vogel. Substrate Interactions of Benzene, Toluene, and para-Xylene during Microbial Degradation by Pure Cultures and Mixed Culture Aquifer Slurries. *Applied and Environmental Microbiology*, 57(10):2981–2985, 1991.

[13] K. Anantharaman, C. T. Brown, L. A. Hug, I. Sharon, C. J. Castelle, A. J. Probst, B. C. Thomas, A. Singh, M. J. Wilkins, U. Karaoz, E. L. Brodie, K. H. Williams, S. S. Hubbard, and J. F. Banfield. Thousands of microbial genomes shed light on interconnected biogeochemical processes in an aquifer system. *Nature Communications*, 7(1):1–11, 10 2016.

[14] E. Annweiler, W. Michaelis, and R. U. Meckenstock. Identical ring cleavage products during anaerobic degradation of naphthalene, 2-methylnaphthalene, and tetralin indicate a new metabolic pathway. *Applied and Environmental Microbiology*, 68(2):852–858, 2002.

[15] P. K. Arora, A. Sharma, and H. Bae. Microbial Degradation of Indole and Its Derivatives. *Journal of Chemistry*, 2015:1–13, 2015.

[16] D. C. Aydin, J. Zamudio Pineres, F. Al-Manji, H. Rijnaarts, and T. Grotenhuis. Direct analysis of aromatic pollutants using a HPLC-FLD/DAD method for monitoring biodegradation processes. *Analytical Methods*, 13(13):1635–1642, 4 2021.

[17] M. J. Baedecker and W. Back. Modern marine sediments as a natural analog to the chemically stressed environment of a landfill. *Journal of Hydrology*, 43(1-4):393–414, 10 1979.

[18] S. Banerjee, A. Bedics, P. Harkai, B. Kriszt, N. Alpula, and A. Táncsics. Evaluating the aerobic xylene-degrading potential of the intrinsic microbial community of a legacy BTEX-contaminated aquifer by enrichment

culturing coupled with multi-omics analysis: uncovering the role of Hydrogenophaga strains in xylene degradation. *Environmental Science and Pollution Research*, 29:28431–28445, 2022.

[19] J. R. Barbaro, J. F. Barker, L. A. Lemon, and C. I. Mayfield. Biotransformation of BTEX under anaerobic, denitrifying conditions: Field and laboratory observations. *Journal of Contaminant Hydrology*, 11(3-4):245–272, 1992.

[20] J. P. Barker, G. C. Patrick, and D. Major. Natural Attenuation of aromatic hydrocarbons in a shallow sand aquifer. *Groundwater Monitoring & Remediation*, 7(1):64–71, 1987.

[21] F. T. Barranco and H. E. Dawson. Influence of aqueous pH on the interfacial properties of coal tar. *Environmental Science and Technology*, 33(10):1598–1603, 5 1999.

[22] D. Barry, H. Prommer, C. Miller, P. Engesgaard, A. Brun, and C. Zheng. Modelling the fate of oxidisable organic contaminants in groundwater. *Advances in Water Resources*, 25(8-12):945–983, 2002.

[23] M. E. Bedessem, N. G. Swoboda-Colberg, and P. J. Colberg. Naphthalene mineralization coupled to sulfate reduction in aquiferderived enrichments. *FEMS Microbiology Letters*, 152(2):213–218, 1997.

[24] H. R. Beller. Metabolic indicators for detecting in situ anaerobic alkylbenzene degradation. *Biodegradation*, 11:125–139, 2000.

[25] H. R. Beller, W.-h. Ding, and M. Reinhard. Byproducts of Anaerobic Alkyibenzene Metabolism Useful as Indicators of in Situ Bioremediation. *Environmental Science & Technology*, 29:2864–2870, 1995.

[26] H. R. Beller, D. Grbic-Galic, and M. Reinhard. Microbial degradation of toluene under sulfate-reducing conditions and the influence of iron on the process. *Applied and Environmental Microbiology*, 58(3):786–793, 1992.

[27] H. R. Beller, S. R. Kane, T. C. Legler, J. R. Mckelvie, B. S. Lollar, F. Pearson, L. Balser, and D. M. Mackay. Comparative assessments of benzene, toluene, and xylene natural attenuation by quantitative polymerase chain reaction analysis of a catabolic gene, signature metabolites, and compound-specific isotope analysis. *Environmental Science and Technology*, 42(16):6065–6072, 8 2008.

[28] C. Berdugo-Clavijo, X. Dong, J. Soh, C. W. Sensen, and L. M. Gieg. Methanogenic biodegradation of two-ringed polycyclic aromatic hydrocarbons. *FEMS Microbiology Ecology*, 81:124–133, 2012.

[29] M. Bhattacharya, S. Guchhait, D. Biswas, and R. Singh. Evaluation of a microbial consortium for crude oil spill bioremediation and its potential uses in enhanced oil recovery. *Biocatalysis and Agricultural Biotechnology*, 18:101034, 3 2019.

[30] X.-Y. Bian, S. M. Mbadinga, Y.-F. Liu, S.-Z. Yang, J.-F. Liu, R.-Q. Ye, J.-D. Gu, and B.-Z. Mu. Insights into the Anaerobic Biodegradation Pathway of n-Alkanes in Oil Reservoirs by Detection of Signature Metabolites. *Scientific Reports*, 5(1):9801, 2015.

[31] M. Bianchi, C. Zheng, C. Wilson, G. R. Tick, G. Liu, and S. M. Gorelick. Spatial connectivity in a highly heterogeneous aquifer: From cores to preferential flow paths. *Water Resources Research*, 47(5):1–18, 2011.

[32] M. F. P. Bierkens and H. J. T. Weerts. Application of indicator simulation to modelling the lithological properties of a complex confining layer. *Geoderma*, 62:265–284, 1994.

[33] P. S. Birak and C. T. Miller. Dense non-aqueous phase liquids at former manufactured gas plants : Challenges to modeling and remediation. *Journal of Contaminant Hydrology*, 105(3-4):81–98, 2009.

[34] P. L. Bjerg, K. Rugge, J. K. Pedersen, and T. H. Christensen. Distribution of Redox-Sensitive Groundwater Quality Parameters Downgradient of a Landfill (Grindsted, Denmark). *Environmental Science and Technology*, 29(5):1387–1394, 1995.

[35] F. Bode, T. Ferré, N. Zigelli, M. Emmert, and W. Nowak. Reconnecting Stochastic Methods With Hydrogeological Applications: A Utilitarian Uncertainty Analysis and Risk Assessment Approach for the Design of Optimal Monitoring Networks. *Water Resources Research*, 54(3):2270–2287, 3 2018.

[36] P. Bombach, H. H. Richnow, M. Kästner, and A. Fischer. Current approaches for the assessment of in situ biodegradation. *Applied Microbiology and Biotechnology*, 86(3):839–852, 2 2010.

[37] K. J. Brassington, R. L. Hough, G. I. Paton, K. T. Semple, G. C. Risdon, J. Crossley, I. Hay, K. Askari, and S. J. Pollard. Weathered hydrocarbon wastes: A risk management primer. *Critical Reviews in Environmental Science and Technology*, 37(3):199–232, 5 2007.

[38] V. Breij, R. Dijcker, N. Hoekstra, C. Jansonius, T. Praamstra, and P. Rood. Aanpak IBC-locaties herzien. Technical report, Bodembreed Forum, 2017.

[39] K. A. Brink. Resultaten van het grondonderzoek uitgevoerd in maart 1988. Technical report, Grondmechanica Delft, Provinciale Waterstaat Utrecht, 1988.

[40] D. G. Brown, L. Gupta, T. H. Kim, H. Keith Moo-Young, and A. J. Coleman. Comparative assessment of coal tars obtained from 10 former manufactured gas plant sites in the Eastern United States. *Chemosphere*, 65(9):1562–1569, 11 2006.

[41] A. Brun and P. Engesgaard. Modelling of transport and biogeochemical processes in pollution plumes: literature review and model development. *Journal of Hydrology*, 256:211–227, 2002.

[42] A. Brun, P. Engesgaard, T. H. Christensen, and D. Rosbjerg. Modelling of transport and biogeochemical processes in pollution plumes: Vejen landfill, Denmark. *Journal of Hydrology*, 256(3-4):228–247, 1 2002.

[43] M. L. Brusseau, E. L. DiFilippo, J. C. Marble, and M. Oostrom. Mass-removal and mass-flux-reduction behavior for idealized source zones with hydraulically poorly-accessible immiscible liquid. *Chemosphere*, 71:1511–1521, 4 2008.

[44] H. Buiter. *Alleen schoon is mooi - de geschiedenis van het Griftpark*. Stokerkade Cultuurhistorische Uitgeverij, 2009.

[45] J. Bumberger, D. Radny, A. Berndsen, T. Goblirsch, J. Flachowsky, and P. Dietrich. Carry-Over Effects of the Membrane Interface Probe. *Ground Water*, 50(4):578–584, 2012.

[46] A. V. Callaghan. Metabolomic investigations of anaerobic hydrocarbon-impacted environments. *Current Opinion in Biotechnology*, 24(3):506–515, 6 2013.

[47] A. V. Callaghan, I. A. Davidova, K. Savage-Ashlock, V. A. Parisi, L. M. Gieg, J. M. Suflita, J. J. Kukor, and B. Wawrik. Diversity of benzyl- and alkylsuccinate synthase genes in hydrocarbon-impacted environments and enrichment cultures. *Environmental Science and Technology*, 44(19):7287–7294, 10 2010.

[48] A. Carvajal, I. Akmirza, D. Navia, R. Pérez, R. Muñoz, and R. Lebrero. Anoxic denitrification of BTEX: Biodegradation kinetics and pollutant

interactions. *Journal of Environmental Management*, 214:125–136, 5 2018.

[49] M.-K. Chang, T. C. Voice, and C. S. Criddle. Kinetics of competitive inhibition and cometabolism in the biodegradation of benzene, toluene, and p-xylene by two Pseudomonas isolates. *Biotechnology and Bioengineering*, 41(11):1057–1065, 5 1993.

[50] W. Chang, Y. Um, and T. R. Pulliam Holoman. Polycyclic aromatic hydrocarbon (PAH) degradation coupled to methanogenesis. *Biotechnology Letters*, 28:425–430, 2006.

[51] F. Chapelle, J. Robertson, J. Landmeyer, and P. Bradley. *Methodology for applying monitored natural attenuation to petroleum hydrocarbon-contaminated ground-water systems with examples from South Carolina.* US Department of the Interior, US Geological Survey, 2001.

[52] I. Chatzis, M. Kuntamukkula, and N. R. Morrow. Effect of Capillary Number on the Microstructure of Residual Oil in Strongly Water-Wet Sandstones. *SPE Reservoir Engineering*, 3(3):902–912, 1988.

[53] J. C. Chee-Sanford, J. W. Frost, M. R. Fries, J. Zhou, and J. M. Tiedje. Evidence for acetyl coenzyme A and cinnamoyl coenzyme A in the anaerobic toluene mineralization pathway in Azoarcus tolulyticus Tol-4. *Applied and Environmental Microbiology*, 62(3):964–973, 1996.

[54] X. Chen, S. Zhang, L. Yi, Z. Liu, X. Ye, B. Yu, S. Shi, and X. Lu. Evaluation of Biodegradation of BTEX in the Subsurface of a Petrochemical Site near the Yangtze River, China. *International journal of environmental research and public health*, 19(24):16449, 12 2022.

[55] J. Cho, M. M. Zein, M. T. Suidan, and A. D. Venosa. Biodegradability of alkylates as a sole carbon source in the presence of ethanol or BTEX. *Chemosphere*, 68(2):266–273, 6 2007.

[56] N. Christensen, D. J. Batstone, Z. He, I. Angelidaki, and J. E. Schmidt. Removal of polycyclic aromatic hydrocarbons (PAHs) from sewage sludge by anaerobic degradation. *Water Science and Technology*, 50(9):237–244, 11 2004.

[57] T. H. Christensen, P. L. Bjerg, S. A. Banwart, R. Jakobsen, G. Heron, and H. J. Albrechtsen. Characterization of redox conditions in groundwater contaminant plumes. *Journal of Contaminant Hydrology*, 45(3-4):165–241, 2000.

[58] T. Christy. A permeable membrane sensor for the detection of volatile compounds in soil. In *11th EEGS Symposium on the Application of Geophysics to Engineering and Environmental Problems*, pages cp–203, LasVegas, Nevada, 1998.

[59] O. A. Cirpka and A. J. Valocchi. Debates—Stochastic subsurface hydrology from theory to practice: Does stochastic subsurface hydrology help solving practical problems of contaminant hydrogeology? *Water Resources Research*, 52(12):9218–9227, 12 2016.

[60] J. D. Coates, R. Chakraborty, and M. J. McInerney. Anaerobic benzene biodegradation—a new era. *Research in Microbiology*, 153(10):621–628, 12 2002.

[61] R. M. Cohen and J. W. Mercer. DNAPL site evaluation. Technical report, GeoTrans, Inc., Sterling, VA (United States)., 1993.

[62] I. M. Cozzarelli, M. J. Baedecker, R. P. Eganhouse, and D. F. Goerlitz. The geochemicai evolution of low-molecular-weight organic acids derived from the degradation of petroleum contaminants in groundwater. *Geochimica et Cosmochimica Acta*, 58(2):863–877, 1994.

[63] I. M. Cozzarelli, R. P. Eganhouse, and M. J. Baedecker. Transformation of Monoaromatic hydrocarbons to organic acids in anoxic groundwater environment. *Environmental Geology and Water Sciences*, 16(2):135–141, 9 1990.

[64] M. L. B. Da Silva, G. M. L. Ruiz-Aguilar, and P. J. J. Alvarez. Enhanced anaerobic biodegradation of BTEX-ethanol mixtures in aquifer columns amended with sulfate, chelated ferric iron or nitrate. *Biodegradation*, 16:105–114, 2005.

[65] F. M. D'Affonseca, P. Blum, M. Finkel, R. Melzer, and P. Grathwohl. Field scale characterization and modeling of contaminant release from a coal tar source zone. *Journal of Contaminant Hydrology*, 102(1-2):120–139, 2008.

[66] F. M. D'Affonseca, H. Prommer, M. Finkel, P. Blum, and P. Grathwohl. Modeling the long-term and transient evolution of biogeochemical and isotopic signatures in coal tar – contaminated aquifers. *Water Resources Research*, 47:1–22, 2011.

[67] H. Darcy. *Les fontaines publiques de la ville de Dijon: exposition et application des principes à suivre et des formules à employer dans les questions de distribution d'eau (Vol. 1).* Victor Dalmont, 1856.

[68] N. Das and P. Chandran. Microbial degradation of petroleum hydrocarbon contaminants: an overview. *Biotechnology Research International*, 2011:13, 2011.

[69] C. Davis, T. Cort, D. Dai, T. Illangasekare, and J. Munakata-Marr. Effects of heterogeneity and experimental scale on the biodegradation of diesel. *Biodegradation*, 14:373–384, 2003.

[70] G. B. Davis, C. Barber, T. R. Power, J. Thierrin, B. M. Patterson, J. L. Rayner, and Q. Wu. The variability and intrinsic remediation of a BTEX plume in anaerobic sulphate-rich groundwater. *Journal of Contaminant Hydrology*, 36(3-4):265–290, 3 1999.

[71] P. O. De Vries, R. N. Comans, K. R. Weytingh, and A. P. Alphenaar. *Handboek gasfabrieken voor bodemingenieurs.* The Three Engineers, 2003.

[72] A. de Wilt, Y. He, N. Sutton, A. Langenhoff, and H. Rijnaarts. Sorption and biodegradation of six pharmaceutically active compounds under four different redox conditions. *Chemosphere*, 193:811–819, 2 2018.

[73] R. A. Deeb and L. Alvarez-Cohen. Temperature Effects and Substrate Interactions During the Aerobic Biotransformation of BTEX Mixtures by Toluene-Enriched Consortia and Rhodococcus rhodochrous. *Biotechnology and Bioengineering*, 62(5), 1999.

[74] R. A. Deeb, H. Y. Hu, J. R. Hanson, K. M. Scow, and L. Alvarez-Cohen. Substrate Interactions in BTEX and MTBE Mixtures by an MTBE-Degrading Isolate. *Environmental Science & Technology*, 35(2):312, 2001.

[75] T. J. Dekker and L. M. Abriola. The influence of field-scale heterogeneity on the infiltration and entrapment of dense nonaqueous phase liquids in saturated formations. *Journal of Contaminant Hydrology*, 42:187–218, 2000.

[76] H. Delottier, A. Pryet, and A. Dupuy. Why Should Practitioners be Concerned about Predictive Uncertainty of Groundwater Management Models? *Water Resources Management*, 31(1):61–73, 1 2017.

[77] P. C. Dennis, B. E. Sleep, R. R. Fulthorpe, and S. N. Liss. Phylogenetic analysis of bacterial populations in an anaerobic microbial consortium capable of degrading saturation concentrations of tetrachloroethylene. *Canadian Journal of Microbiology*, 49(1):15–27, 1 2003.

[78] D. Ding, D. A. Benson, D. Fernàndez-Garcia, C. V. Henri, D. W. Hyndman, M. S. Phanikumar, and D. Bolster. Elimination of the Reaction Rate "Scale Effect": Application of the Lagrangian Reactive Particle-Tracking Method to Simulate Mixing-Limited, Field-Scale Biodegradation at the Schoolcraft (MI, USA) Site. *Water Resources Research*, 53(12):10411–10432, 12 2017.

[79] DINOloket Data en Informatie van de Nedelandse Ondergrond. http://www.dinoloket.nl/, 2019.

[80] B. E. O. Dochartaigh, D. F. Ball, A. M. Macdonald, A. Lilly, V. Fitzsimons, D. Rio, and C. A. Auton. Mapping groundwater vulnerability in Scotland: a new approach for the Water Framework Directive. *Scottish Journal of Geology*, 41(1):21–30, 2005.

[81] S. S. Dyreborg, E. Arvin, and K. Broholm. Effects of creosote compounds on the aerobic bio-degradation of benzene. *Biodegradation*, 7(3):191–201, 1996.

[82] C. Eberhardt and P. Grathwohl. Time scales of organic contaminant dissolution from complex source zones: coal tar pools vs. blobs. *Journal of Contaminant Hydrology*, 59(1-2):45–66, 11 2002.

[83] P. Eckert and C. A. J. Appelo. Hydrogeochemical modeling of enhanced benzene, toluene, ethylbenzene, xylene (BTEX) remediation with nitrate. *Water Resources Research*, 38(9):1130, 8 2002.

[84] A. Edelenbosch. Advies Eindig beheer grote voormalige bodemsanerings-locaties met IBC regime TCB A108. Technical report, Technische Comissie Bodem, 2015.

[85] E. A. Edwards and D. Grbic-Galic. Complete mineralization of benzene by aquifer microorganisms under strictly anaerobic conditions. *Applied and Environmental Microbiology*, 58(8):2663–2666, 1992.

[86] T. Egli, U. Lendenmann, and M. Snozzi. Kinetics of microbial growth with mixtures of carbon sources. *Antonie van Leeuwenhoek*, 63(3-4):289–298, 9 1993.

[87] M. S. Elshahed, L. M. Gieg, M. J. McInerney, and J. M. Suflita. Signature metabolites attesting to the in situ attenuation of alkylbenzenes in anaerobic environments. *Environmental Science and Technology*, 35(4):682–689, 2 2001.

[88] T. Enemark, L. J. Peeters, D. Mallants, and O. Batelaan. Hydrogeological conceptual model building and testing: A review. *Journal of Hydrology*, 569:310–329, 2 2019.

[89] R. Eng. Survey of town gas and by-product production and locations in the US (1880-1950). Technical report, Radian Corp., McLean, VA (USA), 1985.

[90] H. I. Essaid, B. A. Bekins, E. M. Godsy, E. Warren, M. J. Baedecker, and I. M. Cozzarelli. Simulation of aerobic and anaerobic biodegradation processes at a crude oil spill site. *Water Resources Research*, 31(12):3309–3327, 12 1995.

[91] H. I. Essaid, W. N. Herkelrath, and K. M. Hess. Simulation of fluid distributions observed at a crude oil spill site incorporating hysteresis, oil entrapment, and spatial variability of hydraulic properties. *Water Resources Research*, 29(6):1753–1770, 1993.

[92] E. Estévez, M. C. Veiga, and C. Kennes. Biodegradation of toluene by the new fungal isolates Paecilomyces variotii and Exophiala oligosperma. *Journal of Industrial Microbiology and Biotechnology*, 33(1):33–37, 2005.

[93] European Communities. Common implementation strategy for the water framework directive (2000/60/EC). Guidance document no. 26. Guidance on risk assessment and the use of conceptual models for groundwater. Technical report, European Commission, 2000.

[94] A. Fahy, T. J. Mcgenity, K. N. Timmis, and A. S. Ball. Heterogeneous aerobic benzene-degrading communities in oxygen-depleted groundwaters. *FEMS Microbiology Ecology*, 58:260–270, 2006.

[95] M. Farhadian, C. Vachelard, D. Duchez, and C. Larroche. In situ bioremediation of monoaromatic pollutants in groundwater: A review. *Bioresource Technology*, 99(13):5296–5308, 9 2008.

[96] V. A. Feisther, A. A. Ulson De Souza, D. E. G. Trigueros, J. M. M. De Mello, D. De Oliveira, and S. M. A. Guelli Ulson De Souza. Biodegradation kinetics of benzene, toluene and xylene compounds: microbial growth and evaluation of models. *Bioprocess and Biosystems Engineering*, 38, 2015.

[97] C. W. Fetter. *Contaminant Hydrogeology 2.* Waveland Press, Inc., second edi edition, 1999.

[98] A. Fiori, V. Cvetkovic, G. Dagan, S. Attinger, A. Bellin, P. Dietrich, A. Zech, and G. Teutsch. Debates-Stochastic subsurface hydrology from theory to practice: The relevance of stochastic subsurface hydrology to practical problems of contaminant transport and remediation. What is characterization and stochastic theory good for? *Water Resources Research*, 52(12):9228–9234, 12 2016.

[99] A. Fischer, I. Herklotz, S. Herrmann, M. Thullner, S. A. Weelink, A. J. Stams, M. Schlömann, H.-H. Richnow, and C. Vogt. Combined Carbon and Hydrogen Isotope Fractionation Investigations for Elucidating Benzene Biodegradation Pathways. *Environmental Science and Technology*, 42:4356–4363, 2008.

[100] J. Foght. Anaerobic Biodegradation of Aromatic Hydrocarbons: Pathways and Prospects. *Microbial Physiology*, 15(2-3):93–120, 2008.

[101] J. Frank R. Groves. Effect of Cosolvents on the Solubility of Hydrocarbons in Water. *Environmental Science and Technology*, 22(3):282–286, 1988.

[102] M. Fraser, J. F. Barker, B. Butler, F. Blaine, S. Joseph, and C. Cooke. Natural attenuation of a plume from an emplaced coal tar creosote source over 14 years. *Journal of Contaminant Hydrology*, 100(3-4):101–115, 9 2008.

[103] R. A. Freeze. A stochastic-conceptual analysis of one-dimensional groundwater flow in nonuniform homogeneous media. *Water Resources Research*, 11(5):725–741, 10 1975.

[104] R. A. Freeze. The role of stochastic hydrogeological modeling in real-world engineering applications A personal historical perspective. *Stochastic Environmental Research and Risk Assessment*, 18:286–289, 2004.

[105] R. A. Freeze and J. A. Cherry. *Groundwater*. Englewood Cliffs, N.J: Prentice-Hall, 1979.

[106] E. O. Frind and G. E. Hokkanen. Simulation of the Borden Plume Using the Alternating Direction Galerkin Technique. *Water Resources Research*, 23(5):918–930, 1987.

[107] E. O. Frind, J. W. Molson, and D. L. Rudolph. Well Vulnerability: A Quantitative Approach for Source Water Protection. *Groundwater*, 44(5):732–742, 9 2006.

[108] A. D. Fure, J. W. Jawitz, and M. D. Annable. DNAPL source depletion: Linking architecture and flux response. *Journal of Contaminant Hydrology*, 85(3-4):118–140, 5 2006.

[109] C. Gallacher, R. Thomas, R. Lord, R. M. Kalin, and C. Taylor. Comprehensive database of Manufactured Gas Plant tars. Part A. Database. *Rapid Communications in Mass Spectrometry*, 31(15):1231–1238, 8 2017.

[110] C. Gallacher, R. Thomas, R. Lord, R. M. Kalin, and C. Taylor. Comprehensive database of Manufactured Gas Plant tars. Part B. Aliphatic and aromatic compounds. *Rapid Communications in Mass Spectrometry*, 31(15):1239–1249, 8 2017.

[111] S. Gan, E. V. Lau, and H. K. Ng. Remediation of soils contaminated with polycyclic aromatic hydrocarbons (PAHs). *Journal of Hazardous Materials*, 172:532–549, 12 2009.

[112] L. W. Gelhar, C. Welty, and K. R. Rehfeldt. A critical review of data on field-scale dispersion in aquifers. *Water Resources Research*, 28(7):1955–1974, 7 1992.

[113] J. Gerritse and J. C. Gottschal. Two-membered mixed cultures of methanogenic and aerobic bacteria in 02-limited chemost ats. *Journal of General Microbiology*, 139:1853–1860, 1993.

[114] D. Gerstner, T. Scheytt, and C. Faelker. Investigation of subsurface contamination—Chances and limitations of direct push technologies. *Altlasten Spektrum*, 6:316–330, 2006.

[115] D. T. Gibson. *Microbial degradation of organic compounds.* Marcel Dekker Inc., 1984.

[116] D. T. Gibson, J. R. Koch, and R. E. Kallioj. Oxidative Degradation of Aromatic Hydrocarbons by Microorganisms. I. Enzymatic Formation of Catechol from Benzene. *Biochemistry*, 7(7):2653–2662, 1968.

[117] D. T. Gibson, S. M. Resnick, K. Lee, J. M. Brand, D. S. Torok, L. P. Wackett, B. E. Haigler, M. J. Schocken, and B. E. Haigler#. Desaturation, dioxygenation, and monooxygenation reactions catalyzed by naphthalene dioxygenase from Pseudomonas sp. strain. *Journal of Bacteriology*, 177(10):2615–2621, 1995.

[118] L. M. Gieg and J. M. Suflita. Detection of Anaerobic Metabolites of Saturated and Aromatic Hydrocarbons in Petroleum-Contaminated Aquifers. *Environ. Sci. Technol*, (36):3755–3762, 2002.

[119] R. F. Gierczak, J. F. Devlin, and D. L. Rudolph. Combined use of field and laboratory testing to predict preferred flow paths in an heterogeneous aquifer. *Journal of Contaminant Hydrology*, 82(1-2):75–98, 1 2006.

[120] D. Grbic-Galic and T. M. Vogel. Transformation of toluene and benzene by mixed methanogenic cultures. *Applied and Environmental Microbiology*, 53(2):254–260, 1987.

[121] C. Griebler, M. Safinowski, A. Vieth, H. H. Richnow, and R. U. Meckenstock. Combined Application of Stable Carbon Isotope Analysis and Specific Metabolites Determination for Assessing In Situ Degradation of Aromatic Hydrocarbons in a Tar Oil-Contaminated Aquifer. *Environmental Science and Technology*, 38(2):617–631, 2004.

[122] Grondmechanica Delft. Haalbaarheidsstudie diepe schermwanden Eindrapportage geotechnische en geohydrologische aspecten. Technical report, Grondmechanica Delft, Utrecht, 1985.

[123] Grondmechanica Delft. Kwaliteitsbewaking schermwand sanering Griftpark Utrecht Evaluatie monitoring Schermwand. Technical report, Grondmechanica Delft, Provincie Utrecht, 1995.

[124] J. D. Gu and D. F. Berry. Degradation of substituted indoles by an indole-degrading methanogenic consortium. *Applied and Environmental Microbiology*, 57(9):2622–2627, 1991.

[125] W. Guang-lin. The development of sonic drilling technology and its applications. *Exploration Engineering (Drilling and Tunneling)*, 31(3):39–41, 2004.

[126] N. Gülensoy and P. J. J. Alvarez. Diversity and correlation of specific aromatic hydrocarbon biodegradation capabilities. *Biodegradation*, 10:331–340, 1999.

[127] J. D. Haddock. Aerobic degradation of aromatic hydrocarbons: enzyme structures and catalytic mechanisms. In *Handbook of Hydrocarbon and Lipid Microbiology*. Springer-Verlag Berlin Heidelberg, 2010.

[128] F. P. Haeni. *Application of Seismic-refraction Techniques to Hydrologic Studies*. Department of the Interior, US Geological Survey, 1988.

[129] M. J. Hamper. Manufactured gas history and processes. *Environmental Forensics*, 7(1):55–64, 3 2006.

[130] S. M. Harkins, R. S. Truesdale, R. Hill, P. Hoffman, and S. Winters. US production of manufactured gases: assessment of past disposal practices. No. PB-88-165790/XAB. Technical report, Research Triangle Inst., Research Triangle Park, NC (USA), 1988.

[131] A. W. Hatheway. Estimated Number of Manufactured Gas and Other Coal-Tar Sites in the United States. *Environmental and Engineering Geoscience*, 3(1):141–142, 3 1997.

[132] A. W. Hatheway. Manufactured gas plants: Yesterday's pride, today's liability. *Civil Engineering*, 67(11), 1997.

[133] A. W. Hatheway. World history of manufactured gas: A 'world' of land redevelopment possibilities. In *Proceedings of the international symposium and exhibition on the redevelopment of manfactured gas plant sites*, volume 14, pages 171–181, 2006.

[134] E. Hauptfeld, J. Pelkmans, T. T. Huisman, A. Anocic, B. L. Snoek, F. A. von Meijenfeldt, J. Gerritse, J. van Leeuwen, G. Leurink, A. van Lit, R. van Uffelen, M. C. Koster, and B. E. Dutilh. A metagenomic portrait of the microbial community responsible for two decades of bioremediation of poly-contaminated groundwater. *Water Research*, 221, 8 2022.

[135] A. Hazen. Discussion of dams on sand foundations. *A. C. Koenig ed., Transactions of the American Society of Civil Engineers*, 73(3):199–203, 1911.

[136] J. Heider, A. M. Spormann, H. R. Beller, and F. Widdel. Anaerobic bacterial metabolism of hydrocarbons. *FEMS Microbiology Reviews*, 22:459–473, 12 1998.

[137] P. Henner, M. Schiavon, J.-L. Morel, E. Lichtfouse, and E. Lichtfouse Polycyclic. Polycyclic aromatic hydrocarbon (PAH) occurrence and remediation methods. *Analusis Magazine*, 25:M56–M59, 1997.

[138] H. Huang, Y. Jiang, J. Zhao, S. Li, S. Schulz, and L. Deng. BTEX biodegradation is linked to bacterial community assembly patterns in contaminated groundwater ecosystem. *Journal of Hazardous Materials*, 419, 10 2021.

[139] L. Huang, T. Zhao, Y. He, Y. Liu, C. Liu, D. Jin, and X. Jia. Bioremediation of oil-contaminated field by two Pseudomonas aeruginosa strains. *Shengwu Gongcheng Xuebao - Chinese Journal of Biotechnology*, 33(6):957–967, 6 2017.

[140] Y. Huang and L. Li. Biodegradation Characteristics of Naphthalene and Benzene, Toluene, Ethyl Benzene, and Xylene (BTEX) by Bacteria Enriched from Activated Sludge; Biodegradation Characteristics of Naphthalene and Benzene, Toluene, Ethyl Benzene, and Xylene (BTEX) by Bacter. *Water Environment Research*, 86:277, 2014.

[141] H. Huismans, M. v. Vliet, T. Goldberg, and J. Griffioen. Statistische karakterisering van de reactiecapaciteit van de Nederlandse ondergrond ten behoeve van de parametrisering van het modelinstrument NHI-Kwaliteit. Technical report, TNO, 2016.

[142] D. Hunkeler, R. Aravena, and B. J. Butler. Monitoring Microbial Dechlorination of Tetrachloroethene (PCE) in Groundwater Using Compound-Specific Stable Carbon Isotope Ratios: Microcosm and Field Studies. *Environmental Science and Technology*, 33:2733–2738, 1999.

[143] S. R. Hutchins, W. C. Downs, J. T. Wilson, G. B. Smith, D. A. Kovacs, D. D. Fine, R. H. Douglass, and D. J. Hendrix. Effect of Nitrate Addition on Biorestoration of Fuel-Contaminated Aquifer: Field Demonstration. *Groundwater*, 29(4):571–581, 1991.

[144] T. H. Illangasekare, J. L. Ramsey, K. H. Jensen, and M. B. Butts. Contaminant Hydrology Experimental study of movement and distribution of dense organic contaminants in heterogeneous aquifers. *Journal of Contaminant Hydrology*, 20:1–25, 1995.

[145] P. T. Imhoff and C. T. Miller. Dissolution Fingering During the Solubilization of Nonaqueous Phase Liquids in Saturated Porous Media: 1. Model Predictions. *Water Resources Research*, 32(7):1919–1928, 1996.

[146] J. Islam, N. Singhal, and M. O'Sullivan. Modeling biogeochemical processes in leachate-contaminated soils: A review. *Transport in Porous Media*, 43:407–440, 2001.

[147] ITRC. Strategies for Monitoring the Performance of DNAPL Source Zone Remedies. Technical report, ITRC, 2004.

[148] R. Jakobsen and D. Postma. Redox zoning, rates of sulfate reduction and interactions with Fe-reduction and methanogenesis in a shallow sandy aquifer, Rømø, Denmark. *Geochimica et Cosmochimica Acta*, 63(1):137–151, 1 1999.

[149] S. Jiao, W. Chen, E. Wang, J. Wang, Z. Liu, Y. Li, and G. Wei. Microbial succession in response to pollutants in batch-enrichment culture. *Scientific Reports*, 6(1):21791, 2016.

[150] E. Jindrov, M. Citocova, K. Demnerov, and V. Brenner. Bacterial Aerobic Ethylbenzene and Xylene. *Folia Microbiolia*, 47(2):83–93, 2002.

[151] M. T. Jonker, J. M. Brils, A. J. Sinke, A. J. Murk, and A. A. Koelmans. Weathering and toxicity of marine sediments contaminated with oils and polycyclic aromatic hydrocarbons. *Environmental Toxicology and Chemistry*, 25(5):1345–1353, 2006.

[152] J. P. Kaiser, Y. Feng, and J. M. Bollag. Microbial metabolism of pyridine, quinoline, acridine, and their derivatives under aerobic and anaerobic conditions. *Microbiological reviews,*, 60(3):483–498, 1996.

[153] C. M. Kao and C. C. Wang. Control of BTEX migration by intrinsic bioremediation at a gasoline spill site. *Water Research*, 34(13):3413–3423, 2000.

[154] S. W. Karickhoff, D. S. Brown, and S. T. A. Sorption of hydrophobic pollutants on natural sediments. *Water Res.*, 13:241–248, 1979.

[155] G. Kharey, G. Scheffer, and L. M. Gieg. Microorganisms Combined Use of Diagnostic Fumarate Addition Metabolites and Genes Provides Evidence for Anaerobic Hydrocarbon Biodegradation in Contaminated Groundwater. *Microorganisms*, 8(1532), 2020.

[156] S. Killops and V. Killops. *Introduction to Organic Geochemistry*. John Wiley and Sons, Inc., New York, 1993.

[157] M. W. King and J. F. Barker. Migration and natural fate of a coal tar creosote plume. 1. Overview and plume development. *Journal of Contaminant Hydrology*, 39(3-4):249–279, 10 1999.

[158] M. W. King, J. F. Barker, J. F. Devlin, and B. J. Butler. Migration and natural fate of a coal tar creosote plume. 2. Mass balance and biodegradation indicators. *Journal of Contaminant Hydrology*, 39(3-4):281–307, 10 1999.

[159] G. M. Klecka and W. J. Maier. Kinetics of microbial growth on mixtures of pentachlorophenol and chlorinated aromatic compounds. *Biotechnology and Bioengineering*, 31(4):328–335, 1988.

[160] R. Kleemann and R. U. Meckenstock. Anaerobic naphthalene degradation by Gram-positive, iron-reducing bacteria. *FEMS Microbiology Ecology*, 78(3):488–496, 12 2011.

[161] S. Kleinsteuber, K. M. Schleinitz, and C. Vogt. Key players and team play: Anaerobic microbial communities in hydrocarbon-contaminated aquifers. *Applied Microbiology and Biotechnology*, 94(4):851–873, 5 2012.

[162] S. Komukai-nakamura, K. Sugiura, Y. Yamauchi-inomata, H. Toki, K. Venkateswaran, S. Yamamoto, H. Tanaka, and S. Harayama. Construction of Bacterial Consortia That Degrade Arabian Light Crude Oil. *Journal of fermentation and Bioengineering*, 82(6):570–574, 1996.

[163] Koninklijk Nederlands Metereologisch Instituut. https://www.knmi.nl/nederland-nu/klimatologie/uurgegevens, 2022.

[164] J. Kozeny. Über kapillare leitung der wasser in boden. *Royal Academy of Science, Vienna, Proc. Class I*, 136:271–306, 1927.

[165] I. Kraiselburd, T. Bruels, G. Heilmann, F. Kaschani, M. Kaiser, and R. U. Meckenstock. Metabolic reconstruction of the genome of candidate Desulfatiglans TRIP_1 and identification of key candidate enzymes for anaerobic phenanthrene degradation. *Environmental Microbiology*, 21(4):1267–1286, 4 2019.

[166] K. Krivoruchko. Empirical Bayesian Kriging Implemented in ArcGIS Geostatistical Analyst. *ArcUser Fall*, 6(10):1145, 2012.

[167] S. Kuemmel, F.-A. Herbst, A. Bahr, M. Arcia Duarte, D. H. Pieper, N. Jehmlich, J. Seifert, M. Von Bergen, P. Bombach, H. H. Richnow, and C. Vogt. Anaerobic naphthalene degradation by sulfate-reducing Desulfobacteraceae from various anoxic aquifers. *FEMS Microbiology Ecology*, 91(3), 2015.

[168] S. Kuemmel, R. Starke, G. Chen, F. Musat, H. H. Richnow, and C. Vogt. Hydrogen Isotope Fractionation As a Tool to Identify Aerobic and Anaerobic PAH Biodegradation. *Environmental Science & Technology*, 50:3091–3100, 2016.

[169] B. H. Kueper, D. Redman, R. C. Starr, S. Reitsma, and M. Mah. A Field Experiment to Study the Behavior of Tetrachloroethylene Below the Water Table: Spatial Distribution of Residual and Pooled DNAPL. *Groundwater*, 31(5):756–766, 9 1993.

[170] B. H. Kueper, G. P. Wealthall, J. W. N. Smith, S. a. Leharne, and D. N. Lerner. *An illustrated handbook of DNAPL transport and fate in the subsurface*, volume 133. Environment Agency, 2003.

[171] E. P. Kuhn, J. Zeyer, P. Eicher, and R. P. Schwarzenbach. Anaerobic degradation of alkylated benzenes in denitrifying laboratory aquifer columns. *Applied and environmental microbiology*, 54(2):490–496, 1988.

[172] J. E. Landmeyer, F. H. Chapelle, M. Petkewich, and P. M. Bradley. Assessment of natural attenuation of aromatic hydrocarbons in groundwater near a former manufactured-gas plant, South Carolina, USA. *Environmental Geology*, 4:279–292, 1998.

[173] L. S. Lee, P. C. Suresh Rao, I. Okuda, P. Suresh, C. Rao, I. Okuda, and O. Itaru. Equilibrium Partitioning of Polycyclic Aromatic Hydrocarbons from Coal Tar into Water. *Environmental Science and Technology*, 26(11):1111, 1992.

[174] S. H. Lee, H. M. Jin, H. J. Lee, J. M. Kim, and C. O. Jeon. Complete Genome Sequence of the BTEX-Degrading Bacterium Pseudoxanthomonas spadix BD-a59. *Journal of Bacteriology*, 194(2):544–544, 1 2012.

[175] S. K. B. K. B. Lee and S. K. B. K. B. Lee. Substrate utilization patterns during BTEX biodegradation by an o-xylene-degrading bacterium Ralstonia sp. PHS1. *Journal of microbiology and biotechnology*, 12(6):909–915, 2002.

[176] A. Leeson, H. F. Stroo, and P. C. Johnson. Groundwater remediation today and challenges and opportunities for the future. *GroundWater*, 51(2):175–179, 3 2013.

[177] C. Leutwein and J. Heider. Succinyl-CoA:(R)-benzylsuccinate CoA-transferase: An enzyme of the anaerobic toluene catabolic pathway in denitrifying bacteria. *Journal of Bacteriology*, 183(14):4288–4295, 2001.

[178] P. C. Lichtner. Continuum model for simultaneous chemical reactions and mass transport in hydrothermal systems. *Geochimica et Cosmochimica Acta*, 49(3):779–800, 1985.

[179] R. Liedl, A. J. Valocchi, P. Dietrich, and P. Grathwohl. Finiteness of steady state plumes. *Water Resources Research*, 41(12):1–8, 12 2005.

[180] J. W. Lingle and K. L. Brehm. Application of source removal and natural attenuation remediation strategies at MGP sites in Wisconsin. *Remediation Journal: The Journal of Environmental Cleanup Costs, Technologies & Techniques*, 13(4):29–39, 2003.

[181] J. V. Littlejohns and A. J. Daugulis. Kinetics and interactions of BTEX compounds during degradation by a bacterial consortium. *Process Biochemistry*, 43(10):1068–1076, 10 2008.

[182] D. R. Lovley, M. J. Baedecker, D. J. Lonergan, I. M. Cozzarelli, E. J. Phillips, and D. I. Siegel. Oxidation of aromatic contaminants coupled to microbial iron reduction. *Nature*, 339(6222):297–300, 1989.

[183] D. R. Lovley and D. J. Lonergan. Anaerobic Oxidation of Toluene, Phenol, and p-Cresol by the Dissimilatory Iron-Reducing Organism, GS-15. *Applied and environmental microbiology*, 56(6):1858–64, 6 1990.

[184] G. Lu, T. P. Clement, C. Zheng, and T. H. Wiedemeier. Natural attenuation of BTEX compounds: Model development and field-scale application. *Ground Water*, 37(5):707–717, 1999.

[185] A. Luciano, P. Viotti, and M. P. Papini. Laboratory investigation of DNAPL migration in porous media. *Journal of Hazardous Materials*, 176(1-3):1006–1017, 4 2010.

[186] L. Ludvigsen, H. J. Albrechtsen, G. Heron, P. L. Bjerg, and T. H. Christensen. Anaerobic microbial redox processes in a landfill leachate contaminated aquifer (Grindsted, Denmark). *Journal of Contaminant Hydrology*, 33(3-4):273–291, 10 1998.

[187] T. Lueders. The ecology of anaerobic degraders of BTEX hydrocarbons in aquifers. *FEMS Microbiology Ecology*, 93(1), 1 2017.

[188] J. Lyngkilde and T. H. Christensen. Redox zones of a landfill leachate pollution plume (Vejen, Denmark). *Journal of Contaminant Hydrology*, 10(4):273–289, 9 1992.

[189] D. Mackay, W. Y. Shiu, A. Maijanen, and S. Feenstra. Dissolution of non-aqueous phase liquids in groundwater. *Journal of Contaminant Hydrology*, 8(1):23–42, 9 1991.

[190] D. M. Mackay, D. L. Freyberg, P. V. Roberts, and J. A. Cherry. A natural gradient experiment on solute transport in a sand aquifer: 1. Approach and overview of plume movement. *Water Resources Research*, 22(13):2017–2029, 12 1986.

[191] B. Mahjoub, E. Jayr, M. Y. Gourdon, R. Bayard, and R. Gourdon. Phase partition of organic pollutants between coal tar and water under variable experimental conditions. *Water Research*, 34(14):3551–3560, 2000.

[192] S. P. Maletić, J. M. Beljin, S. D. Rončević, M. G. Grgić, and B. D. Dalmacija. State of the art and future challenges for polycyclic aromatic hydrocarbons is sediments: sources, fate, bioavailability and remediation techniques. *Journal of Hazardous Materials*, 365:467–482, 3 2019.

[193] R. Margesin and F. Schinner. Bioremediation (Natural Attenuation and Biostimulation) of Diesel-Oil-Contaminated Soil in an Alpine Glacier Skiing Area. *Applied and Environmental Microbiology*, 67(7):3127–3133, 7 2001.

[194] A. Mariotti, J. C. Germon, P. Hubert, P. Kaiser, R. Letolle, A. Tardieux, and P. Tardieux. Experimental determination of nitrogen kinetic isotope fractionation: Some principles; illustration for the denitrification and nitrification processes. *Plant and Soil*, 62(3):413–430, 10 1981.

[195] P. Martus and W. Püttmann. Formation of alkylated aromatic acids in groundwater by anaerobic degradation of alkylbenzenes. *Science of The Total Environment*, 307(1-3):19–33, 5 2003.

[196] S. M. Mbadinga, L. Y. Wang, L. Zhou, J. F. Liu, J. D. Gu, and B. Z. Mu. Microbial communities involved in anaerobic degradation of alkanes. *International Biodeterioration & Biodegradation*, 65(1):1–13, 1 2011.

[197] M. G. McDonald and A. W. Harbaugh. *A Modular Three-dimensional Finite-difference Ground-water Flow Model.* U.S Geological Survey, 1988.

[198] T. F. McGowan, B. A. Greer, and M. Lawless. Thermal treatment and non-thermal technologies for remediation of manufactured gas plant sites. *Waste Management*, 16(8):691–698, 1996.

[199] W. W. McNab and T. N. Narasimhan. Modeling reactive transport of organic compounds in groundwater using a partial redox disequilibrium approach. *Water Resources Research*, 30(9):2619–2635, 9 1994.

[200] C. Mcrae, C. E. Snape, and A. E. Fallick. Variations in the stable isotope ratios of specific aromatic and aliphatic hydrocarbons from coal conversion processes. *Anaerobic Utilization of Hydrocarbons, Oils, and Lipids*, 123:1519–1523, 1998.

[201] C. McRae, C. G. Sun, C. E. Snape, A. E. Fallick, and D. Taylor. δ13C values of coal-derived PAHs from different processes and their application to source apportionment. *Organic Geochemistry*, 30(8):881–889, 8 1999.

[202] R. U. Meckenstock, M. Elsner, C. Griebler, T. Lueders, C. Stumpp, J. Aamand, S. N. Agathos, H.-J. J. Albrechtsen, L. Bastiaens, P. L. Bjerg, N. Boon, W. Dejonghe, W. E. Huang, S. I. Schmidt, E. Smolders, S. R. Sørensen, D. Springael, and B. M. Van Breukelen. Biodegradation: Updating the Concepts of Control for Microbial Cleanup in Contaminated Aquifers. *Environmental Science and Technology*, 49(12):7073–7081, 2015.

[203] R. U. Meckenstock, B. Morasch, C. Griebler, and H. H. Richnow. Stable isotope fractionation analysis as a tool to monitor biodegradation in contaminated acquifers. *Journal of Contaminant Hydrology*, 75(3-4):215–255, 12 2004.

[204] R. U. Meckenstock, F. Von Netzer, C. Stumpp, T. Lueders, A. M. Himmelberg, N. Hertkorn, P. Schmitt-Kopplin, M. Harir, R. Hosein, S. Haque, and D. Schulze-Makuch. Water droplets in oil are microhabitats for microbial life. *Science*, 345(6197):673–676, 2014.

[205] J. W. Mercer and R. M. Cohen. A review of immiscible fluids in the subsurface: Properties, models, characterization and remediation. *Journal of Contaminant Hydrology*, 6(2):107–163, 9 1990.

[206] B. Morasch, D. Hunkeler, J. Zopfi, B. Temime, and P. Höhener. Intrinsic biodegradation potential of aromatic hydrocarbons in an alluvial aquifer – Potentials and limits of signature metabolite analysis and two stable isotope-based techniques. *Water Research*, 45(15):4459–4469, 10 2011.

[207] D. A. Morris and A. Johnson. Summary of hydrologic and physical properties of rock and soil materials, as analyzed by the hydrologic laboratory of the U.S. Geological Survey. Technical report, US Government Printing Office, 1967.

[208] H. Mouttaki, J. Johannes, and R. U. Meckenstock. Identification of naphthalene carboxylase as a prototype for the anaerobic activation of non-substituted aromatic hydrocarbons. *Environmental Microbiology*, 14(10):2770–2774, 2012.

[209] J. A. Mueller, A. S. Galushko, A. Kappler, and B. Schink. Initiation of anaerobic degradation of p-cresol by formation of 4-hydroxybenzylsuccinate in Desulfobacterium cetonicum. *Journal of Bacteriology*, 183(2):752–757, 2001.

[210] J. G. Mueller, P. J. Chapman, and P. H. Pritchard. Creosote-contaminated sites Their potential for bioremediation. *Environmental Science & Technology*, 23(10), 1989.

[211] A. K. Mukherjee and N. K. Bordoloi. Biodegradation of benzene, toluene, and xylene (BTX) in liquid culture and in soil by Bacillus subtilis and Pseudomonas aeruginosa strains and a formulated bacterial consortium. *Environmental Science and Pollution Research*, 19:3380–3388, 2012.

[212] C. N. Mulligan and R. N. Yong. Natural attenuation of contaminated soils. *Environment International*, 30:587–601, 2004.

[213] M. Mundt, K. Althoff, W. Dott, and J. Hollender. Microbial degradation of tar oil compounds under different redox conditions. *Acta Hydrochimica et Hydrobiologica*, 31(3):204–212, 11 2003.

[214] B. L. Murphy, T. Sparacio, and W. J. Shields. Manufactured gas plants-processes, historical development, and key issues in insurance coverage disputes. *Environmental Forensics*, 6(2):161–173, 6 2005.

[215] F. Musat, A. Galushko, J. Jacob, F. Widdel, M. Kube, R. Reinhardt, H. Wilkes, B. Schink, and R. Rabus. Anaerobic degradation of naphthalene and 2-methylnaphthalene by strains of marine sulfate-reducing bacteria. *Environmental Microbiology*, 11(1):209–219, 1 2009.

[216] I. M. Nambi and S. E. Powers. NAPL dissolution in heterogeneous systems: an experimental investigation in a simple heterogeneous system. *Journal of Contaminant Hydrology*, 44:161–184, 2000.

[217] National Research Council. *In Situ Bioremediation: When Does it Work?* National Academies Press., 1993.

[218] S. Neuman, P. Wierenga, and T. Nicholson. *A comprehensive strategy of hydrogeologic modeling and uncertainty analysis for nuclear facilities and sites*. Division of Systems Analysis and Regulatory Effectiveness, Office of Nuclear Regulatory Research, US Nuclear Regulatory Commission, 2003.

[219] C. J. Neville and C. B. Andrews. Containment Criterion for Contaminant Isolation by Cutoff Walls. *Groundwater*, 44(5):682–686, 2006.

[220] J. Odong. Evaluation of Empirical Formulae for Determination of Hydraulic Conductivity based on Grain-Size Analysis. *The Journal of American Science*, 3(3):1545–1003, 2007.

[221] F. I. Oesterholt, M. P. Pluim, and P. W. De Vries. Groundwater treatment at the former gas work remediation site "griftpark" in Utrecht, The Netherlands. Results of the semi permanent testing facility. *Water Science and Technology*, 35(10):165–172, 1 1997.

[222] Y.-S. Oh, Z. Shareefdeen, B. C. Baltzis, and R. Bartha'. Communication to the Editor Interactions Between Benzene, Toluene, and p-Xylene (BTX) During Their Biodegradation. *Biotechnology and Bioengineering*, 44:533–538, 1994.

[223] J. W. Page, K. Soga, and T. Illangasekare. The significance of heterogeneity on mass flux from DNAPL source zones: An experimental investigation. *Journal of Contaminant Hydrology*, 94(3-4):215–234, 12 2007.

[224] P. Panagos, M. Van Liedekerke, Y. Yigini, and L. Montanarella. Contaminated sites in Europe: Review of the current situation based on data collected through a European network. *Journal of Environmental and Public Health*, 2013, 2013.

[225] F. Pappenberger and K. J. Beven. Ignorance is bliss: Or seven reasons not to use uncertainty analysis. *Water Resources Research*, 42(5), 5 2006.

[226] J. C. Parker and R. J. Lenhard. A Model for Hysteretic Constitutive Relations Governing Multiphase Flow 1. Saturation-Pressure Relations. *Water Resources Research*, 23(12):2187–2196, 1987.

[227] D. L. Parkhurst and C. A. J. Appelo. User's Guide to PHREEQC (Version 2): A Computer Program for Speciation, Batch-Reaction, One-Dimensional Transport, and Inverse Geochemical Calculations, 1999.

[228] L. W. Perelo. Review: In situ and bioremediation of organic pollutants in aquatic sediments. *Journal of Hazardous Materials*, 177(1-3):81–89, 5 2010.

[229] C. D. Phelps, J. Battistelli, and L. Y. Young. Metabolic biomarkers for monitoring anaerobic naphthalene biodegradation in situ. *Environmental Microbiology*, 4(9):532–537, 2002.

[230] G. Pinder and M. Celia. *Subsurface Hydrology*. John Wiley & Sons, 2006.

[231] G. F. Pinder and L. M. Abriola. On the simulation of nonaqueous phase organic compounds in the subsurface. *Water Resources Research*, 22(9S):109S–119S, 8 1986.

[232] W. Poncheewin, G. D. A Hermes, J. C. J van Dam, J. J. Koehorst, H. Smidt, P. J. Schaap, J. Stoye, C. Zhong, S. Jünemann, and P. J. Schaap peterschaap. NG-Tax 2.0: A Semantic Framework for High-Throughput Amplicon Analysis. *Frontiers in Genetics*, 10, 2020.

[233] D. Postma and R. Jakobsen. Redox zonation: Equilibrium constraints on the Fe(III)/SO4-reduction interface. *Geochimica et Cosmochimica Acta*, 60(17):3169–3175, 1996.

[234] H. Prommer, B. Anneser, M. Rolle, F. Einsiedl, and C. Griebler. Biogeochemical and isotopic gradients in a BTEX/PAH contaminant plume: Model-based interpretation of a high-resolution field data set. *Environmental Science and Technology*, 43(21):8206–8212, 2009.

[235] H. Prommer, D. Barry, and C. Zheng. MODFLOW/MT3DMS-based reactive multicomponent transport modeling. *Ground Water*, 41(2):247–257, 2003.

[236] H. Prommer and D. A. Barry. *Modeling bioremediation of contaminated groundwater*. ASM Press, Washington DC, 2005.

[237] H. Prommer, G. Davis, and D. Barry. Geochemical changes during biodegradation of petroleum hydrocarbons: field investigations and biogeochemical modelling. *Organic Geochemistry*, 30(6):423–435, 6 1999.

[238] H. Prommer, M. E. Grassi, A. C. Davis, and B. M. Patterson. Modeling of microbial dynamics and geochemical changes in a metal bioprecipitation experiment. *Environmental Science and Technology*, 41(24):8433–8438, 2007.

[239] T. Ptak, M. Piepenbrink, and E. Martac. Tracer tests for the investigation of heterogeneous porous media and stochastic modelling of flow and transport—a review of some recent developments. *Journal of Hydrology*, 294(1-3):122–163, 7 2004.

[240] M. Rasheed, M. I. Badran, and M. Huettel. Influence of sediment permeability and mineral composition on organic matter degradation in three sediments from the Gulf of Aqaba, Red Sea. *Estuarine, Coastal and Shelf Science*, 57(1-2):369–384, 5 2003.

[241] J. C. Refsgaard, J. P. van der Sluijs, A. L. Højberg, and P. A. Vanrolleghem. Uncertainty in the environmental modelling process – A framework and guidance. *Environmental Modelling & Software*, 22(11):1543–1556, 11 2007.

[242] M. Reinhard, G. D. Hopkins, E. Steinle-Darling, and C. A. LeBron. In Situ Biotransformation of BTEX Compounds Under Methanogenic Conditions. *Groundwater Monitoring & Remediation*, 25(4):50–59, 11 2005.

[243] P. Renard. Stochastic Hydrogeology: What Professionals Really Need? *Groundwater*, 45(5):531–541, 2007.

[244] H. H. Richnow, E. Annweiler, W. Michaelis, and R. U. Meckenstock. Microbial in situ degradation of aromatic hydrocarbons in a contaminated aquifer monitored by carbon isotope fractionation. *Journal of Contaminant Hydrology*, 65(1-2):101–120, 8 2003.

[245] H. H. Richnow, R. U. Meckenstock, L. A. Reitzel, A. Baun, A. Ledin, and T. H. Christensen. In situ biodegradation determined by carbon isotope fractionation of aromatic hydrocarbons in an anaerobic landfill leachate plume (Vejen, Denmark). *Journal of Contaminant Hydrology*, 64(1-2):59–72, 6 2003.

[246] M. O. Rivett and S. F. Thornton. Monitored natural attenuation of organic contaminants in groundwater: priciples and application. *Water Management*, 6(WM6):381–392, 2008.

[247] P. K. Robertson. Interpretation of cone penetration tests-a unified approach. *Canadian Geotechnical Journal*, 46:1337–1355, 2009.

[248] P. K. Robertson and R. G. Campanella. Interpretation of cone penetration tests. Part I: Sand. *Canadian Geotechnical Journal*, 20(4):734–745, 1983.

[249] P. K. Robertson and R. G. Campanella. Interpretation of cone penetration tests. Part II: Clay. *Canadian Geotechnical Journal*, 20(4):734–745, 1983.

[250] M. Rogge, T. M. Christy, and F. de Weirdt. Site contamination fast delineation and screening using the membrane interface probe. In *Field Screening Europe 2001: Proceedings of the Second International Conference on Strategies and Techniques for the Investigation and Monitoring of Contaminated Sites*, pages 91–98. Springer Netherlands., 2002.

[251] W. F. M. Röling and H. W. Van Verseveld. Natural attenuation: What does the subsurface have in store? *Biodegradation*, 13:53–64, 2002.

[252] Royal Haskoning DHV. Griftpark scopeverandering. Historisch onderzoek ten behoeve van nader onderzoek grondwater. Technical report, Royal Haskoning, 2014.

[253] A. N. Roychoudhury and G. L. Merrett. Redox pathways in a petroleum contaminated shallow sandy aquifer: Iron and sulfate reductions. *Science of The Total Environment*, 366(1):262–274, 7 2006.

[254] P. B. Saéz and B. E. Rittmann. Biodegradation kinetics of a mixture containing a primary substrate (phenol) and an inhibitory co-metabolite (4-chlorophenol). *Biodegradation*, 4:3–21, 1993.

[255] M. Safinowski and R. U. Meckenstock. Methylation is the initial reaction in anaerobic naphthalene degradation by a sulfate-reducing enrichment culture. *Environmental Microbiology*, 8(2):347–352, 2006.

[256] A. Samouëlian, I. Cousin, A. Tabbagh, A. Bruand, and G. Richard. Electrical resistivity survey in soil science: a review. *Soil and Tillage Research*, 83(2):173–193, 9 2005.

[257] D. Sarewitz. How science makes environmental controversies worse. *Environmental Science and Policy*, 7(5):385–403, 2004.

[258] E. A. Seagren, B. E. Rittmann, and A. J. Valocchi. A critical evaluation of the local-equilibrium assumption in modeling NAPL-pool dissolution. *Journal of Contaminant Hydrology*, 39(1-2):109–135, 7 1999.

[259] J. S. Seo, Y. S. Keum, and Q. X. Li. Bacterial Degradation of Aromatic Compounds. *International Journal of Environmental Research and Public Health 2009, Vol. 6, Pages 278-309*, 6(1):278–309, 1 2009.

[260] E. Sepic, M. Bricelj, and H. Leskovsek. Toxicity of fluoranthene and its biodegradation metabolites to aquatic organisms. *Chemosphere*, 52(7):1125–1133, 2003.

[261] B. K. Singh and R. Naidu. Cleaning contaminated environment: a growing challenge. *Biodegradation*, 23(6):785–786, 9 2012.

[262] D. G. Smith and N. D. Smith. Sedimentation in anastomosed river systems: examples from alluvial valleys near Banff, Alberta. *Journal of Sedimentary Research*, 50(1):157–164, 1980.

[263] M. R. Smith. The biodegradation of aromatic hydrocarbons by bacteria. *Biodegradation*, 1(2-3):191–206, 6 1990.

[264] K. Soga, J. Page, and T. Illangasekare. A review of NAPL source zone remediation efficiency and the mass flux approach. *Journal of Hazardous Materials*, 110(1-3):13–27, 7 2004.

[265] M. R. Sousa, J. P. Jones, E. O. Frind, and D. L. Rudolph. A simple method to assess unsaturated zone time lag in the travel time from ground surface to receptor. *Journal of Contaminant Hydrology*, 144(1):138–151, 1 2013.

[266] O. D. Sparkman, Z. Penton, and F. G. Kitson. *Gas chromatography and mass spectrometry: a practical guide*. Academic press., 2011.

[267] P. A. Spooner, R. S. Wetzel, C. E. Spooner, C. A. Furman, and E. F. Tokarski. Slurry trench construction for pollution migration control. Technical report, OSTI, 2 1984.

[268] C. I. Steefel, C. A. Appelo, B. Arora, D. Jacques, T. Kalbacher, O. Kolditz, V. Lagneau, P. C. Lichtner, K. U. Mayer, J. C. Meeussen, S. Molins, D. Moulton, H. Shao, J. Šimůnek, N. Spycher, S. B. Yabusaki, and G. T. Yeh. Reactive transport codes for subsurface environmental simulation. *Computational Geosciences*, pages 445–478, 2015.

[269] C. I. Steefel and A. C. Lasaga. A coupled model for transport of multiple chemical species and kinetic precipitation/dissolution reactions with application to reactive flow in single phase hydrothermal systems. *American Journal of Science*, 294(5):529–592, 1994.

[270] A. Steinbach, R. Seifert, E. Annweiler, and W. Michaelis. Hydrogen and carbon isotope fractionation during anaerobic biodegradation of aromatic hydrocarbons a field study. *Environmental Science & Technology*, 38(2):609–616, 2004.

[271] S. Stephens. http://eawag-bbd.ethz.ch/BTEX/BTEX_map.html, 2020.

[272] M. S. Strickland, C. Lauber, N. Fierer, and M. A. Bradford. Testing the functional significance of microbial community composition. *Ecology*, 90(2):441–451, 2 2009.

[273] C. Stumpp, A. J. Żurek, P. Wachniew, A. Gargini, A. Gemitzi, M. Filippini, and S. Witczak. A decision tree tool supporting the assessment of groundwater vulnerability. *Environmental Earth Sciences*, 75(13):1–7, 7 2016.

[274] M. P. Suarez and H. S. Rifai. Biodegradation Rates for Fuel Hydrocarbons and Chlorinated Solvents in Groundwater. *Bioremediation Journal*, 3(4):337–362, 1999.

[275] J. B. Sutherland, T. M. Heinze, M. G. Pearce, J. Deck, A. J. Williams, and J. P. Freeman. Biotransformation of acridine by Mycobacterium vanbaalenii. *Environmental Toxicology and Chemistry*, 28(1):61–64, 2009.

[276] D. J. Sutton, Z. J. Kabala, D. E. Schaad, and N. C. Ruud. The dipole-flow test with a tracer: A new single-borehole tracer test for aquifer characterization. *Journal of Contaminant Hydrology*, 44(1):71–101, 2000.

[277] S. Takahashi, J. Tomita, K. Nishioka, T. Hisada, and M. Nishijima. Development of a Prokaryotic Universal Primer for Simultaneous Analysis of Bacteria and Archaea Using Next-Generation Sequencing. *PLOS ONE*, 9(8):e105592, 8 2014.

[278] A. Tancsics, A. R. Szalay, M. Farkas, T. Benedek, S. Szoboszlay, I. Szabo, and T. Lueders. Stable isotope probing of hypoxic toluene degradation at the Siklós aquifer reveals prominent role of Rhodocyclaceae. *FEMS microbiology ecology*, 94(4):fiy088, 2018.

[279] J. Thierrin, G. B. Davis, C. Barber, B. M. Patterson, T. R. Power, and M. Lambert. Natural degradation rates of BTEX compounds and naphthalene in a sulphate reducing groundwater environment. *Hydrological Sciences Journal*, 38(4):309322, 2009.

[280] R. Thomas. The development of the manufactured gas industry in Europe. *Geological Society, London, Special Publications*, 465(1):137–164, 1 2018.

[281] M. Thullner, F. Centler, H. H. Richnow, and A. Fischer. Quantification of organic pollutant degradation in contaminated aquifers using compound specific stable isotope analysis - Review of recent developments. *Organic Geochemistry*, 42(12):1440–1460, 2012.

[282] M. Thullner, A. Fischer, H. H. Richnow, and L. Y. Wick. Influence of mass transfer on stable isotope fractionation. *Applied Microbiology and Biotechnology*, 97(2):441–452, 2013.

[283] M. Thullner, M. Kampara, H. H. Richnow, H. Harms, and L. Y. Wick. Impact of bioavailability restrictions on microbially induced stable isotope fractionation. 1. Theoretical calculation. *Environmental Science and Technology*, 42(17):6544–6551, 9 2008.

[284] A. Tiehm and S. Schulze. Intrinsic Aromatic Hydrocarbon Biodegradation for Groundwater Remediation. *Oil & Gas Science and Technology-Rev. IFP*, 58(4):449–462, 2003.

[285] D. Tischler. *Microbial Styrene Degradation*. Cham, Switzerland: Springer International Publishing., no. 11725 edition, 2015.

[286] D. E. Trigueros, A. N. Módenes, and M. A. Ravagnani. Biodegradation kinetics of benzene and toluene as single and mixed substrate: Estimation of biokinetics parameters by applying particle swarm optimization. *Latin American Applied Research*, 40:219–226, 2010.

[287] F. T.-C. Tsai. Bayesian model averaging assessment on groundwater management under model structure uncertainty. *Stochastic Environmental Research and Risk Assessment*, 24(6):845–861, 8 2010.

[288] USEPA. Provisional Guidance for Quantitative Risk Assessment of Polycyclic Aromatic Hydrocarbons. Technical report, US EPA, 1993.

[289] E. M. P. M. Van Boekel. Geochemische schematisering van de ondergrond in het STONE model Organisch stofgehalte in de ondergrond. Technical report, Alterra, Wageningen, 2009.

[290] J. van der Sluijs, P. Janssen, A. Petersen, P. Kloprogge, J. Risbey, W. Tuinstra, and J. Ravetz. RIVM/MNP Guidance for Uncertainty Assessment and Communication: Tool Catalogue for Uncertainty Assessment. Technical report, RIVM, 2004.

[291] G. van der Veer. Geochemical soil survey of the Netherlands. Technical report, Geochemical soil survey of the Netherlands, Utrecht, 2006.

[292] M. J. van der Waals, S. Atashgahi, U. N. da Rocha, B. M. van der Zaan, H. Smidt, and J. Gerritse. Benzene degradation in a denitrifying biofilm reactor: activity and microbial community composition. *Applied Microbiology and Biotechnology*, 101(12):5175–5188, 2017.

[293] B. M. van der Zaan, F. T. Saia, A. J. Stams, C. M. Plugge, W. M. de Vos, H. Smidt, A. A. Langenhoff, and J. Gerritse. Anaerobic benzene degradation under denitrifying conditions: Peptococcaceae as dominant benzene degraders and evidence for a syntrophic process. *Environmental Microbiology*, 14(5):1171–1181, 5 2012.

[294] J. A. Van Leeuwen. *Biodegradation of mono-and poly aromatic hydrocarbons in a contaminated aquifer originating from a former Pintsch gas factory site: Laboratory and field investigations.* PhD thesis, Utrecht University, 2021.

[295] J. A. van Leeuwen, J. Gerritse, N. Hartog, S. Ertl, J. R. Parsons, and S. M. Hassanizadeh. Anaerobic degradation of benzene and other aromatic hydrocarbons in a tar-derived plume: Nitrate versus iron reducing conditions. *Journal of Contaminant Hydrology*, 248:104006, 6 2022.

[296] J. A. Van Leeuwen, N. Hartog, J. Gerritse, C. Gallacher, R. Helmus, O. Brock, J. R. Parsons, and S. M. Hassanizadeh. The dissolution and microbial degradation of mobile aromatic hydrocarbons from a Pintsch gas tar DNAPL source zone. *Science of The Total Environment*, 722:137797, 6 2020.

[297] M. M. van Leeuwen, G. B. Heuvelink, J. Wallinga, I. J. de Boer, J. C. van Dam, E. A. van Essen, S. W. Moolenaar, F. P. Verhoeven, J. J. Stoorvogel, and C. R. Stoof. Visual soil evaluation: reproducibility and correlation with standard measurements. *Soil and Tillage Research*, 178:167–178, 5 2018.

[298] A. van Lit. IBC maatregelen Griftpark Utrecht, monitoring grondwater. Technical report, Mourik, Utrecht, 2020.

[299] J. H. van Lopik. *Design of recharge and abstraction well systems in heterogeneous aquifers: modeling and experimental studies*. PhD thesis, Utrecht University, 2020.

[300] S. J. Varjani. Microbial degradation of petroleum hydrocarbons. *Bioresource Technology*, 223:277–286, 1 2017.

[301] J. F. Villaume. Investigations at Sites Contaminated with Dense, Non-Aqueous Phase Liquids (NAPLs). *Groundwater Monitoring & Remediation*, 5(2):60–74, 6 1985.

[302] C. Vogt, C. Dorer, F. Musat, and H. H. Richnow. Multi-element isotope fractionation concepts to characterize the biodegradation of hydrocarbons - from enzymes to the environment. *Current Opinion in Biotechnology*, 41:90–98, 2016.

[303] C. Vogt, F. Musat, and H.-H. Richnow. Compound-Specific Isotope Analysis for Studying the Biological Degradation of Hydrocarbons. In *Anaerobic Utilization of Hydrocarbons, Oils, and Lipids*, pages 285 – 321. Springer Nature Switzerland, 2020.

[304] W. Walker, P. Harremoës, J. Rotmans, J. van der Sluijs, M. van Asselt, P. Janssen, and M. Krayer von Krauss. Defining Uncertainty: A Conceptual Basis for Uncertainty Management in Model-Based Decision Support. *Integrated Assessment*, 4(1):5–17, 3 2003.

[305] N. C. Wardlaw. The Effects of Geometry, Wettability, Viscosity And Interfacial Tension On Trapping In Single Pore-throat Pairs. *Journal of Canadian Petroleum Technology*, 21(3):21–27, 1982.

[306] H. J. T. Weerts and M. F. P. Bierkens. Geostatistical analysis of overbank deposits of anastomosing and meandering fluvial systems; Rhine-Meuse delta, The Netherlands. *Sedimentary Geology*, 85:221–232, 1993.

[307] M. Wehrer, T. Rennert, T. Mansfeldt, and K. U. Totsche. Contaminants at former manufactured gas plants: Sources, properties, and

processes. *Critical Reviews in Environmental Science and Technology*, 41(21):1883–1969, 2011.

[308] J. Weiss and C. Downs. Some of the Constituents of Coke-Oven Tar. *Industrial and Engineering Chemistry*, 15(10), 1923.

[309] F. J. Wentz and S. E. Dickenson. Pore pressure response during high-frequency sonic drilling and SPT sampling in liquefiable sand. In N. Z. CY Chin. Queenstown, editor, *Proceedings of the 19th New Zealand Geotechnical Society Geotechnical Symposium.*, Ed. CY Chin, Queenstown, 2013.

[310] W. B. Whitman, D. C. Coleman, and W. J. Wiebe. Perspective Prokaryotes: The unseen majority. *Proceedings of the National Academy of Sciences of the United States of America*, 95:6578–6583, 1998.

[311] F. Widdel and R. Rabus. Anaerobic biodegradation of saturated and aromatic hydrocarbons. *Current Opinion in Biotechnology*, 12(3):259–276, 6 2001.

[312] T. H. Wiedemeier and P. E. Haas. Designing Monitoring Programs to Effectively Evaluate the Performance of Natural Attenuation. *Groundwater Monitoring & Remediation*, 22(3):124–135, 8 2002.

[313] T. H. Wiedemeier, H. S. Rifai, C. J. Newell, and J. T. Wilson. *Natural attenuation of fuels and chlorinated solvents in the subsurface.* John Wiley & Sons., 1999.

[314] T. H. Wiedemeier, M. A. Swanson, D. E. Moutoux, E. Kinzie Gordon, J. T. Wilson, B. H. Wilson, D. H. Kampbell, J. E. Hansen, and P. Haas. Technical protocol for evaluating natural attenuation of chlorinated solvents in groundwater. Technical report, US EPA, 1998.

[315] R. J. Williams and W. C. Evans. The metabolism of benzoate by Moraxella species through anaerobic nitrate respiration. Evidence for a reductive pathway. *Biochemical Journal*, 148(1):1–10, 1975.

[316] B. H. Wilson, G. B. Smith, and J. F. Rees. Biotransformations of Selected Alkylbenzenes and Halogenated Aliphatic Hydrocarbons in Methanogenic Aquifer Material: A Microcosm Study. *Environmental Science and Technology*, 20(10):997–1002, 1986.

[317] L. Winter, J. J. Linde-Jensen, I. Mikkelsen, T. H. Jensen, and M. Henze. Polytekinsk Forlag, Denmark. Technical report, Spildevand Teknik, 1978.

[318] W. J. Wu, M. Delshad, T. Oolman, and G. A. Pope. Remedial options for creosote-contaminated sites. *Ground Water Monitoring and Remediation*, 20(2):78–86, 2000.

[319] Z. Yan, Y. Zhang, H. Wu, M. Yang, H. Zhang, Z. Hao, and H. Jiang. Isolation and characterization of a bacterial strain Hydrogenophaga sp. PYR1 for anaerobic pyrene and benzo[a]pyrene biodegradation. *RSC advances*, 7(74):46690–46698, 2017.

[320] G. T. Yeh and V. S. Tripathi. A critical evaluation of recent developments in hydrogeochemical transport models of reactive multichemical components. *Water Resources Research*, 25(1):93–108, 1989.

[321] S. Yu and L. Semprini. Kinetics and modeling of reductive dechlorination at high PCE and TCE concentrations. *Biotechnology and Bioengineering*, 88(4):451–464, 11 2004.

[322] D. Zamfirescu and P. Grathwohl. Occurrence and attenuation of specific organic compounds in the groundwater plume at a former gasworks site. *Journal of Contaminant Hydrology*, 53(3-4):407–427, 12 2001.

[323] A. Zech, S. Attinger, A. Bellin, V. Cvetkovic, P. Dietrich, A. Fiori, G. Teutsch, and G. Dagan. A Critical Analysis of Transverse Dispersivity Field Data. *Groundwater*, 57(4):632–639, 7 2019.

[324] J. Zeyer, E. P. Kuhn, and R. P. Schwarzenbach. Rapid microbial mineralization of toluene and 1,3-dimethylbenzene in the absence of molecular oxygen. *Applied and environmental microbiology*, 52(4):944–7, 10 1986.

[325] C. Zhang, H. Yoon, C. J. Werth, A. J. Valocchi, N. B. Basu, and J. W. Jawitz. Evaluation of simplified mass transfer models to simulate the impacts of source zone architecture on nonaqueous phase liquid dissolution in heterogeneous porous media. *Journal of Contaminant Hydrology*, 102(1-2):49–60, 11 2008.

[326] X. Zhang, E. R. Sullivan, and L. Y. Young. Evidence for aromatic ring reduction in the biodegradation pathway of carboxylated naphthalene by a sulfate reducing consortium. *Biodegradation*, 11:117–124, 2000.

[327] C. Zheng and G. D. Bennett. *Applied contaminant transport modeling (Vol. 2)*. New York: Wiley-Interscience., vol 2 edition, 2002.

[328] C. Zheng and P. Wang. MT3DMS: A Modular Three-Dimensional Multispecies Transport Model for Simulation of Advection, Dispersion, and

Chemical Reactions of Contaminants in Groundwater Systems; Documentation and User's Guide. Technical report, US Army Corps of Engineers Engineer Research and Development Center, Alabama, 1999.

[329] Y. Zhong, T. Luan, L. Lin, H. Liu, and N. F. Tam. Production of metabolites in the biodegradation of phenanthrene, fluoranthene and pyrene by the mixed culture of Mycobacterium sp. and Sphingomonas sp. *Bioresource Technology*, 102(3):2965–2972, 2 2011.

[330] Y. Y. Zhou, D. Z. Chen, R. Y. Zhu, and J. M. Chen. Substrate interactions during the biodegradation of BTEX and THF mixtures by Pseudomonas oleovorans DT4. *Bioresource Technology*, 102(12):6644–6649, 6 2011.

Samenvatting

Achtergrond

Grondwaterverontreiniging door koolteer en andere aromatische koolwaterstofmengsels vormt een wereldwijd probleem. Koolteer is een vloeistof die zwaarder is dan water en daardoor, nadat het op het grondoppervlak is gedumpt, diep onder het waterpeil de bodem in kan zakken, waar het een langdurige bron van grondwaterverontreiniging kan worden. Eenmaal opgelost in het grondwater ondergaan aromatische koolwaterstoffen verschillende fysieke, biologische en chemische processen. Om de risico's die gepaard gaan met specifieke verontreinigingen te beoordelen, is het belangrijk om deze processen te kwantificeren. Aangezien ze onderling afhankelijk zijn, is hun kwantificatie verbonden aan de specifieke omstandigheden op de verontreinigde locatie en is de betrouwbaarheid van de kwantificatie sterk afhankelijk van de beschikbaarheid van veldgegevens. In wetenschappelijke literatuur zijn veel gedetailleerd onderzochte veldlocaties gedocumenteerd. Hoewel deze studies bijdragen aan een beter begrip van fundamentele processen, treft men in de 'real-world' advieswereld vaker locaties met zeer complexe condities en beperkte veldgegevens.

Het Griftpark bevindt zich op het terrein van een voormalig industrieel complex waar tot aan de jaren 1960 meerdere gasfabrieken waren gevestigd. Het eerste watervoerende pakket onder de locatie is ernstig verontreinigd met koolteer, dat is gedetecteerd op dieptes variërend van 8 tot 50 meter onder het maaiveld. Om de omliggende watervoerende pakketten veilig te houden, is de bronzone van de verontreiniging afgeschermd met een verticale schermwand. Bovendien wordt, om lekkage van verontreinigingen naar het tweede watervoerende pakket via de enigszins doorlaatbare aquitard te voorkomen, grondwater continu onttrokken aan de afgeschermde zone en afgevoerd naar een zuiveringsinstallatie. Deze beheersmaatregelen, de talrijke, grotendeels onbekende bronlocaties, de aanzienlijke heterogeniteit van de ondergrond, met name de aquitard, evenals de stedelijke omgeving en het openbaar gebruik van

de locatie, beperken de mogelijkheden voor het ontwerpen en uitvoeren van uitgebreide locatieonderzoeken.

Traditioneel gezien hebben de enorme complexiteit en beperkte beschikbaarheid van literatuur, laboratorium- en veldgegevens met betrekking tot de karakterisering van locaties zoals het Griftpark diepgaande (model)studies schijnbaar vruchteloos gemaakt. Als gevolg daarvan is er een aanzienlijke kloof in ons begrip van talrijke real-world locaties en hun potentieel voor (her)ontwikkeling.

Gemotiveerd door deze kennislacune beoogt onze studie de complexe Griftparklocatie te verkennen en te evalueren in hoeverre veldonderzoeken in dergelijke complexe omgevingen kunnen bijdragen aan begrip van het systeem. Ondanks de inherente uitdagingen die worden veroorzaakt door de schaarste aan gegevens, is ons doel waardevolle inzichten te genereren die bijdragen aan risicobeoordelingen en de identificatie van potentiële nieuwe beheers- en saneringsstrategieën.

Dit proefschrift presenteert de bevindingen van ons brede onderzoek, gericht op het verbeteren van het begrip van de hydrogeologische en biochemische processen die van invloed zijn op de verspreiding en concentratie van opgeloste aromatische koolwaterstoffen in het Griftpark. De onderliggende motivatie voor het onderzoek is de ambitie van de gemeente Utrecht om de kostbare actieve beheersprocedures af te bouwen en over te gaan op een nieuwe benadering die is gericht op natuurlijke afbraak. De volgende onderzoeksvragen zijn behandeld:

- Wat zijn de hydrogeologische omstandigheden onder het Griftpark?
- Welke belangrijke biologische afbraakprocessen vinden plaats?
- Wat is de afbraakcapaciteit van de ondergrond en hoe beïnvloedt dit de potentiële effectiviteit van gemonitorde natuurlijke afbraak als beheersoptie?
- Welke kritieke parameters moeten worden overwogen bij het uitvoeren van een risicobeoordeling voor mogelijke beheersopties in het Griftpark?

Methodes

Om deze onderzoeksvragen te beantwoorden, werden verschillende technieken toegepast, variërend van laboratorium- en veldonderzoek tot numerieke analyses op veldschaal.

Verschillende boortechnieken werden gebruikt om informatie te verkrijgen over fysieke ondergrondse parameters en de aanwezigheid van koolteercomponenten, zoals sonderingen, inclusief cone penetration tests (CPT) en

membrane inter-phase probing (MIP), en sonische bemonstering. Een reeks hydraulische tests werd uitgevoerd om beter inzicht te krijgen in de verbinding tussen het eerste en tweede watervoerende pakket, evenals de lekdichtheid van de schermwand.

Bodem-, grondwater- en teermonsters werden in het laboratorium bestudeerd om bodemtypen te identificeren (zeefanalyse) en om samenstellingen en concentraties van verontreinigingen te meten (gas chromatography-mass spectrometry). Verschillende analyses werden uitgevoerd om de van nature voorkomende biologsiche afbraak van opgeloste koolteercomponenten te beoordelen. Deze onderzoeken omvatten de bepaling en kwantificering van microbiële DNA (real-time polymerase chain reaction) en metabolieten (qualitative tandem liquid chromatography quadrupole time of flight mass spectrometry), evenals de analyse van specifieke isotopen (gas chromatography isotope ratio mass spectroscopy) en elektronacceptoren in het grondwater (ion-exchange chromatography and inductively coupled plasma-optical emission spectrometry).

Om diepgaander inzicht te krijgen in de gecombineerde effecten van grondwaterstroming, transport van verontreinigingen, biologische afbraak en daaropvolgende geochemische reacties, als mede het faciliteren van een risicobeoordeling van de locatie, werd een driedimensionaal numeriek reactief transportmodel gemaakt voor het Griftpark. Het model werd gebouwd in PHT3D, een softwarecode die de mogelijkheden van de veelgebruikte MODFLOW/MT3DMS stromings- en transportsimulator integreert met die van de geochemische reactiesimulator van de PHREEQC-2 code.

Resultaten

Geologie

Weerstandsprofielen van sonderingen en visuele inspectie van bodemmonsters onthulden de aanwezigheid van heterogeniteiten in de ondergrond van het Griftpark, met name binnen de aquitard. Verder onderzoek, inclusief hydraulische tests, suggereerde dat hoewel communicatie tussen de twee watervoerende pakketten door de aquitard plaatsvindt, de vertikale stroming wordt belemmerd door de aanwezigheid van meerdere kleiafzettingen van verschillende grootte en dikte. Analyse van verontreinigingen en redoxgegevens wees uit dat er geen verontreiniging en de daarmee gepaard gaande biologische afbraak plaatsvindt in het tweede watervoerende pakket. Dit wijst erop dat de aquitard in combinatie met de grondwateronttrekking effectief verhindert dat zowel koolteer in pure fase als opgelost in het grondwater het tweede

watervoerende pakket in lekt. Dit toont ook de effectiviteit van de huidige beheersmaatregelen.

Numerieke modellering toonde aan dat het aannemen van modellagen inclusief kleiafzettingen in de aquitard, in plaats van homogene modellagen, resulteerde in verhoogde waterfluxen de afgeschermde zone in en uit. Er werd ook waargenomen dat dit leidde tot een sterkere verspreiding van de verontreinigingspluim en hogere concentraties in de kern van de pluim. Desalniettemin was het effect op de verontreinigingsconcentraties relatief gering in vergelijking met andere parameters. Daarom wordt het toevoegen van expliciete heterogeniteit als een waardevolle bijdrage aan het numerieke model beschouwd met name wanneer ruimtelijke evolutie van de verontreinigingspluim in het tweede watervoerende pakket van belang is.

Verontreinigingsbronnen

De talrijke potentiële dumplocaties van teer en de intrinsiek onvoorspelbare aard van verspreiding ervan in heterogene ondergrond, stelden aanzienlijke uitdagingen aan het vaststellen van verontreinigingsbronzones in het Griftpark. Tijdens het onderzoek werd koolteer in pure fase consequent aangetroffen op verdachte locaties of werden indicaties gevonden voor de aanwezigheid van pure teer vlakbij het testpunt. De dieptes waarop koolteer werd aangetroffen varieerde sterk. Zo werd op een locatie teer aangetroffen op een diepte van slechts 4 m onder het maaiveld, en op een diepte van 49.5 m onder het maaiveld (46.5 m onder de grondwaterpeil) op een andere.

Het onderzoek leverde onvoldoende informatie op om een volledig driedimensionaal begrip van de distributie van de bronzones te verkrijgen. Desalniettemin gaf het reactief transportmodel aan dat het volume verontreinigde grond aanzienlijk invloed heeft op de concentraties die de tweede watervoerende pakket bereiken wanneer grondwaterpompen worden uitgeschakeld. Dit toont het belang van grondig onderzoek om de distributie van de bronzones nauwkeurig te karakteriseren.

Analyse van een koolteermonster onthulde dat het gewicht is samengesteld uit 92% polycyclische aromatische koolwaterstoffen, voornamelijk naftaleen (39% van het totale gewicht) en verschillende gemethyleerde naftalenen (43% van het totale gewicht), evenals indeen en indaan (1% en 6% van het totale gewicht). De overige 8% van het monster bestond uit mono-aromatische koolwaterstoffen, waarvan meer dan de helft bestond uit benzeen, tolueen, ethylbenzeen en xylenen (BTEX)-verbindingen.

Biologische afbraak

Het onderzoek naar natuurlijke biologische afbraak in het Griftpark benadrukte de belangrijke rol van biologische afbraak bij het verminderen van aromatische koolwaterstofconcentraties. De studie toonde aan dat conventionele onderzoeksbenaderingen om natuurlijke biologische afbraak te beoordelen, doorgaans toegepast om processen in verontreinigingspluimen te bestuderen, effectief de aanwezigheid van biologische afbraak kunnen aantonen, ook in afwezigheid van een direct traceerbare pluim.

IJzer en sulfaat werden geïdentificeerd als de belangrijkste elektronacceptoren voor afbraak in het Griftpark. Het reactieve transportmodel onthulde dat de temporele verandering in de afbraakcapaciteit van het systeem nauw verbonden is met uitputting van biologisch beschikbaar ijzer in sediment en sulfaat in grondwater. Terwijl sulfaat grotendeels is uitgeput in grondwater op locaties met hoge aromatische koolwaterstofconcentraties, wijzen juist sterk verhoogde sulfaatconcentraties op andere plekken op de aanwezigheid van sulfaatbronnen (bijvoorbeeld gips uit fabriekspuin). Hoewel geen sedimentanalyse is uitgevoerd om de beschikbaarheid van ijzer in de ondergrond te beoordelen, geven de onderzoeksresultaten aan dat ijzeruitputting heeft plaatsgevonden rond verontreinigingsbronzones. Na verloop van tijd zal naar verwachting biologische afbraak beperkt worden door sulfaat aangevuld door regenval en grondwater, evenals door methanogenese.

Hoewel de gegevens van het Griftpark terrein het voorkomen van biologische afbraak bevestigen, belemmert het ontbreken van een direct traceerbare verontreinigingspluim het maken van massabalansen die gebruikt kunnen worden om afbraaksnelheden te berekenen. We toonden aan dat afbraaksnelheden een cruciale rol spelen bij het bepalen van de verontreinigingsconcentraties die het tweede watervoerende pakket bereiken wanneer grondwateronttrekking wordt stopgezet. Literatuurwaarden bieden een breed scala aan potentiële afbraaksnelheden als gevolg van variaties in fysieke, chemische en biologische omstandigheden op verschillende locaties. Bij het Griftpark zou het gebruik van de bovengrens van snelheden aangetroffen in de literatuur resulteren in een volledig veilige situatie in het tweede watervoerende pakket na het stopzetten van de grondwateronttrekking, terwijl de ondergrens leidt tot concentraties die aanzienlijk boven interventiewaarden liggen. Dit benadrukt het belang van het bepalen van mogelijke afbraaksnelheden specifiek voor deze locatie om meer betekenisvolle risicobeoordelingen te kunnen uitvoeren.

Kritieke parameters

Het reactieve transportmodel van het Griftpark heeft inzicht gegeven in significante processen die zich afspelen in de ondergrond. De bevindingen wijzen

op de belangrijkste overwegingen voor de ontwikkeling van een risicobeoordelingsmodel voor de mogelijke toepassing van gemonitorde natuurlijke afbraak op deze locatie.

Simulaties waarbij, door het stopzetten van grondwateronttrekking, verontreiniging het tweede watervoerende pakket in kon lekken, toonden aan dat ook na 100 jaar, biologische afbraak de aromatische koolwaterstofconcentraties onder interventieniveaus hield bij het gebruik van gemiddelde afbraaksnelheden aangetroffen in de literatuur. Aangezien de vele aannames in het referentiemodel (met betrekking tot verontreinigingsbronnen, afbraaksnelheden en de samenstelling van het grondwater van de eerste en tweede watervoerende pakket) het momenteel nog ongeschikt houden ter ondersteuning van besluitvorming, zijn de resultaten veelbelovend. Dit biedt een basis om het onderzoek naar gemonitorde natuurlijke afbraak als een beheersoptie voor het Griftpark voort te zetten. De gevoeligheidsanalyse van het model toonde aan dat het volume van de ondergrond dat verontreinigd is met teer en de afbraaksnelheden van de aanwezige koolwaterstoffen de kritieke factoren zijn bij het bepalen van de potentiële doorbraakconcentraties in het tweede watervoerende pakket.

De resultaten van ons onderzoek tonen aan dat, ondanks de beperkte beschikbaarheid van data, de combinatie van veldonderzoek en numerieke modellering waardevolle inzichten kan opleveren in het begrip van complexe locaties. Dit werk onderstreept het potentiële belang van het gebruik van dergelijke tools en methoden bij het onderzoeken van locaties vergelijkbaar met het Griftpark, of daar ook beheersmaatregelen worden toegepast of niet.

Aerobe lab experimenten

Daarnaast werd er een reeks aerobe batch-experimenten uitgevoerd om de interacties tussen substraten te onderzoeken bij de verontreinigende stoffen die zijn aangetroffen in het Griftpark. De experimenten toonden aan dat inheemse micro-organismen van het Griftpark alle geteste verbindingen, te weten benzeen, tolueen, ethylbenzeen, xyleen, indeen, indaan en naftaleen (BTEXIeIaN), volledig kunnen afbreken onder aerobe omstandigheden. Bovendien werd vastgesteld dat de aanwezigheid van indeen, indaan en naftaleen de afbraak van benzeen, tolueen, ethylbenzeen en o-xyleen remt.

Deze bevindingen laten zien dat de gelijktijdige aanwezigheid van meerdere verontreinigende stoffen leidt tot variaties in afbraakprocessen en de ontwikkeling van de microbiële gemeenschap. Deze complexiteit vormt een extra uitdaging bij het bepalen van afbraaksnelheden op specifieke veldlocaties, evenals een beperking bij het extrapoleren van snelheden die zijn verkregen op één locatie naar een andere.

Aanbevelingen

Om het referentiemodel te verbeteren, raden we ten zeerste aan om aanvullende veldonderzoeken uit te voeren om belangrijke kennislacunes aan te pakken. Ten eerste is het van belang om een uitgebreider beeld te krijgen van de mate van koolteer verontreinigingen in pure fase, aangezien de onzekerheid in deze parameter van aanzienlijke invloed is op de voorspellende capaciteiten van het reactieve transportmodel. Door gebruik te maken van technologieën zoals de MIP op verdachte en niet-verdachte locaties, zou er meer inzicht kunnen worden verkregen in het totale verontreinigde volume en de hoeveelheid verontreiniging.

Hoewel het verkrijgen van nauwkeurige schattingen van de massa-balans en afbraaksnelheden uitdagingen met zich meebrengt in afwezigheid van een direct traceerbare verontreinigingspluim, biedt regelmatige bemonstering langs convergerende stroomlijnen naar grondwateronttrekkingsputten een mogelijkheid om een idee van mogelijke snelheden te verkrijgen.

Om het inzicht in de afbraakcapaciteit van de ondergrond te verbeteren, wordt aanbevolen om ijzerspeciatie-analyses uit te voeren op bodemmonsters uit zowel het eerste als het tweede watervoerende pakket, van verscheidene locaties waar verschillende omstandigheden heersen. Deze analyse zou de beoordeling van de hoeveelheid en het type biologisch beschikbaar ijzer in de ondergrond mogelijk maken, evenals de huidige mate van uitputting. Ook wordt aanbevolen om aanvullende bronnen van sulfaat en ijzer in sedimenten te identificeren (zoals gips- en slakafzettingen), aangezien ze een belangrijke rol kunnen spelen in de afbraakcapaciteit van de ondergrond van het Griftpark op de langetermijn.

Verder wordt geadviseerd om het biologische afbraakpotentieel in het tweede watervoerende pakket te evalueren. Aangezien hier niet sulfaat- maar nitraatreducerende omstandigheden overheersen en er momenteel geen waargenomen verontreiniging met koolteer aanwezig is, is het potentieel voor biologische afbraak in het tweede watervoerende pakket nog onbekend. Dit is een aanzienlijk kennisgebrek, aangezien het afbraakpotentieel van het tweede watervoerende pakket grotendeels de risico's zal bepalen die gepaard gaan met mogelijke lekkage van verontreinigingen naar deze laag.

Door deze onderzoeken uit te voeren, zal de voorspellende capaciteit van het model voor de verspreiding en afbraak van koolwaterstoffen op lange termijn aanzienlijk verbeteren. Dit zou vervolgens het model tot een onmisbaar instrument maken voor het uitvoeren van risicobeoordelingen en het evalueren van mogelijke toekomstige beheersmaatregelen voor het Griftpark.

Er moet worden opgemerkt dat gezien de hoge graad van heterogeniteit en complexiteit van de ondergrond op deze locatie, een zekere mate van onzeker-

heid zal blijven bestaan in het ondergrondmodel. Daarom is het raadzaam om voorafgaand aan het uitvoeren van definitieve beheersmaatregelen, potentiële noodmaatregelen te onderzoeken die effectief onverwacht hoge niveaus van koolwaterstoffen in het tweede watervoerende pakket kunnen aanpakken. Dergelijke noodoplossingen kunnen bijvoorbeeld het stimuleren van biologische afbraak omvatten, bijvoorbeeld door middel van sulfaat- of zuurstofinjectie. Sommige van dit type onderzoeken zijn al gaande in het Griftpark en worden besproken in het laatste deel van deze samenvatting.

Vooruitzicht

Op dit moment worden verschillende onderzoeksactiviteiten uitgevoerd om nader inzicht te verkrijgen in de potentie van (gestimuleerde) biologische afbraak in het Griftpark. Deze activiteiten omvatten een aantal specifieke pilotprojecten in het Griftpark, evenals het internationale MiBiRem-project.

MiBiRem Het project 'Microbiomes for bio-based innovation and environmental applications' (MiBiRem) is gestart om een IT-modelleringsinstrument te ontwerpen dat microbiologische, chemische, hydrologische en fysische gegevens en processen integreert om de potentie van bioremediatie op verschillende verontreinigde locaties te voorspellen en besluitvorming te ondersteunen. Het instrument zal bestaande numerieke modellen combineren en de processen op verschillende schalen integreren in een enkele interface. De casestudy van het Griftpark zal als input voor dit instrument worden gebruikt, zowel door observatiegegevens op te nemen als door gebruik te maken van het reactieve transportmodel, dat voor dit doel zal worden vertaald naar de Python-versie van MODFLOW (FlowPy) en PHREEQC (PhreeqPy). Het door de EU gefinancierde project wordt uitgevoerd door een groot internationaal consortium waar de Universiteit Utrecht betrokken zal zijn bij het verwerken van veldgegevens en hoofdverantwoordelijk zal zijn voor de ontwikkeling van het modelleringsinstrument.

Pilotprojecten 2023/2024 Om het potentieel van beheersbenaderingen op basis van biologische afbraak in het Griftpark te onderzoeken, worden momenteel vier pilotprojecten ontwikkeld.

- Pilot 1: In-situ stimulatie van biologische afbraak door nitraatinjectie
  - Dit pilotproject omvat de installatie van een onttrekkingsput in het tweede watervoerende pakket met als doel daaraan nitraathoudend water te onttrekken. Het onttrokken water wordt vervolgens in het eerste watervoerende pakket geïnjecteerd, waarna monitoring

zal plaatsvinden om de biologische afbraak van de daar aanwezige aromatische koolwaterstoffen te beoordelen.

  - Het primaire doel van deze pilot is om het potentieel voor biologische afbraak van de koolteerverontreiniging in het Griftpark te onderzoeken in het tweede watervoerende pakket, waar nitraatreducerende omstandigheden heersen. Het onderzoek heeft tot doel vast te stellen of natuurlijke afbraakprocessen alleen in staat zijn om opgeloste verontreinigingen, die mogelijk aan het afgeschermde gebied ontsnappen na deactivatie van de huidige actieve beheersmaatregelen, voldoende af te breken. Daarnaast zal de pilot de mogelijkheid onderzoeken om biologische afbraak met nitraat te stimuleren als aanvullende fallback-optie.

- Pilot 2: In-situ stimulatie van biologische afbraak door sulfaatinjectie

  - Deze pilot omvat de installatie van putten op een ernstig verontreinigde locatie in het Griftpark, gekenmerkt door uitgeputte sulfaatniveaus, en de injectie van sulfaat om biologische afbraak te stimuleren.
  - Het belangrijkste doel van deze pilot is om te onderzoeken of sulfaatdosering de biologische afbraak van koolteeraromaten kan stimuleren tot een mate waarin de migratie van verontreinigingen naar de tweede watervoerende pakket effectief wordt voorkomen na de deactivatie van de grondwateronttrekking uit het begrensde gebied.
  -

- Pilot 3: In-situ aërobe stimulatie van biologische afbraak door injectie van nano- en microbellen

  - Deze pilotstudie richt zich op de installatie van putten voor de injectie van nano- en microbellen in het grondwater en het monitoren van de daaropvolgende aërobe biologische afbraak van koolteeraromatische koolwaterstoffen.
  - Het belangrijkste doel van deze pilot is om de kosteneffectiviteit van nano- en microbellen te demonstreren en te vergelijken met het effect van macrobellen voor het inbrengen van lucht in de verontreinigde ondergrond. Verwacht wordt dat nano- en microbellen een betere optie vormen voor de gestimuleerde biologische afbraak van aromatische koolwaterstoffen.

- Pilot 4: Ex-situ behandeling van verontreinigd grondwater in een constructed wetland

- Deze pilot omvat de installatie van een 'constructed wetland' bij de grondwaterzuiveringsinstallatie, waarbij het binnenkomende verontreinigde grondwater wordt behandeld met behulp van een combinatie van helofytenfilters (moerasfilters), microbellen en actieve kool.
- Het belangrijkste doel van deze pilot is om de mogelijkheden van constructed wetlands te demonstreren bij de afbraak van aromatische koolwaterstoffen, terwijl tegelijkertijd verstoring van de omgeving wordt voorkomen. Het uiteindelijke doel is om de potentie van on-site constructed wetlands te onderzoeken om te vermijden dat verontreinigd grondwater altijd naar de op 3 km afstand gelegen zuiveringsinstallatie gepompt hoeft te worden.

De eerste drie pilots zullen worden uitgevoerd door *SARPI/TAUW*, en de vierde door *hmvt*. Het doel van de pilots is om te bepalen welke van deze methoden geschikt zijn om het beheer van aromatische koolwaterstoffen op het Griftpark terrein en vergelijkbare locaties in de toekomst duurzamer en kostenefficiënter te maken.